A study of the consequences of thermal treatments of the dioxide and lower oxides of manganese.

Newnham, Colin E.

Award date:
1975

Awarding institution:
University of Bath

A Study of the Consequences of Thermal Treatments of the Dioxide and Lower Oxides of Manganese

Submitted by Colin E. Newnham
for the degree of Ph.D.
of the University of Bath

1975

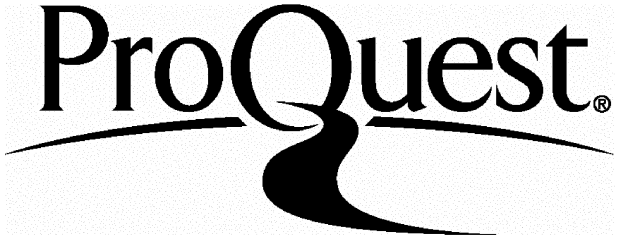

ABSTRACT

An electrodeposited γ-manganese dioxide has been studied by thermal analysis in vacuum, oxygen and water vapour environments between room temperature and 450°C. Water was the predominant desorption product and five types have been identified. Textural changes occuring as a result of dehydration were monitored by nitrogen adsorption at liquid nitrogen temperature and the isotherms obtained analysed by the α_s method. A micropore network was generated on outgassing above 160°C due to elimination of hydroxyl groups from the oxide lattice.

The products obtained by partial chemical reduction of γ- manganese dioxide have been characterised by X-ray diffraction and magnetic measurements and their thermal behaviour investigated. The microporosity revealed on outgassing was evaluated by nonane adsorption and the results compared with those obtained from nitrogen adsorption data.

The thermal decomposition of γ- and α- MnOOH has been studied in vacuum and at low oxygen pressures (10 Torr). In vacuum, γ- MnOOH decomposed below 400°C to a mixture of Mn_5O_8, α-Mn_3O_4 and water. Above this temperature Mn_5O_8 was converted to α-Mn_3O_4 as a result of oxygen removal. The vacuum dehydration of α-MnOOH led to a new modification of manganese sesquioxide (Mn_2O_3) isostructural with corundum (α- Al_2O_3). In oxygen both oxyhydroxides decomposed to β-MnO_2. γ-MnOOH transformed

directly to β-MnO_2 whilst α-MnOOH appeared to proceed via Mn_2O_3.

The existence of two new oxides of manganese, namely Mn_7O_{12} and Mn_7O_{10} has been established by thermal measurements and chemical analysis.

CONTENTS

ACKNOWLEDGMENTS

The work for this thesis was carried out in the laboratories of The Ever Ready Company (Holdings) Ltd. I would like to thank Dr. F.L. Tye for the opportunity to register for a higher degree and for his invaluable comments throughout the period in which the work was carried out.

I would also like to express my appreciation to my supervisors Dr. J.A. Lee (Ever Ready Co.) and Professor F.S. Stone (University of Bath) for very many valuable discussions.

I would also like to record my debt of thanks to the following; Mr. C.R. St.Claire-Smith for construction of the apparatus which was used for the thermal and gas adsorption experiments; Mr. P. Skidmore for recording the majority of the X-ray diffractometer traces and Mr. T.W. Baker of A.E.R.E., Harwell, for the remainder; Dr. R. Giovanoli for supplying a sample of Mn_5O_8; Dr. A. Hagan for instruction in the use of the magnetic susceptibility apparatus installed at the University of Bath; Mrs. J. Hitchcock for obtaining the thermal hygrometric data and Mrs. M.P. Jackson for typing the manuscript.

Finally I would like to thank the Directors of The Ever Ready Co.(Holdings) Ltd. for permission to carry out and submit this programme of work.

CHAPTER 1

Introduction

1.1. Oxides and Oxyhydroxides of Manganese

1.1.(i) General introduction

Manganese can exist in a multiplicity of oxidation states from +1 to +7 and oxides corresponding to several of these valency states are known. In addition to the simple oxides of Mn(II), Mn(III) and Mn(IV) there are oxides containing manganese in more than one valency state. At least two oxyhydroxides of manganese have been well characterised. The oxides and oxyhydroxides relevant to this work are described below.

1.1.(ii) Manganese dioxide MnO_2

Although the literature on manganese dioxide is extensive there is a good deal of confusion as to how many modifications exist. At least fourteen different Greek letters have been used to denote the various types of MnO_2[1] although it now seems certain that only two true modifications exist.

The common form β-MnO_2 is found widespread in nature as pyrolusite and crystallises with the rutile structure[2]. The structure consists of a somewhat distorted hexagonal close packing of oxygen ions with Mn(IV) ions occupying half of the octahedral sites. The other modification occurs in nature as the rare mineral ramsdellite. This has the same structure as the mineral diaspore (α-AlOOH)[3]. As for β-MnO_2 the structure can be regarded as derived from hexagonal close packing of the oxygen ions with half of the octahedral sites containing Mn(IV) ions. β-MnO_2 differs from ramsdellite in the way in which the manganese ions are arranged[4]. β-MnO_2 may be thought of as consisting of single chains of MnO_6

octahedra running parallel to the c axis whilst the ramsdellite structure can be considered as consisting of alternating double chains. This relationship is illustrated in fig.1.1. Ramsdellite is apparently metastable and transforms to β-MnO_2 at about 300°C in air.

It is possible for structural intergrowth to occur between the pyrolusite and ramsdellite structures to produce a manganese dioxide designated as γ-MnO_2[5]. These dioxides are used widely in the battery industry and a detailed account of their properties is given later in the chapter.

1.1.(iii) Pentamanganese octoxide Mn_5O_8

This was first reported by Feitknecht[6] who obtained Mn_5O_8 by two different routes: a) decomposition of γ-MnOOH at low oxygen pressures at 400°C b) oxidation of Mn_3O_4 having a surface area between 10 and 80 m^2g^{-1} at temperatures between 250°C and 550°C in the presence of nitrogen-oxygen mixtures. Other preparative routes have since been reported[7]. The X-ray powder pattern of Mn_5O_8 has been indexed by Oswald, Feitknecht and Wampetich[8] and shows Mn_5O_8 to be monoclinic. The formula may be written as $Mn_2^{II}Mn_3^{IV}O_8$ as Mn_5O_8 has been found to be isostructural with $Cd_2Mn_3O_8$. A complete structure determination[9] using single crystals of Mn_5O_8 shows that there is a distorted octahedral arrangement of oxygen atoms around Mn(IV) and a distorted trigonal prism around Mn(II). The chemical behaviour of Mn_5O_8 has received little attention in the literature but has been shown by DTA and TG to decompose in air and oxygen atmospheres at 550°C to α-Mn_2O_3[8]. Mn_5O_8 produced from finely divided α-MnOOH in an oxygen stream is reported[10] to oxidise

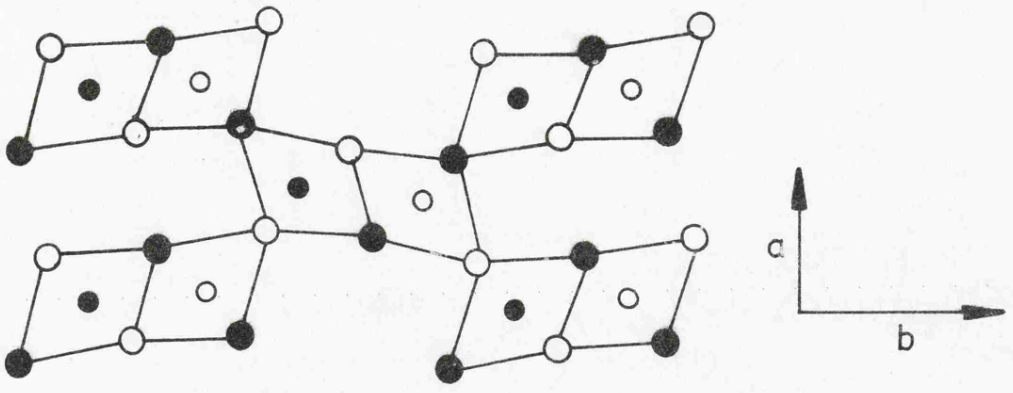

(a)

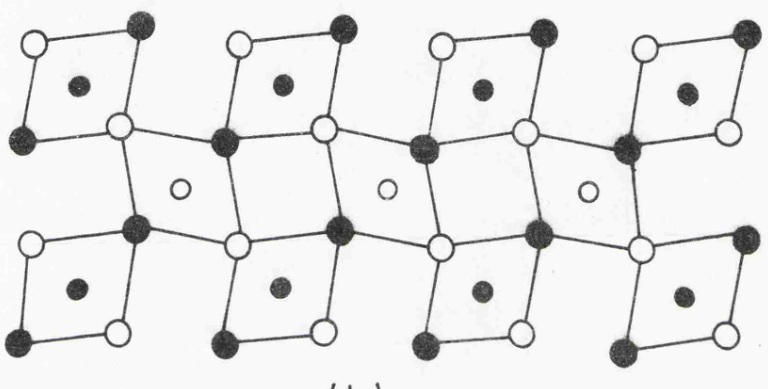

(b)

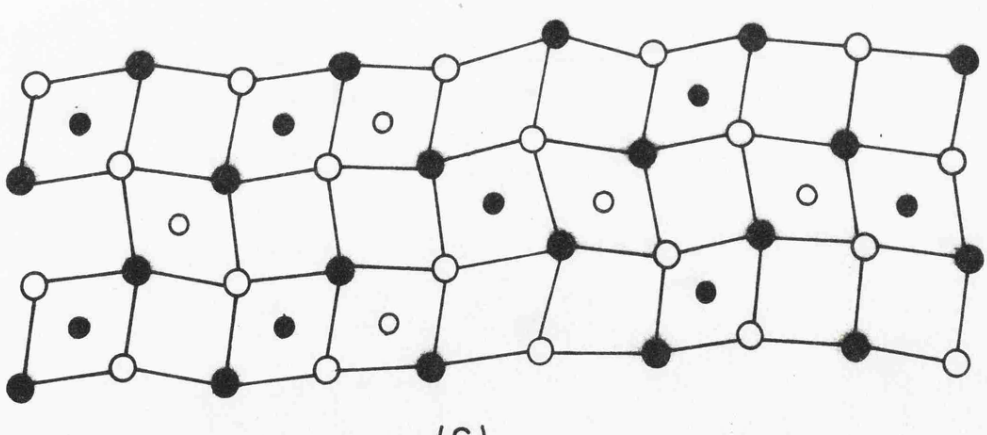

(C)

Fig.1.1 Idealised structures for a) ramsdellite and b) β-MnO_2 viewed along the c axis. The larger circles are oxygen, the smaller manganese. The shaded circles indicate atoms at ¾c, the open circles representing atoms at ¼c.

c) Random layer model for γ-MnO_2 as proposed by de Wolff[5].

to β-MnO_2 at 300°C.

1.1.(iv) Manganese sesquioxide Mn_2O_3

This is reported to exist in two modifications[2]. The stable form, generally designated α-Mn_2O_3, is obtained by heating many manganese compounds in air between 600-800°C. A cubic C- type sesquioxide structure has been assigned to α-Mn_2O_3[11] but it has recently been shown that deviation from body-centred cubic symmetry occurs and is more accurately described as primitive orthorhombic[12].

A second modification (γ-Mn_2O_3) has been referred to in the literature on numerous occasions. It was first reported by Dubois[13] who claimed to have obtained this sesquioxide by vacuum dehydration of γ-MnOOH at 250°C, the latter having been obtained by addition of aqueous ammonia to manganous sulphate solution in the presence of hydrogen peroxide. Verwey and de Boer[14] repeated this experiment and found the γ-Mn_2O_3 to have an X-ray diffraction pattern very similar to that of α-Mn_3O_4 although no numerical data were reported. The formation of γ-Mn_2O_3 was re-investigated by Moore, Ellis and Selwood[15] who prepared this compound by two different routes a) Vacuum dehydration of manganese oxyhydroxide b) Thermal decomposition of γ-MnO_2 at 500°C in vacuum. The materials had identical X-ray diffraction patterns which were very similar to α-Mn_3O_4 except for the appearance of an extra line at d=1.83Å. It should be noted, however, that chemical analysis of the two samples obtained by Moore, Ellis and Selwood differed from each other (for sample a, x in MnO_x = 1.47 and for sample b, x in MnO_x = 1.56) and that

whereas the sample obtained by Dubois readily oxidised at moderate temperatures, those of Moore, Ellis and Selwood showed no such tendency. Recent work by Schmier and Sterr[16] indicated that the ideal formula for γ-Mn_2O_3 cannot be attained and that this phase only exists in the range $MnO_{1.33}$ to $MnO_{1.40}$. Doubts must therefore exist as to whether γ-Mn_2O_3 is a true modification of Mn_2O_3.

A third modification of Mn_2O_3 has been reported by Lima-de-Faria and Lopes-Vieira[17]. These authors studied the transformation of α-MnOOH (groutite) into β-MnO_2 (pyrolusite) at 300°C in air. During this transformation weak spots were observed on X-ray oscillation photographs which could not be ascribed to β-MnO_2. It was concluded that these spots were due to an Mn_2O_3 isostructural with α-Fe_2O_3 (haematite). This has not to date been confirmed by other authors.

1.1.(v) Trimanganese tetroxide Mn_3O_4

All oxides and oxyhydroxides of manganese when heated in air at about 1000°C form Mn_3O_4. At room temperature Mn_3O_4 has a distorted spinel structure[2] and is designated α-Mn_3O_4. It occurs in nature as the mineral hausmannite. Above 1170°C the distorted spinel structure is reported to become cubic[18] and is designated β-Mn_3O_4.

1.1.(vi) Manganese oxide MnO

MnO can be prepared by the thermal decomposition of $MnCO_3$ or MnC_2O_4 in vacuum. With increasing decomposition temperature the particle size increases which is accompanied by a

corresponding decrease in activity. MnO crystallises with a cubic structure similar to NaCl[2] and occurs in nature as the mineral manganosite.

1.1.(vii) Manganese oxyhydroxide MnOOH

There is confusion in the literature concerning the nature of the various oxyhydroxides of Mn(III). Two oxyhydroxides, α-MnOOH (groutite) and γ-MnOOH (manganite) have been well characterised and will be discussed in detail. A third phase β-MnOOH has been reported in the literature but insufficient evidence is available to confirm its existence.

α-MnOOH occurs in nature as the mineral groutite. A reliable synthetic route was first reported by Gabano, Morignat, Fialdes, Emery and Laurent[19] who obtained α-MnOOH by chemical reduction of γ-MnO_2 in a xylene medium using cinnamyl alcohol. This was later modified by Giovanoli and Leuenberger[10] who showed that the crystallite size of α-MnOOH depended on the particle size of γ-MnO_2. The crystal structure of α-MnOOH was first studied by Gruner[20] who showed that the X-ray data could be indexed on the basis of an orthorhombic unit cell and noted that it was isostructural with α-FeOOH (goethite) and α-AlOOH (diaspore). A complete structure determination was carried out by Collin and Lipscomb[21] which was later refined by Dent-Glasser and Ingram[22]. This showed that the oxygen atoms formed distorted octahedra around the manganese atoms. Four of the bonds which formed a rough square about the manganese atom were considerably shorter

than the other two and this was attributed to the Jahn-Teller effect.

A number of authors have looked at the effect of thermal treatment on α-MnOOH and these studies can be conveniently divided into two types a) Isothermal studies b) Thermogravimetric analysis (TG). The isothermal studies have to a large extent been confined to natural samples in oxygen or air environments. The investigations by Lima-de-Faria and Lopes-Vieira[17] and by Dent-Glasser and Smith[4] show that α-MnOOH transforms topotactically to β-MnO_2 rather than ramsdellite with which α-MnOOH is isostructural. This appears to contradict the results of Klingsberg and Roy[23] who did obtain ramsdellite but probably results from the different experimental conditions. Giovanoli and Leuenberger[10] found that synthetic samples of α-MnOOH followed a different decomposition path. In an oxygen stream finely divided α-MnOOH decomposed to Mn_5O_8 which further oxidised to γ-MnO_2. More crystalline α-MnOOH was observed to decompose directly to γ-MnO_2 when the temperature was below 300°C. It therefore appears that at atmospheric pressure in air or oxygen natural α-MnOOH samples decompose directly to β-MnO_2 whereas the product from a synthetic sample is more complex and depends upon such parameters as temperature, period of heating and particle size. TG studies on α-MnOOH have been restricted to the work of Praliaud, Rousseau and Mathieu[24]. A synthetic sample was reported to decompose in air via γ-MnO_2 as shown below.

$$\alpha\text{-MnOOH} \xrightarrow{200\text{-}250^{\circ}C} \gamma\text{-}MnO_2 \xrightarrow{420\text{-}450^{\circ}C} \alpha\text{-}Mn_2O_3 \xrightarrow{880^{\circ}C} \alpha\text{-}Mn_3O_4 \qquad (1.1.)$$

In vacuum dehydroxylation led directly to the formation of α-Mn_2O_3.

$$\alpha\text{-MnOOH} \xrightarrow{230^{\circ}\text{-}250^{\circ}\text{C}} \alpha\text{-}Mn_2O_3 \xrightarrow{420^{\circ}\text{C}} \alpha\text{-}Mn_3O_4 \qquad (1.2)$$

γ-MnOOH occurs naturally as the mineral manganite. Its preparation usually involves the oxidation of manganese(II) salt solutions. The products that can result from the oxidation of divalent manganese in basic solution are diverse and strict control of the concentration of the base, nature of the oxidising agent and temperature of the reaction must be maintained[15]. A reliable synthesis by such a route has been given by Giovanoli and Leuenberger[10]. γ-MnOOH crystallises in the monoclinic system[25] but unlike α-MnOOH is not isostructural with any of the oxyhydroxides of aluminium or iron. Its structure is very similar to β-MnO_2, the manganese - oxygen octahedra forming strings along the C- axis by sharing edges.

The thermal behaviour of γ-MnOOH has been investigated by a number of workers. As for α-MnOOH the bulk of the studies have been carried out on natural samples in oxygen or air environments. The majority of the results from DTA studies suggest that β-MnO_2 is the first decomposition product[29,30] and isothermal experiments tend to substantiate these ideas[26,27] but there are other views[28]. Isothermal and DTA experiments give no insight into the reaction path involved in the conversion of γ-MnOOH to β-MnO_2. The decomposition of synthetic γ-MnOOH using TG was first

looked at by Dubois[13]. In air γ-MnOOH transformed to β-MnO_2 at about 200°C which subsequently decomposed to α-Mn_2O_3 around 600°C. The decomposition step leading to the formation of β-MnO_2 did not appear to be as straightforward as would be expected from the reaction

$$4MnOOH + O_2 \rightarrow 4MnO_2 + 2H_2O \qquad (1.3)$$

A weight loss in excess of that predicted by equation (1.3) was followed by a weight increase to give overall the desired weight loss. Sato and co-workers[31] have recently investigated the decomposition of synthetic γ-MnOOH using TG and DTA. In air β-MnO_2 was formed at 220°C via a similar weight loss-weight gain phenomenon as noted by Dubois. It was concluded that the thermal transformation in air took place via the successive reactions formulated below

$$2\ MnOOH \rightarrow Mn_2O_3 + H_2O \qquad (1.4)$$

$$2\ Mn_2O_3 + O_2 \rightarrow 4\ MnO_2 \qquad (1.5)$$

However, no evidence was presented to confirm the formation of Mn_2O_3 as an intermediate and no suggestions were made as to the nature of the Mn_2O_3 produced.

The decomposition of γ-MnOOH in an inert environment has received scant attention compared to that in oxygen. Dubois[13] obtained a modification of Mn_2O_3 by dehydroxylation of γ-MnOOH at 250°C which was later designated as γ-Mn_2O_3. The subsequent decomposition of this compound was not reported. The decomposition of γ-MnOOH in nitrogen has

been investigated by Sato and co-workers[31]. The results obtained were difficult to interpret as a compound of composition $MnO_{1.63}$ was obtained at 250°C which changed to α-Mn_2O_3 at 640°C. In view of the uncertainty that exists regarding the decomposition products of γ-MnOOH, together with the debatable existence of γ-Mn_2O_3, a re-investigation of the thermal behaviour of γ-MnOOH was considered desirable.

The existence of β-MnOOH was first proposed by Feitknecht and Marti[32] and later substantiated by Feitknecht, Bruner and Oswald[33] who claimed that manganese(II) hydroxide could be topotactically oxidised to β-MnOOH. Schmier and Sterr[16] suggested that this phase had the composition $2MnO_2.Mn(OH)_2$ but in a recent publication Meldau, Newesely and Strunz[34] claim to have determined the lattice parameters of β-MnOOH and shown it to be isostructural with $Mn(OH)_2$.

1.2 γ-Manganese Dioxide

1.2.(i) Structure

γ-MnO_2 was first described by Glemser[35] in 1939 but its structure has been the subject of much controversy. Kedesdy, Katz and Levin[36] observed that X-ray diffraction patterns of synthetic γ-MnO_2 were similar to those of ramsdellite[37] except for small deviations in line intensity, position and broadening. Calculated values of lattice parameters and cell volume showed reasonable agreement with those of ramsdellite although definite deviations were evident and were attributed to shifts in the atomic parameters. These results could be explained by assuming that the double

strings of oxygen octahedra had been rotated around the c direction by 27° with respect to their position in the ramsdellite structure. That this hypothesis could account for the anomalous diffraction phenomena shown by γ-MnO_2 was however dismissed by de Wolff[5] who examined the X-ray patterns of several γ-MnO_2 samples and noticed that they contained many comparatively sharp lines in identical positions. Nevertheless, certain broad lines showed considerable differences in position. A random layer model based on the introduction of a 'pyrolusite layer' in the ramsdellite matrix was postulated (see Fig.1.1). This model predicted that lines with k in hkl even would match strong ramsdellite lines. For lines with k odd such as 110, 131 etc., the line would shift to higher diffraction angles by an amount dependent on the pyrolusite concentration. A simultaneous peak broadening would also be observed. Recent work by Giovanoli, Maurer and Feitknecht[38] endorsed the ideas put forward by de Wolff. Using a combination of X-ray diffraction, electron microscopy and selected area electron diffraction they proposed that the pyrolusite concentration in the ramsdellite matrix was in the form of microdomains which were randomly distributed and did not exceed more than one unit cell dimension in the b direction.

The findings of de Wolff and Giovanoli, Maurer and Feitknecht provide us with a way of interpreting the X-ray diffraction patterns of γ-MnO_2. Lines that are common to all γ-MnO_2

samples such as the 021, 121, 221 and 002 planes (with respect to the diaspore unit cell) are indicators of crystallite size[1]. These lines are due to the close packing of the oxygen ions and are not dependent on the position of the manganese ions. Therefore they are independent of pyrolusite concentration and will broaden only with decrease in crystallite size. Other lines with k odd may or may not be present in the diffraction pattern depending on the degree of structural intergrowth. The 110 plane in particular is very sensitive to the degree of structural disorder[1].

1.2.(ii) Nature of sorbed water

Manganese dioxide has been used as the cathode of the Leclanché cell since its development in 1868. Despite the long history controversy still exists as to the detailed mechanism of the electrode reactions. However, it has been shown from the manner in which the cell voltage varies with discharge time that the manganese dioxide reduction is a one phase reaction[39]. In essence the γ-MnO_2 on discharge is thought to accept protons and electrons which can move about in the lattice as the discharge proceeds. The reduction of MnO_2 may be expressed as

$$MnO_2 + H^+ + e \longrightarrow MnOOH \qquad (1.6)$$

It has been suggested that water associated with the γ-MnO_2 structure plays an important role during the discharge of γ-MnO_2 as this facilitates proton migration[40] by allowing the protons to diffuse more readily through the 'built-in' water.

Sasaki and Kozawa[41] observed that the capacity of a cell containing γ-MnO_2 showed a marked dependence on the pre-treatment temperature of the MnO_2. They noticed that up to 250°C the cell capacity was inversely proportional to the outgassing temperature. This could not be caused by any structural changes as γ-MnO_2 is stable in air below 250°C. A relationship was established between the decrease in capacity and the amount of water released from γ-MnO_2 during thermal treatment.

Many studies have been performed on the nature of the water associated with γ-MnO_2 and it is generally agreed that there is a qualitative relationship between the water and the electrochemical characteristics. Sasaki and Kozawa[42] considered that the water released by heating below 110°C was physisorbed whilst that lost between 110°C and 300°C was termed 'combined' water and could not be restored upon cooling to room temperature. Tvarusko[43] found that the water content of a sample depends on its type, origin and conditions of preparation. Water lost at 110°C increased in the series natural ore < electrodeposited < chemical < synthetic hydrous manganese dioxide. The findings of Sasaki and Kozawa were also substantiated by Tvarusko but the irreversibly lost water was termed constitutional water. The classification of water in γ-MnO_2 is controversial; combined water, water of addition, water of constitution, bound water, physisorbed water and water of hydration are terms frequently employed in the

literature to describe the water associated with MnO_2. The irreversibly lost water may be present as H_2O, OH^- or H_3O^+ inside the lattice whilst the presence of surface hydroxyl groups is also likely. Covington, Cressey, Lever and Thirsk[44] suggested that the combined water on γ-MnO_2 was present as surface hydroxyl groups but Muller, Tye and Wood[45] from ion exchange measurements considered that there was a better correlation of potassium ion exchange with the physisorbed water content than with the combined water, which suggests that the latter is not entirely surface water. The presence of OH groups in the lattice of γ-MnO_2 has been established by I.R. spectroscopy[46] and it has been suggested[47] that these are associated with Mn(III) ions. A number of chemical formulae have been assigned to γ-MnO_2 to take into account the presence of both internal molecular water and hydroxyl groups but the feasibility of this has been questioned[48]. Brenet et al[49] have claimed that molecular water and OH groups inside the lattice may be distinguished by DTA, the loss of molecular water being observed as an endotherm in the range 100-180°C and the dehydroxylation as an exothermal process between 200 and 350°C. Although it is doubtful whether such resolution can be ascribed to lattice molecular water and hydroxyl groups the results of Gabano et al[19] provide convincing evidence for the presence of both; however, it is not clear from their work whether the loss of molecular water originates from the surface or the lattice. Also no separation between the various types of water was observed by TG. A relationship

between surface hydroxyl groups and electrochemical activity has been hinted at in the literature[50] and a quantitative determination of surface hydroxyl groups on manganese dioxides is claimed[51].

1.2.(iii) Chemical reduction

As mentioned above the reduction of MnO_2 is believed to be the first step in the discharge process taking place at the cathode of the Leclanché cell. As a consequence of this the reduction mechanism has attracted much interest. Feitknecht, Oswald and Feitknecht-Steinmann[52] showed that the chemical reduction of γ-MnO_2 proceeded in the same manner as the electrochemical reaction. The unit cell volume increased approximately linearly with decrease in Mn(IV) content and was considered to be a one phase reaction. Among the different reducing media used to effect the reduction have been hydrazine sulphate[52], hydrazine hydrate[53], cinnamyl alcohol[19] and potassium iodide in dimethylformamide[54]. Gabano et al[19] made a detailed study of the lattice parameters of the compounds produced by partial reduction of γ-MnO_2. They observed that the variation of the parameters as a function of sample composition could not be described by a single linear relationship but consisted of two linear components that intersected at a composition corresponding to fifty per cent reduction. It was considered that the reduction took place in two stages as two of the Mn(IV) ions in the unit cell of γ-MnO_2 were thought to be more easily

reduced than the remaining two. However Giovanoli, Bernhard and Feitknecht[55] proposed that all the cations in the diaspore structure are identical relative to the OH^- and O^{2-} ions. The oxidation of α-MnOOH to γ-MnO_2 was considered not to be single phase and the discontinuity was attributed to the presence of two crystal species. At an intermediate stage in the reaction the 021, 121 and 221 lines in the X-ray diffraction pattern could be seen both for the starting material and the end product[10].

The thermal behaviour of the products obtained by partial chemical reduction of γ-MnO_2 has been looked at in various environments. Gabano et al[19] studied the decomposition of the compounds by TG in nitrogen. The weight loss up to 400°C increased with the degree of reduction and was attributed to the loss of water of addition and constitution. A linear relationship between the water loss and sample composition enabled the proportions of water of addition and constitution to be determined. Laragne and Brenet[54] using TG and a nitrogen atmosphere confirmed Gabano's relationship but no attempt was made to determine how this water loss arose. The decomposition in air and vacuum has been investigated by Brouillet, Grund, Jolas and Mellet[47] using TG. They reported that the loss of water in vacuum at 250°C was due to the decomposition of MnOOH.

$$2MnOOH \rightarrow Mn_2O_3 + H_2O \qquad (1.7)$$

In oxygen the curves were found to be virtually the same for all samples and it was considered that this was due to the reaction

$$4MnOOH + O_2 \rightarrow 4MnO_2 + 2H_2O \qquad (1.8)$$

The loss of water is almost balanced by the uptake of oxygen, and therefore the TG curves become virtually independent of MnOOH content. Coeffier and Brenet[53] using TG in air observed a slight weight increase between 240° and 260° which was not mentioned by the previous authors. This was attributed to either chemisorption of oxygen or more probably to a slight reoxidation.

Although good evidence has been presented to suggest that water associated with the γ-MnO_2 structure plays an important role in the discharge mechanism of a dry cell its classification has been somewhat arbitrary. A detailed study of the nature of this water was thought desirable and in the present research it has been investigated using a thermal technique. The thermal behaviour of the products obtained by chemical reduction of γ-MnO_2 does not appear to have been studied in sufficient detail and attempts have therefore been made to clarify the results reported in the literature.

1.3 Temperature Programmed Desorption

1.3.(i) Introduction

The technique of temperature programmed desorption (TPD) has been widely used to obtain information on adsorbed species and can provide information on several adsorption parameters such as the mobility of the adsorbed state and its apparent activation energy of desorption. In view of the readiness in obtaining such data the TPD technique has

been applied in this work to the study of water desorption from the γ-MnO_2 surface.

1.3.(ii) Theory

The removal of a gas from a solid surface by means of programmed heating is termed thermal desorption. The flash filament technique, a specific type of thermal desorption has been widely used to investigate the kinetics of desorption of gases from metal surfaces in ultra high vacuum[56]. This technique involves the recording of the total pressure inside a closed system as the adsorbed species is desorbed by heating of the sample. The resulting pressure-time curve is referred to as a 'desorption-spectrum' which on analysis can provide useful information about the activation energy of desorption. This method was modified by Amenomiya and Cvetanovic[67] to enable the desorption of gases from catalyst surfaces to be studied. The adsorbed species is desorbed into a stream of inert carrier gas and its concentration determined by a sensitive gas chromatographic detector. This method is generally known as temperature programmed desorption (TPD) and is not restricted in use to ultra high vacuum and metal surfaces.

While the measurement of pressure and thermal conductivity are convenient ways of counting the number of molecules desorbed from the surface any experimental technique that can be used to determine the number of molecules remaining on or escaping from the surface can, in principle, be used. Thus Czanderna[58] was able to develop equations to analyse

thermal desorption spectra obtained with a microbalance.

The equation describing the desorption of a gas from a surface is assumed to be of the form

$$-\frac{dn_i}{dt} = n_i^{x} \nu \exp\left(\frac{-E_D}{RT}\right) \qquad (1.9)$$

where $-\frac{dn_i}{dt}$ = rate of desorption

n_i = number of adsorbed molecules at time t

ν = frequency factor

E_D = Activation energy of desorption

T = temperature (^{o}K)

x = order of reaction

This may be more conveniently expressed[58] when using a microbalance technique to measure the number of desorbing molecules by

$$\frac{-dw_i}{dt} = w_i^{x} \nu \exp\left(\frac{-E_D}{RT}\right) \qquad (1.10)$$

where w_i = weight of adsorbed species at time t

Using a linear heating programme it can be shown[56] that for a first order process

$$\frac{\beta E_D}{RT_p^{2}} = \nu \exp\left(\frac{-E_D}{RT_p}\right) \qquad (1.11)$$

where

β = heating rate

Tp = temperature at the maximum rate of desorption

Equation (1.11) can be written in the form[57]

$$2 \log Tp - \log \beta = \frac{2.303E_D}{R} \frac{1}{T_p} + \log \frac{2.303E_D}{\nu R} \qquad (1.12)$$

The activation energy of desorption E_D can be obtained from the slope of a plot of 2 log Tp - log β versus T_p^{-1} and the frequency factor ν from the intercept. The latter may provide information about the mobility of the adsorbate as this contains an entropy term[60]. The absolute rate theory predicts that the frequency factor is a product of three terms[61] i.e.

$$\nu = \bar{r} \frac{kT}{h} \frac{\bar{F}^{\ddagger}}{F_{init}} \qquad (1.13)$$

where $\bar{r}$ = average transmission coefficient

$F^{\ddagger}$ = partition function of the activated complex

F_{init} = partition function of the reactant

and the activation entropy $\Delta S^{\ddagger}$ is defined as

$$\Delta S^{\ddagger} = R \ln \frac{\bar{F}^{\ddagger}}{F_{init}} \qquad (1.14)$$

Very often the product $\bar{r} \frac{\bar{F}^{\ddagger}}{F_{init}}$ is taken to be unity and then ν has the value 10^{13} sec^{-1}. However calculations of ν have in many instances produced much larger values and this has often been interpreted as being due to changes in $\frac{\bar{F}^{\ddagger}}{F_{init}}$ and attributed to supermobile adsorption. It is unlikely that the transmission coefficient $\bar{r}$ will be equal to one which is nearly always assumed. Petermann[62] has recently shown that large values of frequency factor may well result from the temperature dependence of $\bar{r}$. Therefore too much emphasis should not be placed on data obtained from equation (1.12) concerning the mobility of the adsorbate

although changes in frequency factor with parameters such as coverage or temperature may well be informative. Equation (1.11) predicts that Tp is independent of coverage for a first order reaction with constant E_D and thus E_D can be found directly from measurements of Tp as a function of heating rate β. If Tp decreases with increasing coverage this is either indicative of a second order process or a first order reaction with E_D dependent on coverage[56].

1.3.(iii) TPD of water from oxides

This technique has been used by many workers in order to evaluate desorption energies of surface and bulk water. Some of the relevant work that has appeared in the literature is reviewed below so as to demonstrate the wide range of materials that have been studied and the activation energies expected for a particular water species. Except where specifically stated TPD refers to the chromatographic technique as developed by Amenomiya and Cvetanovic.

Yakerson and Rubinshtein[63] studied the desorption of water from alumina by TPD. They observed one broad desorption peak whose peak temperature was a function of coverage. As the fractional coverage increased from 0.06 to 0.27 E_D dropped from 46 to 26 kcal $mole^{-1}$. The wide range of E_D values was interpreted as being due to surface heterogeneity and the presence of both molecular and dissociated water.

The interaction of water vapour with the rutile surface has been investigated by Munuera and Stone[64]. Two TPD peaks were observed. The peak at 370°C was independent of coverage and ascribed to the dissociative adsorption of water on titanium and oxygen sites. An activation energy of desorption of 25.5 kcal $mole^{-1}$ was calculated. A second peak, the Tp of which was a function of coverage and was observed at 250°C in the most hydrated sample, was assigned to a molecular water species.

Stakebake[65] investigated the interaction between water vapour and plutonium dioxide using a mass spectrometric thermal desorption technique. Chemisorbed water was found to be desorbed in two temperature ranges. The desorbed entity found between 100° and 150°C had an activation energy of desorption of 20 kcal $mole^{-1}$ and was attributed to double hydrogen bonding of water molecules to underlying surface hydroxyl groups. The second peak at 300-350°C had an E_D of 68 kcal $mole^{-1}$ and was thought to be due to a surface dehydroxylation. Frequency factors of $4x10^{9}sec^{-1}$ and $4x10^{12}sec^{-1}$ respectively were reported.

Krylova, Filonenko and Sitonite[66] investigated the desorption of water from silica and alumina by TPD and recorded the pressure of the desorbed gas as a function of sample temperature. Two desorption peaks were observed for each oxide. Alumina produced peaks at 70°-90° and 280-300°C from which activation energies of desorption

of 6.5 and 25 kcal $mole^{-1}$ were calculated by means of equation (1.11). Silica gave desorption maxima at 140°C and 250°C from which E_D values of 6.5 and 19 kcal $mole^{-1}$ respectively were obtained.

Sedlak and Beebe[67] studied the removal of water from amorphous calcium phosphate. From the amount of water lost it was considered that 25% of that amount could be held in an adsorbed monolayer, the remainder being bound inside the amorphous particles as hydrate water. The 'desorption spectrum' exhibited one peak whose Tp varied from 65°C (β= 3°C min^{-1}) to 100°C (β= 32°C min^{-1}). Application of equation (1.12) to the data revealed two linear segments with activation energies of 10.5 and 20.0 kcal $mole^{-1}$. The former is assigned to the loosely bound surface water whilst the latter is thought to be consistent with an internal hydrate species. The validity of equation (1.12) for obtaining approximate activation energies for bulk dehydration studies in solids has been established by the above authors[67].

For the investigation of the γ-MnO_2 surface the conventional gas chromatographic detector has been replaced by a microbalance and the technique, to avoid confusion, is termed gravimetric TPD in the ensuing pages.

1.4 Textural Studies

1.4.(i) Introduction

Changes in the texture of a solid as a result of heat treatment may be conveniently followed by gas adsorption

studies. Information may be obtained on the surface area and porosity of a sample by selection of an appropriate adsorbate. Nitrogen adsorption at 78 K is a popular technique for evaluating the former when this exceeds a few m^2g^{-1} whilst the presence of micropores may be detected by a technique involving adsorption of a hydrocarbon at liquid nitrogen temperature.

1.4.(ii) Physical adsorption of gases on solids

When a molecule comes into contact with a surface it will remain there for a certain period of time before evaporating. When a number of molecules continually strike the surface it may happen that the concentration of gas at the surface is greater than that of the bulk. This phenomenon is called adsorption and the relationship between the amount of gas adsorbed and the relative vapour pressure of the gas at constant temperature is called an adsorption isotherm.

Brunauer, Deming, Deming and Teller[68] divided the physical adsorption isotherms into five types. Type I isotherms are associated with solids where adsorption is limited to a monolayer, the remainder involving multilayer adsorption. Of the theories proposed to interpret the adsorption isotherm that of Brunauer, Emmett and Teller[69] is the best known. These authors using a kinetic approach derived an equation (now known as the BET equation) from which the specific surface of the material could be calculated. The BET equation is usually written in the form

$$V = \frac{V_m c p}{(p^o - p)\{1 + (c-1)\frac{p}{p^o}\}} \qquad (1.15)$$

where V = volume of gas adsorbed at pressure p

V_m = volume of adsorbate in a completely filled monolayer

p^o = saturation vapour pressure of the adsorbate

The value of c is given approximately by

$$c = e^{(E_1 - E_L)/RT} \qquad (1.16)$$

where E_1 = average heat of adsorption in the first layer

E_L = heat of liquefaction

The term $E_1 - E_L$ is known as the net heat of adsorption. The BET equation may be transformed into

$$\frac{p}{V(p^o - p)} = \frac{1}{V_m c} + \frac{c-1}{V_m c}\frac{p}{p^o} \qquad (1.17)$$

and a plot of $\frac{p}{V(p^o-p)}$ versus $\frac{p}{p^o}$ should yield a straight line from which a value for V_m can be obtained from the slope and intercept. The surface area can be calculated from the relationship

$$S = \frac{V_m}{M.W} \cdot N. A. \times 10^{-20} \qquad (1.18)$$

where S = surface area ($m^2 g^{-1}$)

$M.W$ = molecular weight of adsorbate

N = Avogadro's Number

A = Cross sectional area of the adsorbate

The range of relative pressures in which the BET equation is

usually employed is from $\frac{p}{p^o} \sim 0.05$ to $\frac{p}{p^o} \sim 0.30$.

It was initially proposed that the BET equation was applicable to all types of isotherms although it now appears that the values of surface area obtained for microporous materials ($d<20\text{Å}$)[70] can only be approximate[71]. If monolayer adsorption and micropore filling are occurring simultaneously then the BET monolayer capacity is not strictly valid. De Boer and Sing have developed methods whereby these processes may be separated.

The t-plot of Lippens and de Boer[72] consists in plotting the volume of nitrogen adsorbed on the solid against the statistical thickness t of adsorbed nitrogen on a non-porous reference solid. For a non-porous material under investigation a straight line will be obtained which on extrapolation to t=o will pass through the origin. The slope of the line provides a value of the surface area which can be calculated from the relationship,

$$S_t = \frac{15.47\ V_a}{t} \qquad (1.19)$$

Departure from linearity was interpreted in terms of either micropore filling or capillary condensation. Although providing a simple and ingenious way of detecting porosity there are limitations associated with the method[73]. The standard isotherm is not, as was first thought, applicable to all materials, the adsorption isotherm depending to a certain extent on the chemical nature of the surface and

the porosity. The t-plot method is not completely independent of the BET method and cannot readily be extended to isotherms with low 'c' values. An attempt at overcoming these difficulties was made by Sing[74] who modified the t-plot of Lippens and de Boer by replacing t with α_s where $\alpha_s = V/V_{0.4}$ and $V_{0.4}$ is the amount of gas adsorbed at $p/p^o = 0.4$. α_s was chosen to equal 1 at $p/p^o = 0.4$ as both monolayer coverage and micropore filling occur at $p/p^o < 0.4$ whereas capillary condensation takes place at $p/p^o > 0.4$. The α_s plot takes the form of adsorption on the sample under study plotted against α_s for the appropriate standard. Values of surface area are calculated from the slope of the α_s plot by using a proportionality factor which is obtained from the standard isotherm on the non-porous material of known BET surface area. The presence of capillary condensation causes an upward departure from the standard isotherm. Micropore filling is revealed by a positive intercept on the volume axis when the α_s plot is extrapolated to $\alpha_s = 0$. Thus the α_s plot is capable of quantitatively assessing the micropore volume and providing internal and external surface areas of a material.

To obtain meaningful micropore volumes and surface area data from α_s and t-plots careful consideration has to be given to the selection of an appropriate standard. The reference material must be non-porous and ideally possess a similar chemical structure to the sample under investigation[75].

It has also been pointed out[76] that the standard data employed should have a 'c' constant of comparable magnitude to that of the unknown. The 'c' constant affects the shape of the isotherm at low relative pressures and large differences between the 'c' values of the reference solid and the unknown may lead to erroneous estimates of microporosity. Nicolaon and Teichner[77] however, have recently proposed that meaningful microporosity data could be obtained for solids even if differences in 'c' values were evident provided only α_s values above 0.75 ($p/p^o > 0.2$) are taken into account.

1.4.(iii) Nitrogen adsorption on γ-MnO_2 and its reduction products

The majority of nitrogen adsorption studies on γ-MnO_2 reported in the literature have been confined to surface area and porosity measurements on the 'as-received' sample. For an electrodeposited γ-MnO_2 Dakri, Tye and Whiteman[78] obtained a type IV adsorption isotherm with hysteresis. A BET surface area of 61 m^2g^{-1} was reported and a pore size analysis showed a maximum near 20Å radius. The work of Le Tran[79] was in close agreement with these results. There is only one report in the literature on the application of nitrogen adsorption studies to determine the texture of γ-MnO_2 as a function of outgassing temperature. Praliaud, Rousseau and Mathieu[24] working with an electrodeposited γ-MnO_2 obtained a type II isotherm with no hysteresis for a sample outgassed at ambient temperature. On heating in

vacuum hysteresis appeared and the surface area increased slightly from 45 m^2g^{-1} at 25°C to 52 m^2g^{-1} at 183°C. At 250°C the surface area had increased to 72 m^2g^{-1} but further heating resulted in a gradual decrease in area. These authors also carried out a similar study on α-MnOOH. Up to 220°C the BET area increased from 42 m^2g^{-1} to about 80 m^2g^{-1} and was accompanied by a corresponding increase in pore volume. Additional thermal treatment resulted in a gradual reduction of the surface area. There appears to be no published data on gas adsorption studies on the intermediate reduction products of γ-MnO_2.

In order to understand more fully the processes taking place during the thermal desorption of water from γ-MnO_2 and its reduction products nitrogen adsorption experiments have been carried out in situ. The α_s method has been used to differentiate between internal and external water removal.

1.4.(iv) Nonane adsorption

Gregg and Langford[80] have described a method by which the micropore contribution of a carbon black may be evaluated. They were able to demonstrate that nonane adsorbs in the micropores at liquid nitrogen temperature and is retained by the sample on warming to room temperature. The difference between the nitrogen adsorption isotherms determined before and after adsorption of nonane provides a measure of the micropore volume. Parfitt, Urwin and Wiseman[81] reported that this was also true of microporous oxide surfaces.

Although no details were given in the paper the compounds being characterised at that time were Al_2O_3, SiO_2 and TiO_2.

There is no mention in the literature of any nonane adsorption measurements having been conducted on oxides or oxyhydroxides of manganese. Nonane adsorption experiments have therefore been carried out on certain products obtained by chemical reduction of γ-MnO_2 and the extent of microporosity assessed by the α_s method.

1.5 Magnetic Behaviour

1.5.(i) Theory

Chemical substances may be classified on the basis of their behaviour when placed in a non-uniform magnetic field. Substances which tend to move from a weaker to a stronger part of the field are termed paramagnetic, this behaviour generally being exhibited by an atom possessing unpaired electrons. As most transition metal compounds possess unpaired electrons much useful information concerning the valency state and bonding in such compounds can be obtained from magnetic data[82]. In magnetic experiments the experimentally determined quantity is the magnetic susceptibility (χ_M) with a temperature dependence nominally given by the relation

$$\chi_M = \frac{N^2\mu^2}{3RT} \qquad (1.20)$$

where μ = magnetic moment

N = Avogadro's Number

This gives χ_M for a mole of the compound being studied and

in order to obtain χ_M for the atom of interest a diamagnetic correction must be made for all the atoms present in the molecule.

i.e. $\chi_M^{corr.} = \chi_M$ + diamagnetic corrections (1.21)

Equation (1.20) can then be rearranged so that the effective magnetic moment μ_{eff} is given by

$$\mu_{eff} = 2.84(\chi_M^{corr.} \times T)^{\frac{1}{2}} \quad (1.22)$$

At the end of the nineteenth century Curie found that for a number of paramagnetic materials

$$\chi_M^{corr.} = \frac{C}{T} \quad (1.23)$$

where C = Curie constant

If this relationship is true μ_{eff} is a constant. Later work showed that a more exact relationship is given by

$$\chi_M^{corr.} = \frac{C}{T+\theta} \quad (1.24)$$

where θ = Curie temperature

This is known as the Curie-Weiss Law and may be rearranged to give

$$\frac{1}{\chi_M^{corr.}} = \frac{1}{C}.T + \frac{\theta}{C} \quad (1.25)$$

Thus obedience of the Curie-Weiss Law should give a slope of $\frac{1}{C}$ and an intercept on the temperature axis of θ. When θ is known μ_{eff} is usually calculated from the expression

$$\mu_{eff} = 2.84\{\chi_M^{corr.}(T+\theta)\}^{\frac{1}{2}} \quad (1.26)$$

Re-arranging equation (1.24) gives $C = \chi_M(T+\theta)$ and therefore

$$\mu_{eff} = 2.84C^{\frac{1}{2}} \quad (1.27)$$

The magnetic moment which provides information on the valency state of the metal atom can therefore be obtained from the gradient of the Curie-Weiss plot. θ which is a measure of the interaction between neighbouring metal atoms[83] can be obtained from the intercept on the temperature axis.

It can also be shown that for many first row transition metals an approximate value for the magnetic moment can be obtained from the 'spin-only' formula

$$\mu_{so} = \{n(n+2)\}^{\frac{1}{2}} \qquad (1.28)$$

where n = number of unpaired electrons

1.5(ii) γ-MnO_2 and its reduction products

Transition metal oxides are often magnetically concentrated and give rise to large interactions between the paramagnetic ions. Most are antiferromagnetic and have magnetic moments lower than those predicted by the spin-only formula. β-MnO_2 whether obtained naturally or by synthesis has a typical susceptibility[84,85] (χ_{Mn}) of about $26\text{-}30\times10^{-6}$ which is less than that expected for a compound containing Mn(IV). However, Selwood, Eischens, Ellis and Wethington[84] found that a synthetic sample of γ-MnO_2 obeyed the Curie-Weiss Law down to liquid nitrogen temperature and had a magnetic moment of 3.7 B.M., close to the spin-only value of 3.87 B.M. for 3 unpaired electrons. Since this discovery magnetic measurements have been used extensively to study the electrochemical reduction of γ-MnO_2 in the Leclanché cell as this is the only paramagnetic constituent[86,87]. The spin-only magnetic

moments of manganese with oxidation states of (IV), (III) and (II) are very close to 3.9, 4.9 and 5.9 B.M. respectively. A linear relationship thus exists between μ and sample composition from Mn(IV) through to Mn(II) and therefore it is not possible to determine whether the reduction of Mn(IV) goes initially to Mn(III) or Mn(II).

There is only one paper in the literature concerned with the magnetic behavior of the products obtained from the chemical reduction of γ-MnO_2. Labat and Gabano[88] made a detailed study of this system and observed that down to about 75% reduction μ was a linear function of sample composition and very close to the theoretical spin-only values. Further reduction resulted in the formation of a ferromagnetic structure causing abnormally high values of μ and θ. One of the authors[19] had previously reported a discontinuity in the variation of the lattice parameters of the reduced samples as a function of composition. This occurred after about 50% reduction and was possibly indicative of a structural change. Such a reorganisation of the lattice might be expected to lead to changes in μ and θ but no evidence of this was observed.

In order to obtain additional information on the structure of the compounds obtained from the chemical reduction of γ-MnO_2 their magnetic behaviour has been reinvestigated. An attempt has been made to correlate anomalies in μ and θ with structural changes in the solid.

1.6 Present Work

The aims of the work presented in this thesis may be summarised as follows:

(a) to determine the nature of the water associated with γ-MnO_2;

(b) to elucidate the structural changes that take place on the removal of water by thermal treatment;

(c) to characterise the compounds produced by the chemical reduction of γ-MnO_2;

(d) to investigate the thermal behaviour of α-MnOOH, γ-MnOOH and Mn_5O_8.

CHAPTER 2

Experimental

2.1 Materials

2.1.(i) General introduction

Several oxides and oxyhydroxides of manganese have been studied in this work and their preparative routes are described below. Some samples are of commercial origin or have been supplied by other workers and details of these are given when known.

2.1.(ii) γ- Manganese dioxide

The majority of the work on γ-MnO_2 was carried out on a commercially electrodeposited material of Japanese origin. A sufficient quantity of the sample was taken at the start of the investigation to ensure that all subsequent experiments were carried out on the same batch. The γ-MnO_2 was produced by electrolysis of an acidified manganous sulphate solution using a carbon anode[89] and analysed as $MnO_{1.946}$. An X-ray diffractometer trace of the sample is shown in fig.2.1 and is typical of an electrodeposited γ-MnO_2[90]. The BET area obtained by nitrogen adsorption at liquid nitrogen temperature on the 'as-received' sample was 33.7 m^2g^{-1} which is also typical of an electrodeposited sample[90]. The term 'as-received' refers to the commercial sample that has not been subjected to an outgassing treatment above ambient temperature. Chemical analysis showed that the major impurities were C, 0.5%; SO_4^{2-}, 1.1% and NH_3, 0.1%.

Two other γ-manganese dioxides were studied, a synthetic sample and a naturally occurring variety. The former was obtained by the disproportionation of Mn_3O_4 in nitric acid

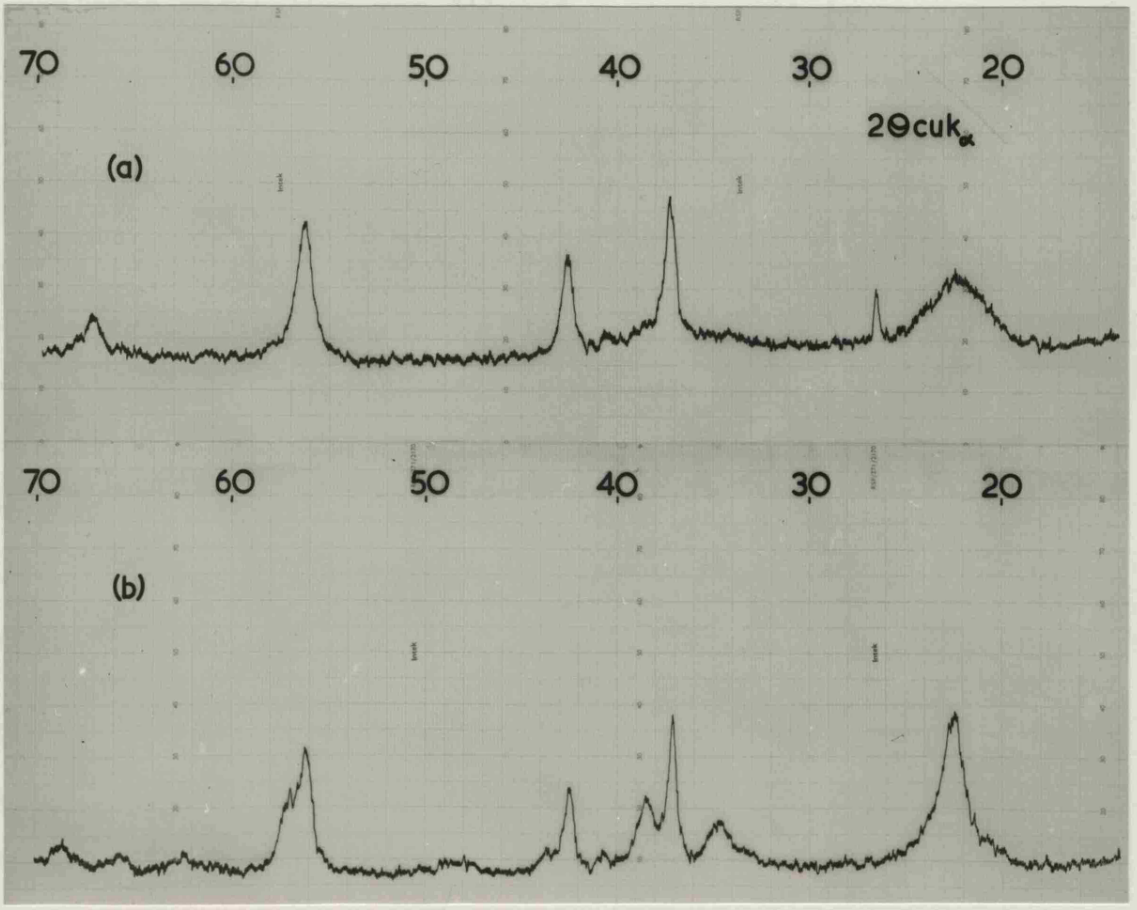

Fig. 2.1 X-ray diffractometer traces (Cu K_α) of (a) commercially electrodeposited γ-MnO_2 and (b) synthetic γ-MnO_2.

based on a method used by Giovanoli, Maurer and Feitknecht[38]. $MnCl_2$ solution (0.5M, 800 ml) and NaOH (1.0M, 800 ml) were heated separately to 60°C and then mixed together. The resulting suspension was diluted with distilled water (2400 ml) and oxidised by bubbling a stream of oxygen through the mixture for six hours whilst maintaining the temperature at 60°C. The Mn_3O_4 was removed by filtration, washed several times with distilled water and dried under vacuum at 25°C. The Mn_3O_4 structure was confirmed by X-ray diffraction. Mn_3O_4 (7.0 g) was then refluxed with nitric acid (1.0M, 614 ml) for 22 hours. The product was filtered, washed with distilled water and dried under vacuum. Chemical analysis showed a stoichiometry of $MnO_{1.96}$ and the structure of γ-MnO_2 was confirmed by X-ray diffraction (fig.2.1).

The naturally occurring sample came from Ghana and analysed as $MnO_{1.96}$. X-ray diffraction showed it to be a crystalline specimen with FeO and SiO_2 as the principal impurities.

2.1.(iii) β- Manganese dioxide

Isolated experiments were conducted on two different samples of β-MnO_2, one a synthetic variety, the other a naturally occurring ore. The former was obtained by the method of Ambrose[91] from the thermal decomposition of manganous nitrate.

Manganous nitrate hexahydrate (40 g) was heated in a round bottomed flask at 150-170°C over which a stream of oxygen was passed. After the resulting black mass had solidified

distilled water was added and the mixture boiled. This was then filtered and the solid air dried at 110°C. To remove lower oxides of manganese the solid (∿2g) was refluxed with 1:1 nitric acid (250 ml) for 4 hours, washed with distilled water and dried at 110°C. The material was finally heated at 400°C in a stream of oxygen. The structure was confirmed by X-ray diffraction and the solid analysed as $MnO_{1.99}$.

The natural sample was a Moroccan pyrolusite ore which analysed as $MnO_{1.99}$ and contained a small amount of iron as impurity. X-ray diffraction showed a well crystallised material with the pyrolusite structure.

2.1.(iv) Chemical reduction products of γ-MnO_2

In the presence of γ-MnO_2 hydrazine decomposes in the following way[53]

$$N_2H_4 \rightarrow N_2 + 4H^+ + 4e \qquad (2.1)$$

γ-MnO_2 present is reduced according to

$$\gamma\text{-}MnO_2 + H^+ + e \rightarrow MnOOH \qquad (2.2)$$

the overall reaction being

$$4MnO_2 + N_2H_4 \rightarrow 4MnOOH + N_2 \qquad (2.3)$$

Two sources of hydrazine, namely hydrazine sulphate and hydrazine hydrate were used to effect the reduction. The sulphate was used initially but was superseded by the hydrate owing to the greater solubility of the latter and the absence of any interfering sulphate ions. To ensure that this change

did not affect the structure of the product a sample of the same composition was prepared by both routes. The thermal behaviour and X-ray diffraction patterns of the materials were identical.

1. Preparation with hydrazine sulphate

Hydrazine sulphate (0.24 - 1.47 g) was added to a suspension of γ-MnO_2 (9.5 g) in distilled water (100 ml). N_2 was passed over the reaction vessel maintained at 24±0.2°C throughout the reduction period of two hours. The solid was then filtered off, washed with water and vacuum dried at ambient temperature. The dependence of product composition on reducing agent concentration is shown in figure 2.2.

2. Preparation with hydrazine hydrate

Hydrazine hydrate solution (60% W/W) was diluted 10X with distilled water. An aliquot of this standard solution (0 - 18.8 ml) was added to γ-MnO_2 (9.5 g) and the procedure continued as for hydrazine sulphate. Chemical analysis of the products showed that the reduction as given in equation (2.3) was quantitative for the hydrate whereas a simple calculation using data from fig.2.2 showed that this was not true with hydrazine sulphate.

2.1(v) γ- Manganese oxyhydroxide

The preparation of three samples was attempted based on a method described by Giovanoli and Leuenberger[10]. The most crystalline specimen (sample A) was prepared by the

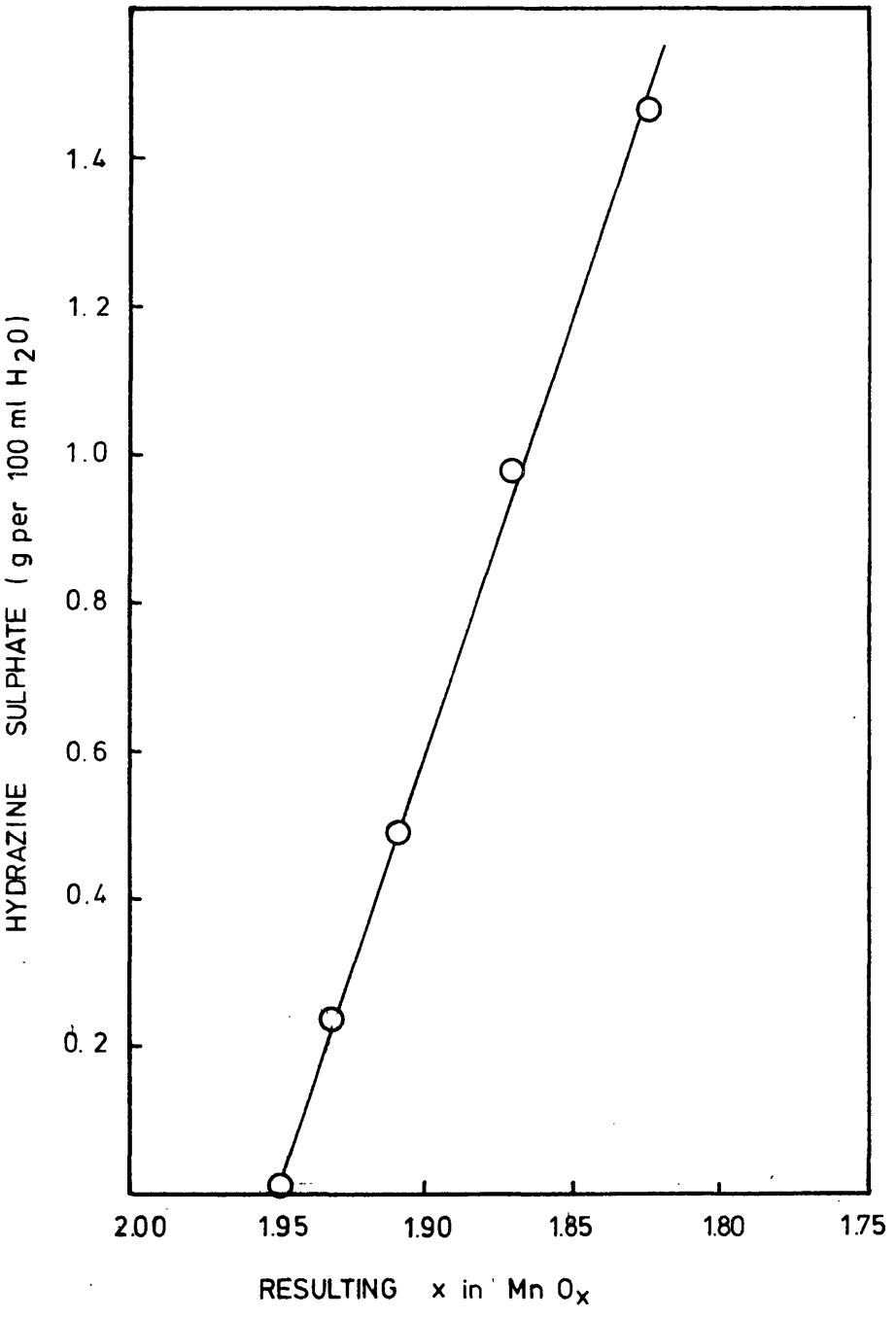

Fig.2.2 Chemical reduction of γ-MnO_2.

addition of aqueous ammonia (150 ml, 0.2M) to a stirred solution of manganous sulphate (5.07 g, 500 ml H_2O) containing hydrogen peroxide (10.2 ml, 30% W/V) at room temperature. A chocolate brown precipitate formed instantaneously and this was heated in the aqueous solution to 100°C and refluxed for 26 hours. The yellow-brown solid was filtered off and air dried at 100°C for 12 hours. This analysed as $MnO_{1.51}$ and had a BET surface area of 19.7 m^2g^{-1}. A second sample (sample B) was prepared in a similar manner except that after precipitation at room temperature the sample was filtered off and vacuum dried at that temperature. The nitrogen BET area was 87.7 m^2g^{-1} and the solid analysed as $MnO_{1.55}$. The third sample (sample C) was obtained by precipitation at 5°C, filtered off, washed thoroughly with water and dried under vacuum overnight at ambient temperature. Chemical analysis showed a sample composition of $MnO_{1.52}$.

2.1.(vi) α-Manganese oxyhydroxide

The preparation was based on a procedure reported by Giovanoli and Leuenberger[10]. Well crystallised γ-MnO_2 (2.0 g) prepared by the disproportionation of Mn_3O_4 in hot dilute nitric acid as described in (ii) was heated in a round bottomed flask at 90°C together with cinnamyl alcohol (2.4 g) and xylene (40 ml) for 6 days. The product was filtered off, washed thoroughly with industrial methylated spirits and air dried at 25°C. Interplanar distances taken from an X-ray diffraction trace are compared with those of natural groutite given in the ASTM[92] card (Table 2.1). All the lines in the pattern

TABLE 2.1

X-RAY DIFFRACTION DATA FOR SYNTHETIC AND NATURAL GROUTITE (α-MnOOH)

Synthetic α-MnOOH			Natural α-MnOOH		
d(Å)	I/I^{o}	hkl	d(Å)	I/I^{o}	hkl
			5.34	20	020
4.19	100	110	4.20	100	110
			3.47	20	120
2.86	35	130	2.81	70	130
2.68	85	040	2.67	70	040
2.54	50	021	2.54	5	021
			2.42	5	101
2.39	80	111	2.38	40	111
2.31	55	140	2.30	60	140
			2.28	5	200
2.22	35	210	2.22	10	210
			2.10	5	220
			2.01	5	131
			1.91	20	041,150
			1.781	5	060
			1.762	10	211
			1.737	40	240
1.694	90	221	1.695	50	221
1.62	25	151	1.608	40	151
			1.561	30	250
1.514	25	061	1.515	30	061
			1.487	5	
			1.463	30	
1.440	30		1.449	40	

can be indexed on the basis of α-MnOOH although some of the weaker lines reported for natural groutite cannot be detected. Chemical analysis indicated that reduction had continued slightly beyond MnOOH, x in MnO_x being equal to 1.45 instead of the expected 1.50.

2.1.(vii) Pentamanganese octoxide

A sample was kindly supplied by Dr. R. Giovanoli of the University of Berne, Switzerland. It had been prepared by controlled oxidation of finely divided MnO obtained from the decomposition of Mn(II) oxalate in hydrogen. Its X-ray pattern corresponded to that given in the literature[93].

2.1.(viii) Other materials

A sample of non-porous hydroxylated alumina (Degussa 'Aluminiumoxid C') was kindly supplied by Degussa Forschung Chemie, Frankfurt, W.Germany. It had been manufactured by the flame hydrolysis of $AlCl_3$. Koch-Light puriss grade (> 99%) nonane used in the adsorption studies was dried over molecular sieve type 3A and subjected to several freeze-pump-thaw cycles before use.

Nitrogen and oxygen for gas adsorption or TPD work were BOC Research Grade.

Water used in TPD runs was triple distilled over potassium permanganate and permanent gases removed by the freeze-pump-thaw technique.

Iron(III) stabilised oxalate solution used in the chemical analysis of manganese oxides was prepared by dissolving 13.399 g of sodium oxalate in 400 ml of sulphuric acid (10% V/V). 5 g of ferric ammonium sulphate were added and the solution diluted to 1 litre with distilled water. It was stored in an amber-coloured bottle.

2.2 Equipment

2.2(i) TPD apparatus

The gravimetric TPD arrangement (fig.2.3) was based on a Cahn RG electromagnetic microbalance. The balance was rigidly mounted on a welded box girder frame supported on a heavy pedestal which constituted an efficient shock absorber when isolated from the floor by six 1" corks. Suspended from the arm of the balance were two nichrome wires to which were attached a sample and a counterweight respectively, both being contained in either a thin glass or silica holder. These in turn were surrounded by hangdown tubes of quartz (for the sample) or glass (for the counter-weight) enabling sample temperatures of up to 700^{o}C to be reached.

The linear temperature programme was provided by a Stanton Redcroft programmer (Model LVP/CA 10) and furnace (Model VB 100) giving nominal rates of heating of 0-10^{o}C min^{-1}. The sample temperature was monitored continuously with a chromel-alumel thermocouple, its junction positioned 2 mm below the sample bucket. The emf was measured to $\pm$ 10μV by means of a millivoltmeter (Digitek, Model 451S) and a 10 mV potential

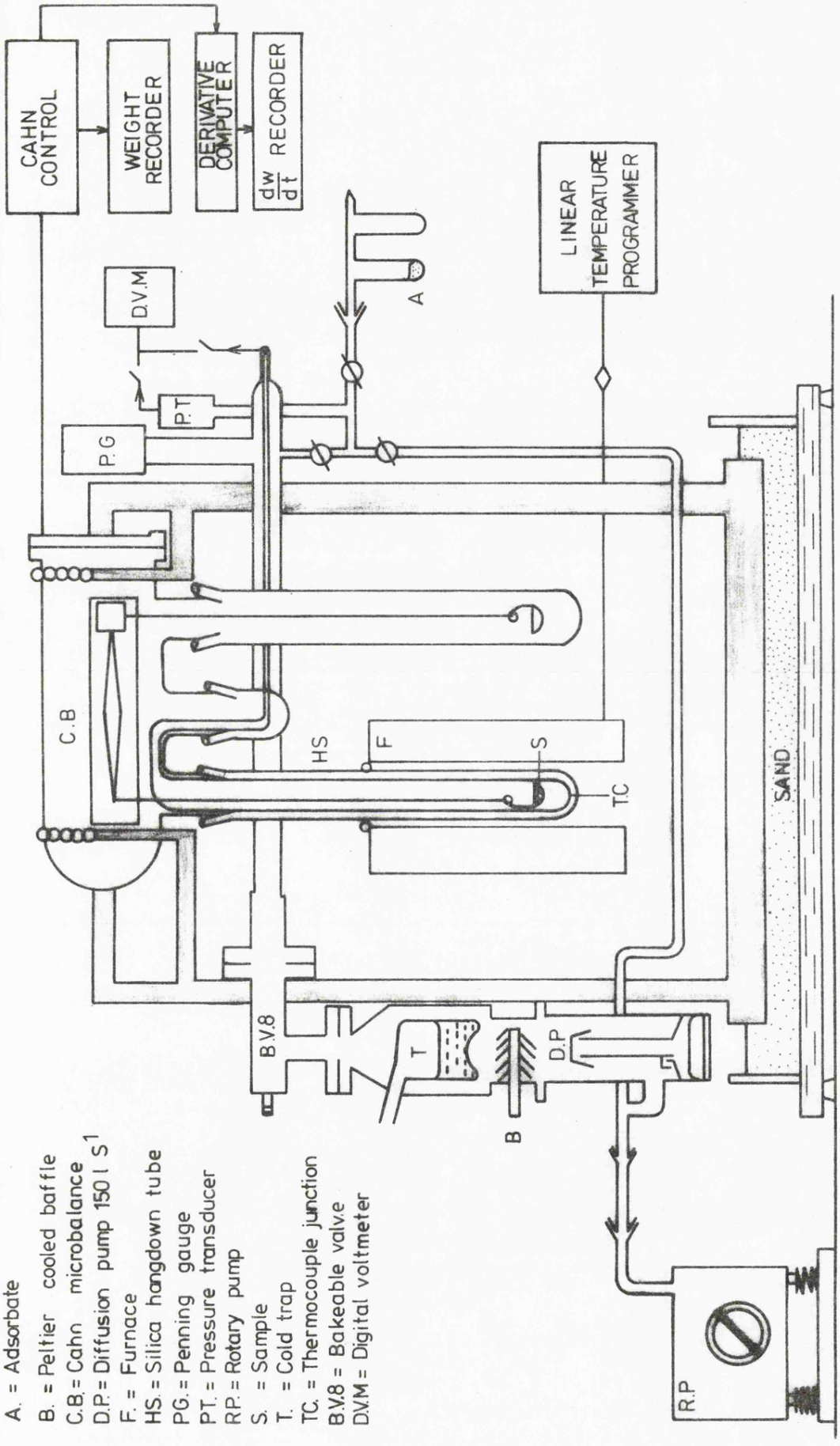

Fig.2.3 Gravimetric TPD and gas adsorption system.

back-off arrangement (Digital Measurements, Model DM 2201). The thermocouple had been previously calibrated at $0^{o}C$, $231.9^{o}C$ and $327.8^{o}C$ the melting points of ice, tin and lead respectively. The response was found to be linear and within $1^{o}C$ of the maker's calibration.

The output from the Cahn balance was fed into a Leeds and Northrup Speedomax recorder and to a Cahn time-derivative computer. The latter was connected to a Bryans 27000 1mV X-t recorder and provided directly a rate of weight loss as a function of heating time. This enabled easy identification of the time at which a peak occurred. A continuous record of sample weight versus heating time could be obtained from the former.

The vacuum pumping system consisted of an Edwards EM2 mercury diffusion pump (speed 150 l sec^{-1}), DCB2B baffle and NTM2A liquid nitrogen cold trap. This system evacuated the balance arrangement through a B 'V8 1' bakeable valve to a pressure of 10^{-6} Torr. The pressure inside the balance case could be observed continuously during a run with a Penning gauge sealed directly into the system.

2.2.(ii) Gas adsorption

Nitrogen adsorption isotherms were determined gravimetrically using the Cahn balance arrangement employed in the thermal work. Both hangdown tubes were immersed to a depth of 25 cm in liquid nitrogen throughout the determination of an isotherm. Pressure measurements were made with a Bell and Howell type

4-326 pressure transducer covering the pressure range 0-760 Torr. As well as being easy to operate, the arrangement eliminated any possible contamination of the sample by mercury vapour[94] from a conventional manometer. The type 4-326 transducer consists of a stainless steel diaphragm the displacement of which induces a stretching of a tungsten wire wound in the form of a Wheatstone bridge network. An input voltage of 10 V was applied to one pair of arms by a stabilised D.C. power supply (Coutant Electronics power supply, Bell and Howell stabiliser type 3-141-1) and the output across the opposite pair was measured. The output pressure sensitivity of the transducer was 12.28 Torr mV^{-1} which was inconvenient for use with the Digitek voltmeter. This could be altered to 86.71 Torr mV^{-1} when used in conjunction with a suitable voltage divider. The transducer had previously been checked against the manufacturer's calibration with air using a conventional mercury manometer. The saturated vapour pressure of nitrogen (p^o) was measured directly with a nitrogen vapour pressure thermometer situated close to the apparatus. In a few of the later runs p^o was taken as being equal to atmospheric pressure owing to breakage of the nitrogen thermometer.

2.2.(iii) Additional techniques

Mass spectrometric analysis of the desorption products resulting from the thermal treatment of γ-MnO_2 was carried out at the B.C.U.R.A. Laboratories using an AEI MS10 mass spectrometer with a continuous sampling system for bleeding

off part of the gases evolved from the oxide. The temperature of the sample was raised in 40-60^{o} steps to 410^{o}C allowing a total of 40 minutes at each temperature. The partial pressures of water, oxygen, carbon dioxide and nitrogen were measured at the maximum desorption rates.

Differential thermal analysis (DTA) of the samples was made either with a Stanton Redcroft 6-73 or Mettler Thermoanalyser. The runs were carried out by the Stanton Redcroft Consultancy Service and by employees at Mettler Instrumente AG, Switzerland.

X-ray diffraction data were obtained on powdered samples at room temperature using a Philips 1130 X-ray unit equipped with a diffractometer and operating at a current of 40 mA and at a potential of 45 kV. Ni filtered Cu k_{α} radiation was used throughout. Unless specifically stated otherwise, diffractometer traces were obtained with the following settings; sensitivity 200 counts sec^{-1}, time constant 4 sec with a goniometer scan of 1^{o} min^{-1} and a chart speed of 300 mm hr^{-1}.

Scanning electron micrographs were obtained on a Cambridge Scientific Instruments Stereoscan 600.

Magnetic measurements were made by the author in the University of Bath on an apparatus constructed and described in detail by Hagan[95]. Data were obtained by the Gouy method using an enclosed Cahn RG electrobalance. By means of a suitable cryostat arrangement susceptibility measurements were obtained from room temperature down to 80 K. Facilities

were available for recording measurements over a wide range of field settings (3000-5500 gauss) but this was limited to 3300 gauss at the lowest temperatures in this study because of oscillation of the Gouy tube with subsequent sticking to the sides of the hangdown tube.

2.3 Procedure

2.3.(i) Outgassing treatment

Prior to TPD and gas adsorption experiments the samples were outgassed in vacuum for a set period of time. The sample size was variable (60-115 mg) and was generally distributed as a loosely packed bed in the glass or silica sample holder. For room temperature outgassing the system was pumped down to $\sim 5 \times 10^{-5}$ Torr over a period of 3-4 hours. Degassing at an elevated temperature was achieved by following the procedure employed for the room temperature runs and then raising the sample temperature and continuing pumping for a further 2 hours.

2.3.(ii) TPD runs

Commencement of the linear heating programme could be made either from the outgassing temperature on completion of the outgassing procedure or after cooling the sample to room temperature. The former method was used for the determination of apparent activation energies of desorption whilst the latter was employed in all other cases. To obtain the temperature at which a desorption peak appeared on the time derivative computer trace it was necessary to measure the emf of the thermocouple as a function of time by an accurate stopwatch.

It was then simple to relate the desorption rate to temperature and obtain the peak temperature. The true heating rate β was obtained from the slope of a plot of sample temperature versus heating time. If small deviations from linearity were apparent near the region of interest β was obtained as a tangent at that point.

During a run the pressure in the system was very rarely allowed to exceed 5×10^{-4} Torr so that spurious mass changes resulting from thermomolecular flow (TMF) were eliminated[96]. As well as vacuum studies runs were carried out in static gas environments. After vacuum outgassing the samples were cooled to room temperature, 10 Torr of gas admitted and TPD carried out as for the vacuum runs. No TMF forces were evident at that pressure.

2.3.(iii) Adsorption measurements

Nitrogen adsorption isotherms were determined gravimetrically using the Cahn RG microbalance. After outgassing of the sample as described above this was cooled to room temperature with the balance case open to the vacuum pumps and pumping was continued overnight at that temperature. Nitrogen ($\sim$ 10 Torr) was then admitted and both hangdown tubes immersed in liquid nitrogen. Equilibration was usually complete after 30 minutes. Isotherms were constructed up to $\sim p/p^{o} = 0.75$, a time interval of 15 minutes being adequate for attainment of equilibrium. It has been pointed out[97] that there can be an appreciable temperature difference between the adsorbent and the surrounding liquid nitrogen bath.

Because of this BET surface areas are lower than those calculated from conventional volumetric isotherms[97-99]. Cutting[97] showed that this difference could be allowed for by recording the temperature of both the sample and cryostat bath with subsequent correction of the experimental data. Alternatively allowance may be made by the use of appropriate standard adsorption data[98]. This procedure is based on the fact that isotherms are determined at the same temperature on the samples of interest even though the registered value of p^o is not the true saturation pressure of nitrogen at the adsorbent temperature. This method has been adopted in the ensuing work and no correction has been made to the isotherms or α_s plots for temperature differences.

The procedure employed to investigate the microporous structure generated on heat treatment, by means of pre-adsorption of nonane, was as follows:

A nitrogen adsorption isotherm was determined on the sample in the manner outlined above. The nitrogen was then removed by opening the balance chamber to the vacuum pumps followed by exposure of the sample to nonane vapour at 78 K for several hours. The sample was then allowed to warm up to room temperature and excess nonane pumped away overnight. A nitrogen isotherm was then determined at 78 K.

2.3.(iv) Chemical analysis

Compositions of manganese oxides are frequently expressed in the form MnO_x where x ranges from 1.0 for MnO to 2.0 for

MnO_2. The ratio of tetravalent manganese ions to the total manganese content of the samples is given by y, where x = 1+y. Methods of analysis are based on the determination of these two quantities. In acid solution Mn(III) readily disproportionates into Mn(II) and Mn(IV)[100] and will therefore be determined as such. Tervalent manganese ions in the solid are therefore considered to be composed of equal parts of Mn(II) and Mn(IV) ions for the purpose of calculating the sample composition. Mn_2O_3 becomes $MnO_{1.50}$ where x = 1.50 and y = 0.50 $\left(= \frac{Mn(IV)}{Mn(II) + Mn(IV)}\right)$.

Although the procedure employed varied with the available sample size the basis of the analysis remained unaltered. Mn(IV) was determined by a modified oxalic acid method[101]. Oxalic acid is oxidised by tetravalent manganese and the excess oxalate back titrated with potassium permanganate. The reactions may be represented by:

$$Mn(IV) + (COO)_2^{2-} \rightarrow Mn(II) + 2CO_2 \qquad (2.4)$$

$$2\ Mn(VII) + 5\ (COO)_2^{2-} \rightarrow 2\ Mn(II) + 10CO_2 \qquad (2.5)$$

The determination of total manganese was based on the potentiometric method of Karplus and Lingane[102]. All of the manganese ions in the sample are reduced to the +2 oxidation state. These are titrated with $KMnO_4$ in neutral pyrophosphate solution, Mn(II) being oxidised to Mn(III) which is stabilised in the presence of pyrophosphate. The reaction may be represented by:

$$4\ Mn^{2+} + MnO_4^- + 8H^+ + 15H_2P_2O_7^{2-} \rightarrow 5\ Mn(H_2P_2O_7)_3^{3-} + 4\ H_2O \quad (2.6)$$

When the available sample weight was in excess of 600 mg the procedure employed was as follows.

Mn(IV)

The oxide (0.41-0.48 g) was refluxed with standard sodium oxalate solution (0.2N, 50 ml) and sulphuric acid (20% V/V, 25 ml) for 30 minutes until dissolution was complete. The solution was diluted to 150 ml and titrated at 80°C with potassium permanganate (0.05N).

Total manganese

The oxide (0.2 g) was transferred to a conical beaker containing distilled water (4 ml) and hydrochloric acid (S.G.1.18, 4 ml). The solution was heated gently until chlorine evolution had ceased and then gently boiled for a further 30 minutes. After cooling the solution was transferred to a volumetric flask (100 ml), sulphuric acid added (20% V/V, 6 ml) and diluted to volume. An aliquot (50 ml) was added to a saturated solution of sodium pyrophosphate (150 ml) and the pH adjusted to between 6.5 and 7.0 with either sodium hydroxide or sulphuric acid. This was titrated potentiometrically with potassium permanganate (0.05N), the potential of a platinum electrode being measured with respect to a saturated calomel electrode.

The analysis procedure was modified to accommodate the small sample sizes produced during a thermal run and this was based on a technique employed by Vetter and Jaeger[103].

This method has several advantages over the technique described above in that (a) only one sample is required which eliminates errors due to different moisture contents (b) the exact sample weight is not required (c) the exact molarity of the sodium oxalate and potassium permananate solution is not required. The sample weight used depended on the mean oxidation state of the manganese. For x in MnO_x equal to 2.0, 1.5 or 1.3 sample weights of the order of 17, 31 and 45 mg were used. This enabled the back titration of excess oxalate to be similar for each sample. The procedure employed was as follows:

A suitable sample weight was refluxed in sodium oxalate solution (10 ml, 0.025M) containing sulphuric acid (2 ml, 20% V/V) for 30 minutes by which time dissolution of the sample was complete. The solution was diluted to 25 ml, heated to 80°C and titrated with $KMnO_4$ (0.01M) (V_1). To the same solution was added potassium pyrophosphate ($\sim$ 4 g) which was dissolved by stirring. The pH was then adjusted to 6.5 to 7.0 by the addition of sodium hydroxide pellets and titrated potentiometrically with 0.02M $KMnO_4$ (V_2). Finally the volume of $KMnO_4$ (V_o) required to standardise 10 mls of sodium oxalate solution was noted. x in MnO_x was calculated from the relationship

$$x = 1 + \{5(V_o - V_1)/8(V_2 - 0.25V_1)\} \qquad (2.7)$$

2.3.(v) Characterisation of MnOOH

Well-crystallised α- and γ- MnOOH can be distinguished from

each other by means of their X-ray diffraction patterns. However, when a mixture is present or the components are finally divided this becomes difficult. Giovanoli and Leuenberger[10] developed a method whereby it was possible to differentiate between these two oxyhydroxides on the basis of their behaviour in nitric acid. They showed that MnOOH disproportionates in hot dilute nitric acid in the following way:

$$2\ MnOOH + 2\ HNO_3 \rightarrow MnO_2 + Mn(NO_3)_2 + 2H_2O \qquad (2.8)$$

γ- MnOOH forms β- MnO_2 whereas α- MnOOH forms γ- MnO_2. The dioxides are more readily distinguished from each other by X-ray diffraction than their precursors. The procedure involved refluxing the sample in dilute nitric acid (1N) for 1 hour, filtering the resulting solid and finally drying in an air oven at 100°C. A mole ratio of $MnOOH:HNO_3$ = 5:1 was used.

2.3.(vi) Ion exchange

The ion exchange capacity of some of the products obtained by chemical reduction of γ-MnO_2 was investigated using the following procedure:

The sample (1.0 g) was transferred to a volumetric flask (100 ml) and diluted to volume with potassium chloride (0.1N). This was left to equilibrate for 28 days with intermittent shaking[45]. The pH of the potassium chloride solution was measured before addition of the oxide and on attaining equilibrium.

2.3.(vii) Magnetic susceptibility

Prior to the recording of the magnetic measurements the samples were outgassed in vacuum overnight at room temperature. The experiments were conducted in the presence of a small amount of helium (2 Torr). It can be shown[104] that in the presence of helium the susceptibility of a uniform rod of a specimen suspended in a non-homogenous magnetic field is given by

$$\chi_g = \frac{\frac{2\,g\,l\,\Delta w}{H^2}}{W} = \frac{B\,\Delta w}{W} \qquad (2.9)$$

where χ_g = gram susceptibility

l = length of specimen

H = magnetic field strength

Δw = weight change in and out of field

W = sample weight

B is obtained by recording the force exerted on a compound of known susceptibility at a series of field settings and at a fixed temperature. Mercury tetrathiocyanato cobaltate $HgCo(CN)_4$ was used as the calibrant, its susceptibility at any temperature being given by[105]

$$\chi_g = \frac{4985 \times 10^{-6}}{(T+10)} \qquad (2.10)$$

Although B should be independent of temperature, measurements were obtained in the range 209-272 K as a check and a mean value of B at each field setting calculated. In order to evaluate B the weight change in and out of the magnetic field had to be corrected for the diamagnetism of the glass sample tube. This was accomplished by weighing the empty tube in and out of the magnetic field at several different

field settings and over the temperature range 80-293 K (the diamagnetic corrections are shown in Table 2.2 and values of B after correction in Table 2.3). The gram susceptibilities for each of the compounds over the whole of the temperature range were calculated from equation (2.9). These values were converted to magnetic susceptibility per mole of manganese by use of equation

$$\chi_{Mn} = \frac{B \, \Delta w \, 5494}{W \, x} \qquad (2.11)$$

where x = % manganese in the weighed out sample.

TABLE 2.2

DIAMAGNETIC CORRECTIONS FOR GLASS SAMPLE TUBE

Field Setting		Temperature (K)												
Dial Setting	Gauss	291	275	257	239	225	209	194	178	163	145	130	115	99	82
		Diamagnetic Correction (mg)													
2.25	3000	0.15	0.15	0.15	0.14	0.14	0.15	0.15	0.14	0.13	0.13	0.12	0.10	0.09	0.09
2.50	3307	0.18	0.18	0.18	0.17	0.18	0.18	0.17	0.17	0.16	0.15	0.14	0.13	0.12	0.11
2.75	3559	0.21	0.21	0.21	0.20	0.20	0.20	0.20	0.19	0.18	0.18	0.16	0.15	0.13	0.12
3.00	3765	0.23	0.23	0.23	0.22	0.23	0.23	0.22	0.22	0.21	0.20	0.18	0.16	0.15	0.14
3.50	4101	0.28	0.28	0.27	0.27	0.27	0.27	0.26	0.25	0.24	0.24	0.21	0.19	0.18	0.16
4.00	4369	0.32	0.32	0.31	0.30	0.31	0.30	0.30	0.28	0.28	0.26	0.24	0.22	0.21	0.17
4.50	4579	0.35	0.35	0.34	0.33	0.34	0.33	0.33	0.31	0.30	0.29	0.27	0.24	0.22	0.18
5.50	4885	0.40	0.39	0.38	0.38	0.38	0.38	0.37	0.35	0.34	0.33	0.30	0.28	0.25	0.19
6.50	5134	0.44	0.43	0.43	0.42	0.42	0.41	0.41	0.38	0.38	0.36	0.34	0.31	0.28	0.21
8.00	5454	0.47	0.49	0.48	0.47	0.48	0.47	0.46	0.44	0.43	0.41	0.38	0.35	0.31	0.24

TABLE 2.3

VARIATION OF TUBE CONSTANT (β) WITH FIELD STRENGTH

Field Setting		Temperature (K)												
		292		275		257		240		225		209		Mean Value of β
Dial Setting	Gauss	Δw mg	βx10^4	Δw mg	βx10^4	Δw mg	βx10^4	Δw mg	βx10^4	Δw mg	βx10^4	Δw mg	βx10^4	
2.25	3000	2.28	12.34	2.45	13.05	2.65	12.88	2.85	12.79	3.06	12.67	3.21	12.96	0.001278
2.50	3307	2.79	10.82	3.02	10.59	3.21	10.63	3.41	10.69	3.66	10.59	3.96	10.51	0.001064
2.75	3559	3.25	9.29	3.42	9.35	3.71	9.20	3.99	9.14	4.20	9.23	4.54	9.17	0.000923
3.00	3765	3.62	8.34	3.87	8.26	4.18	8.17	4.43	8.23	4.75	8.16	5.14	8.10	0.000821
3.50	4101	4.30	7.02	4.59	6.97	4.95	6.89	5.27	6.92	5.65	6.86	6.11	6.81	0.000691
4.00	4369	4.92	6.13	5.25	6.09	5.61	6.08	6.04	6.03	6.37	6.09	6.89	6.04	0.000608
4.50	4579	5.37	5.62	5.74	5.57	6.20	5.50	6.56	5.56	7.05	5.50	7.54	5.52	0.000555
5.50	4885	6.17	4.89	6.47	4.94	7.00	4.88	7.47	4.88	8.02	4.83	8.61	4.83	0.000488
6.50	5134	6.75	4.47	7.23	4.42	7.73	4.42	8.33	4.38	8.86	4.38	9.47	4.39	0.000441
8.00	5454	7.60	3.97	8.14	3.93	8.72	3.91	9.41	3.87	10.01	3.87	10.74	3.87	0.000390

CHAPTER 3

γ- Manganese dioxide

3.1 TPD under dynamic vacuum

A typical TPD curve obtained by outgassing γ-MnO_2 to $5x10^{-5}$ Torr and continuously pumping away the desorption products is illustrated in fig.3.1. The main desorption peak (Type II) occurs at about 200°C. The majority of the less strongly bound water (Type I) is removed during the initial outgassing procedure. A small amount remains and is observed as a shoulder on Type II. Beyond Type II there is a hint of a third desorption process (Type III) before oxygen loss predominates above 400°C. The oxygen evolution at high temperatures results from the decomposition of the manganese dioxide

$$4\ MnO_2 \rightarrow 2\ Mn_2O_3 + O_2 \qquad (3.1)$$

Preliminary experiments were designed to establish the nature of the desorbing species in the temperature range of interest and to investigate the reversibility of the main desorption process around 200°C. Previous unpublished work in these laboratories suggested that the weight loss up to 400°C was due to water desorption. Fig.3.2 shows the partial pressure of gases released on heating γ-MnO_2 to 400°C in 40°-60° steps allowing 40 minutes at each temperature. The weight loss around 210°C (fig.3.1) is seen to be associated with the loss of water although subsidiary evolution of carbon dioxide and nitrogen are also observed. Oxygen loss begins at 260°C which shows that both oxygen and water removal contribute to the weight loss in the region of 360°C (Type III).

The following procedure was used to determine the reversibility

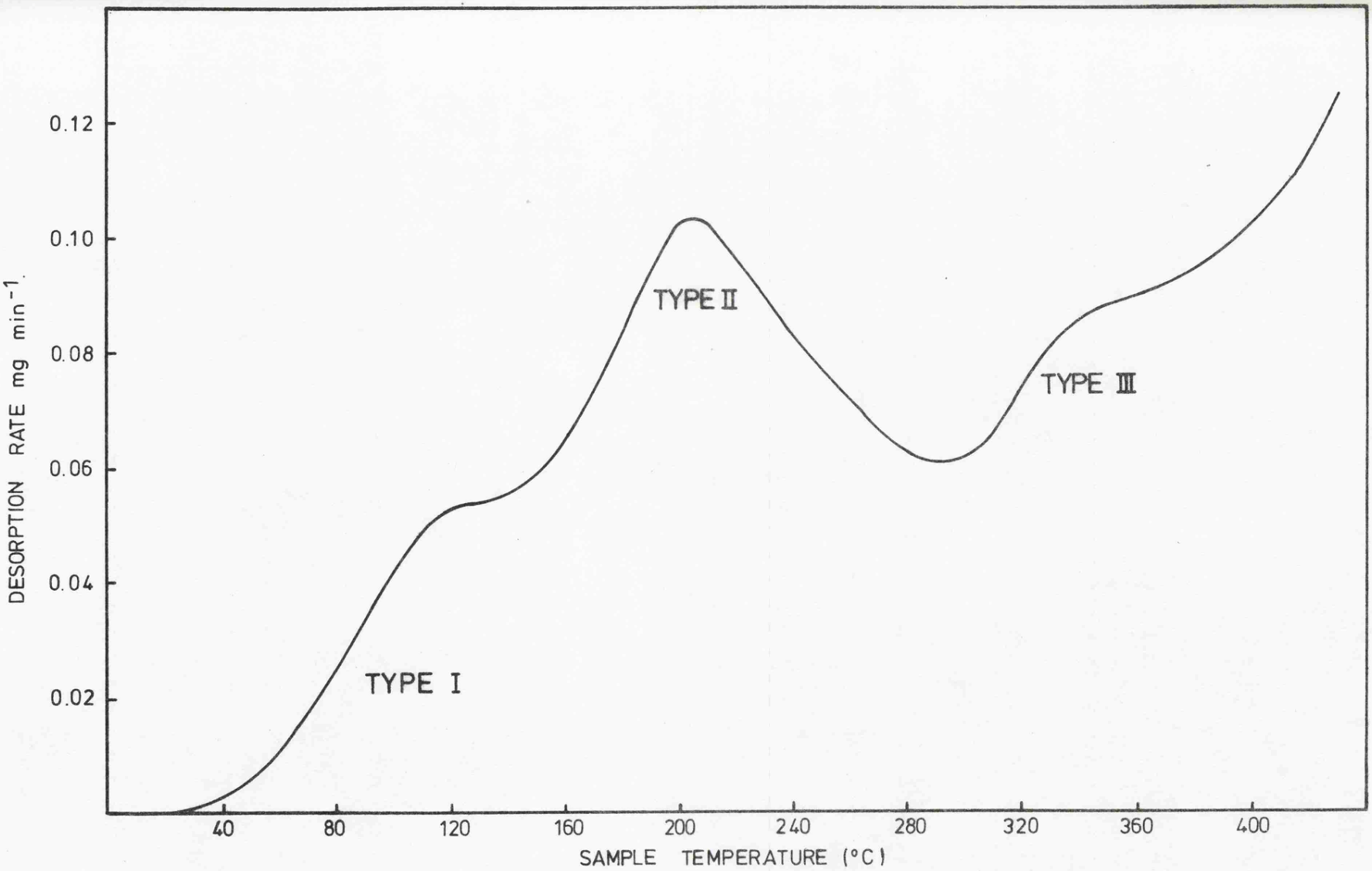

Fig.3.1 Typical TPD curve of γ-MnO_2 in a dynamic vacuum.

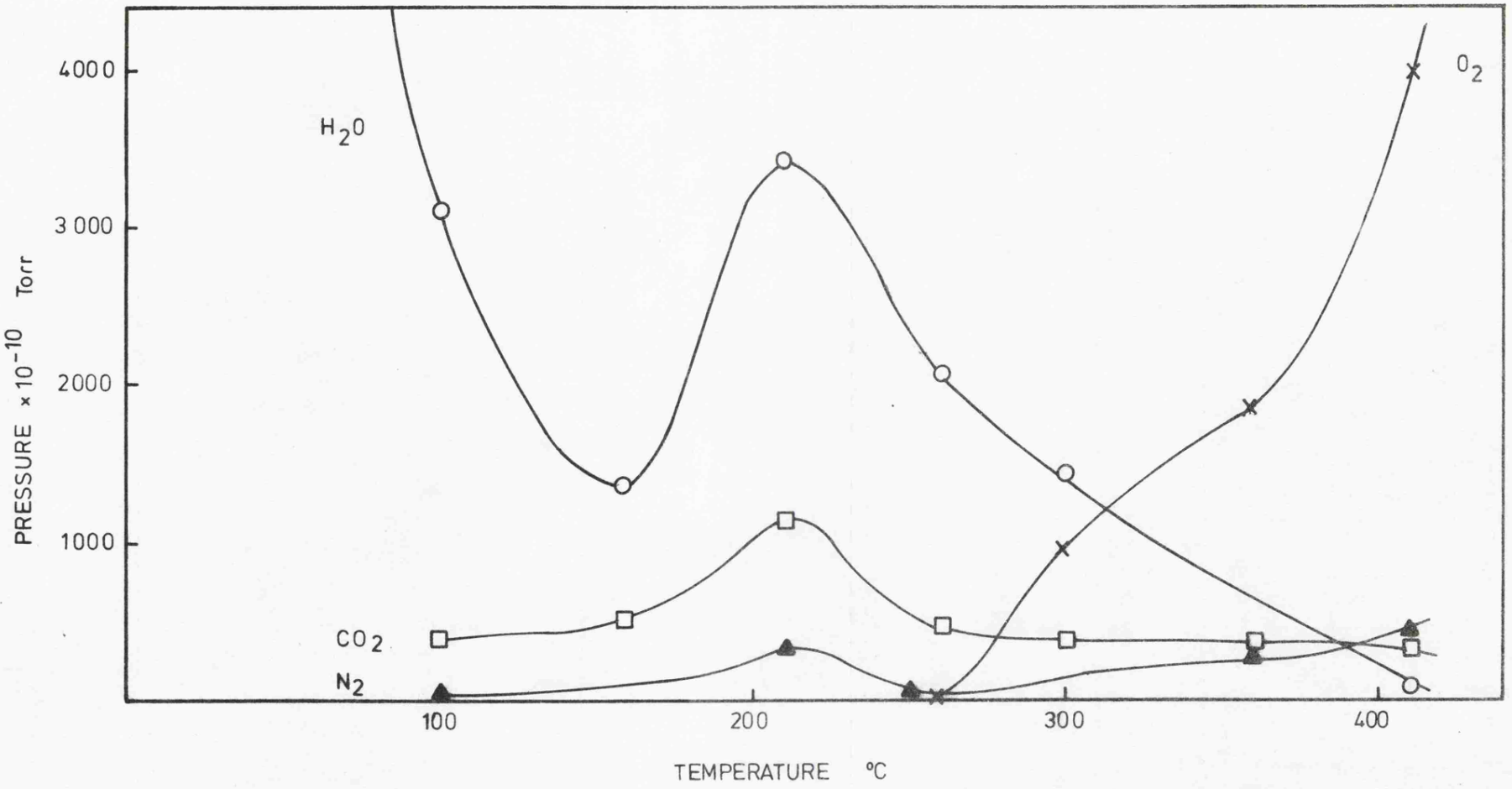

Fig.3.2 Mass spectrometric analysis of desorbed products from γ-MnO_2.

of the desorption processes. The temperature of the γ-MnO_2 sample was first raised to 270°C by a linear temperature programme. On attaining 270°C the sample was cooled to room temperature and then left in contact with water vapour ($\sim$ 7 Torr) overnight. After removing excess water by room temperature evacuation, TPD from γ-MnO_2 showed that readsorption had taken place up to $\sim$60°C. However, the water associated with Type II had not been restored (fig.3.3). In view of the irreversible nature of the water a fresh sample had to be used for each run.

Outgassing γ-MnO_2 at room temperature and application of a linear heating programme produced TPD curves as in fig.3.4. The temperature at which the desorption rate was a maximum (Tp) shifted to higher temperatures as the heating rate increased. The apparent activation energy of desorption for the Type II water species was obtained from a plot of equation (1.12) assuming a first order process. Application of a least squares fit to the data in fig.3.5a gave a value for E_D of 23.5 kcal $mole^{-1}$ (98 k J mol^{-1}). This was of the same order as found by Sedlak and Beebe[67] for internal molecular water in calcium phosphate (20 kcal $mole^{-1}$) and by Munuera and Stone[64] for dissociative chemisorption of water on rutile (25.6 kcal $mole^{-1}$). The magnitude of E_D indicates that the water is chemically associated with γ-MnO_2 although it is not possible to differentiate between surface and internal water. The pre-exponential factor obtained from the intercept in fig.3.5a was equal to 3×10^8 sec^{-1}. This may be indicative of supermobile adsorption but frequency factors of this order give no insight

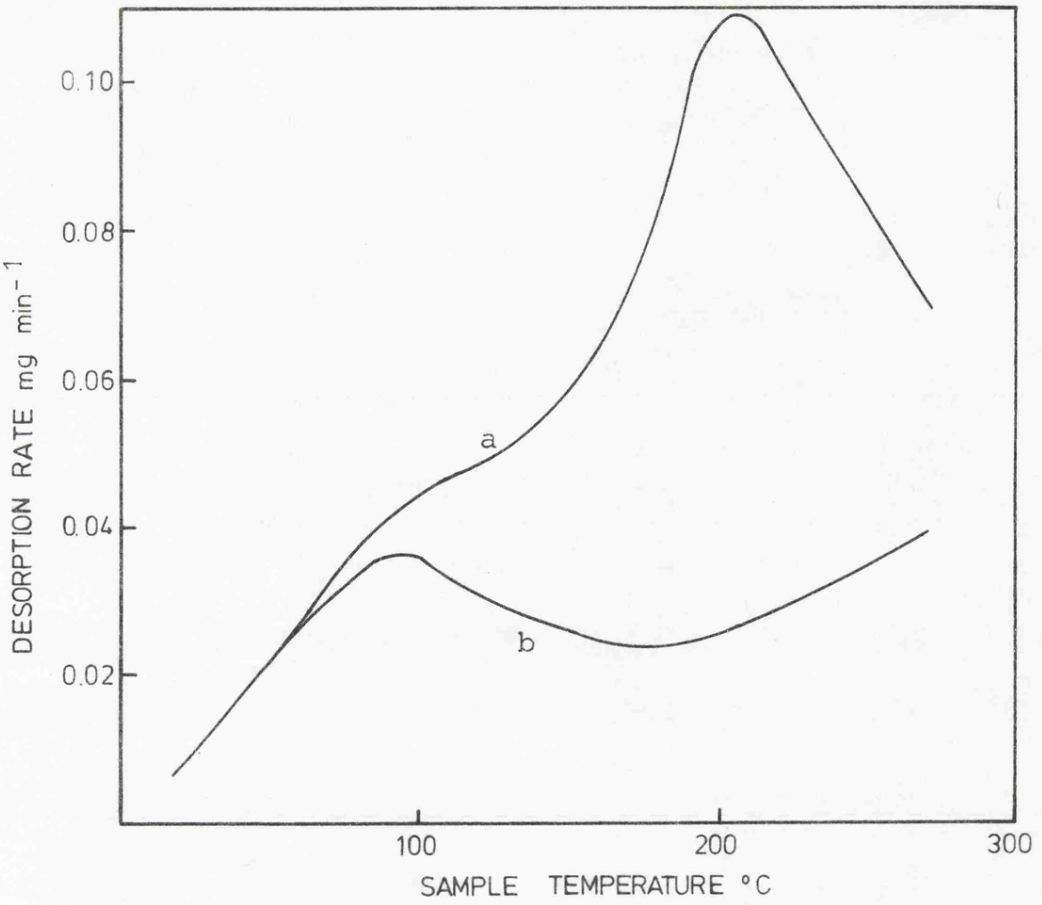

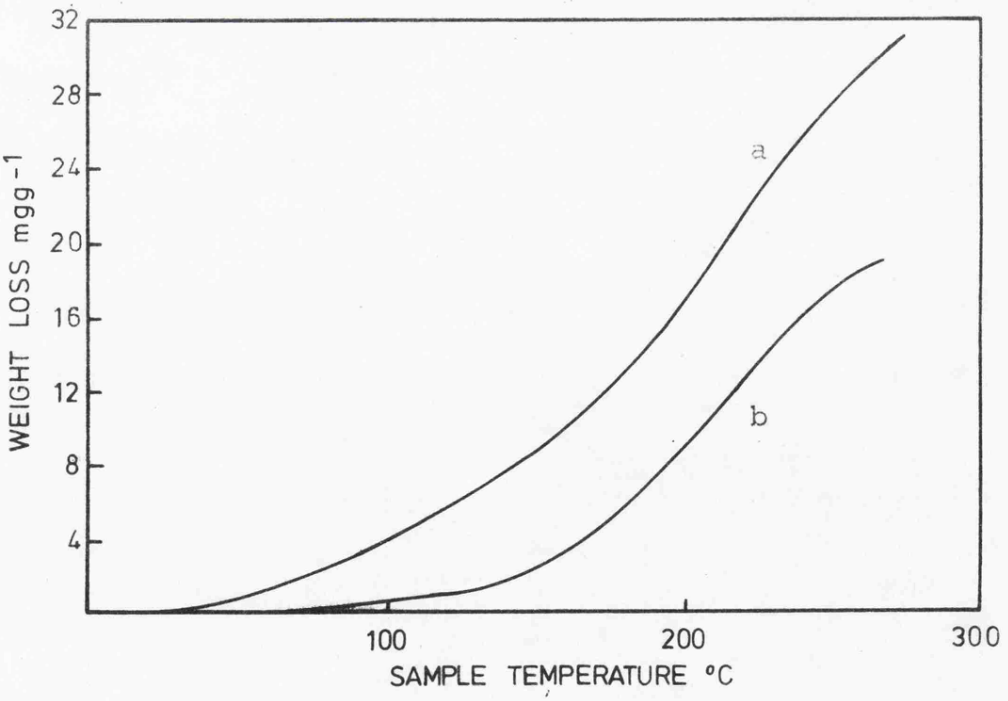

Fig.3.3 Top. Gravimetric TPD curves of a) γ-MnO_2 b) γ-MnO_2 after heating to 270°C and equilibrating in 7 Torr water vapour for 12 hours.

Bottom. a) Total weight loss and b) irreversible weight loss as a function of sample temperature for γ-MnO_2.

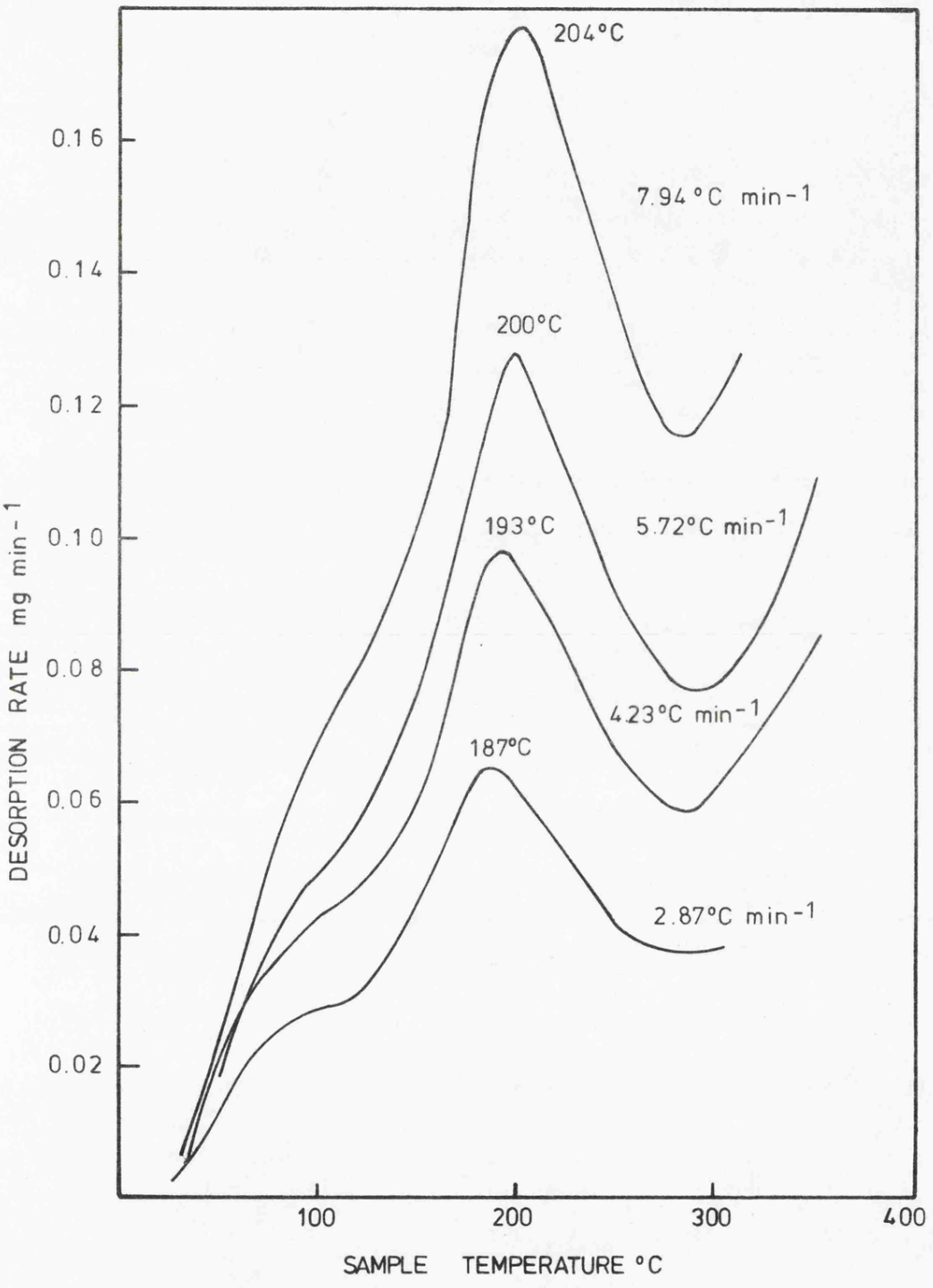

Fig.3.4 Peak temperature (Tp) as a function of heating rate for desorption of type II water from γ-MnO_2.

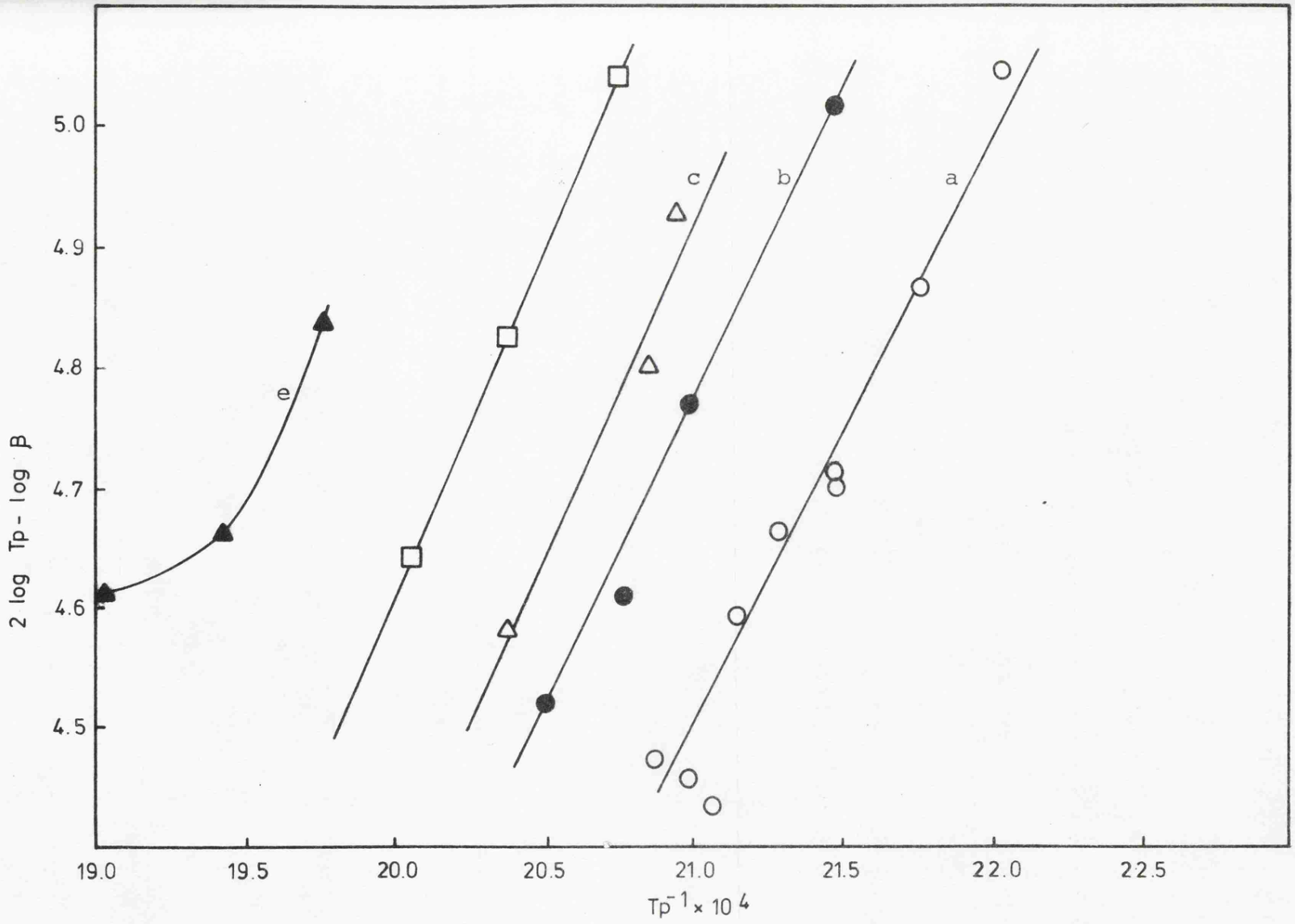

Fig.3.5 2 log Tp - log β versus Tp^{-1} for γ-MnO_2 evacuated at room temperature in vacuum to 6×10^{-5} Torr followed by 2 hours outgassing at 23°C (○), 123.5° (●), 136° (△), 145° (□) and 160°C (▲) prior to gravimetric TPD.

as to the nature of the water species. Munuera[106] obtained a value of $\nu = 2.7 \times 10^{8}$ sec^{-1} for surface hydroxyl groups on TiO_2 whereas Stakebake[65] found that for surface molecular water doubly hydrogen bonded to underlying hydroxyl groups, $\nu = 4 \times 10^{9}$ sec^{-1}.

It was of interest to establish the dependence of Tp on coverage. For a homogeneous set of adsorption sites Tp is independent of coverage whilst an increase in Tp with decrease in coverage is indicative of surface heterogeneity. The amount of water on the surface prior to TPD analysis was progressively decreased by outgassing at selected temperatures. The weight losses corresponding to various outgassing conditions are recorded in fig.3.6. The curves resulting from TPD analysis after reduction of coverage in this way are illustrated in fig.3.7. The shift of peak temperature confirms the dependence of E_D on coverage. E_D may be calculated by substitution of Tp, obtained at different initial coverages, into equation (1.11). However, this assumes that the frequency factor is independent of coverage and although this was the approach adopted by Amenomiya and Cvetanovic[57] it is not fully justified. As the pre-exponential factor contains an entropy term this may alter with coverage leading to erroneous values of E_D. The approach adopted was to record Tp at varying heating rates for a constant outgassing temperature and plot the data as for the room temperature treatments. Except for the highest outgassing temperature case, linear plots were obtained (fig.3.5), enabling E_D and ν to be determined as a function of outgassing temperature. Results are given in fig.3.8.

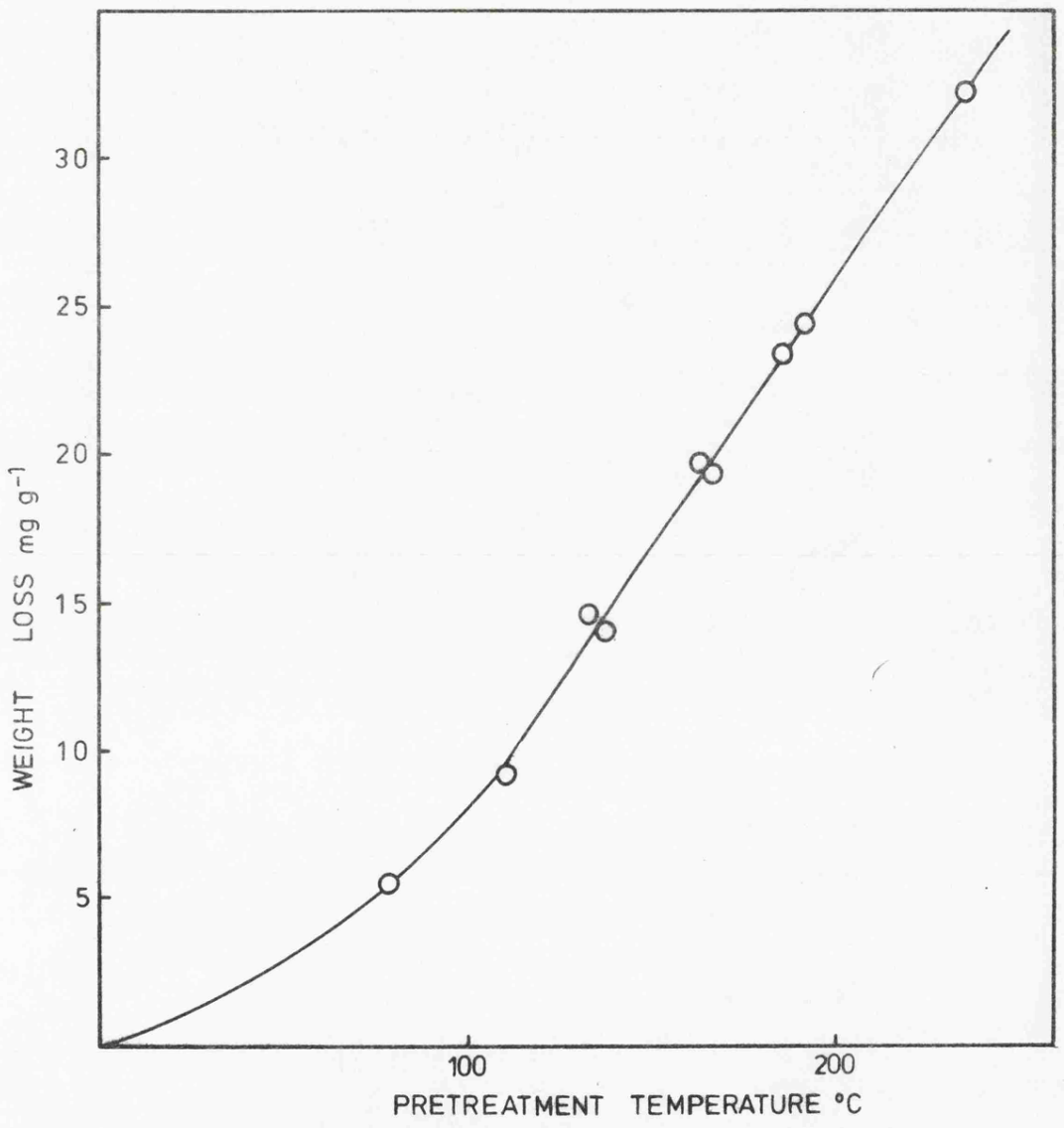

Fig.3.6 Water desorption from γ-MnO_2 during two hour thermal pretreatments.

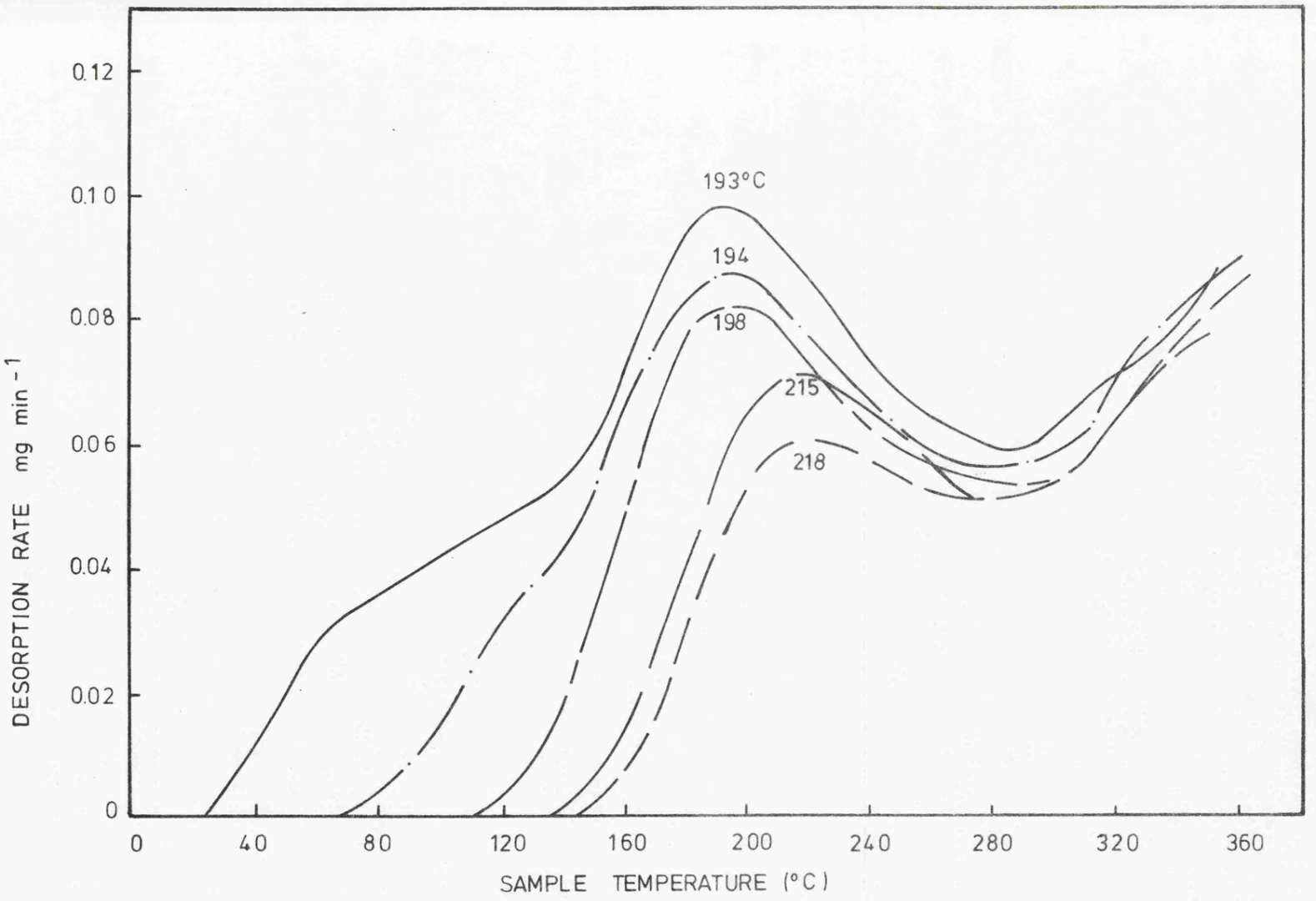

Fig.3.7 Gravimetric TPD from γ-MnO_2 after evacuating in vacuum to 6×10^{-5} Torr at room temperature followed by two hour thermal pretreatments at (——) 23°C, (— ·—) 65°C, (— — —) 108°C, (— —) 136°C and (— — —) 145.5°C.

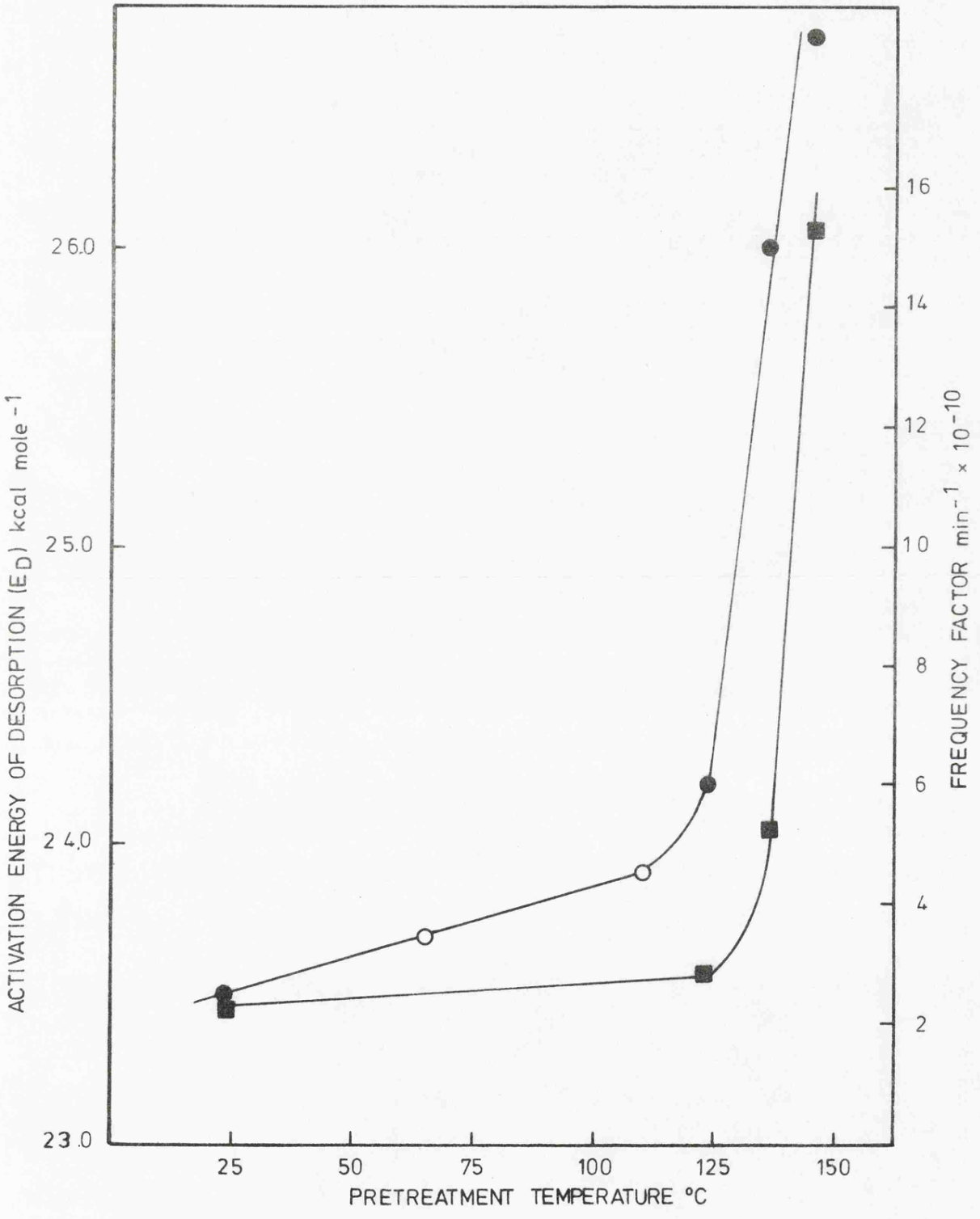

Fig.3.8 Activation energy of desorption (●) and frequency factor (■) as a function of pretreatment temperature. E_D values at 65°C and 110°C were calculated using $\nu = 2.6 \times 10^{10}$ min^{-1}. The remainder were obtained directly from the gradients in fig.3.5.

Up to 120°C E_D increases slightly due to the removal of very small amounts of Type II water. Above this temperature more substantial amounts are desorbed giving rise to increased activation energies. The dependence of ν on coverage parallels that of E_D and may reflect the presence of less mobile states. At 160°C there was an unexpected departure from linearity in the plots shown in fig.3.5. This anomaly is almost certainly a result of a dehydroxylation process which, as will be seen later, is initiated at that temperature.

In order to ascertain the dependence of E_D on coverage for Type II it is necessary to know the amount of water associated with the desorption process. Due to overlap of peaks in the TPD curve it is not possible to obtain a reliable estimate of the weight losses involved. An indirect approach has been attempted although its validity is uncertain. It can be shown[107] that

$$\frac{dn_i}{dTp} = \frac{N_{io}.\beta.E_D}{R.Tp^2.e} \qquad (3.2)$$

where $\frac{dn_i}{dTp}$ = maximum rate of desorption

N_{io} = initial coverage

β, E_D, Tp have the same meaning as previously defined

For a particular outgassing temperature the maximum rate of desorption $\frac{dn_i}{dTp}$ should be directly proportional to $\frac{\beta}{Tp^2}$, the slope of the plot providing a value of coverage if E_D is known. By comparing initial coverages for various outgassing pre-treatments the fractional coverage θ may be ascertained. Linear plots were obtained in all cases (fig.3.9). θ was determined

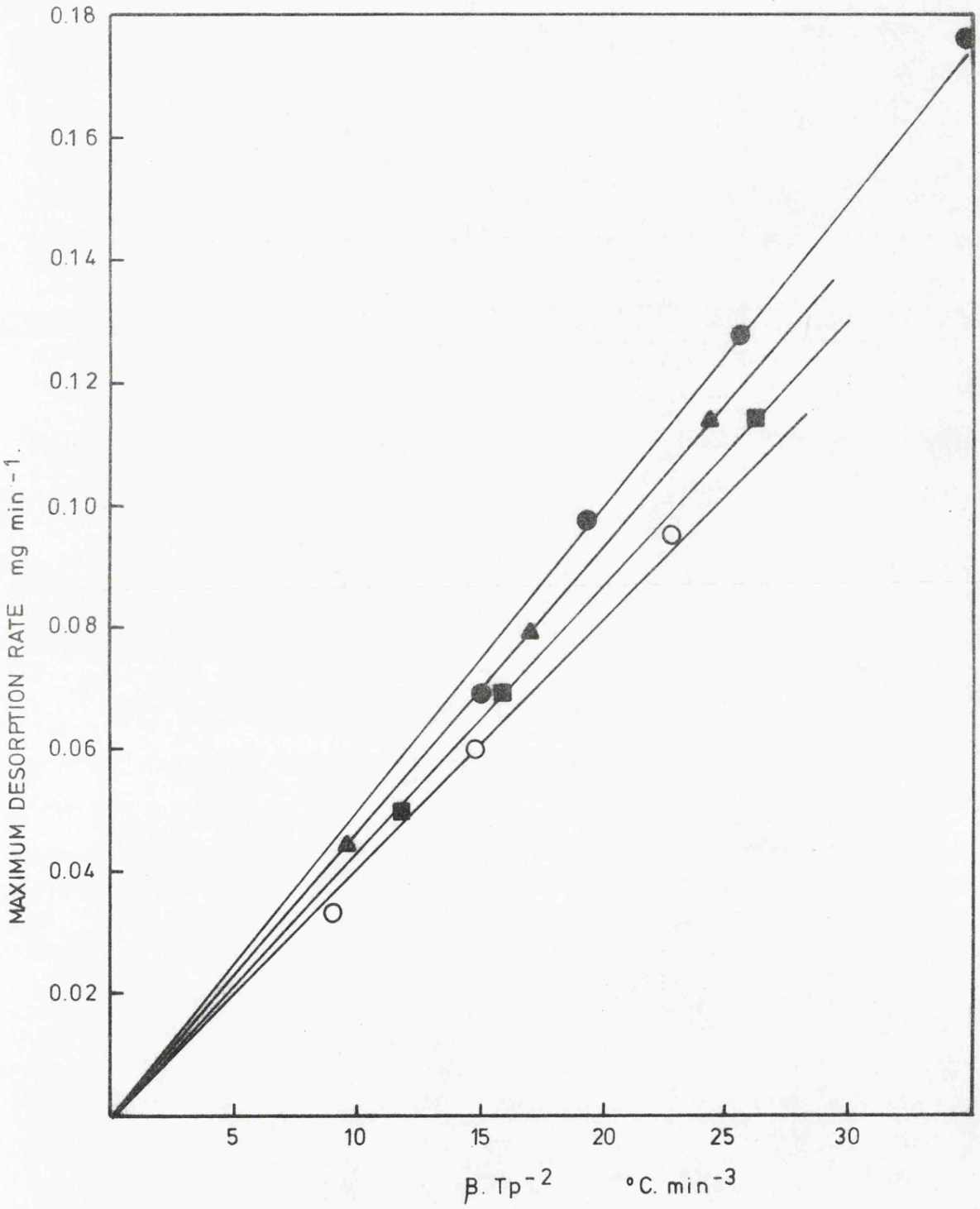

Fig.3.9 Plot of eq. (3.2). ●, ▲, ■ and O refer to 2 hour thermal pretreatments at 23°, 123.5°, 136° and 145.5°C respectively.

by inserting E_D values calculated from fig.3.5 and $\theta = 1.0$ for room temperature outgassing was assumed. Values of θ are given in Table 3.1.

TABLE 3.1

TYPE II WATER AS A FUNCTION OF OUTGASSING TEMPERATURE

Outgassing Temperature ^oC	Fraction of Type II water remaining θ
23	1.00
123.5	0.88
136	0.77
145.5	0.70

Fig.3.10 depicts the dependence of E_D on coverage using θ values from Table 3.1. An approximate linear relationship within a limited range of coverage is evident.

The amounts of water associated with Types I and II have been estimated to be 5 and 18 mg g^{-1} respectively. These figures were obtained by dropping verticals from the inflection and minima points on the corresponding rate curve to the temperature axis and integrating the included area. Although the method is somewhat inaccurate it is less subjective than deconvolution to produce individual rate curves for types I and II and subsequent integration.

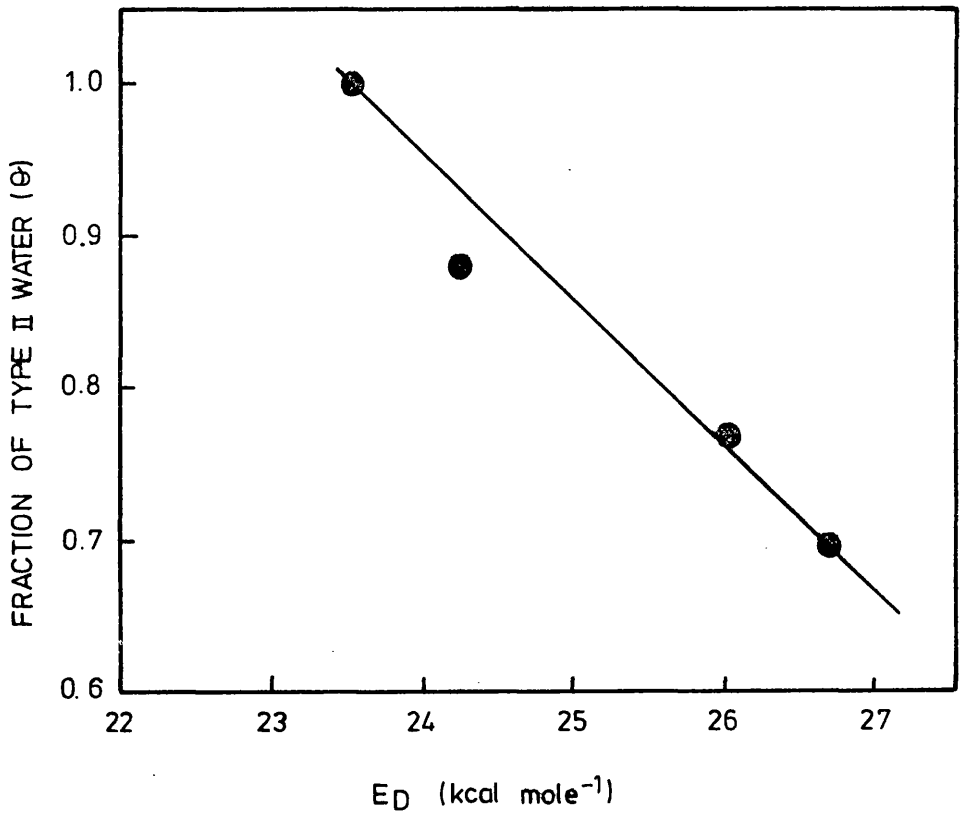

Fig.3.10 Dependence of activation energy of desorption (E_D) on coverage.

Of paramount importance in establishing the nature of this water is a knowledge of the surface structure of γ-MnO_2. Assuming an idealised γ-MnO_2 model as proposed by Bystrom[37] the structures of the low index crystal planes are readily envisaged. The choice of such planes on which a discussion may be based is partially justified by the fact that the crystals are rapidly electrodeposited which favours their production[108]. A more important factor governing the surface structure of the material is the coordination number of the metal ions[109]. In the bulk solid the manganese ions are each surrounded by six oxygen atoms. Therefore the predominating surface planes are likely to be those where the coordination of the manganese ions is kept as close as possible to six. In the 001 and 010 planes the Mn ions are four coordinate whereas in the 100 plane only threefold coordination is achieved. The 001 plane is depicted in fig.3.11. Only half of the metal ions would be accessible to surface hydration, the remainder lying at a distance ½ c below the surface and being coordinatively saturated. This results in a density of 4.3 Mn ions nm^{-2}. The maximum amount of water that could be desorbed as molecular water or as a result of a deyhdroxylation reaction from the 001 plane would be 4.8 mg g^{-1}. In an analogous manner 4.3 mg g^{-1} could be desorbed from the 010 plane. This is much less than the amount of water associated with Type II which suggests that Type II is not primarily surface water.

However, this quantity is consistent with Type I although

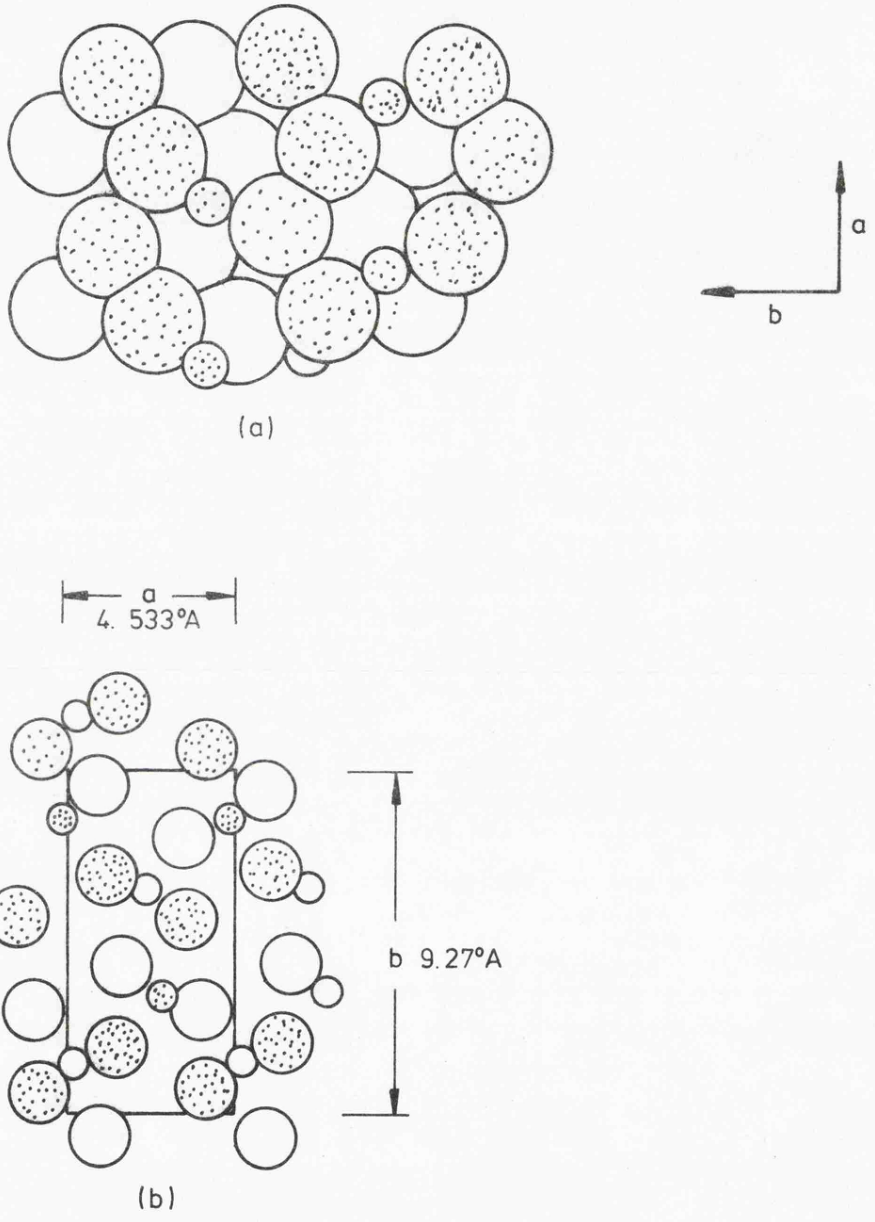

Fig.3.11 a) A packing drawing of the 001 plane of ramsdellite.

The larger circles are oxygen, the smaller manganese. The shaded circles indicate atoms at ¾c, the open circles representing atoms at ¼c. Axes 'a' and 'b' are in the plane of the paper, 'a' vertical and 'b' horizontal.

b) The 001 plane of ramsdellite. Legend as above.

the desorption temperatures indicate that this is unlikely to be associated with dissociated water or with water strongly bound to cation sites. It may well be that Type I arises from the adsorption of molecular water on to surface hydroxyl groups, the molecule being held by a hydrogen bond between the oxygen of the water molecule and the hydrogen atoms of the underlying hydroxyl groups. On many oxides[110] the surface hydroxyl groups are formed by a dissociative mechanism, the hydroxyl group of the water molecule adsorbing on the cation, and the proton forming a second hydroxyl with an adjacent surface O^{2-} ion. A layer of water on this hydroxylated surface will be localised by double hydrogen bonding and desorption temperatures of the order found for Type I would be expected. The mechanism for the adsorption of water on γ-MnO_2 which gives rise to Type I is shown in fig.3.12.

3.2. TPD in the presence of gases and water vapour

The effect of environment on the TPD curves is depicted in fig.3.13. The recordings in nitrogen and helium were very similar to that obtained in vacuum except for a slight displacement of the maximum desorption rate to higher temperatures as a result of an increase in partial pressure above the sample. The difference between nitrogen and helium is attributed to the higher thermal conductivity of the latter.

The desorption curve in oxygen was more complex. The oxygen environment suppressed the decomposition of manganese dioxide and led to the clearer resolution of a third peak at about

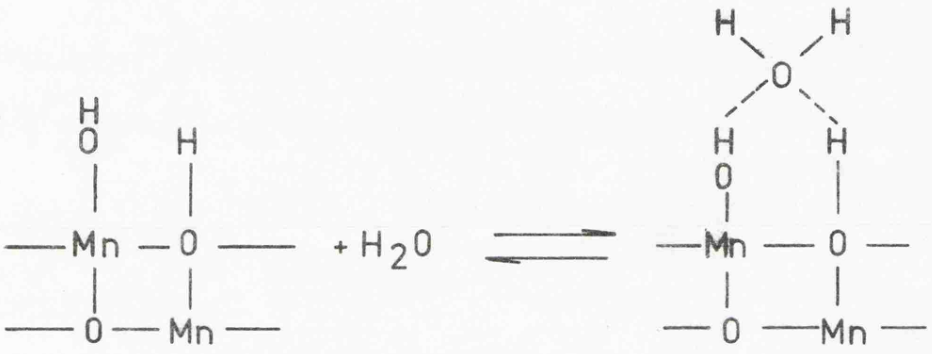

Fig.3.12 Proposed mechanism for the formation of Type I water on γ-manganese dioxide.

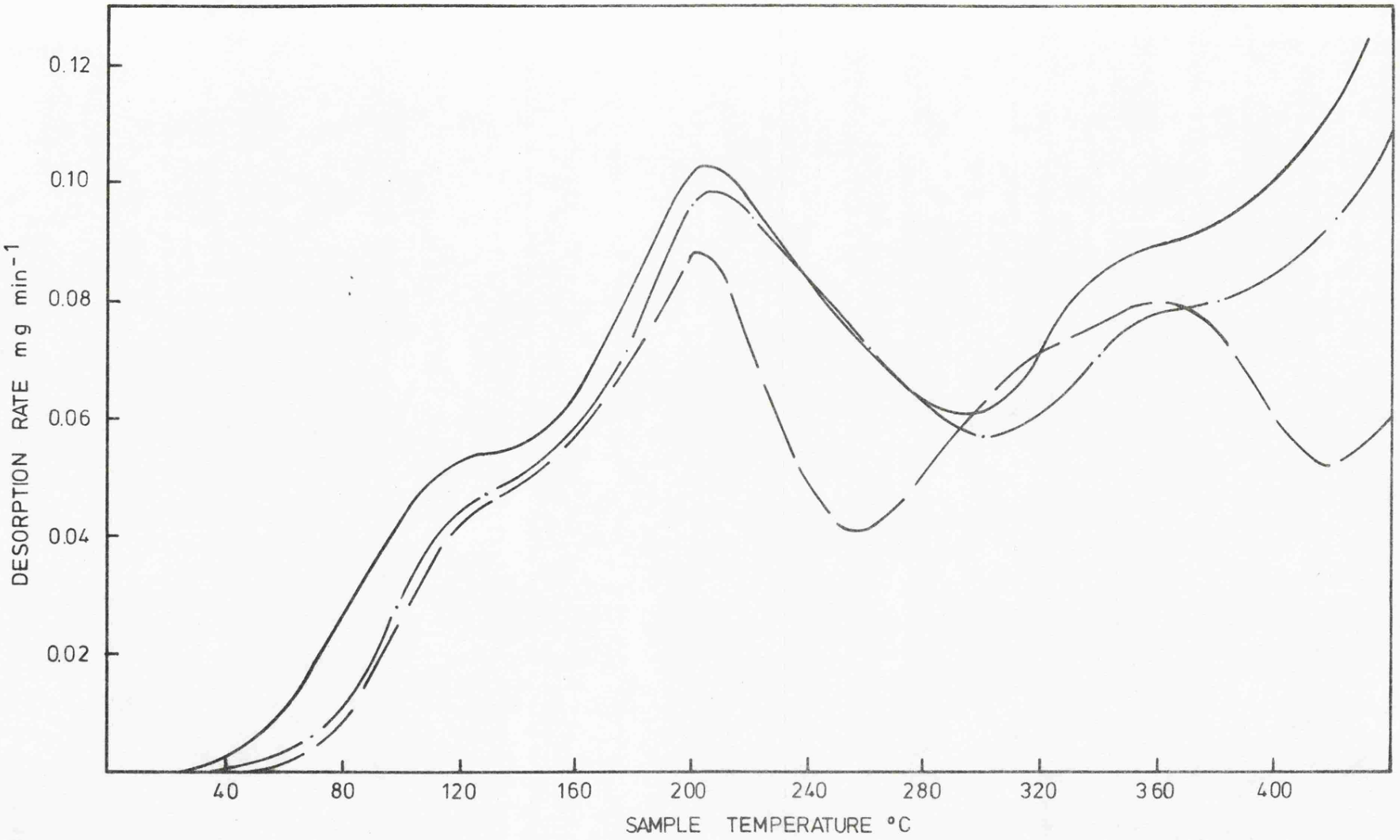

Fig.3.13 Gravimetric TPD curves of γ-MnO_2 in static environments (10 Torr) of helium (——), nitrogen (——·) and oxygen (– – –).

360°C only a hint of which was seen in the vacuum runs. Type II is also markedly affected. The desorption rate beyond Tp is considerably less than that recorded in other environments. This appears to result from oxygen uptake and additional evidence in support of this was obtained from DTA of γ-MnO_2 recorded in an oxygen atmosphere (fig.3.14). The endothermal process at 120°C in fig.3.14 corresponds to the removal of physisorbed water and the hydrogen bonded molecular water, the former not being observed in the TPD runs described earlier because of its removal during the initial outgassing treatment. Associated with the loss of Type II is an exothermic peak confirming that oxygen sorption is the probable cause of the lower rate curve around 200°C in the TPD trace. Beyond 200°C the weight loss and DTA data do not coincide. The maximum desorption rate of Type III appears as a minimum in the DTA trace whilst an exothermic shoulder at $\sim$ 270°C corresponds to the minimum between Types II and III in the weight loss curve. This suggests that Type III is not a simple desorption or decomposition process but is accompanied by other complicating factors. The final DTG and endothermic peaks mark the decomposition of manganese dioxide.

Additional information concerning Types I and II has been obtained by recording TPD curves in controlled water vapour environments. A typical TPD run recorded in 6.0 Torr ambient water vapour pressure after room temperature outgassing is shown in fig.3.15 curve a. Type I is now clearly evident whilst Type II appears to be partially resolved into two

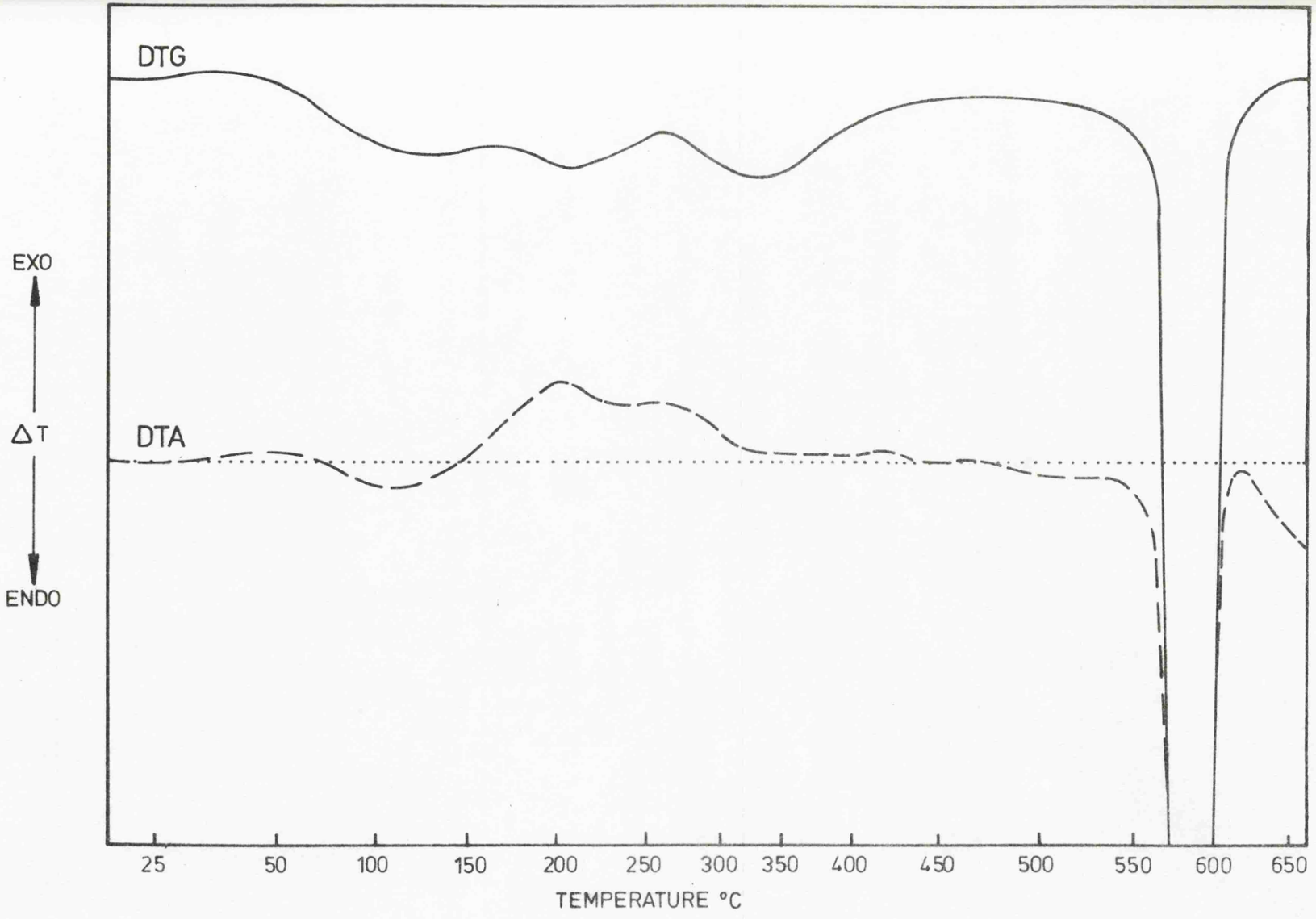

Fig.3.14 DTG and DTA runs on γ-MnO_2 in a dynamic oxygen environment. Oxygen flow rate 4ℓ hr^{-1}, heating rate 4°C min^{-1}.

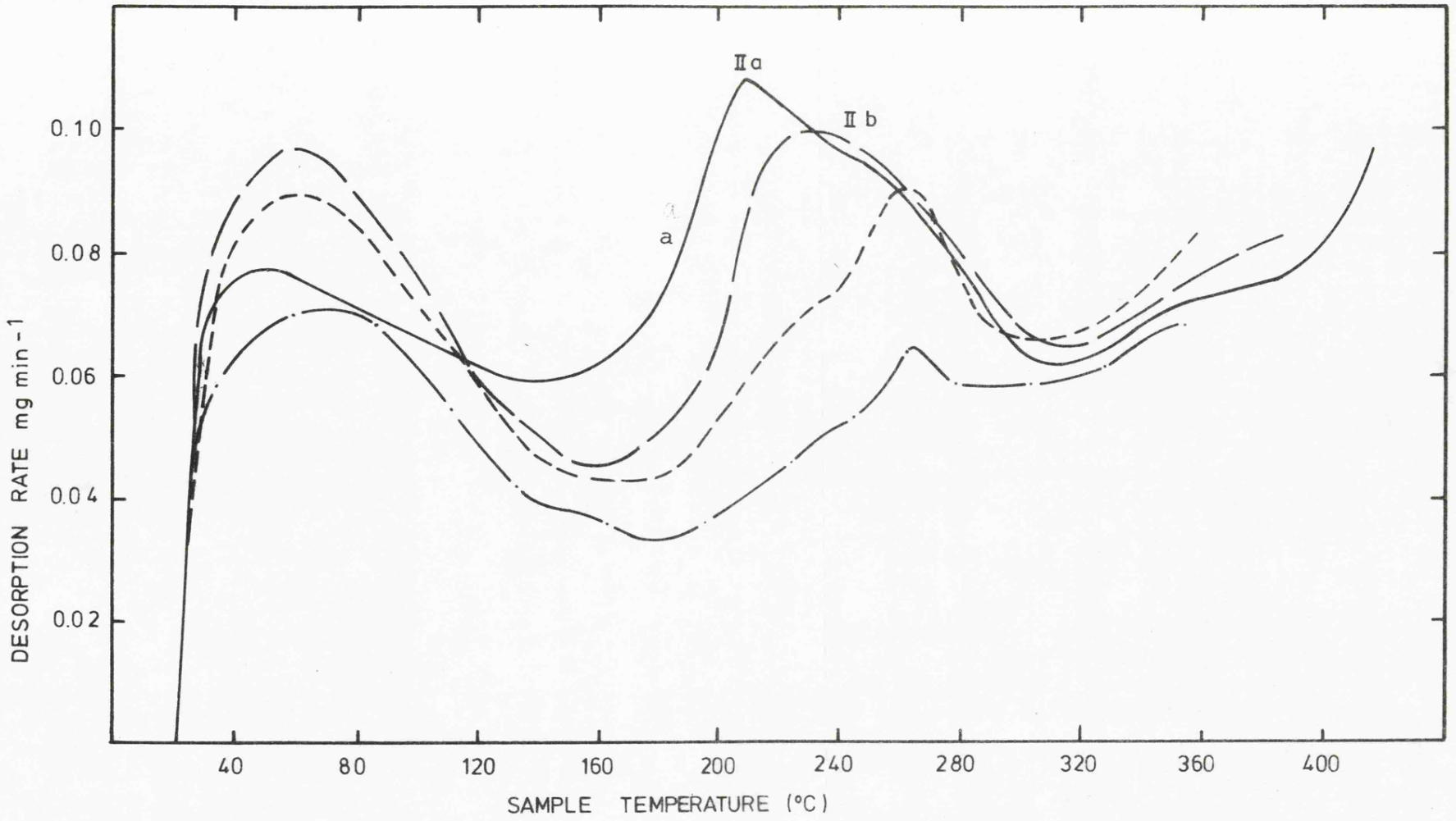

Fig.3.15 Gravimetric TPD curves of γ-MnO_2 in static environments of water vapour (6.0 Torr). Prior to TPD the samples were evacuated at room temperature to 5×10^{-5} Torr and then outgassed for a further 2 hrs. at 23°C (——), 145°C (— —), 165°C (– – –) and 191°C (— ·).

components. Increasing the water vapour pressure increased the amount of water associated with Type I whilst Type II remained unaltered (see fig.3.16). In a water vapour environment Type I is more correctly described as being made up of two species. On application of a linear heating programme physisorbed molecular water, the exact quantity depending on the pressure, is first removed followed by a monolayer of hydrogen bonded water, the two quantities being unresolved under the conditions of the experiment and observed as a single peak at about 70°C. The independence of Type II on water vapour pressure supports the earlier view of a chemisorbed entity.

Fig.3.15 also shows the effect of the pre-treatment temperature on the TPD curves. It can be seen that up to an outgassing temperature of 165°C selective removal of the water contributing to the initial part of Type II takes place leading to improved resolution of a more energetic component. Type II therefore appears to be made up of two entities which will henceforth be referred to as IIa and IIb (fig.3.15).

As mentioned earlier the weight loss associated with Type II was considerably greater than the amount required for complete surface coverage (i.e. 1 H_2O per surface Mn ion). If the water originates from the bulk of the sample (as well as from the adsorbed state) then its removal might be expected to lead to changes in surface area. The surface area obtained by nitrogen adsorption on samples degassed and subjected to the various two hour thermal pre-treatments prior to TPD are

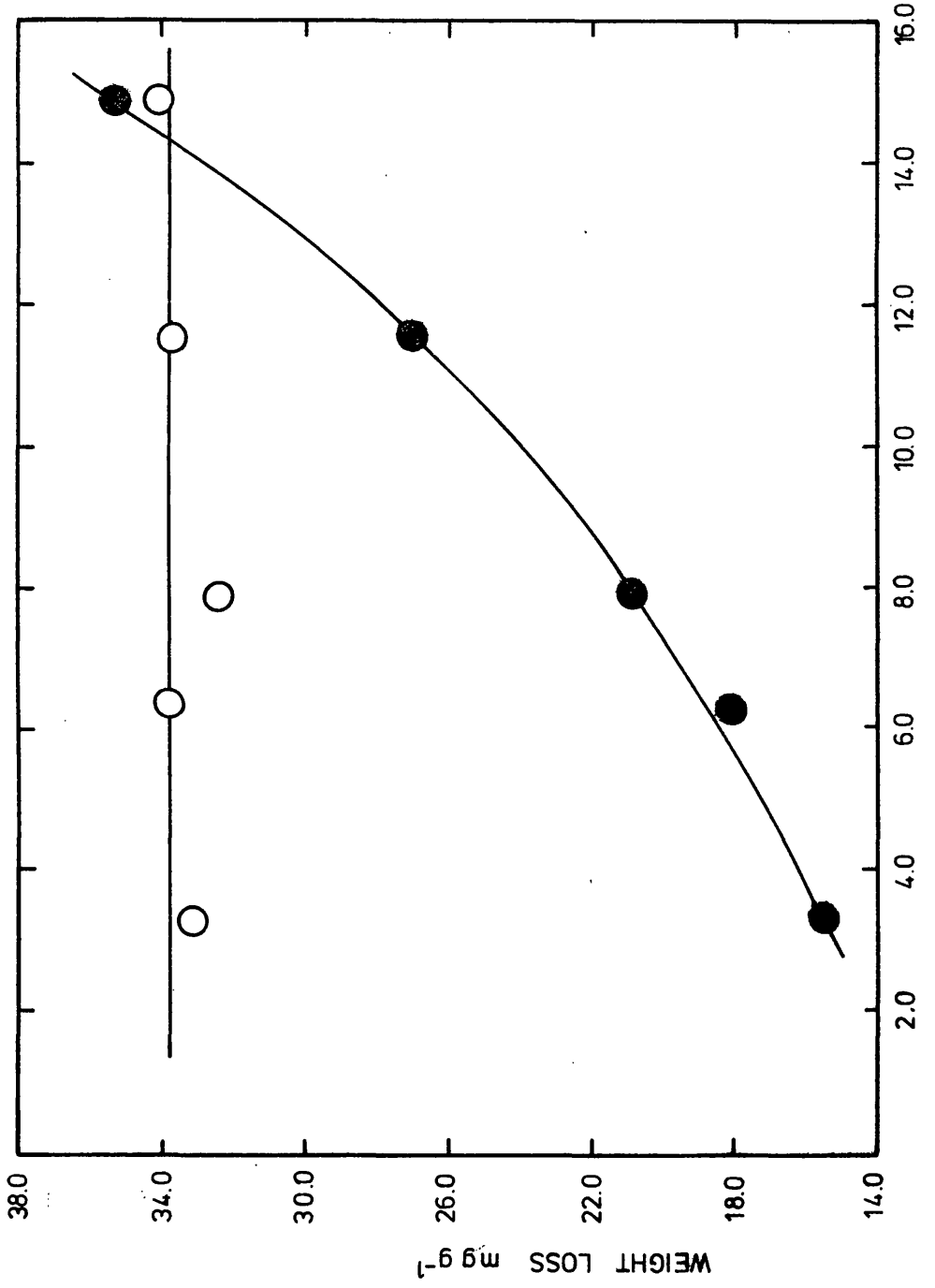

Fig.3.16 Dependence of type I (●) and type II (○) on water vapour pressure.

depicted in fig.3.17. Between ambient outgassing and 160°C the change in surface area follows a similar path to that of activation energy of desorption and frequency factor. Up to 120°C very little change is apparent in surface area, the primary effect of these pre-treatments being the removal of physisorbed water. Between 120° and 160°C the increase in surface area is concurrent with the removal of IIa water. α_s plots obtained by analysis of the nitrogen adsorption data are shown in fig.3.18. Up to 160°C the changes in surface area may be ascribed to the development of an external surface whilst at higher temperatures of pre-treatment (>160°C) the increase in surface area results from the generation of a micropore volume which is apparently associated with the removal of the more energetically bound Type IIb.

The energy of desorption from Type IIa is 23.5 kcal $mole^{-1}$ which is consistent with IIa being ascribed to either bulk molecular water or water dissociatively chemisorbed on coordinatively unsaturated manganese and oxygen surface sites. However, several important features have emerged from this study which are not in agreement with IIa being ascribed to a surface species. The disappearance of Type IIa after outgassing treatments at 145° and 165° is associated with an increase in surface area. In addition the water loss is greater than that expected for a chemisorbed monolayer and the constancy of the BET 'c' value for nitrogen adsorption below 165°C outgassing (fig.3.17) suggests that the state of surface hydroxylation has not been drastically affected[81, 111] by the removal of IIa water. Finally the water cannot be

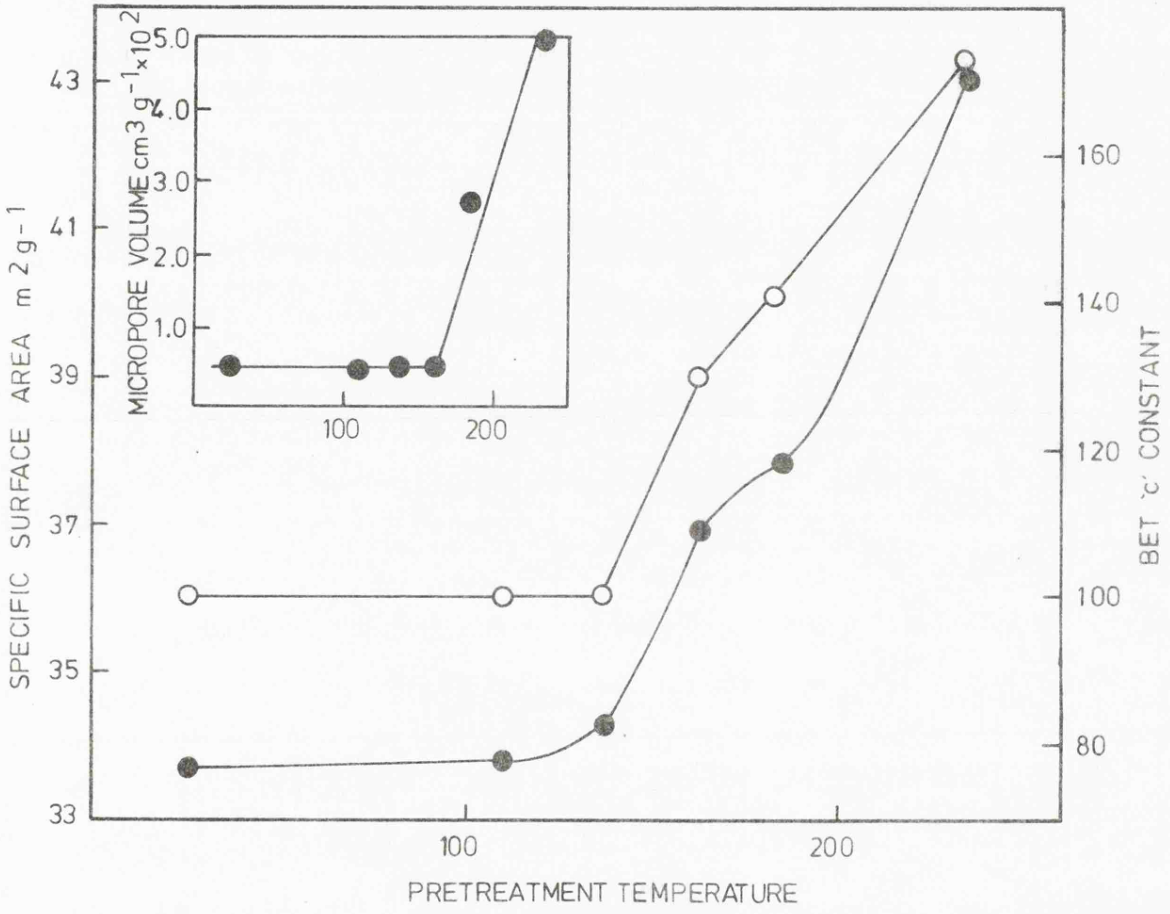

Fig.3.17 BET area (●) and 'c' constant (O) as a function of pretreatment temperature. Insert - micropore volume as a function of pretreatment temperature.

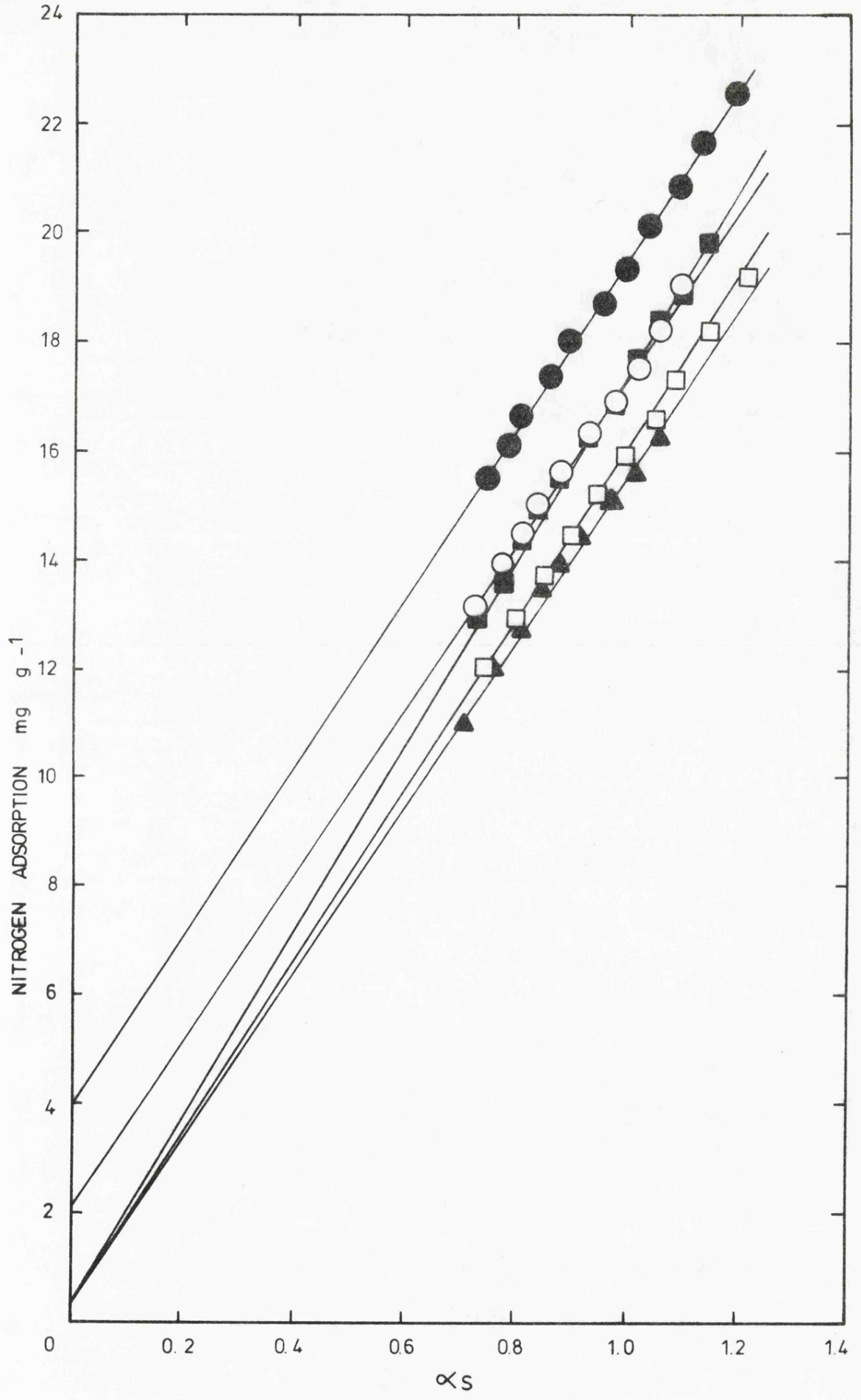

Fig.3.18 α_s plots for nitrogen adsorption on γ-Manganese dioxide pretreated at 110°C (Δ), 137°C (□), 163°C (■), 185°C (○) and 235°C (●).

replaced by re-exposure to water vapour. All of these features indicate that Type IIa water is coming primarily from sub-surface layers. The nature of IIa water, although contained within the bulk of γMnO_2, must however be speculative. It is possible that during preparation water molecules 'dissolve' in γ-MnO_2 (as has been suggested for silica[112]) or are trapped inside the structure in some other manner as a result of the preparative procedure.

On outgassing γ-MnO_2 at temperatures > 165°C a microporous structure is exposed (Fig.3.17 inset). This may arise from the progressive emptying of fine pores within the crystallites or result from the removal of hydroxyl groups which may be present in our sample. Although the temperature is on the high side for the desorption of molecular water from micropores Gammage, Fuller and Holmes[111] found that tenaciously bound micropore water in ThO_2 required temperatures in the region 200-400°C to remove it. Stronger evidence against IIb being micropore water in the accepted sense is its irreversibility and the volume generated by its removal. The nitrogen α_s plot indicates that between 165° and 235°C outgassing pre-treatments a micropore volume of $\sim$ 5 $\mu l g^{-1}$ is generated. Taking the density of water as 1.0 g cm^{-3} the maximum amount of water that can be contained in this volume is 5 mg g^{-1} which is considerably less than the observed weight loss even allowing for the fact that IIa is desorbing at the same time.

3.3. TPD of chemically reduced γ-MnO_2

Brouillet, Grund, Jolas and Mellet[47] have previously shown by TG, that the products obtained by the chemical reduction

of γ-MnO_2 produced a smaller weight loss in air than in vacuum. This was attributed as outlined on p.17 to the thermal behaviour of the MnOOH component. It was not possible to compare the decomposition temperature of MnOOH recorded by Brouillet et al with that of Type II owing to the low sensitivity employed by these authors. In order to establish whether Type II was due to a dehydroxylation reaction, controlled amounts of hydroxyl groups were introduced into the γ-MnO_2 structure as outlined in the experimental section. TPD curves recorded in 6.0 Torr of water vapour are shown in fig.3.19. As the hydroxyl content increased, Type II greatly increased in extent whilst at the same time the desorption process beyond Type II was suppressed. The peak temperatures for Type II (Table 3.2) corresponded with the temperature of Type IIb for the 'as-received' sample. Type IIb is therefore associated with the removal of surface and bulk hydroxyls since its population is directly related to the degree of reduction of the manganese dioxide.

TABLE 3.2

VARIATION OF PEAK TEMPERATURE (Tp) WITH SAMPLE COMPOSITION FOR TYPE II

x in MnO_x	Tp(^{o}C)
1.946	210
1.931	243
1.908	239
1.870	243
1.825	245

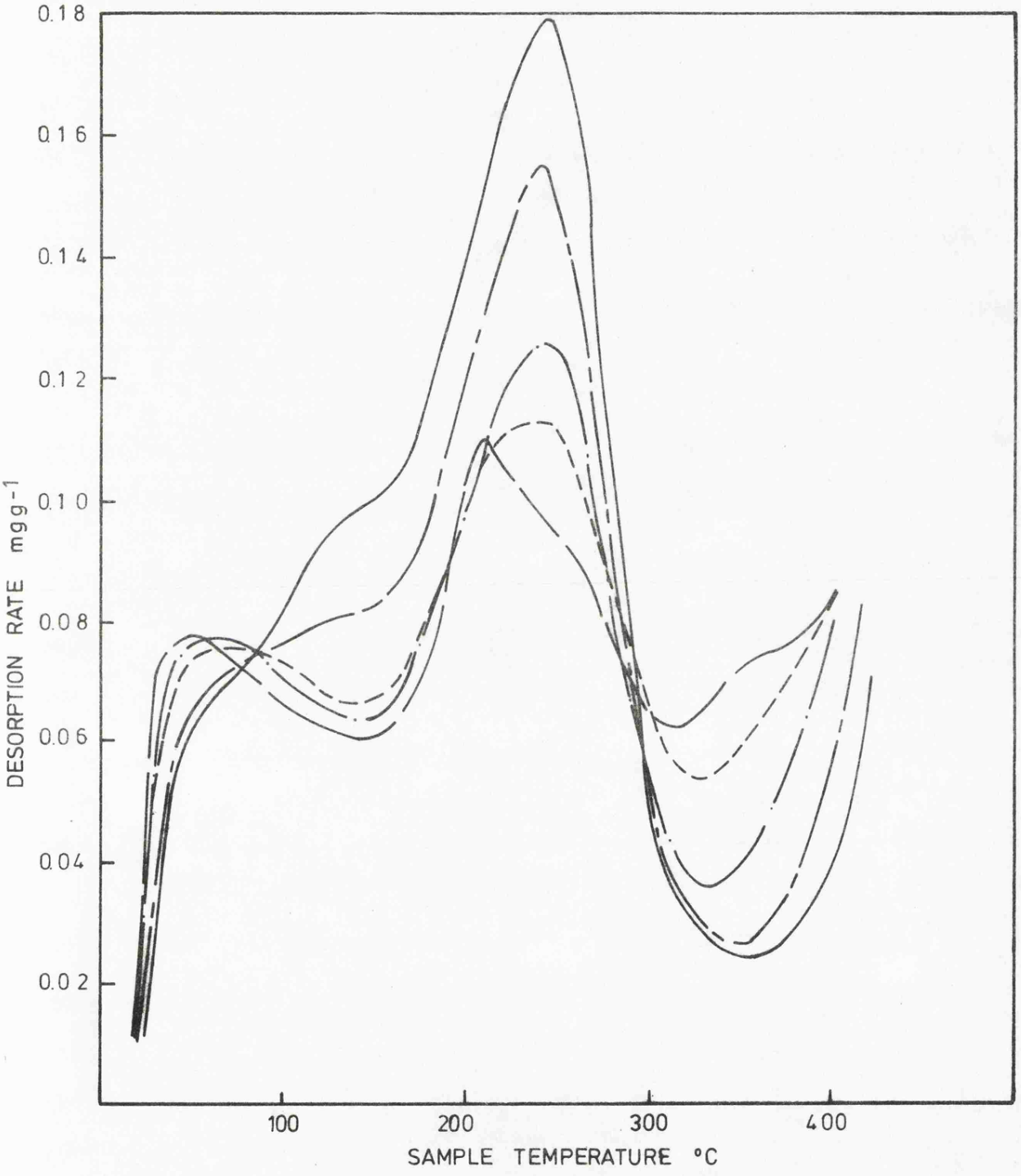

Fig.3.19 Gravimetric TPD curves in a static water vapour environment (6.0 Torr) of partially reduced γ-MnO_2.x in MnO_x = 1.946 (— —), 1.931 (– – –), 1.909 (——·), 1.870 (—— –) and 1.825 (—— –).

A dehydroxylation process from within the bulk will be a disruptive process and probably accounts for the generation of the micropore volume on outgassing above 165°C. Although no gas adsorption measurements were made Lima-de-Faria[113] observed that dehydration of goethite (α-feOOH) and diaspore (α-AlOOH) led to a well developed pore system. More recent work by several authors[77, 98, 114] using gas adsorption data has shown that the removal of hydroxyl groups from the interior of a solid leads to the generation of a microporous network.

The suppression of the rate curve beyond Type IIb (Fig.3.19) results from the partial replacement of MnO_2 by MnOOH. This leads to less oxygen loss from the composition change $MnO_2 \rightarrow Mn_2O_3$. As the degree of reduction increases a new shoulder appears at 120°-140°C in the TPD curves between Type I and Type II. This is very similar in position to the shoulder present on Type II in vacuum runs and which was ascribed to hydrogen bonded molecular water. It is also found at a similar temperature to a water state described by Munuera[106] which appeared after water adsorption on a sample of TiO_2 that had undergone surface reduction. Fig.3.19 shows that as this new state develops with the degree of reduction so less physisorbed water (peak at 70°C) is lost. It might be expected that surface hydroxylation would increase as the degree of reduction increases leading to a more ordered state (i.e. more hydrogen bonding) in the adsorbed water.

3.4. TPD from synthetic γ-MnO_2

Having established that Type II is comprised of two components IIa and IIb, the quantity of the latter being directly proportional to the sample composition, it was of interest to know if IIa was dependent on composition and an essential part of the γ-MnO_2 structure. TPD curves were obtained in vacuum and oxygen (10 Torr) from a synthetic γ-MnO_2 and are shown in fig.3.20. Both were similar to traces obtained from the electrodeposited sample. In vacuum the main desorption peak was observed at 245^{o}C and was preceded by a shoulder at $\sim$140^{o}C. In oxygen a Type III peak was evident at 360^{o}C and the peak width of Type II narrower compared to the vacuum study. In vacuum integration of the area beneath the TPD curve up to the minimum immediately following Type II provides an estimate of the weight loss associated with the removal of types I + IIa + IIb. In oxygen the same procedure gives very nearly the weight loss for types I + IIa. An estimate of the amount of IIb can be obtained by subtracting the weight loss in oxygen from the weight loss in vacuum. This assumes that in oxygen the water loss associated with the dehydroxylation reaction (IIb) is exactly annulled by the uptake of oxygen. Equation (1.3) shows that the ratio of water loss to oxygen gain is 36:32. The amount of IIb obtained from the TPD runs has to be multiplied by the factor 9/8 to obtain a more exact value. Subtracting this from the weight loss in vacuum provides a value of Type (I + IIa). Applying this procedure to the TPD data from the synthetic and electrodeposited γ-MnO_2 the amounts of Types I + IIa are

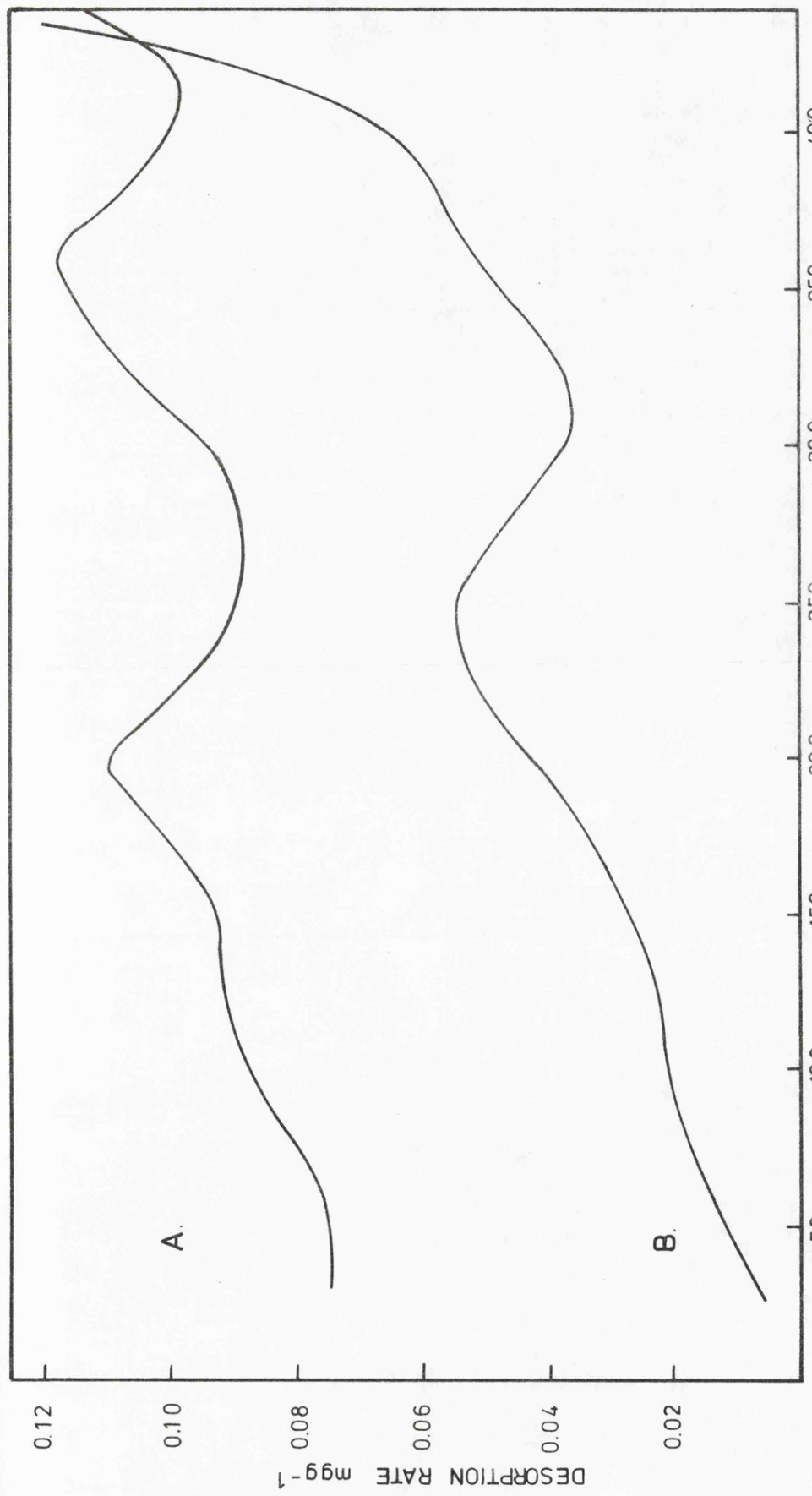

Fig.3.20 Gravimetric TPD curves of synthetic γ-MnO_2 in (A) oxygen (10 Torr) (B) vacuum. The curve in oxygen is offset by 0.07 mg g^{-1}.

8.7 and 22.8 mg g^{-1} respectively. As approximately 5 mg g^{-1} of Type I is adsorbed on the commercial sample the amount of water associated with IIa is of the order of 18 mg g^{-1}. The amount of Type I adsorbed on the synthetic sample is not known with certainty but nevertheless the amount of IIa is clearly considerably less than on the other sample. As the composition of the samples are similar it is unlikely that there is any relationship between Type IIa water and Mn(IV) or Mn(III) content. It can also be shown that γ-MnO_2 is capable of existence in the absence of this sub-surface molecular water. Heating the synthetic γ-MnO_2 in oxygen to 280°C removes IIa water. An X-ray diffractometer trace of the product confirmed a γ-MnO_2 structure which tends to suggest that IIa water is not an integral part of the structure but merely water trapped in some manner in the material during preparation.

3.5. Further investigations of the Type III feature

Interpretation of the shoulder present in the vacuum TPD traces from γ-MnO_2 (Fig.3.1) between the removal of Type II water and the decomposition of MnO_2 was difficult. This feature appeared as a peak in TPD traces recorded in oxygen (fig.3.13) and was designated Type III. Analysis of the desorption products obtained from the decomposition of γ-MnO_2 in vacuum did not provide an obvious explanation as to the nature of Type III. Although loss of water and oxygen were taking place in the region of 360°C it was considered that their release was spread over too wide a temperature interval to enable a peak to be observed in the TPD trace. A thermal hygrometric technique has been used successfully

in these laboratories for a number of years to establish the temperature range in which water is released from various types of manganese dioxides used in the battery industry. This technique has been comprehensively described by Hitchcock and Pelter[115] and in essence involves passage of the volatiles released by application of TG through an electrical hygrometer. Water present is electrolysed and the current produced, which is proportional to the water content, is recorded continuously as a function of sample temperature. This technique has an advantage over mass spectrometric analysis in the present situation as the run can be carried out in an oxygen environment. The curve obtained by application of this technique to γ-MnO_2 is shown in fig.3.21. It can be seen that Type III is comprised of two components, the water peak at $320^{o}C$ in the thermal hygrometric trace corresponding to the lower temperature component of Type III.

It was not known with any degree of certainty whether Type III occurred as a result of an impurity present in the electro-deposited sample or was a characteristic common to all manganese dioxides. The only impurity present in the concentration needed to produce this weight loss ($\sim$ 20 mg g^{-1}) was carbon but addition of increasing amounts of this contaminant did not enhance the weight loss. Examination of the TPD curve of the synthetic γ-MnO_2 reported earlier showed that a Type III peak was also present albeit of lower intensity (9.1 mg g^{-1}). Type III was unlikely therefore to be associated with any impurity as the preparative route for the two samples differed. A number of other manganese dioxide samples were investigated

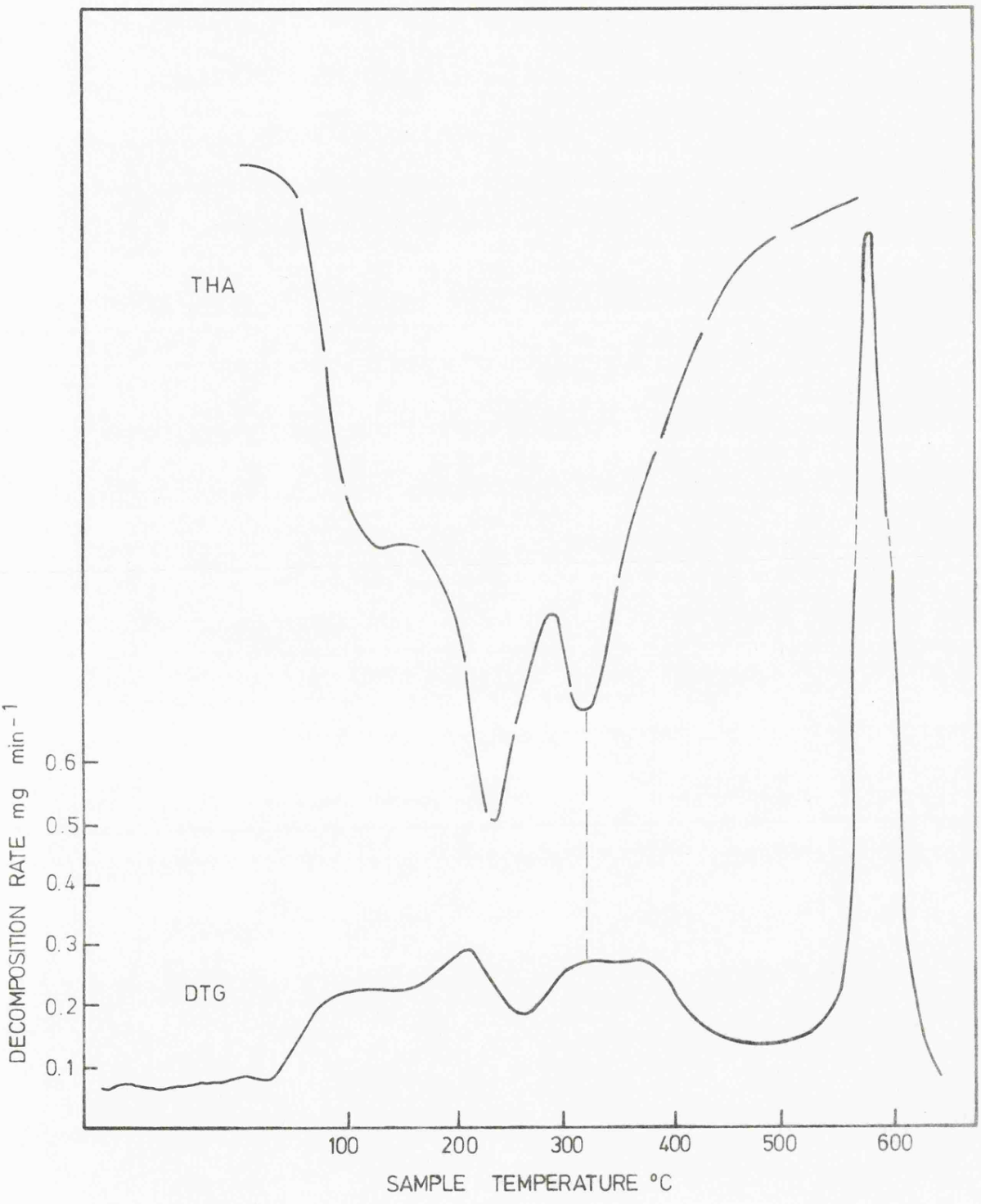

Fig.3.21 Thermal hygrometric and DTG curves of γ-MnO_2 in a dynamic oxygen environment (760 Torr). The abscissa for the DTG curve is as indicated, that of the THA is arbitrary.

in an effort to throw more light on the nature of Type III (see fig.3.22). Unfortunately because of impurity effects and the uncertain composition of some of the samples it was not possible to establish from these traces whether Type III was present in all γ-manganese dioxides. However, it was evident that Type III was absent from β-manganese dioxides.

Additional experiments to determine the nature of Type III were carried out using the synthetic γ-MnO_2 as better definition of the feature was available. X-ray diffractometer traces of the products obtained by heating γ-MnO_2 in oxygen to temperatures corresponding to the onset and completion of Type III showed a reasonably well crystallised γ-MnO_2 and a developing β-MnO_2 structure respectively. A thermal transformation from γ→β-MnO_2 has been observed by other authors[116, 117] but there are no reports of this being accompanied by a simultaneous loss in weight. Chemical analysis of the products indicated a change in sample composition from $MnO_{1.98}$ prior to the removal of Type III to $MnO_{1.91}$ on completion. The loss of oxygen expected from this compositional change (13 mg g^{-1}) was in very good agreement with the weight loss obtained by integration of the area beneath the TPD peak. This was indicative of oxygen removal being the only species contributing towards Type III for the synthetic γ-MnO_2.

It is interesting to note that values of x in MnO_x for β phase manganese dioxides are almost without exception very close to 2.0 and therefore a weight increase in going from γ → β-MnO_2 would be the expected reaction path. It is

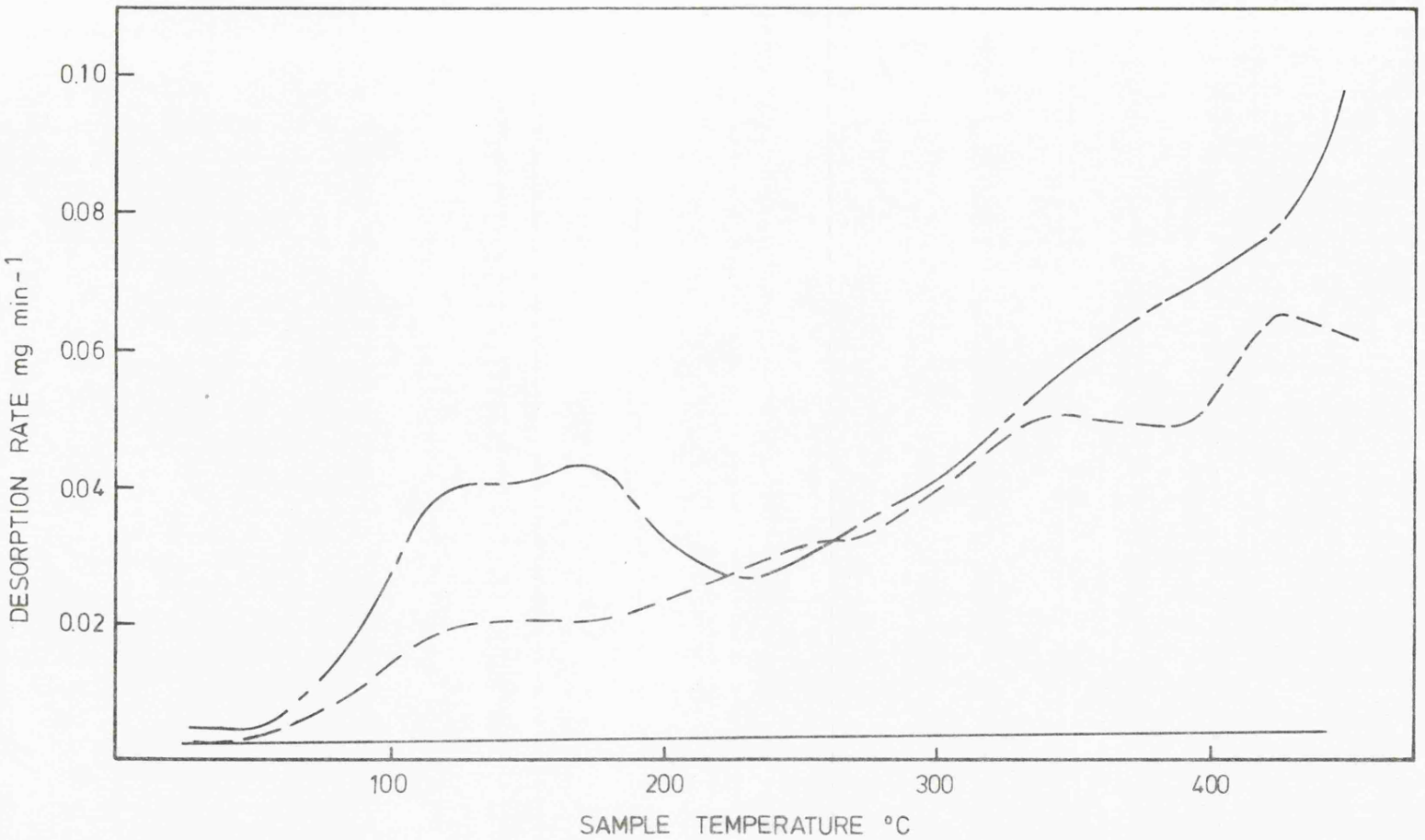

Fig.3.22 TPD curves of a commercial chemically precipitated γ-MnO_2 (——·—), naturally occurring gamma ore from Ghana (— — —) and a synthetic β-MnO_2 (———).

tempting to suggest that as the X-ray data is indicative of β-MnO_2 and that as the sample composition corresponds to $MnO_{1.91}$ a crystallographic shear (CS) phase has been produced. The term crystallographic shear was first applied by Wadsley[118] and is a means by which oxygen deficiency in an oxide can be accommodated by insertion of planar faults across which the normal cation-anion coordination is modified. One compound that has been studied extensively is rutile and to date two series of ordered structures described by the formula Ti_nO_{2n-1} have been obtained by elimination of oxygen[119]. When n = 4-10 crystallographic shear occurs at the 121 planes and the normal edge sharing of the TiO_6 octahedra is replaced by face sharing. The elimination of oxygen leads to a change in the oxidation number and ionic radius of the cation. For CS to occur in rutile like compounds the tervalent metal must be capable of forming a stable trivalent metal oxide[120]. Of the first row transition metal oxides which possess a rutile structure, CS structures have been reported for Ti, V and Cr. These metals all form a trivalent oxide possessing a corundum type structure, the electron configuration of the cations being d^1, d^2 and d^3 respectively. It is worth noting that β-MnO_2 has a rutile type structure. It also forms at least one stable trivalent oxide and probably another metastable variety which possesses a corundum type structure (see Chapter 5). Although CS systems based on MnO_2 have not been reported previously it may be that $MnO_{1.91}$ (i.e. the stoichiometry of the sample on removal of Type III) is a member of a homologous series based on β-MnO_2. Evidence

is presented in Chapter 5 which adds additional support to the possible existence of CS phases in manganese oxide systems. It must be added that when chemical analysis was repeated on the thermally produced samples the composition after removal of Type III was $MnO_{1.99}$ indicating that in this instance oxygen uptake had readily taken place.

An identical set of experiments were performed on the electrodeposited sample and similar results obtained although these did not provide such convincing evidence for the existence of CS. X-ray diffraction data confirmed the formation of γ and β-MnO_2 before and after removal of Type III respectively. The analytical composition of the samples was $MnO_{1.96}$ and $MnO_{1.93}$ respectively, which failed to account for the whole of the weight loss associated with Type III. It appears therefore that in the case of the synthetic γ-MnO_2 Type III can be ascribed solely to the removal of oxygen as a result of the thermal transformation from $\gamma \rightarrow \beta$-MnO_2 and which satisfactorily accounts for its absence from β-MnO_2. In the electrodeposited sample Type III is probably made up of oxygen from the $\gamma \rightarrow \beta$-MnO_2 conversion and water originating from an unknown source.

The release of oxygen during the γ-β MnO_2 transition provides a possible explanation of the complex DTA trace of γ-MnO_2 shown in fig.3.14. In the temperature region 250-360^{o}C the weight loss peaks are not coincident with those in the DTA curve. β-MnO_2 is the thermodynamically stable phase of manganese dioxide and it is reasonable therefore to expect that the γ-β MnO_2 transformation would be an exothermic

process. Accompanying this change would be the loss of oxygen which would be an endothermic reaction. The two processes appear to annul each other which results in the absence of a peak in the DTA trace when there is a maximum in the DTG curve.

CHAPTER 4

Chemically Reduced γ-MnO_2

4.1 TPD in vacuum and oxygen

Gravimetric TPD curves of the products obtained by the introduction of controlled amounts of hydroxyl groups into the γ-MnO_2 lattice were discussed in the previous Chapter. These were recorded in a static water vapour atmosphere and this study has now been extended to vacuum and oxygen environments (10 Torr). The TPD curves recorded in vacuum are shown in fig.4.1. As expected the increase in height of Type II was directly proportional to the hydroxyl content. The curves were similar to those obtained in water vapour except for obvious differences prior to the desorption of Type II, this being due to physisorbed water present in a water vapour environment being removed by room temperature evacuation before commencing a vacuum run.

The TPD curves recorded in oxygen are illustrated in fig.4.2. Several interesting features are immediately apparent. In the region of 200^{o}C there is no dependence of peak height on the degree of reduction as was found in vacuum and water vapour. This situation arises because the MnOOH component rather than decomposing to Mn_2O_3 as in an inert environment oxidises to MnO_2, this reaction path being independent of the degree of reduction (see eq. {1.3}). Type IIa water which has been shown to be sub-surface molecular water would not be expected to be influenced to any extent by the degree of reduction. However, it appears that a part of Type IIa is removed during chemical reduction as the TPD

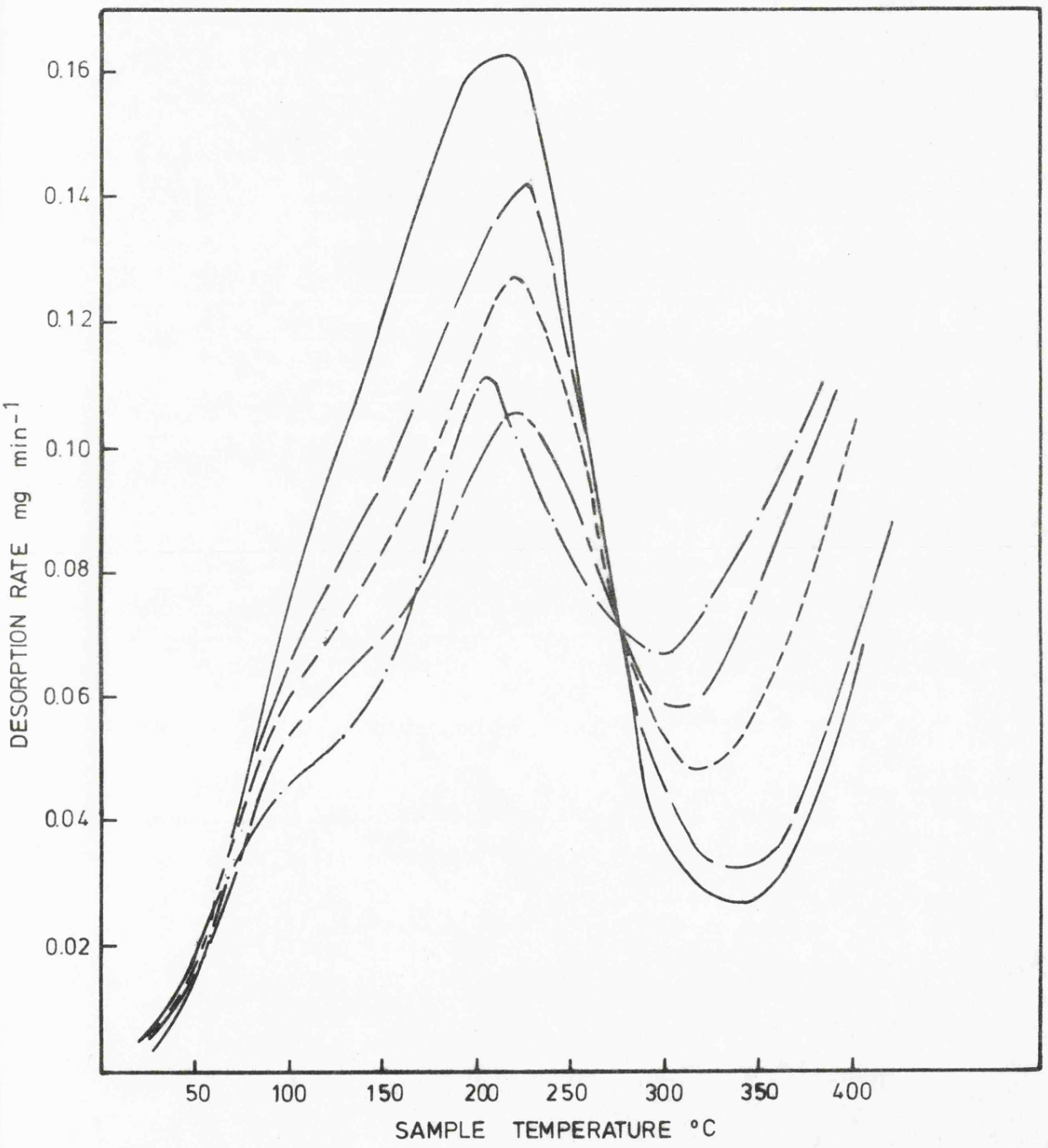

Fig.4.1 Gravimetric TPD curves in vacuum of partially reduced γ-MnO_2.x in MnO_x= 1.946 (——·), 1.931 (— — —), 1.909 (- - -), 1.870 (— · —) and 1.825 (———).

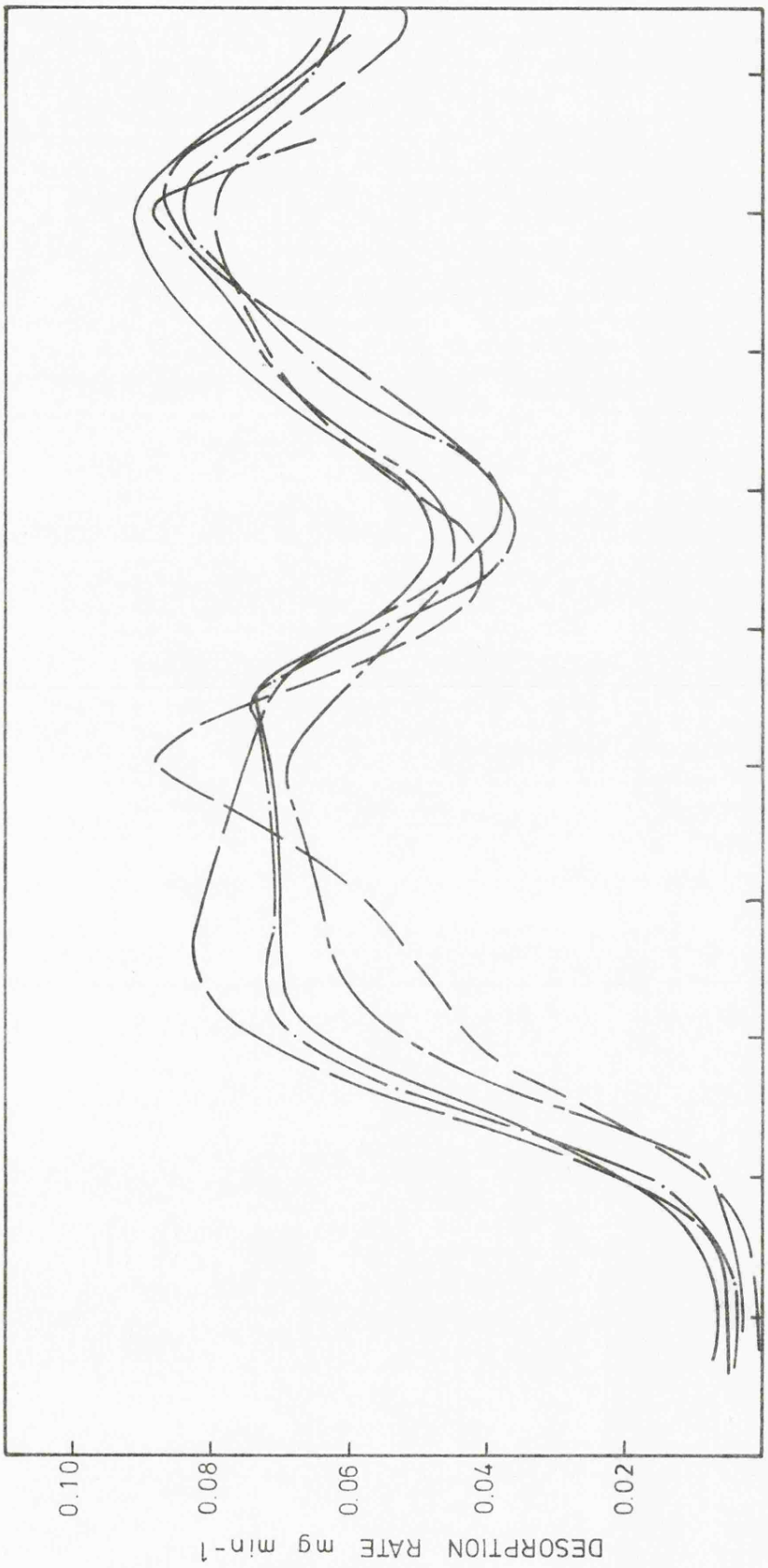

Fig.4.2 TPD curves of partially reduced γ-MnO_2 in a static oxygen atmosphere (10 Torr). x in MnO_x = 1.946 (— — —), 1.931 (——— —), 1.909 (———), 1.870 (——— • ———) and 1.825 (——— ———).

curve for the 'as-received' sample differs from its reduction products in the region of IIa. Observation of IIa is complicated by a low temperature shoulder which is dependent on sample composition. This corresponds to the water state that appeared at 120-140^{o}C in the TPD runs recorded in water vapour.

Depicted in fig.4.3 are the weight losses associated with the desorption processes in the various environments. These were taken directly from the TG traces and were the losses recorded from the commencement of the heating programme (ambient temperature) up to the temperature corresponding to the minimum following Type II in the TPD trace. The desorption processes taking place within this temperature range depends upon the nature of the environment. The observed linear relationships between the loss in weight and degree of reduction for vacuum and water vapour runs reflects the increase in hydroxyl content of the solid with increase in the state of reduction. They are nearly parallel to each other because the desorption processes making up the TPD curve are the same in water vapour as in vacuum except that in the former weakly held physisorbed water is also removed. The vertical separation between the lines represents the amount of physisorbed water on the sample at an ambient water vapour pressure of 6.0 Torr and corresponds to about 16 mg g^{-1}.

Compared to studies recorded in an inert environment the weight losses in oxygen are lower and nearly independent of the degree of reduction. This is a result of the thermal

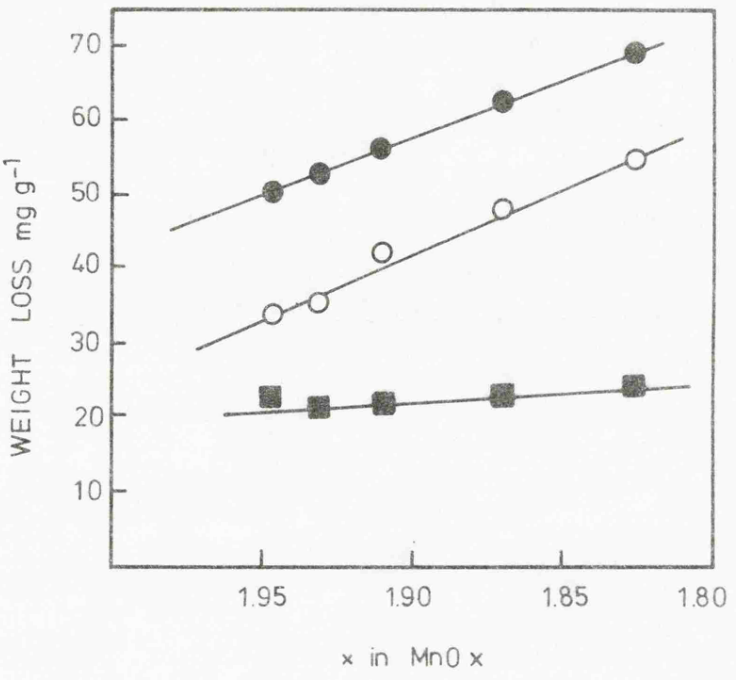

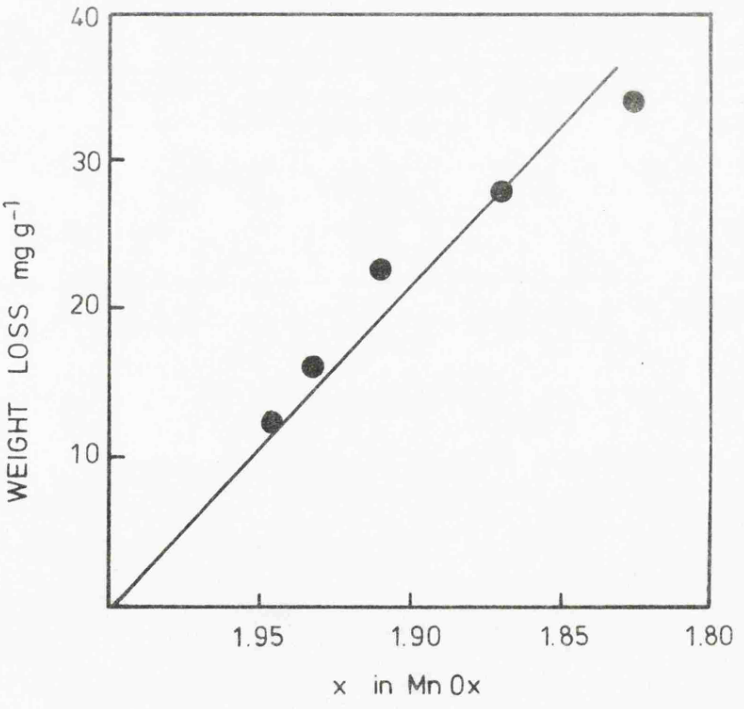

Fig.4.3 Top. Weight losses associated with the decomposition of the chemical reduction products of γ-MnO_2 in (●) water vapour (6.0 Torr), (Θ) vacuum and (■) oxygen (10 Torr).

Bottom. Water loss due to dehydration of MnOOH as a function of sample composition. (——) theoretical loss calculated from the sample composition. (●) experimental points.

behaviour of MnOOH in the oxidising atmosphere. A measure of the water loss expected from the decomposition of the MnOOH component can be obtained from the separation between the vacuum and oxygen recordings in the same way as was described earlier for γ-MnO_2 (see p.95). The results are shown graphically in fig.4.3 and compared with the theoretical values calculated from the sample composition assuming that each Mn(III) ion is associated with one hydroxyl group. The agreement is seen to be satisfactory.

All of the TPD curves in oxygen contained a desorption peak in the region of 360°C which has been assigned to Type III. The maximum desorption rate was independent of degree of reduction as was the temperature at which this occurred (see Table 4.1). However, a narrowing of the peak on the

TABLE 4.1

DEPENDENCE OF PEAK TEMPERATURE (Tp) AND MAXIMUM DESORPTION RATE $\left(\frac{dw}{dt}\right)_{max}$ ON DEGREE OF REDUCTION FOR TYPE III

x in MnO_x	Tp(°C)	$\left(\frac{dw}{dt}\right)_{max}$ mg min^{-1}	Ambient oxygen pressure Torr
1.946	360	0.080	9.79
1.931	360	0.086	9.86
1.909	357	0.080	9.82
1.870	362	0.083	9.83
1.825	363	0.083	9.82

low temperature side tending towards an increase in symmetry was evident. It was shown earlier that Type III results from the elimination of oxygen and water from the structure, the former as a result of the $\gamma \rightarrow \beta$-MnO_2 transformation. As the decomposition of MnOOH in oxygen produces γ-MnO_2 the sample composition prior to the removal of Type III will correspond with γ-MnO_2 regardless of the initial degree of reduction. The oxygen contribution to Type III will therefore remain constant and independent of the degree of reduction. If the oxygen loss is invariant the peak narrowing can be ascribed to less water desorption from the sample. It was not possible in the previous Chapter, with the limited amount of evidence available at that time, to put forward any ideas concerning the nature of this water species. It has been proposed that the formation of electrodeposited γ-MnO_2 proceeds via an intermediate of composition $Mn(OH)_4$ [121]. It is possible that a small amount remains after the dehydration of this species to γ-MnO_2, this being the final step in the production process. A possible decomposition path in oxygen may be as below:

$$Mn(OH)_4 \rightarrow MnO_2 + 2H_2O \qquad (4.1)$$

The amount of water associated with Type III will therefore be dependent on the $Mn(OH)_4$ content. During the chemical reduction of γ-MnO_2 two possible routes may be envisaged for the reduction of any $Mn(OH)_4$ present:

$$Mn(OH)_4 + H^+ + e \rightarrow MnOOH + 2H_2O \qquad (4.2)$$

$$Mn(OH)_4 + 2H^+ + 2e \rightarrow Mn(OH)_2 + 2H_2O \qquad (4.3)$$

Whichever path is followed the $Mn(OH)_4$ content of the sample is dependent on the degree of reduction and Type III will exhibit a dependence on the extent of the reduction.

In an effort to obtain additional information on the nature of Type III increased amounts of hydroxyl groups were introduced into the γ-MnO_2 structure and the products obtained investigated by gravimetric TPD in an oxygen environment. As discussed above, when x in MnO_x > 1.82 the dehydroxylation reaction (IIb) was almost independent of composition and Type III, although showing partial dependence on the degree of reduction did not increase in extent or experience any displacement along the temperature axis. However, when 1.77 > x > 1.54 this simple dependence was not observed. Fig.4.4 illustrates the TPD curves obtained in oxygen (10 Torr). Type IIb increased with increase in Mn(III) content and was followed by a process involving uptake of oxygen. In the most reduced sample (x = 1.54) a weight increase was observed in the region of 250^{o}C which completely masked the presence of Type III. A plot of Type IIb peak height versus sample composition is shown in fig.4.5. The discontinuity corresponding to an analytical composition of about $MnO_{1.75}$ suggests that the products obtained by partial reduction of γ-MnO_2 differ structurally either side of this value. This is the first time that a discontinuity has been observed in a plot based on the thermal behaviour of the reduction products of γ-MnO_2 although other workers have obtained similar relationships in studies involving the

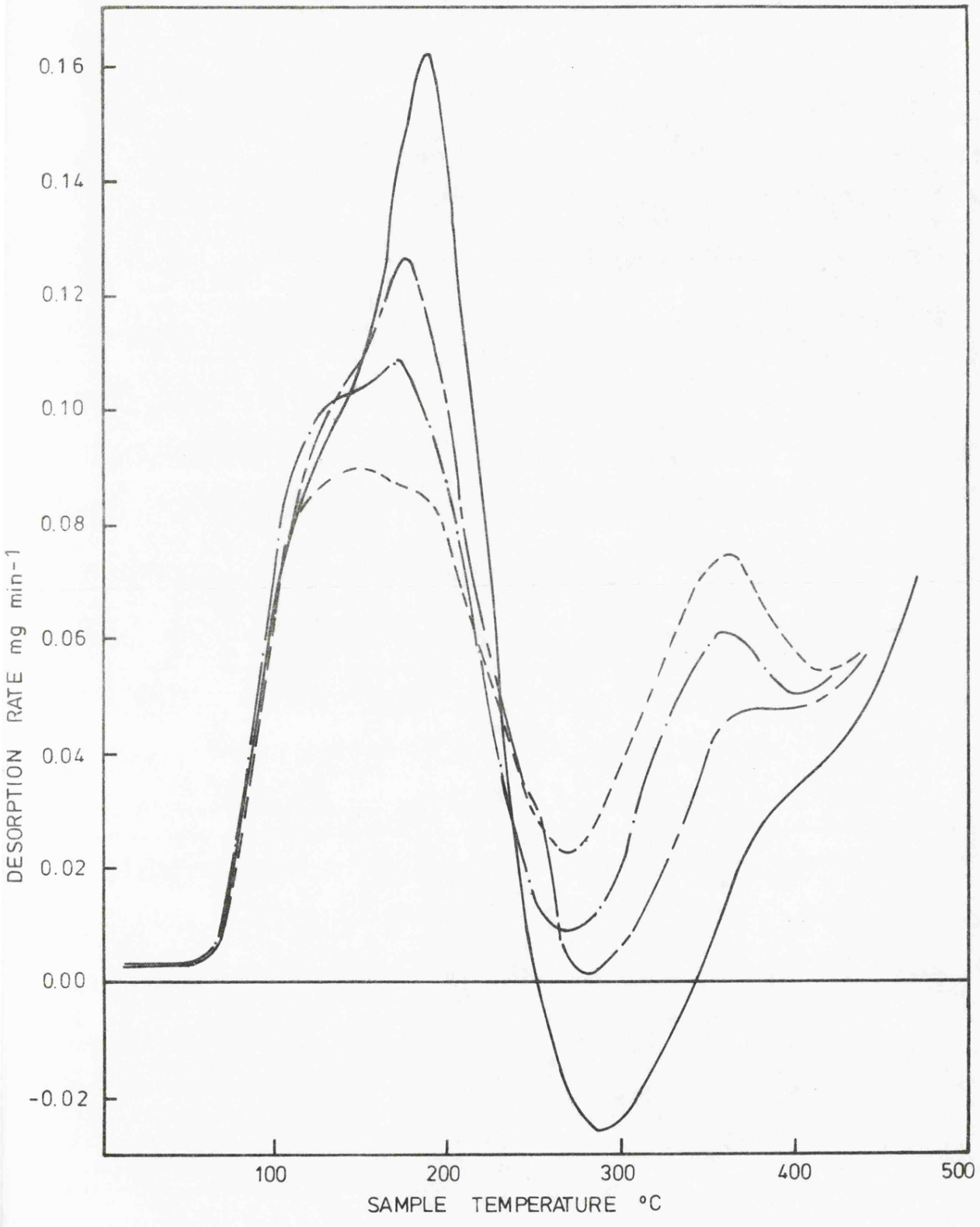

Fig.4.4 Gravimetric TPD curves in oxygen (10 Torr) of partially reduced γ-MnO_2. x in MnO_x = 1.73 (— — —), 1.65 (——·——), 1.62 (——·—·——) and 1.54 (——·——·——).

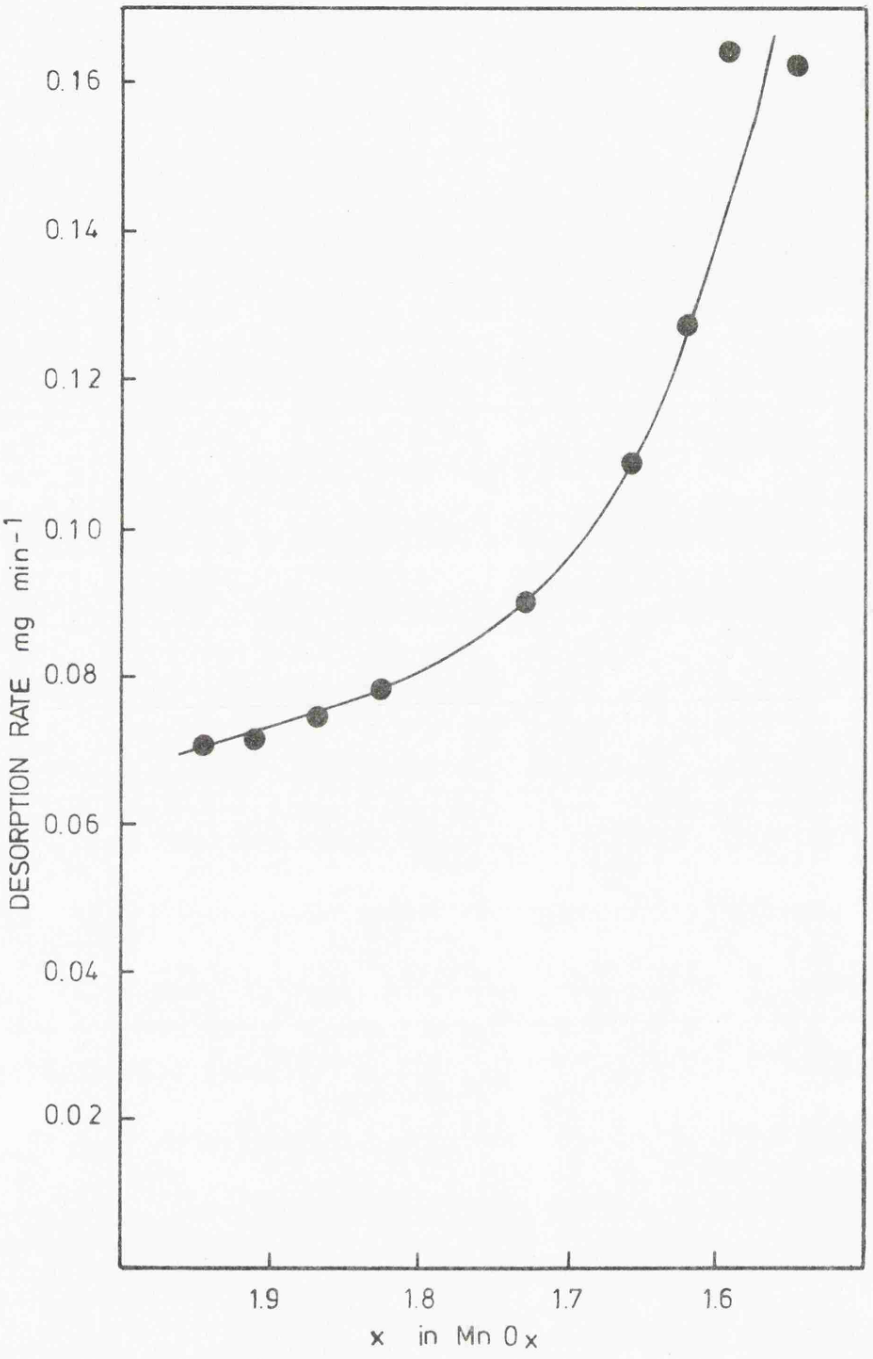

Fig.4.5 Maximum desorption rate in oxygen (10 Torr) as a function of sample composition for partially reduced γ-MnO_2

measurement of certain physical properties of these materials. Gabano and co-workers[19] measured the lattice parameters of the products obtained from the reduction of γ-MnO_2 with cinnamyl alcohol and reported a break in a plot of unit cell volume versus sample composition at $MnO_{1.75}$. This was later confirmed by Giovanoli, Bernhard and Feitknecht[55]. Electronic conductivity measurements on these samples also showed a discontinuity in the region of x = 1.75 when the activation energy was plotted as a function of sample composition[122]. The explanations given in the literature for this behaviour were mentioned in Chapter 1 but are not entirely satisfactory.

In an attempt to interpret the TPD behaviour in oxygen it was considered desirable to obtain additional information on the structure of the reduction products and with this aim in view their X-ray parameters have been redetermined and their magnetic and ion-exchange behaviour investigated.

4.2 Characterisation of chemical reduction products

4.2.(i) X-ray diffraction

Fig.4.6 shows the X-ray diffractometer traces of the reduction products and fig.4.7 depicts the interplanar distances of the prominent X-ray lines as a function of sample composition. Observed 'd' spacings are reported rather than lattice parameters for two reasons, (i) only a small number of reflections are present which is insufficient for the calculation of accurate lattice parameters[123] (ii) the majority of the lines are of very low intensity which hinders

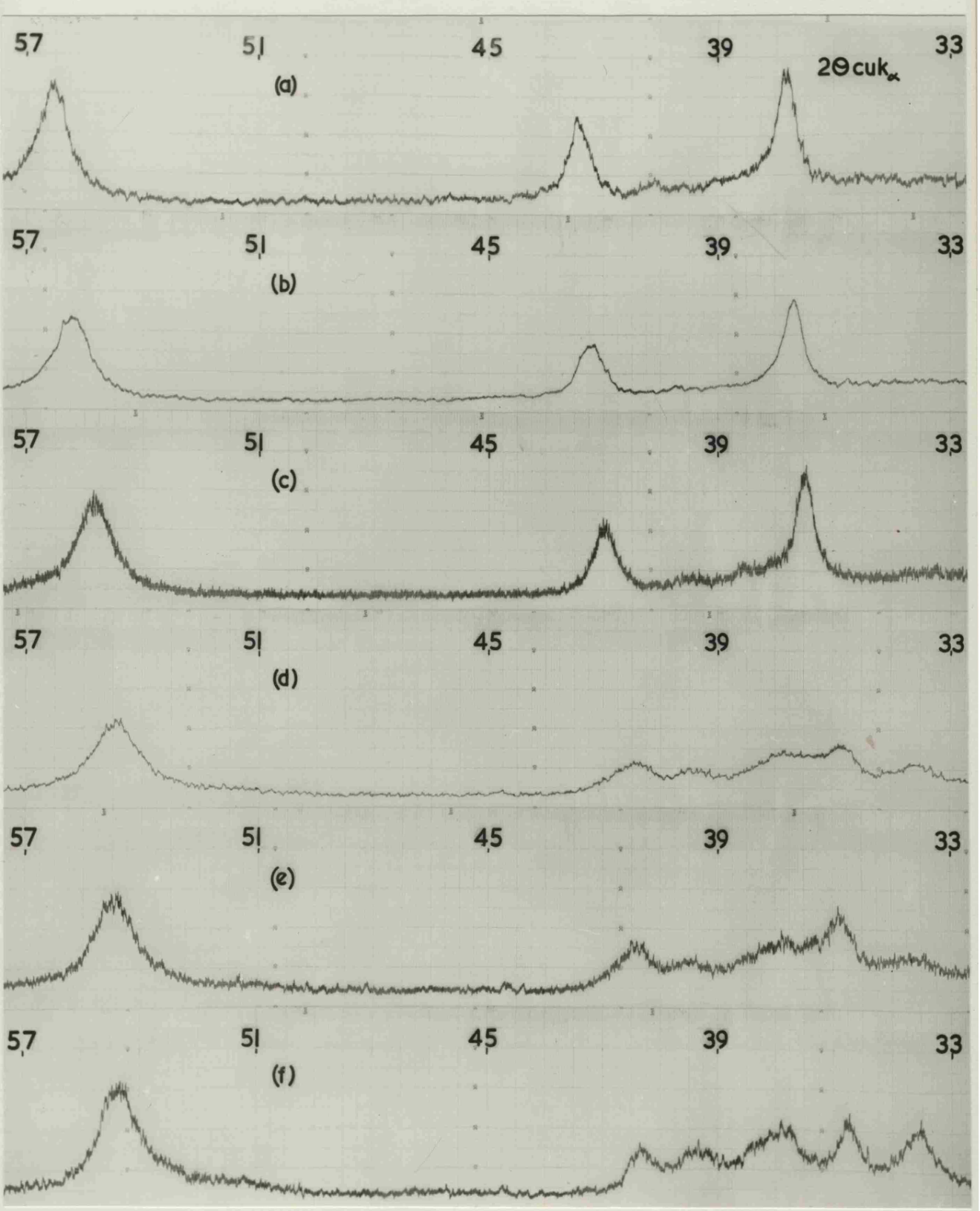

Fig.4.6 X-ray diffractometer traces (Cu K_α) of partially reduced γ-MnO_2. x in MnO_x (a) 1.946 (b) 1.870 (c) 1.804 (d) 1.65 (e) 1.62 and (f) 1.54.

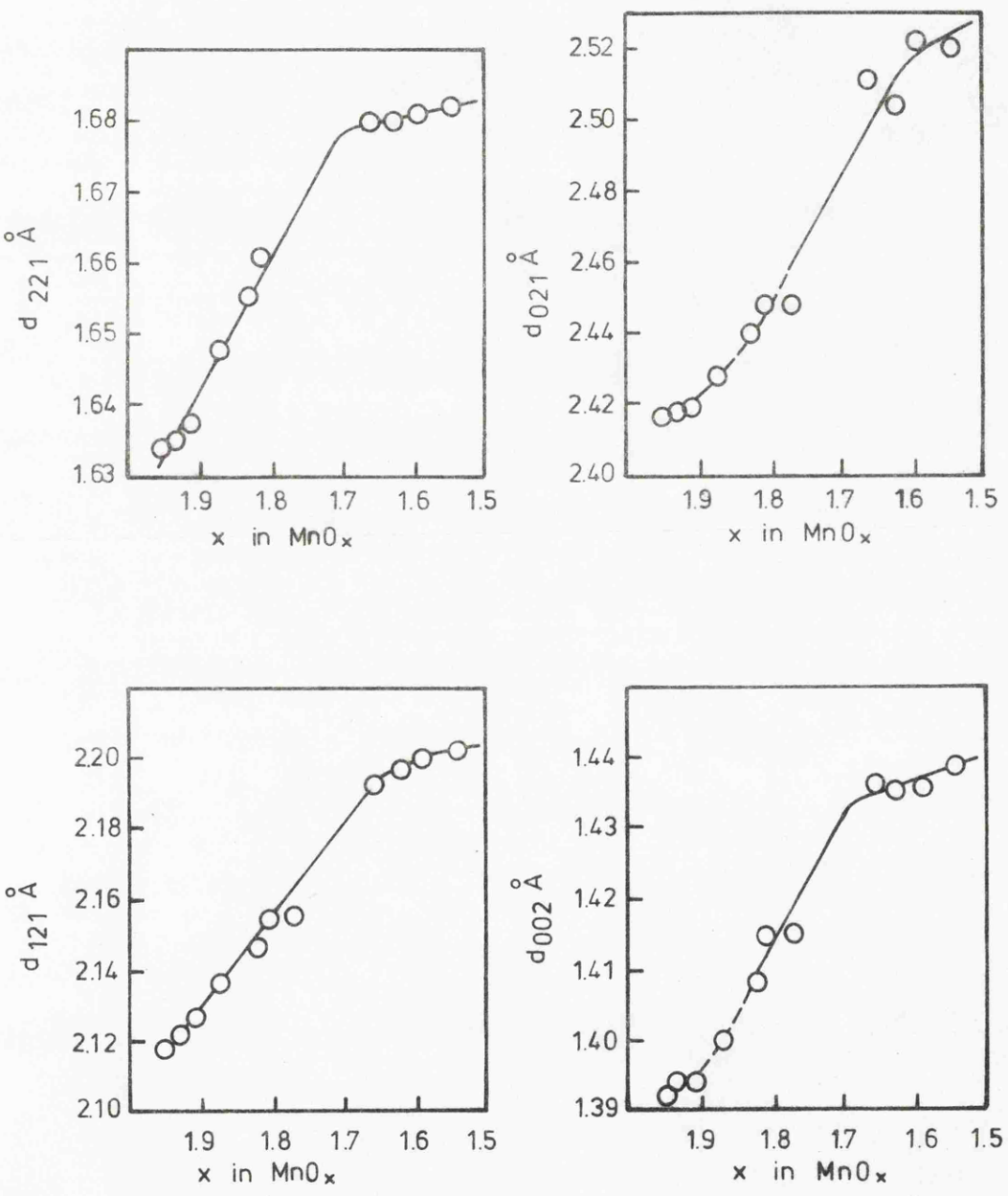

Fig.4.7 Interplanar separation (d) as a function of composition for partially reduced γ-MnO_2.

any precise measurement of their position.

In the range $70^{o} > 2\theta > 10^{o}$ five reflections are present for the samples with $x > 1.77$ namely 110, 021, 121, 221 and 002 (indexed on the basis of a diaspore unit cell). These shifted to lower angles of diffraction as the Mn(III) content increased and no new lines were apparent. This behaviour is consistent with a solid solution process and is in agreement with previous investigations[10, 19].

When $x < 1.77$ the traces are more complex. For $x = 1.65$ the diffraction pattern is extremely poor. Reflections due to the 021, 221 etc. can still be identified but are much weaker in intensity. Further reduction results in sharper diffraction traces but only very small changes in line position are apparent. Also present are additional lines which were not observed in the traces when $x > 1.77$. It appears from the very poor nature of the traces that in the region $x = 1.65 - 1.77$ the structure is undergoing a structural transition. The discontinuity in fig.4.5 strongly speaks against a continuous solid solution from MnO_2 to MnOOH.

Extrapolation of the plots in fig.4.7 to a sample composition of $MnO_{1.50}$ should provide the 'd' values of the 021, 121, 221 and 002 planes of α-MnOOH (groutite). Table 4.2 compares the experimental values with those reported in the literature for groutite[92]. The extrapolated 'd' spacing for the 021 plane is about 2.53Å. This is in reasonable agreement with

TABLE 4.2

X-RAY DIFFRACTION DATA FOR CHEMICALLY REDUCED γ-MnO_2($MnO_{1.50}$) AND NATURAL GROUTITE (α-MnOOH)

Index plane hkl	Interplanar distance d(Å)	
	experimental	literature[92]
040	2.64	2.67
021	2.52	2.54
111	2.40	2.38
210	2.21*	2.22
221	1.685	1.695
002	1.44	1.45**

* assigned to the 121 reflection in γ-MnO_2

** not assigned to a particular index plane

the reported value for groutite (2.54Å). Also good agreement is found for the 221 plane i.e. the extrapolated value of 1.683 compares well with the literature value of 1.695. An extrapolated value for the 121 plane of 2.20Å could not be compared with that in the literature as no figure for that index plane was available. The ASTM card does give a line at 2.22Å but assigns this to the 210 reflection. Also it was not possible to compare the value found for the 002 plane (1.44Å) as no value is quoted in the literature. A line is found at 1.45Å in α-MnOOH but this is not assigned to any particular reflection. It appears therefore that these lines do show a strong resemblance to those of α-MnOOH. Of

the new lines that appear in the diffractometer traces when $x < 1.77$ only the positions of two of these could be determined accurately. These reflections occur at d = 2.40Å and 2.64Å and correspond closely to the positions found for the 111(2.38Å) and 040(2.67Å) planes respectively in α-MnOOH. All of the measured reflections in the X-ray trace at $1.77 > x > 1.54$ can therefore be indexed on the basis of an α-MnOOH unit cell.

Klingsberg[124] studied the hydrothermal conversion of α-MnOOH→ MnO_2 and concluded that there was no solid solution behaviour between these two compounds. It was found however, that this conversion went via an intermediate which was called groutellite. More recently Muller and Joubert[125] have prepared a modification of vanadium oxyhydroxide which is isotypic with diaspore. These authors found that this converted to vanadium dioxide by thermal treatment in air. The vanadium dioxide formed was also isotypic with diaspore and this system is therefore analagous to that of ramsdellite (MnO_2) and α-MnOOH. It is significant that although the modifications of VOOH and VO_2 possessed the same structure no evidence of a solid solution was found during their inter conversion as was true for the MnOOH - MnO_2 system. The similarity between the two systems also extends to the formation of an intermediate during the transformation of the oxyhydroxide to the dioxide. Muller and Joubert suggested that the intermediate phase was identical to one described earlier by Evans and Mrose[126] and could be represented by the formula $V_2O_3(OH)$.

In view of these important results it is considered that the following interpretation satisfactorily accounts for the observed X-ray data obtained on the chemical reduction products of γ-MnO_2. In the range $MnO_{1.95}$ - $MnO_{1.77}$ the chemical reduction takes place in solid solution as shown by the linear displacement in the interplanar distance. Substitution of oxide ions by hydroxyl groups with a corresponding change in oxidation state of the cation from (IV) to (III) occurs within a single phase which can conveniently be represented by the formula $(1-x)MnO_2.x\ MnOOH$. In the region between $MnO_{1.77}$ and $MnO_{1.65}$ a structural reorganisation takes place resulting in the formation of a disordered state as shown by the very weak X-ray diffractometer trace at $MnO_{1.65}$. This may well result from Jahn-Teller distortion in the structure due to the presence of Mn(III). Below $MnO_{1.65}$ the reduction may continue either in one phase (but a phase which is distinct from the solid solution existing above $MnO_{1.77}$) or it may continue as a two phase system, α-MnOOH being formed at the expense of the intermediate. The invariance of the reflections and the increase in intensity in going from $MnO_{1.65}$ to $MnO_{1.54}$ together with the results of Klingsberg[124] and Muller and Joubert[125] suggest that the latter is more likely.

4.2.(ii) Magnetic properties

Further information on the structure of the products prepared by chemical reduction of γ-MnO_2, was obtained from magnetic susceptibility measurements. First, however it was of prime importance to establish the independence of the magnetic

susceptibility of these compounds on field strength. Ferromagnetic impurities present in the sample would cause the susceptibility to vary with field strength and an attempt at correcting for this would be necessary. Equation (2.9) can be rearranged to give

$$\chi_g = \frac{2gl}{W} \cdot \frac{\Delta w}{H^2} = \frac{k\Delta w}{H^2} \qquad (4.4)$$

A linear plot of Δw against H^2 with a gradient equal to $\chi_g k^{-1}$ and which passes through the origin would establish the independence of susceptibility on field strength. Fig.4.8 shows such a plot for $MnO_{1.946}$, the linearity and absence of an intercept confirming the independence of χ_g on H.

The variation of magnetic susceptibility as a function of temperature for the samples of γ-MnO_2 that had undergone partial chemical reduction is shown in fig.4.9. Curie-Weiss plots are depicted in fig.4.10. The shape of the former are typical of normal paramagnetic materials. The Curie-Weiss plots were linear in the range 290-140 K but below 140 K there was a downward departure from linearity probably due to a ferromagnetic effect. Magnetic moments calculated from the slopes of the plots are shown graphically in fig.4.11(Top). μ increased with degree of reduction due to the substitution of Mn(IV) (μ_{so} = 3.87 B.M.) by Mn(III) (μ_{so} = 4.90 B.M.). In the range $1.95 > x > 1.80$ the magnetic moments were close to the spin only values reflecting the absence of any appreciable orbital contribution from Mn(IV) in a perfect octahedral environment[127]. Below x = 1.80 two important features are evident in fig.4.11(Top). When $x > 1.62$

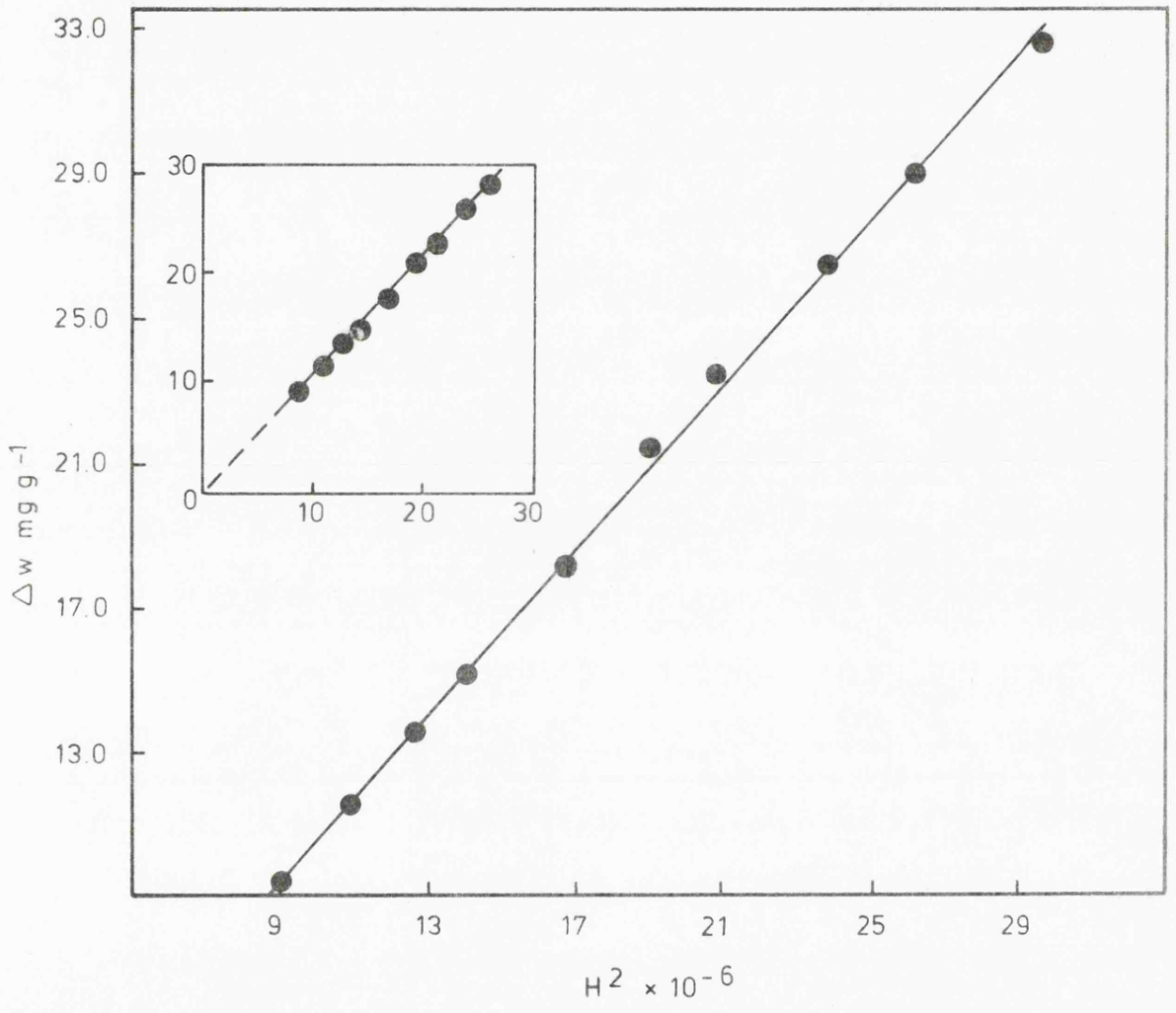

Fig.4.8 Weight change (Δw) as a function of field strength for $MnO_{1.946}$.

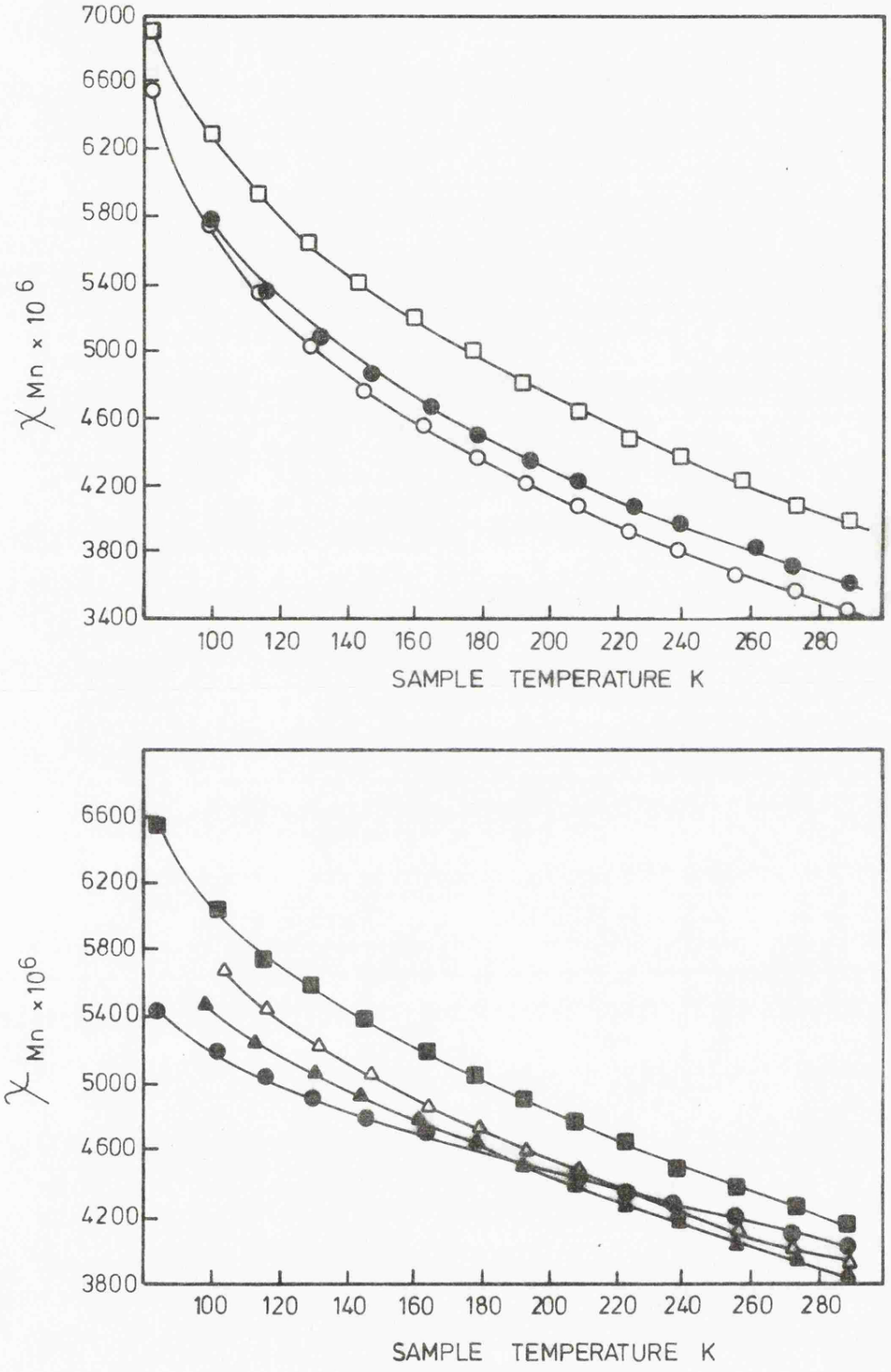

Fig.4.9 Magnetic susceptibility as a function of temperature for partially reduced γ-MnO_2. x in MnO_x . Top, 1.946 (O), 1.870 (●), 1.804 (□). Bottom, 1.77 (▲), 1.65 (△), 1.62 (■) and 1.54 (●).

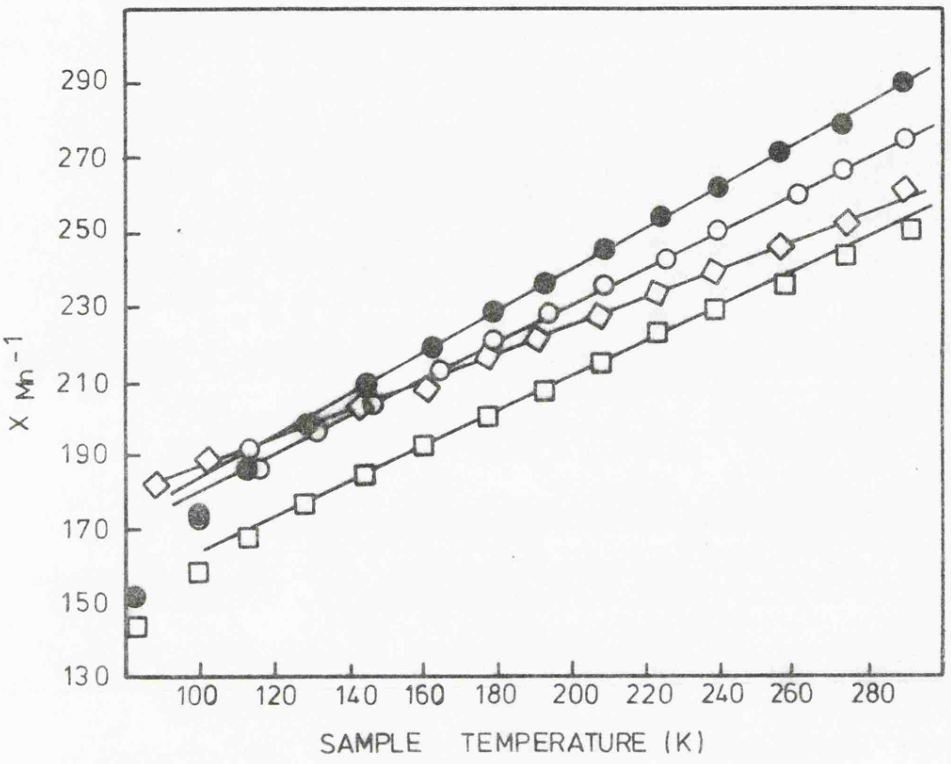

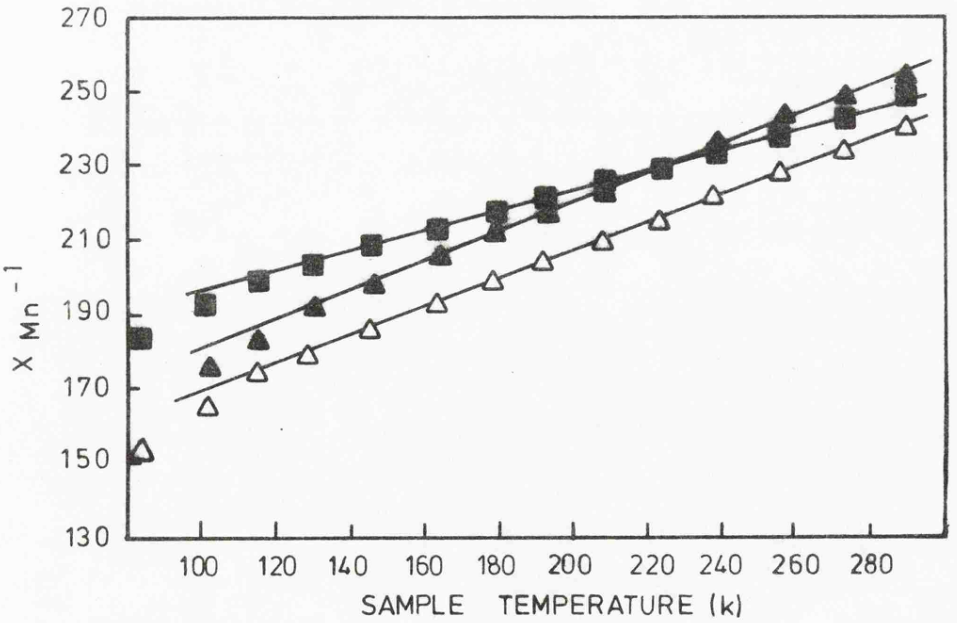

Fig.4.10 Curie-Weiss plots for partially reduced γ-MnO_2.x in MnO_x = 1.946 (●), 1.870 (○), 1.804 (□), 1.77 (◊), 1.65 (△), 1.62 (▲) and 1.54 (■).

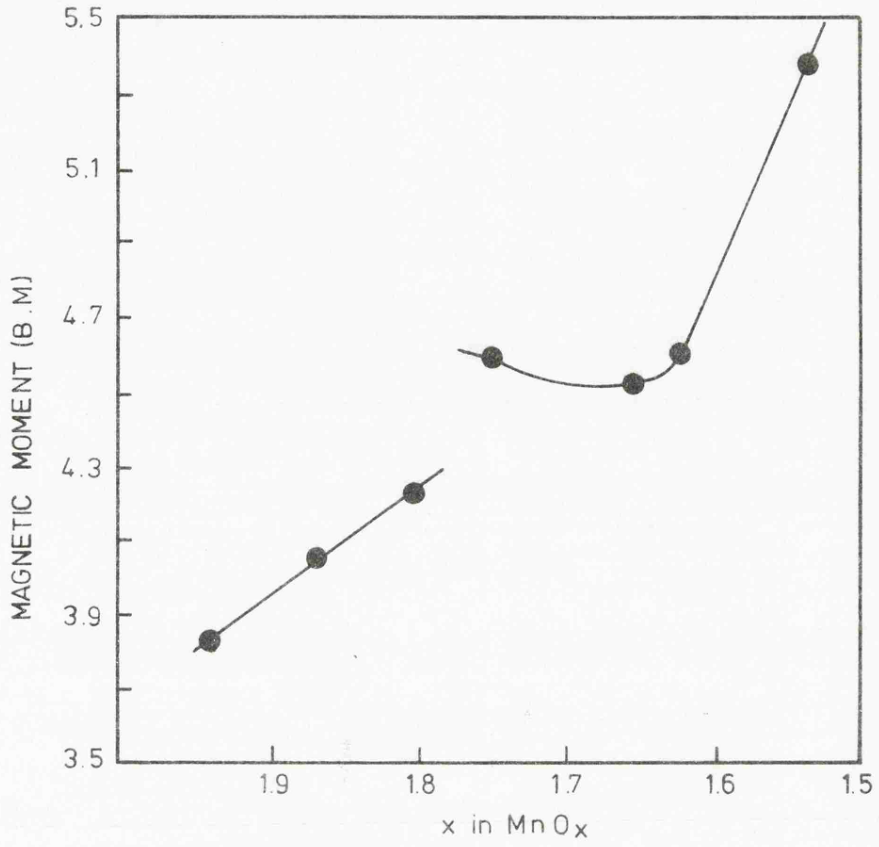

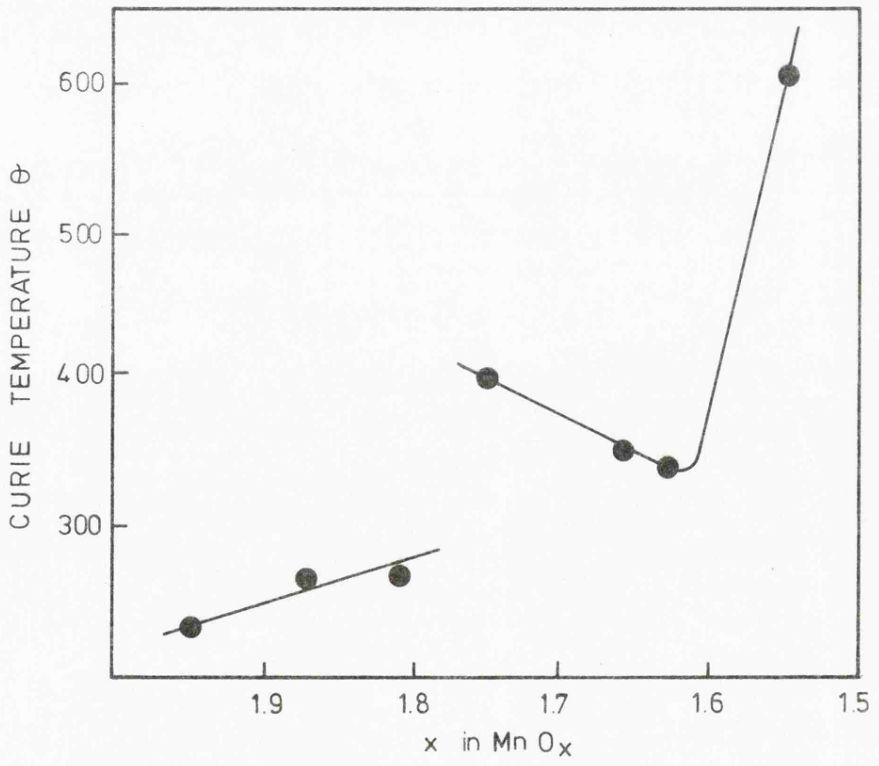

Fig.4.11 Top. Magnetic moment as a function of sample composition for partially reduced γ-MnO_2.

Bottom. As above but Curie temperature (θ) in place of magnetic moment.

abnormally high values of μ were obtained possibly due to an increased orbital contribution as a result of a structural change. Secondly there appeared to be a discontinuity in the region of x = 1.75. This may have resulted from an error in the experimental determination but is considered unlikely. These results were consistent with the X-ray data which suggested a structural reorganisation in the region x = 1.75 - 1.62.

Extrapolation of the linear portion of the Curie-Weiss plot to $\chi_{Mn}^{-1} = 0$ (i.e. determination of the Curie temperature θ) provides a measure of the interaction energy between neighbouring ions. This is shown as a function of sample composition in fig.4.11(Bottom). This is seen to be similar in shape to the plot in fig.4.11(Top) and indicative of a structural transition after replacement of about 50% of the quadrivalent manganese ions by tervalent ions.

A possible lattice reorganisation could also be inferred from the susceptibility - temperature plots shown in fig.4.9. The susceptibility recorded at three different temperatures as a function of sample composition (Fig.4.12) attains a maximum value at about x = 1.62 and exhibits a region of discontinuity at about x = 1.75.

The only previous magnetic investigation of this system[88] showed a similar dependence of magnetic moment and Curie temperature on sample composition except that a break was

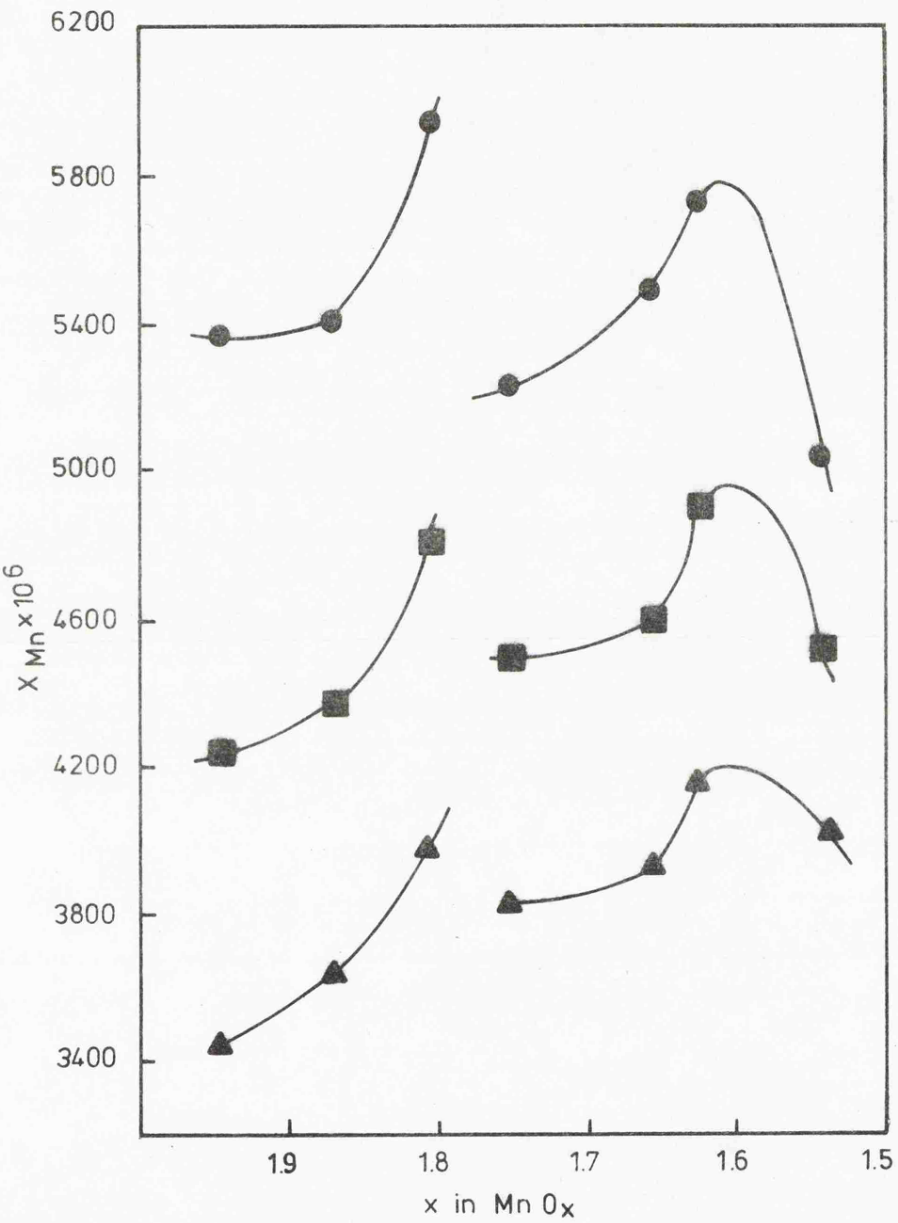

Fig.4.12 Magnetic susceptibility as a function of sample composition for partially reduced γ-MnO_2 recorded at 114 K (●), 194 K (■) and 290 K (△).

not reported at x = 1.75. It is possible that this may have been a consequence of the omission of a sample in the critical region of x = 1.75. When the same authors repeated the study on samples of γ-MnO_2 that had undergone a limited electrochemical reduction the magnetic moment of the sample corresponding to x = 1.75 did deviate upwards from a line joining the moments obtained for x = 1.91 and 1.67, which was consistent with the present data.

4.2.(iii) Ion exchange

The X-ray diffractometry and magnetic investigations have established that chemical reduction of γ-MnO_2 introduces hydroxyl groups into the oxide lattice and, in order to maintain electrical neutrality, is accompanied by a corresponding change in the valency of the manganese ions from (IV) to (III). Chemical reduction would also be expected to lead to a progressive increase in the surface population of trivalent manganese ions.

It has been known for many years that manganese dioxide has the ability to adsorb cations from an external solution with an equivalent increase in the hydrogen ion concentration of that solution. Muller, Tye and Wood[45] have made a detailed study of the ion exchange properties of several manganese dioxides in potassium chloride solutions of varying pH. Using the conditions established by these authors this technique has been employed to investigate the release of hydrogen ions by the partially reduced oxides.

It is known that the acidity of a hydroxyl group is dependent upon the valency state and radius of the cation to which it is associated[128]. Hydroxyl groups on the surface of γ-MnO_2 would therefore be expected to become less acidic on substitution of the quadrivalent manganese ions by trivalent ions. Fig.4.13 shows the concentration of hydrogen ions released on exchange with potassium ions as a function of degree of reduction. It can be seen that the magnitude of the hydrogen ion release diminishes with increase in degree of reduction consistent with a progressive increase in the surface concentration of manganese(III) ions.

4.3 Nature of intermediate formed during TPD of chemically reduced γ-MnO_2 in oxygen

The observed dependence of the desorption rate on the degree of reduction below x = 1.75 for TPD runs recorded in oxygen may be attributed to the presence of α-MnOOH as a separate phase. This appears to decompose to γ-MnO_2 via an intermediate that is capable of existing for a finite time in the oxidising atmosphere before its eventual oxidation. It is possible to demonstrate that oxidation of the intermediate to γ-MnO_2 is taking place at the same time as undecomposed α-MnOOH breaks down to form the intermediate.

The total weight loss from a decomposition process should be independent of heating rate. Application of a linear heating programme in the range 1^{o}-$10^{o}C\ min^{-1}$ to the decomposition of $MnO_{1.54}$ in oxygen resulted in an increase in the maximum

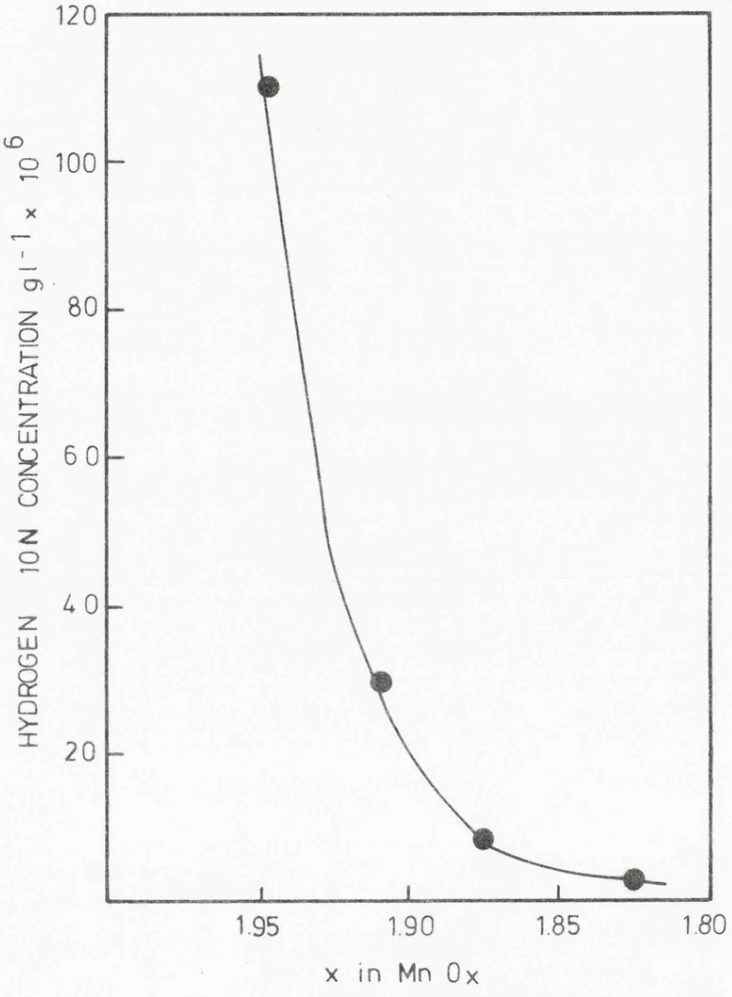

Fig.4.13 Hydrogen ion release from partially reduced γ-MnO_2 as a function of sample composition.

desorption rate as β increased. This was accompanied by a corresponding increase in the amount of oxygen uptake. The weight loss from the commencement of the heating programme to a temperature corresponding to the onset of the weight increase was plotted as a function of β and shown in fig.4.14. This dependence is indicative of two competing reactions, namely the breakdown of α-MnOOH to the intermediate and its subsequent oxidation to γ-MnO_2.

The nature of the intermediate and the reasons for its formation have been investigated. Giovanoli and Leuenberger[10] observed that finely divided α-MnOOH when heated isothermally in oxygen at 200°-275°C converted to Mn_5O_8 after a period of about twenty minutes and which further oxidised to γ-MnO_2 after a period ranging from a few hours to days. This could account for the observed TPD curves in oxygen. Mn_5O_8 resulting from the decomposition of the α-MnOOH component would be subsequently oxidised to γ-MnO_2. The first reaction may be represented by:

$$20\,MnOOH + O_2 \rightarrow 4\,Mn_5O_8 + 10\,H_2O \qquad (4.5)$$

This could give rise to the desorption peak in the temperature interval 160°-190°C (Fig.4.4) and would be dependent on the oxyhydroxide concentration as found experimentally. The second stage could result from its oxidation:

$$Mn_5O_8 + O_2 \rightarrow 5\,MnO_2 \qquad (4.6)$$

which would give rise to the weight increase in the region of 300°C.

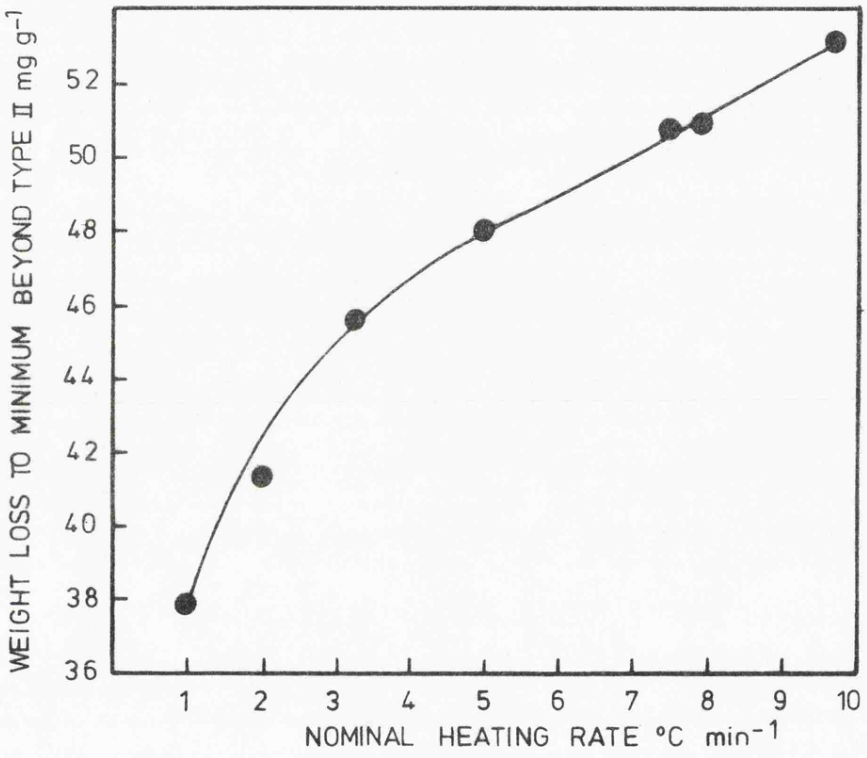

Fig.4.14 Decomposition of $MnO_{1.54}$ in oxygen (10 Torr) as a function of heating rate.

Alternatively, the intermediate associated with the 'desorption-absorption' phenomena may be Mn_2O_3, its formation being accounted for by the following mechanism:

$$2\,MnOOH \rightarrow Mn_2O_3 + H_2O \qquad 2\,Mn_2O_3 + O_2 \rightarrow 4\,MnO_2 \qquad (4.7)$$

The formation of Mn_2O_3 may be a necessary step during the conversion of α-MnOOH to γ-MnO_2 or merely an artefact as a result of insufficient oxygen reaching the sample under the conditions of the experiment. Oxygen ingress into the sample may be inhibited as a result of the low oxygen pressure in which the experiments were conducted (10 Torr). However experiments performed in a flowing oxygen environment at atmospheric pressure produced similar weight loss curves.

Attempts were made to isolate the intermediate by stopping a TPD run of $MnO_{1.54}$ in oxygen at selected temperatures during the decomposition and characterising the sample by X-ray diffraction. This failed to provide any additional information on the intermediate, the diffractometer traces being indicative of either $MnO_{1.54}$ or its ultimate decomposition product γ-MnO_2.

Further investigations were carried out by recording the TPD curves in oxygen at pressures other than 10 Torr. These are illustrated in fig.4.15. On increasing the oxygen pressure the rate of weight loss peak centred at about 220^{o}C diminished and less oxygen uptake in the region of 300^{o}C was observed. This is consistent with the formation of Mn_2O_3 as an intermediate. An increase in the oxygen pressure would be expected to facilitate the oxidation of Mn_2O_3 (see eq. 4.7). This would

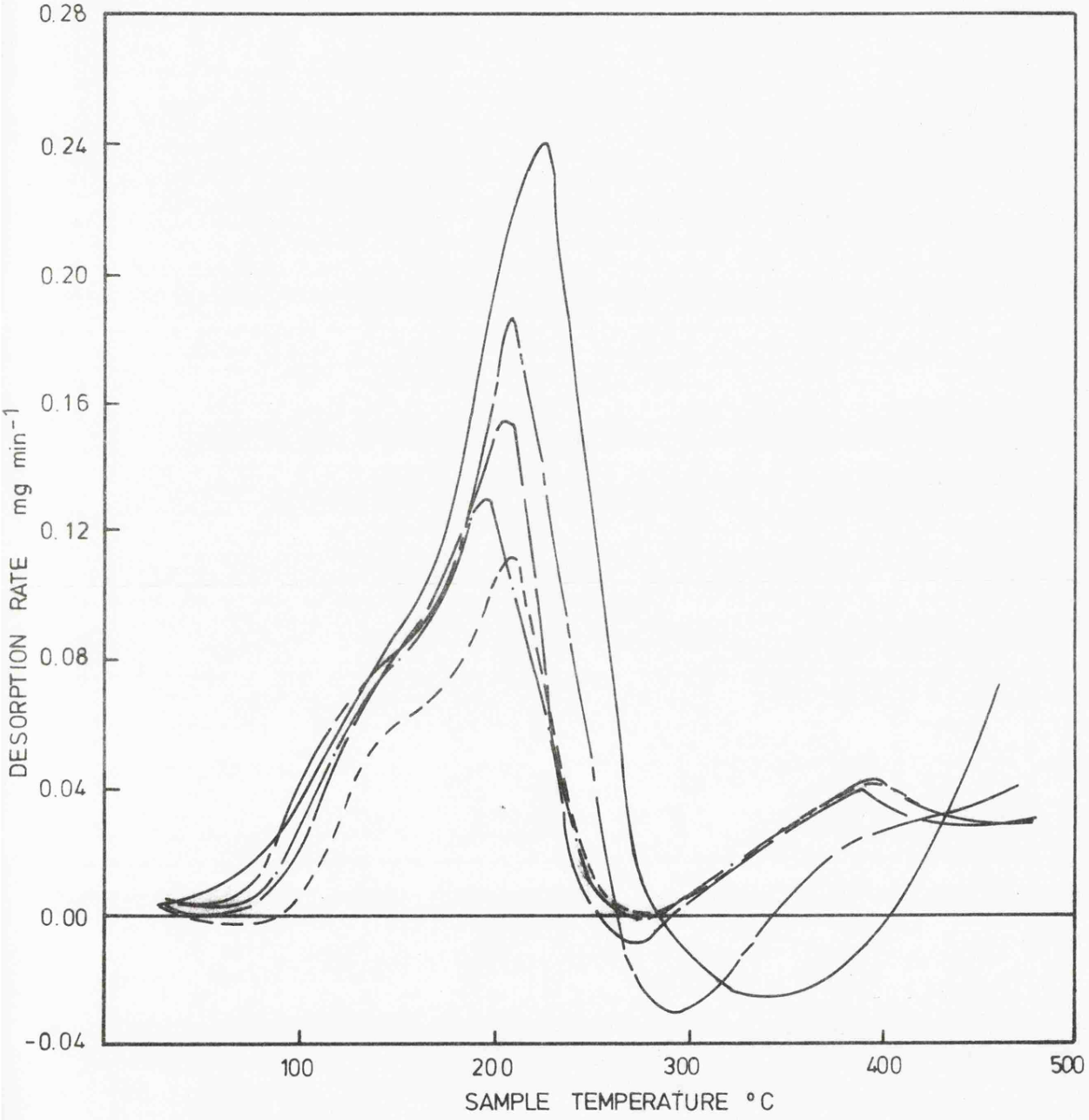

Fig.4.15 Decomposition of $MnO_{1.54}$ in static oxygen environments of varying pressure.

Ambient oxygen pressures were 4 (——), 53 (——), 258 (— - —), 358 (——·) and 456 Torr (— — —).

lead to a diminution of the desorption peak in accordance with the experimentally observed behavior. The mechanism of Mn_5O_8 formation is more complex, oxygen being involved in both reaction steps (see eq. 4.5 and 4.6). An increase in pressure might enhance both the desorption and adsorption stages, the shape of the resulting TPD curve being difficult to predict.

Strong evidence that the TPD behaviour in oxygen involved the formation of Mn_2O_3 was obtained from the decomposition of a synthetic α-MnOOH sample. This was prepared as outlined in Chapter 2 and a detailed account of its thermal behaviour is presented later in Chapter 5. The experiment relevant to this discussion is described below. α-MnOOH was heated in oxygen to a temperature just before the onset of the weight increase. This was followed by cooling of the sample to room temperature, oxidation being prevented by opening the tap to the vacuum pump during this period. An X-ray diffractometer trace showed this to be Mn_2O_3 although not possessing the common C - sesquioxide structure. Its structure will be discussed in detail in Chapter 5.

4.4 Textural studies

4.4(i) Nitrogen adsorption

In order to obtain meaningful microporosity data from nitrogen adsorption isotherms, standard data on a well characterised non-porous solid is essential. Payne and Sing[129] have recorded nitrogen isotherms on samples of Degussa 'Aluminiumoxid C' a γ-Al_2O_3 of discrete, nearly spherical particles. This was

shown to be non-porous and was subsequently used as the reference solid to study porosity in aluminas. Recently Nicolaon and Teichner[77] measured the adsorption of argon on this material and used the data to estimate the microporosity generated during the thermal decomposition of $Ni(OH)_2$ to NiO.

The interpretation of nitrogen adsorption data on γ-MnO_2 and related oxides was initially based on Degussa 'Aluminiumoxid C' as the reference solid. Gravimetric sorption data on this material are given in Table 4.3 and a BET plot is shown in fig.4.16. The latter was linear in the p/p^o range 0.05 - 0.24 from which a surface area of 95.2 m^2g^{-1} was calculated. The nitrogen molecule was assumed to occupy an area of 16.2 $\mathring{A}^2$. The surface area compared favourably with values reported by other workers[77, 129]. Included in Table 4.3 is the α_s data from which α_s plots for the oxides and oxyhydroxides under study may be constructed. It can be shown that the external area of a non-porous solid is given by

$$A_s = k \frac{w}{\alpha_s} \qquad (4.8)$$

where A_s = external surface area

$\frac{w}{\alpha_s}$ = slope of the α_s plot

For a non-porous material $A_s = A_{BET}$ and $k = A_{BET} \cdot \frac{\alpha_s}{w}$.

For Degussa 'Aluminiumoxid C' k was calculated to be 2.33. The external surface area of γ-MnO_2 and its chemical reduction products can therefore be calculated from the relationship

$$A_s = 2.33 \frac{w}{\alpha_s} \qquad (4.9)$$

TABLE 4.3

STANDARD ADSORPTION DATA FOR NITROGEN AT -196°C ON DEGUSSA 'ALUMINIUMOXID C'

Adsorption mg g^{-1}	Relative p/p^{o}	Reduced Adsorption α_s	Adsorption μ moles m^{-2}	Adsorption μ moles m^{-2} according to Sing
19.52	0.0147	0.477	7.3	8.0
21.73	0.0265	0.531	8.2	8.7
23.22	0.0387	0.568	8.7	9.2
24.59	0.0521	0.601	9.2	9.6
25.57	0.0632	0.625	9.6	9.9
26.78	0.0783	0.655	10.0	10.3
27.69	0.0934	0.677	10.4	10.6
28.71	0.111	0.702	10.8	10.9
29.51	0.129	0.722	11.1	11.2
31.55	0.164	0.771	11.8	11.8
32.86	0.198	0.803	12.3	12.3
34.15	0.232	0.835	12.8	12.8
35.61	0.266	0.871	13.4	13.3
36.94	0.301	0.903	13.9	13.8
38.38	0.339	0.938	14.4	14.5
40.07	0.382	0.980	15.0	15.2
41.71	0.425	1.020	15.6	16.0
43.34	0.465	1.060	16.3	16.6
45.32	0.512	1.108	17.0	17.4
47.42	0.558	1.159	17.8	18.4
49.58	0.606	1.212	18.6	19.5
51.75	0.651	1.265	19.4	20.7
54.03	0.691	1.321	20.3	21.9
56.96	0.737	1.393	21.4	23.4

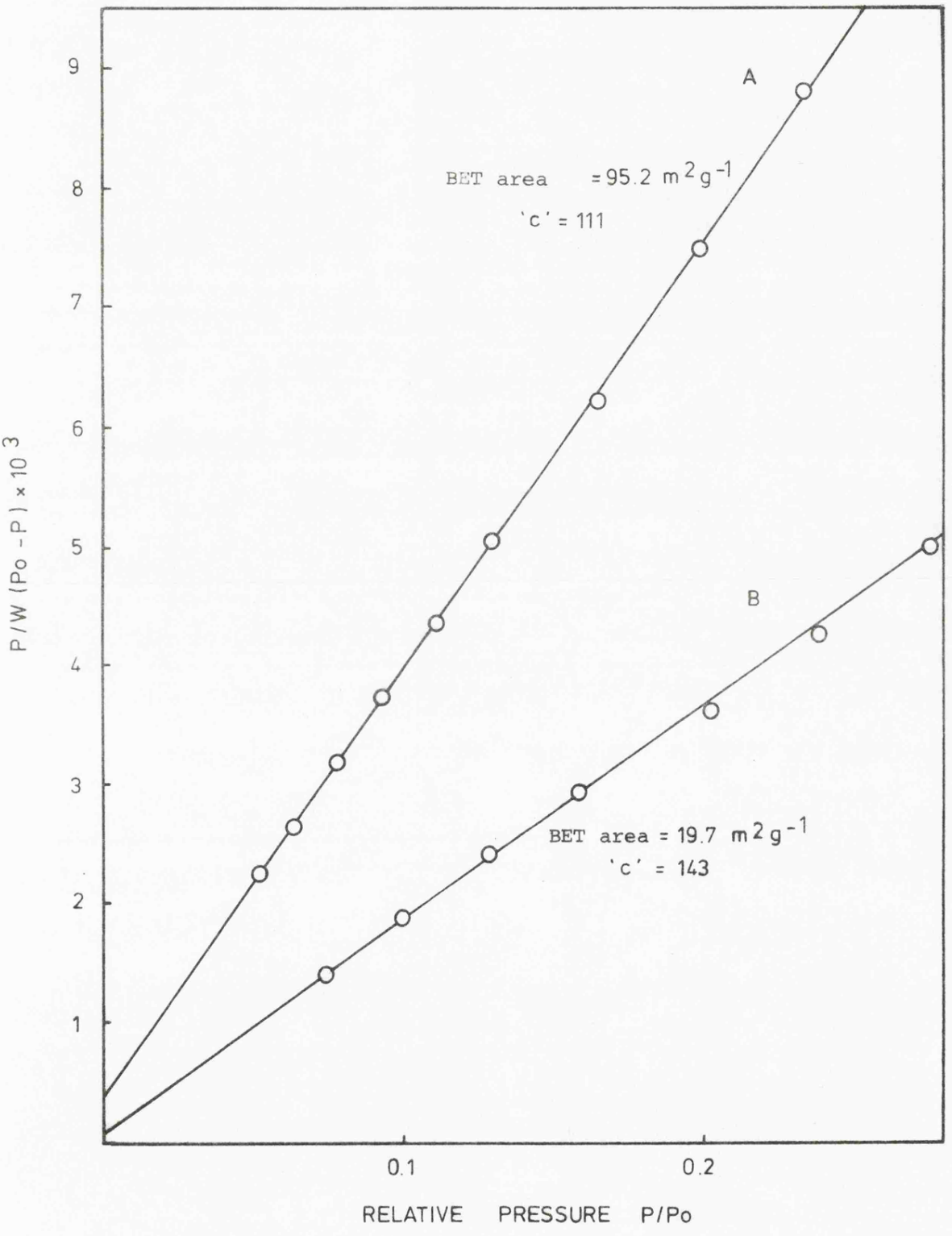

Fig.4.16 BET plots for nitrogen adsorption at -196°C on (A) Degussa Aluminiumoxid 'C' and (B) γ-MnOOH.

Although this would have been a suitable standard from which information concerning the development of microporosity could be obtained, it is preferable to use as standard a material of similar chemical nature to the sample under investigation[75]. Of the oxides and oxyhydroxides of manganese used in this work a synthetic sample of γ-MnOOH (manganite) was considered to meet all of the requirements necessary of a reference solid. Nitrogen adsorption data on γ-MnOOH is presented in Table 4.4 and a BET plot in fig.4.16. The surface area of 19.7 m^2g^{-1} was high enough to be suitable as a standard if porosity could be shown to be absent. An α_s plot based on Degussa 'Aluminiumoxid C' was constructed and shown in fig.4.17. Absence of microporosity was established by extrapolation of the α_s plot through the origin. The linearity of the plot indicated the absence of porosity in the mesopore range. Additional evidence supporting the absence of microporosity in γ-MnOOH was obtained from scanning electron micrographs. These showed the crystals to be rod-like cylinders (Fig.4.18). An attempt at measuring the surface area from the micrographs was only partially successful owing to the uncertain diameter of the cylinders. Surface areas were of the order 10-30 m^2g^{-1} which indicated the absence of any appreciable porosity. It was decided to use this material as a standard and α_s plots reported in this thesis refer to γ-MnOOH as the reference solid. External areas of the manganese oxides were calculated from the relationship:

$$A_s = 2.25 \frac{w}{\alpha_s} \qquad (4.10)$$

TABLE 4.4

STANDARD ADSORPTION DATA FOR NITROGEN AT -196°C ON γ-MnOOH

Adsorption mg g^{-1}	Adsorption μ moles m^{-2}	Relative Pressure p/p^o	Reduced Adsorption α_s
5.11	9.3	0.037	0.58
5.35	9.7	0.053	0.61
5.67	10.3	0.074	0.65
5.86	10.6	0.099	0.67
6.11	11.1	0.128	0.70
6.35	11.5	0.157	0.73
6.97	12.6	0.202	0.80
7.30	13.2	0.238	0.83
7.64	13.9	0.278	0.87
8.10	14.7	0.323	0.925
8.48	15.4	0.365	0.97
8.89	16.1	0.416	1.015
9.31	16.9	0.461	1.06
9.71	17.6	0.508	1.11
10.04	18.2	0.555	1.15
10.42	18.9	0.600	1.19
11.06	20.1	0.654	1.26
11.47	20.8	0.705	1.31
12.18	22.1	0.759	1.39
12.80	23.2	0.814	1.46
13.75	24.9	0.858	1.57

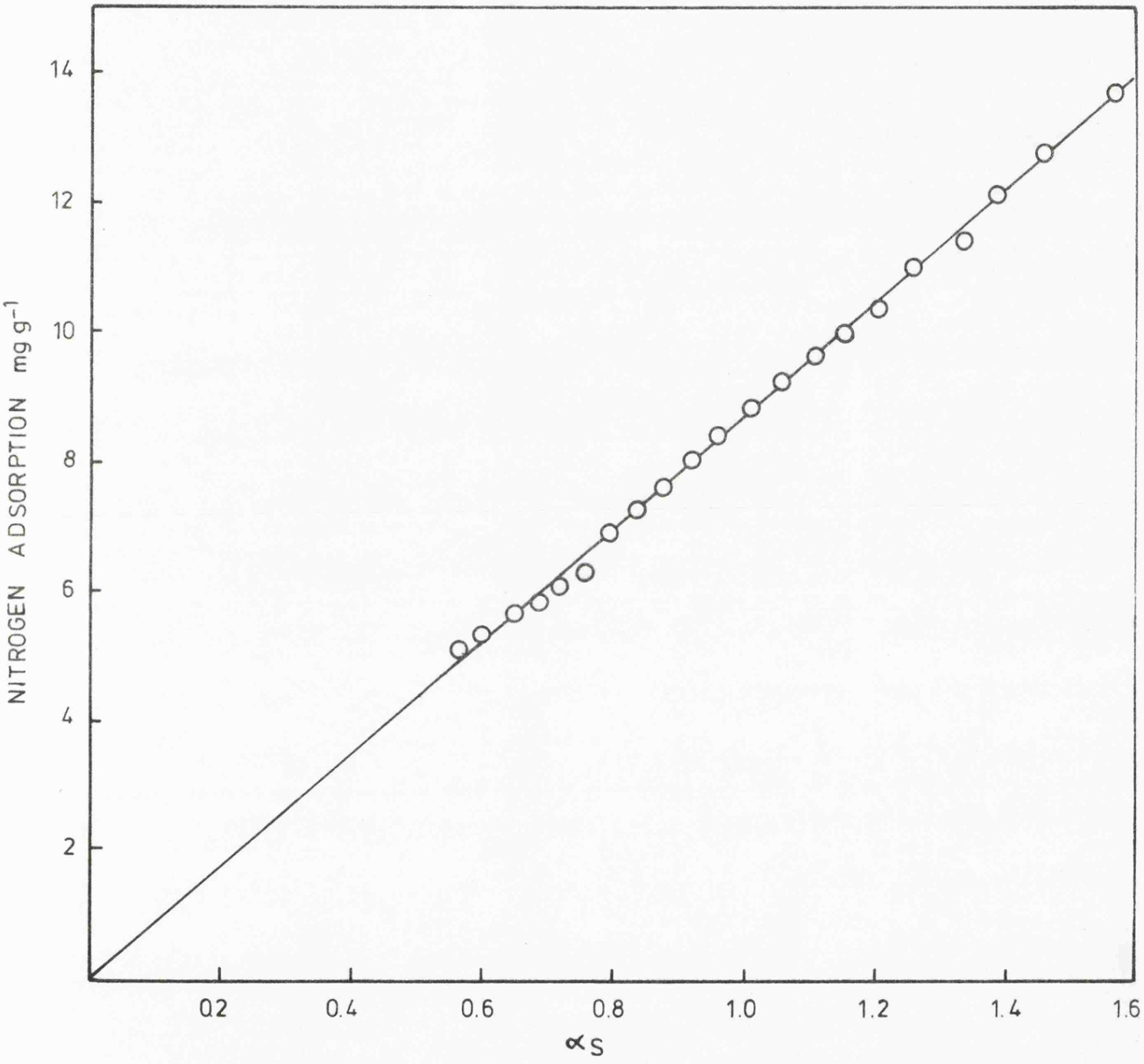

Fig.4.17 α_s plot for nitrogen adsorption on γ-MnOOH using Degussa 'Aluminiumoxid C' as the reference solid.

Fig.4.18 Scanning electron migrograph of γ-MnOOH (X20,000).

where the factor 2.25 was obtained by calibration against the BET area of γ-MnOOH.

Surface areas of the chemical reduction products of γ-MnO_2 were calculated from nitrogen adsorption isotherms and are shown graphically in fig.4.19. Contrary to a previous report in the literature[54] the BET surface area decreased from 33.7 m^2g^{-1} for the 'as-received' sample to 20.7 m^2g^{-1} for the most highly reduced sample. This reduction in surface area was not linearly dependent on the sample composition. After the initial gradual decrease in area from $MnO_{1.95}$ to $MnO_{1.80}$ a constant value was maintained until a composition of $MnO_{1.62}$ was reached when there was a sharp decrease in area. This complex relationship may be connected with the structural reorganisation that was postulated to take place in the region of $MnO_{1.65}$ - $MnO_{1.75}$. The only reference in the literature to the determination of the surface area of these materials appears in the work of Laragne and Brenet[54]. These authors measured the BET surface area of two reduced samples having compositions of $MnO_{1.94}$ and $MnO_{1.67}$ and found the variation in surface area to be very small, obtaining values of 32.4 and 31.9 m^2g^{-1} respectively. Fig.4.20 shows the α_s plots for nitrogen adsorption on the chemical reduction products. A small amount of microporosity was present in all but the most reduced sample. The change in external surface area followed a similar trend to the areas obtained by the BET procedure.

It was of interest to observe the change in porosity on conversion of MnOOH to Mn_2O_3. Alario Franco, Baker and Sing[98]

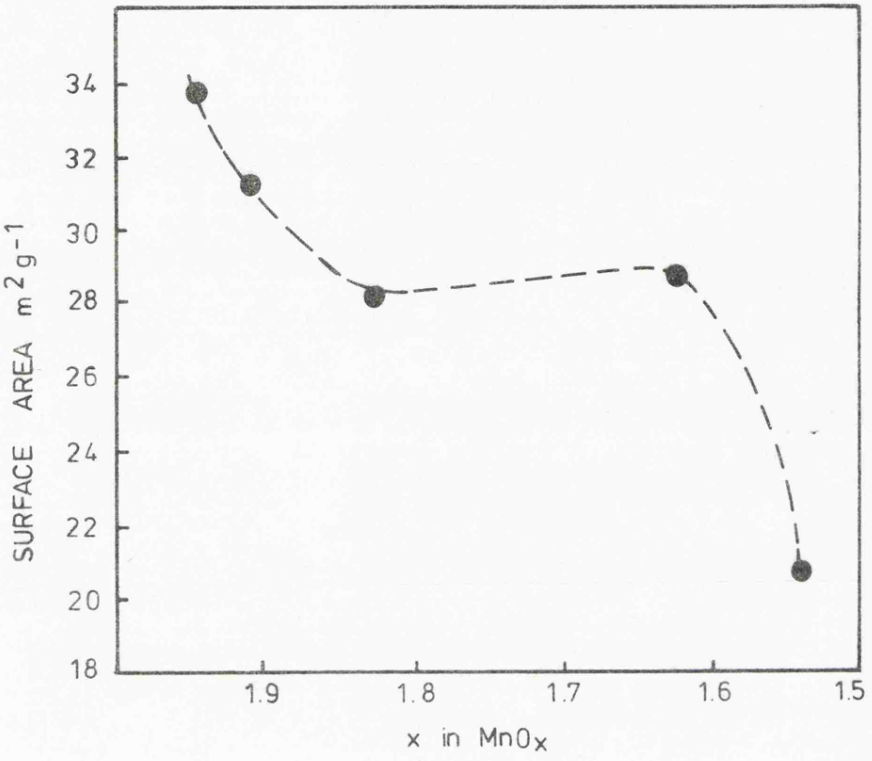

Fig.4.19 Surface area as a function of sample composition for partially reduced γ-MnO_2.

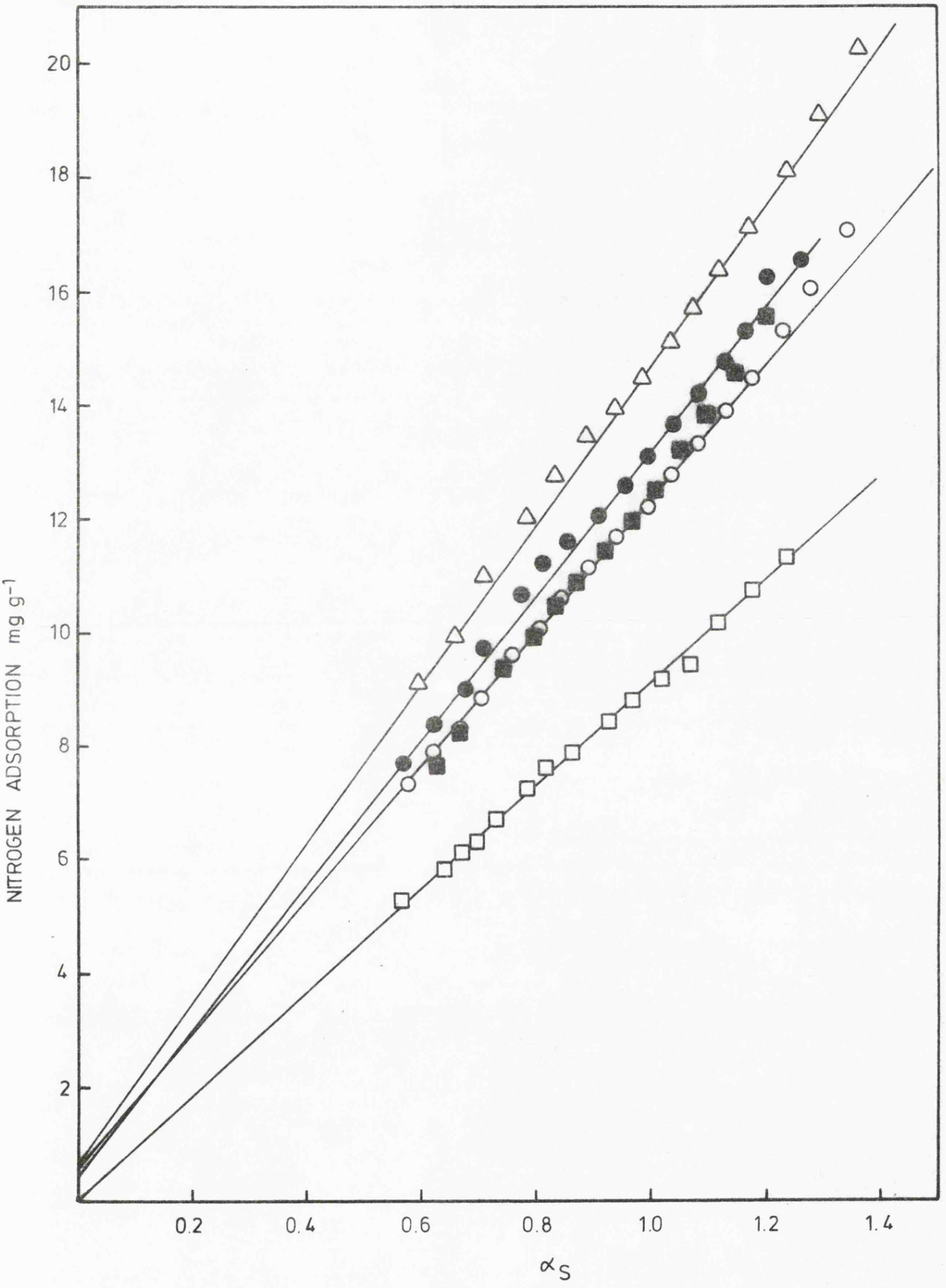

Fig.4.20 α_s plots for nitrogen adsorption on partially reduced γ-MnO_2. x in MnO_x = 1.946 Δ, 1.909 ●, 1.825 ⊖, 1.62 ■ and 1.54 □.

found that the thermal decomposition of chromium oxyhydroxide to chromium sesquioxide via chromium dioxide in vacuo resulted in a surface area increase from 15 m^2g^{-1} at 25°C to 124 m^2g^{-1} at 630°C before decreasing to 23 m^2g^{-1} at 800°C. Nicolaon and Teichner[77] observed an increase in surface area during the decomposition of $Ni(OH)_2$ (18.3 m^2g^{-1}) to NiO (141 m^2g^{-1}). Dehydroxylation in vacuo of the chemical reduction products was also expected to produce surface area changes and a typical α_s plot for $MnO_{1.54}$ outgassed at 200°C is illustrated in fig.4.21. The BET surface area increased from 20.7 m^2g^{-1} at 25°C to 60.7 m^2g^{-1} at 200°C and it is apparent from the α_s plot that this was primarily due to an increase in micro-porosity. Similar results were obtained on other reduction products and the data are presented in Table 4.5. It is

TABLE 4.5

EFFECT OF OUTGASSING TEMPERATURE ON THE SURFACE AREA OF PARTIALLY REDUCED γ-MnO_2

x in MnO_x	surface area after evacuation at 25°C m^2g^{-1}	surface area after outgassing at 200°C m^2g^{-1}	surface area increase m^2g^{-1}
1.946	33.7	41.7	8.0
1.825	28.1	39.5	11.4
1.62	28.8	59.2	30.4
1.54	20.7	60.7	40.0

interesting to note that a plot of generated micropore volume as a function of sample composition (Fig.4.22) was linear with

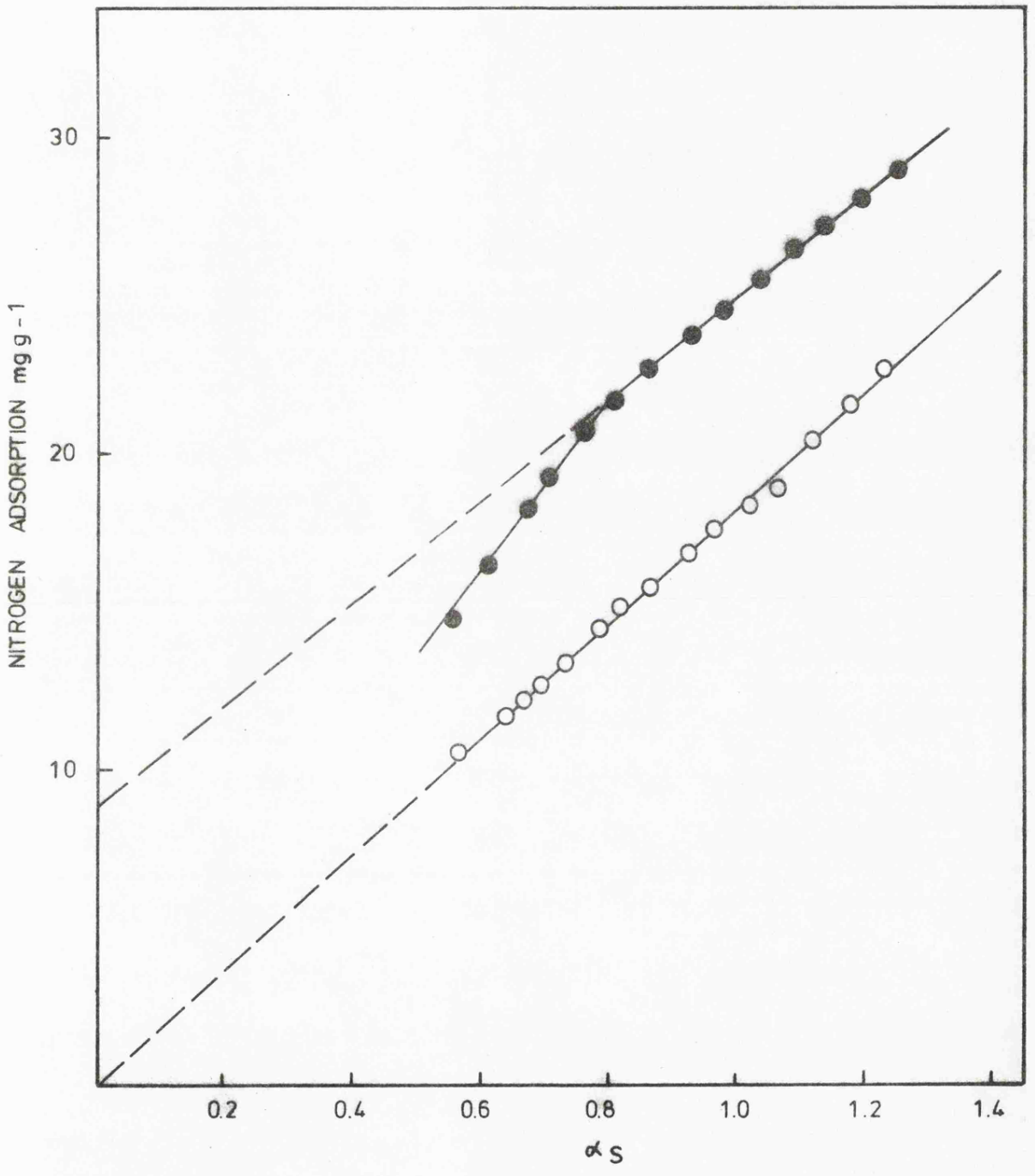

Fig.4.21 α_s plot for nitrogen adsorption on $MnO_{1.54}$ outgassed at 25°C (O) and 200°C (●).

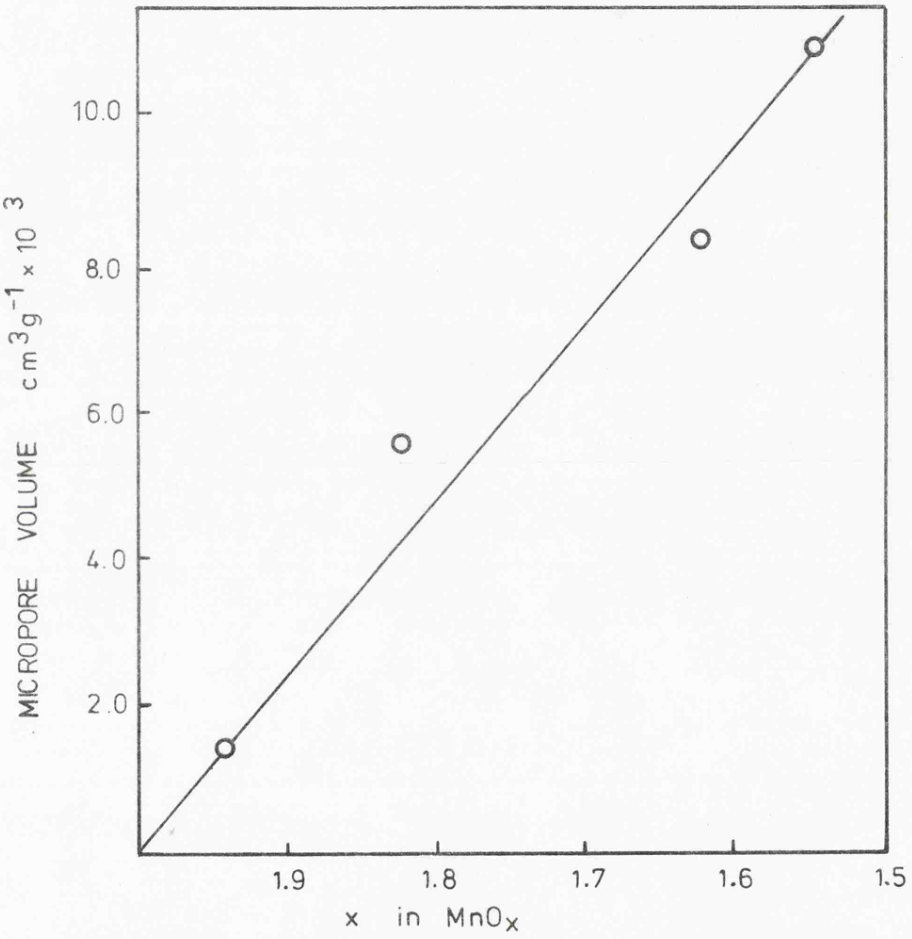

Fig.4.22 Micropore volume as a function of sample composition for the chemical reduction products of γ-MnO_2 outgassed at 200°C.

a gradient that passed through the origin. This confirms that the porosity revealed on outgassing at 200°C is a result of the removal of hydroxyl groups from the interior of the solid.

4.4(ii) Nonane adsorption

Gregg and Langford[80] developed a technique whereby micropores in carbons could be detected by adsorption of nonane. Changes in nitrogen isotherm character before and after pre-adsorption of the hydrocarbon vapour could be interpreted in terms of micropore blockage. There is a limited amount of data available in the literature concerning the extension of this technique to oxidic materials. This method has therefore been applied to some oxides of manganese as an independent method of micropore assessment and the results compared with those obtained from α_s plots.

Nitrogen isotherms obtained before and after pre-adsorption of nonane on $MnO_{1.54}$ outgassed at 200°C are shown in fig.4.23(Top). It can be seen that the nitrogen uptake by $MnO_{1.54}$ is greater prior to adsorption of the hydrocarbon vapour. The two isotherms are nearly parallel in the multilayer region, the vertical separation between the curves being a measure of the micropore contribution. It appears therefore that nonane is capable of being strongly held by the micropores in this particular oxide of manganese.

Fig.4.23(Bottom) depicts the BET plots calculated from the nitrogen adsorption data. The surface available for nitrogen

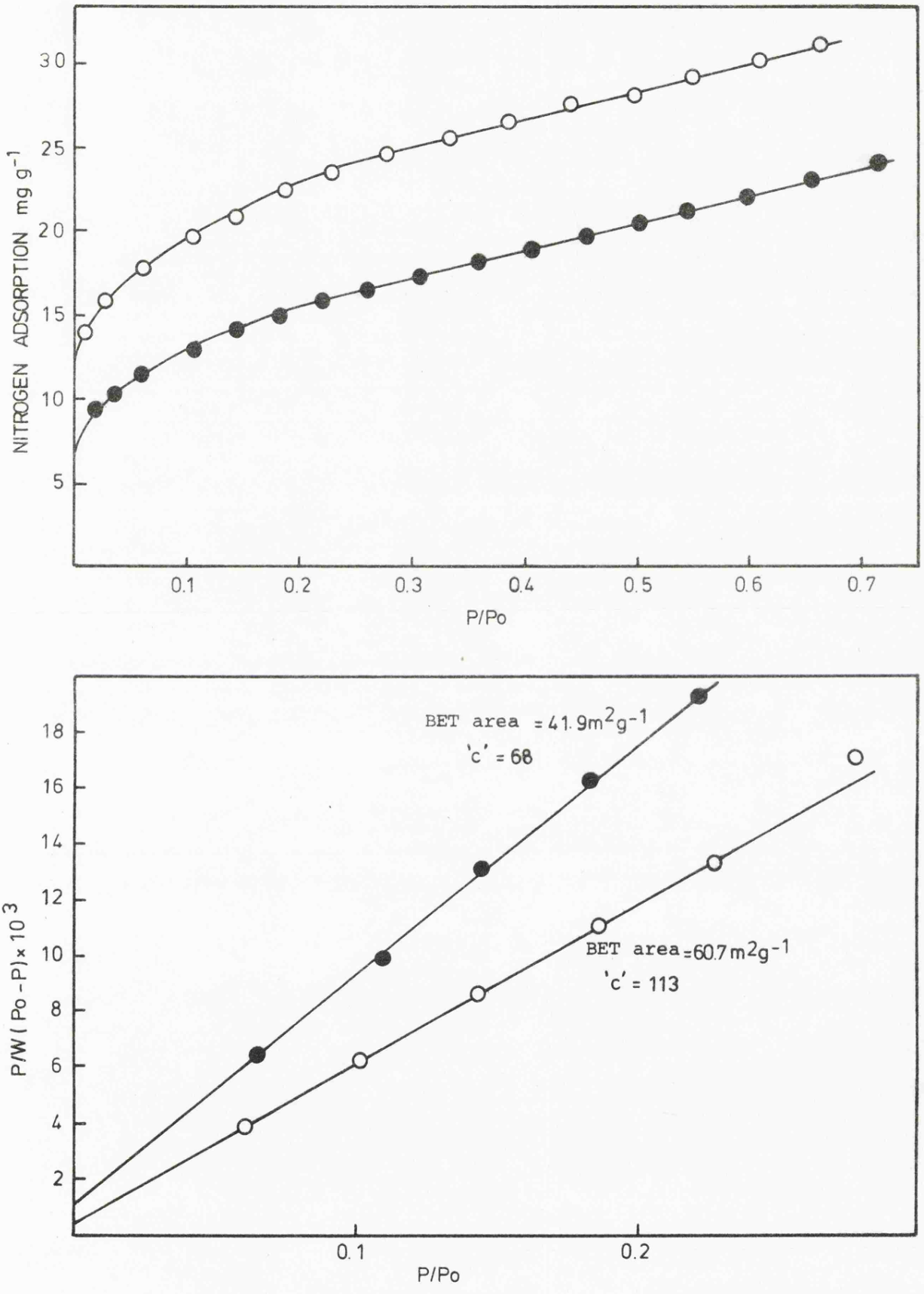

Fig.4.23 Top. Nitrogen adsorption isotherms for $MnO_{1.54}$ outgassed at 200°C. Before (O) and after (●) pre-adsorption of nonane.

Bottom. BET plots calculated from the adsorption data shown above.

adsorption had decreased from 60.7 m^2g^{-1} prior to nonane adsorption to 41.9 m^2g^{-1} after sorption of the alkane. The change in the BET 'c' value from 113 to 68 is significant. 'c' is a measure of the interaction energy between the adsorbate and adsorbent[130]. The only difference as far as the nitrogen molecule is concerned between the two samples studied above is that in one sample sorption can occur both on the open surface and in micropores whereas in the other nitrogen adsorption takes place only on the open surface. It is known that the heat of adsorption in micropores is greater than on an open surface[130]. Differences in 'c' therefore reflect solely changes in the microporosity of the sample. In other words if outgassing a sample at an elevated temperature is accompanied by the formation of micropores this effect will tend to increase 'c' irrespective of any changes in the chemical nature of that surface. It cannot therefore be assumed that increases in the value of 'c' sometimes obtained upon outgassing oxidic materials results solely from surface dehydroxylation. Increase in 'c' may result from changes in the micropore contribution or from the removal of surface hydroxyl groups or a combination of these two effects.

α_s plots for nitrogen adsorption on $MnO_{1.54}$ before and after pre-adsorption of nonane are shown in fig.4.24. These confirm that the primary effect of the nonane was to adsorb strongly in the micropores and reduce the surface available for nitrogen adsorption. The linear part of the α_s plot for the sample with

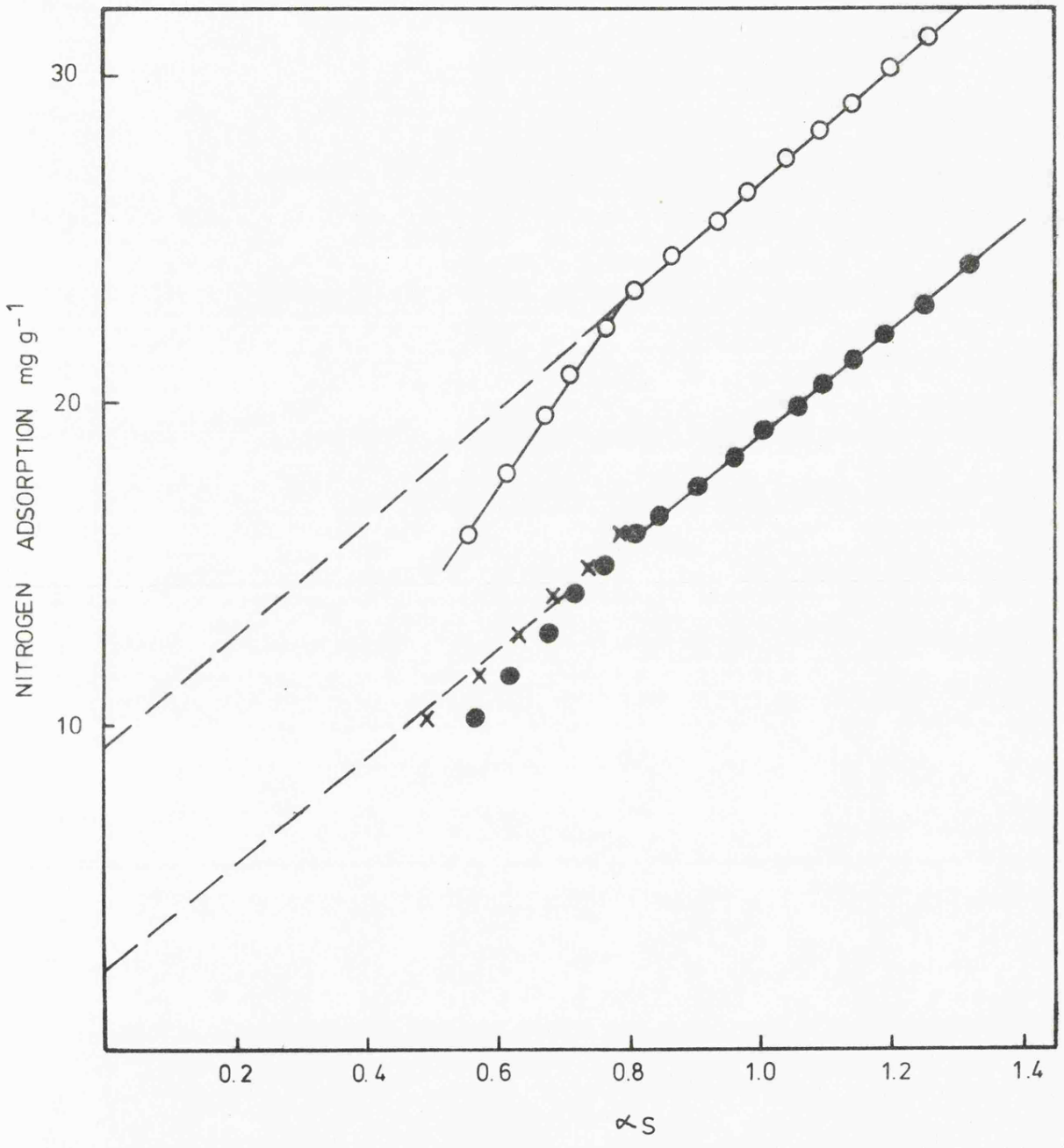

Fig.4.24 α_s plots for nitrogen adsorption on $MnO_{1.54}$ outgassed at 200°C before (O) and after (●) pre-adsorption of nonane. X denotes values obtained after application of Dubinin's procedure[133] to take into account the difference in BET 'c' value between the sample and the standard.

pre-sorbed nonane does not extrapolate to the origin, i.e. total blocking of the micropores was not achieved. The time allowed for nonane adsorption on to the sample ($\sim$ 2 hours) was considered adequate and extension of the equilibration time to 16 hours did not remedy the situation. It seems likely that steric factors contribute to the observed behaviour.

It is of interest to compare the amount of nitrogen uptake by the micropores with that of nonane. The micropore volume of the outgassed solid should be equal to the total volume (calculated as liquid) of the adsorbate whether nitrogen or nonane is held in the micropores.

The amount of nitrogen adsorbed in the volume occupied by nonane = 6.75 mg g^{-1} from the α_s plots in fig.4.24. This is equivalent to a micropore volume of (6.75×10^{-3}). $\rho_{N_2}^{-1}$ cm^3 g^{-1}. Taking the density of nitrogen (ρ_{N_2}) at 77 K as 0.81 g cm^{-3} the micropore volume is equal to 8.3×10^{-3} cm^3 g^{-1}. The amount of nonane uptake was measured directly and found to be 6.87 mg g^{-1}. The density of liquid nonane at 77 K may be calculated from the relationship[131].

$$\rho_t = \rho_s + 10^{-3}\ \alpha(t - t_s) + 10^{-6}\ \beta(t - t_s)^2 \qquad (4.11)$$

where for nonane at 77 K

$$t = -195.2\ ,\ \alpha = -0.75 \text{ and } \beta = -0.455.$$

This gives a value of 0.90 g cm^{-3} for the density of nonane at 77 K. The micropore volume is accordingly (6.87×10^{-3}) $(0.90)^{-1} = 7.7 \times 10^{-3}$ cm^3 g^{-1}. Thus there is good agreement between the micropore volumes calculated from the two adsorbates. Gregg and Langford[80] found that this was not true for nonane

adsorption on carbon and attributed this to two disturbing features arising from the narrowness of the pores, (a) the modification of the density of the adsorbate from that of the bulk liquid (b) steric effects which will interfere with the normal packing of the molecules. The fact that a discrepancy is not present in our case may result from a difference in the size of the micropores in this oxide of manganese compared to those of carbon. However, there are presumably some very small pores in the oxide as judged by the fact that total blocking by nonane could not be achieved.

Extrapolation of the four data points at lowest α_s in fig.4.24 intercepts the ordinate at a negative value. This is a consequence of the difference in 'c' value between the reference material and the sample under study[132]. In a recent publication Dubinin[133] outlined a procedure whereby a number of standard t or α_s plots corresponding to different BET 'c' values could be calculated from a single experimental curve. The manganese oxyhydroxide reference material has a BET 'c' value of 143 compared to 68 for the outgassed $MnO_{1.54}$ containing pre-adsorbed nonane. Modification of the α_s data on the reference material using Dubinin's procedure to take into account the change in 'c' value from 143 to 68 alters the shape of the α_s plot (lower) in fig.4.24 below $\alpha_s = 1.0$. The improved points are denoted by a cross. Application of this technique has the effect of decreasing the α_s value at $c = 68$ compared to $c = 143$ enabling extrapolation of the α_s plot in the low relative pressure region to intercept nearer

the origin. It has however very little effect on the value of micropore volume as determined by extrapolation of the linear portion of the plot above α_s = 1.0 on to the vertical axis.

Nonane adsorption experiments have also been carried out on $MnO_{1.62}$ after outgassing at 200°C in order to generate a micropore network. Nitrogen adsorption isotherms determined before and after pre-adsorption of nonane are shown in fig. 4.25(Top). These are similar to those obtained on $MnO_{1.54}$ indicating that sorption of nonane had resulted in micropore blocking. BET plots (Fig.4.25 Bottom) indicated a change in surface area from 59.2 $m^2\ g^{-1}$ prior to nonane adsorption to 39.0 $m^2\ g^{-1}$ after pore blocking. α_s plots for the two samples however (Fig.4.26) differed from those obtained for $MnO_{1.54}$. It appeared that complete filling of the micropores had been achieved but that the linear portions of the α_s plots were not completely parallel. The α_s plot was also complicated by departure from linearity in the high pressure region due to capillary condensation which was not evident for $MnO_{1.54}$. The surface area of 37.9 $m^2\ g^{-1}$ after pre-adsorption of nonane as determined from the slope of the α_s plot was in close agreement with the BET surface area (39.0 $m^2\ g^{-1}$) confirming the validity of the extrapolation in fig.4.26. The external surface area of 42.5 $m^2\ g^{-1}$, determined from the slope of the α_s plot prior to nonane adsorption, was demonstrably greater than that found after sorption of the hydrocarbon. This may result from nonane remaining on the open surface but evidence

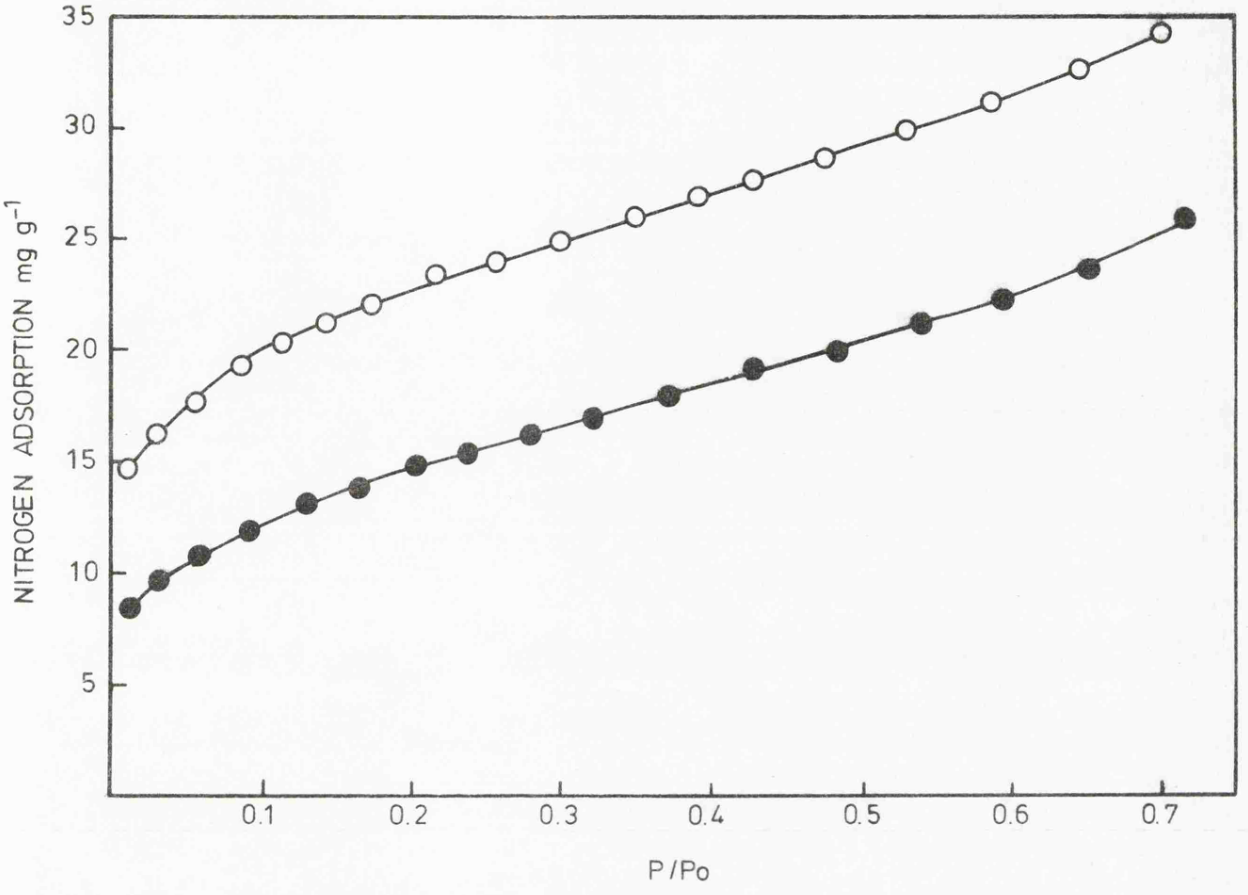

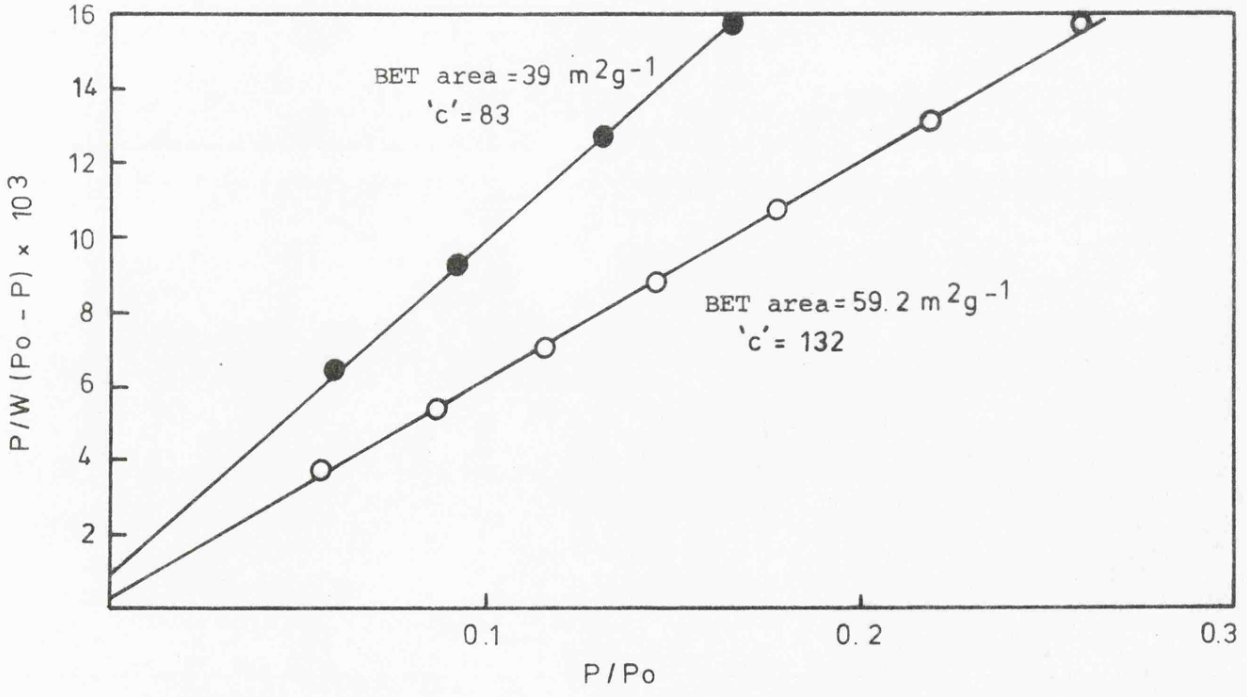

Fig.4.25 Top. Nitrogen adsorption isotherms for $MnO_{1.62}$ outgassed at 200°C. (O) before and (●) after pre-adsorption of nonane.

Bottom. BET plots calculated from the adsorption data shown above.

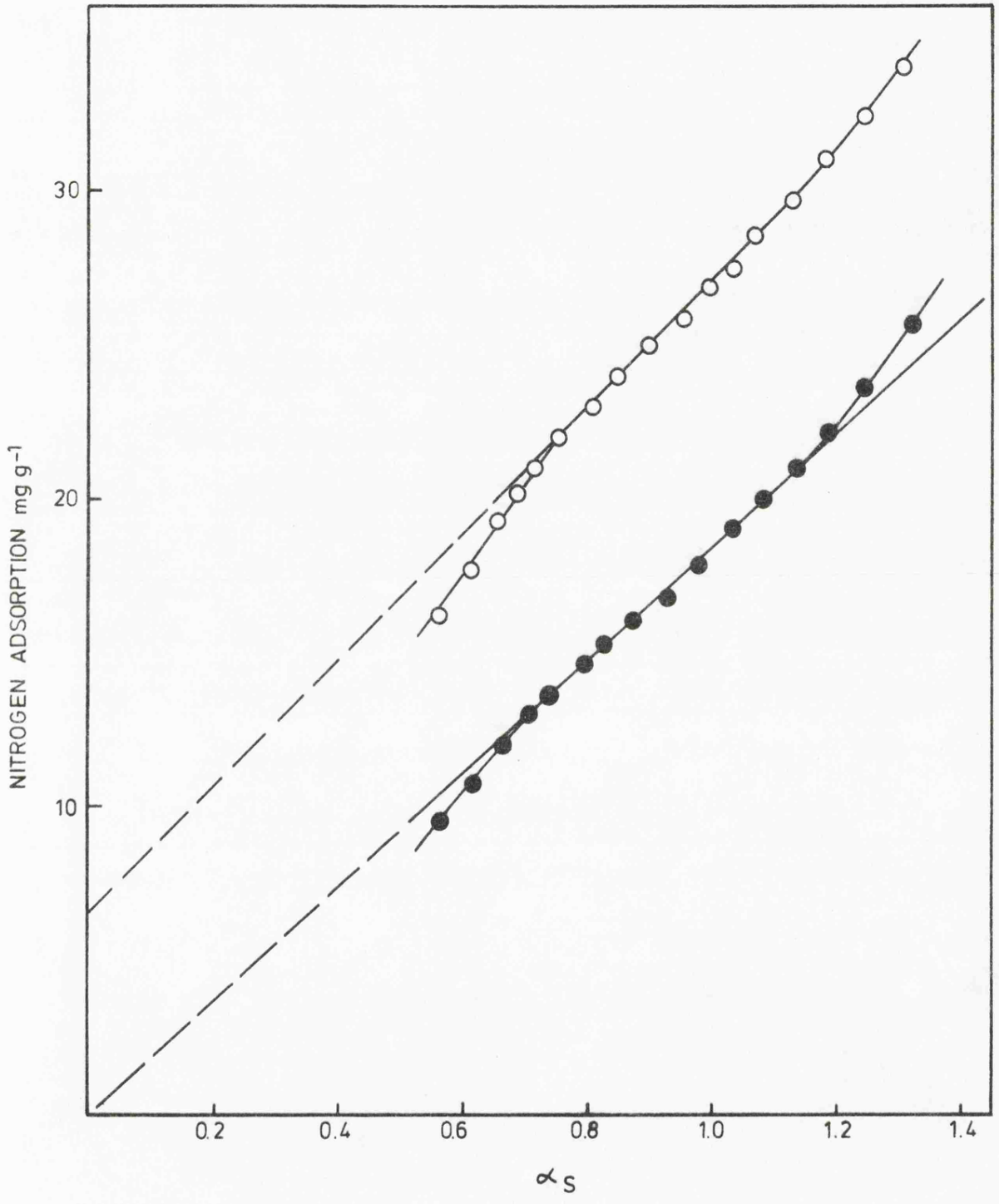

Fig.4.26 α_s plots for nitrogen adsorption on $MnO_{1.62}$ outgassed at 200°C. (O) before and (●) after pre-adsorption of nonane.

in favour of this is lacking. Nitrogen adsorption isotherms determined on the non-porous γ-MnOOH reference material before and after exposure to nonane vapour were identical indicating that chemisorption of nonane had not occurred. It would therefore be unlikely to take place on $MnO_{1.62}$ in view of the similar chemical nature of the surfaces.

The micropore volume formed on outgassing was calculated from the intercept of the α_s plot and directly from the amount of nonane adsorbed as previously outlined. The values obtained were 8.2 and 8.4 x 10^{-3} cm^3 g^{-1} respectively, again showing good agreement. The microporosity was difficult to determine accurately by extrapolation of the linear segment of the α_s plot and so such good agreement was a little surprising. Nevertheless in both cases studied the micropore volumes generated by outgassing the oxides of manganese and determined from the nitrogen and nonane adsorption data are of the same order in contrast to Gregg and Langford's findings for carbon.

CHAPTER 5

Manganese Oxyhydroxide and Oxides of Manganese

5.1 Thermal decomposition of γ-MnOOH

5.1.(i) Vacuum. Isolation of Mn_2O_3 isostructural with corundum

The thermal behaviour of γ-MnOOH has received scant attention in the literature and the products obtained upon thermal treatment have been insufficiently characterised. The majority of the studies have been performed on samples obtained by oxidation of manganous sulphate solutions in alkaline media. As mentioned in Chapter 2 the nature of the products obtained can be diverse and therefore it is not sufficient to assume that the precipitated material is necessarily γ-MnOOH. Giovanoli and Leuenberger[10] obtained a well crystallised specimen of γ-MnOOH based on this synthetic route and details given by these authors have been used to obtain the samples investigated in this present study. Three different samples were prepared by varying the temperature at which the precipitation was carried out.

The TPD curve obtained from the thermal decomposition in vacuum of the sample prepared at 100°C (sample A) is illustrated in fig.5.1. Two rate of weight loss peaks were present between ambient temperature and 700°C. The first occurred at 298°C and was followed by a smaller weight loss at 535°C. The weight loss of 10.7% associated with the initial decomposition step is in good agreement with the expected water removal resulting from the dehydroxylation of γ-MnOOH to Mn_2O_3 (10.2%).

The thermal decomposition of γ-MnOOH was first reported by

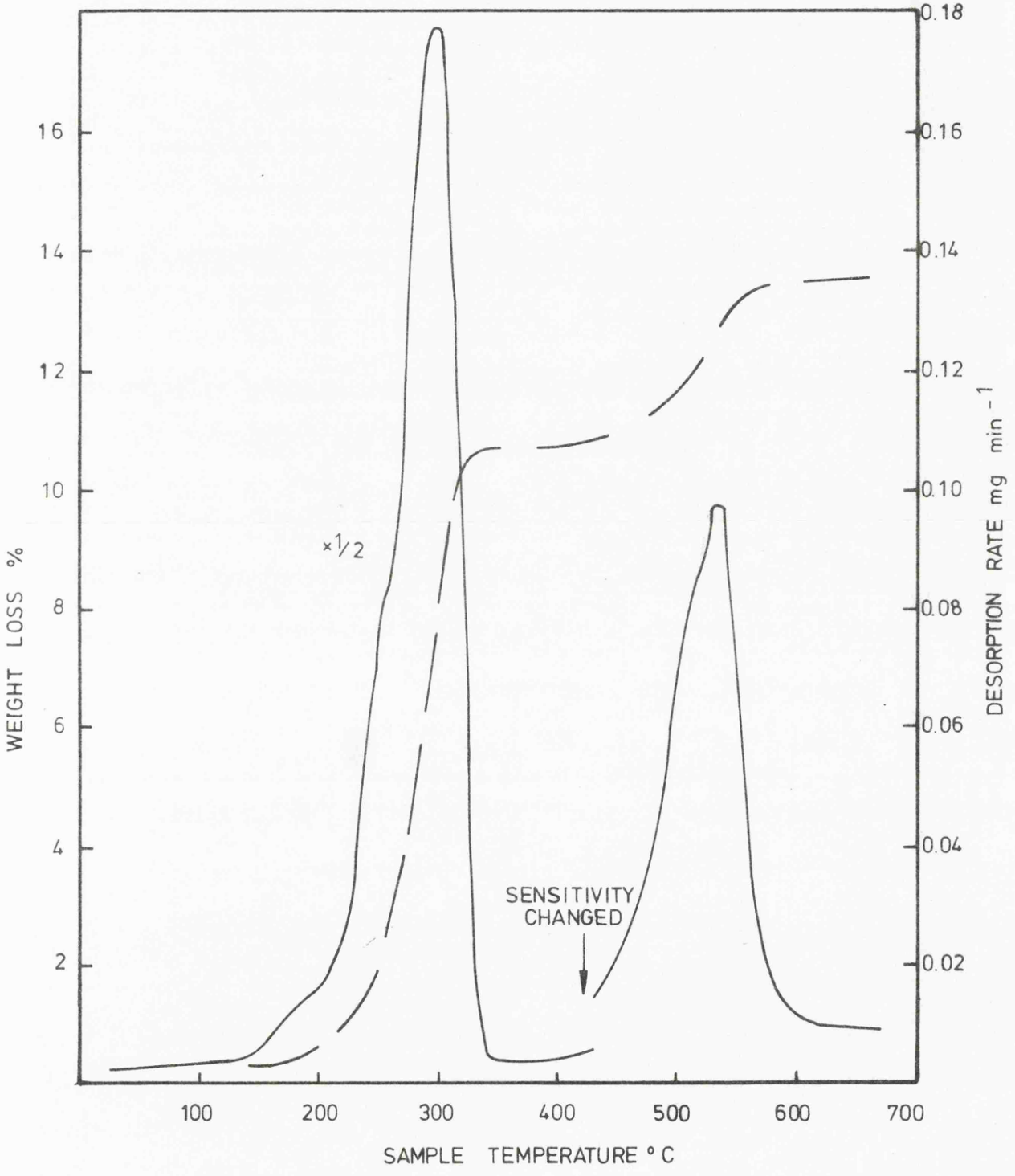

Fig.5.1 Thermal decomposition in vacuum of Sample A. Weight loss (— —) and rate of decomposition (———) curves. Sample weight 63.1 mg.

Dubois[13]. He observed that the oxyhydroxide obtained by oxidation of manganese sulphate in an alkaline medium decomposed at 250°C in vacuum to produce a variety of Mn_2O_3 which differed from the common C-type sesquioxide. Although an X-ray line diagram was presented which strongly resembled α-Mn_3O_4, the absence of a suitable scale along the abscissa prevented any comparison of the data with that described later in this thesis. Verwey and de Boer[14] repeated the preparation of this variety of Mn_2O_3 and suggested that its structure could be described by an Mn_3O_4 lattice containing cation vacancies. The relationship between this modification of Mn_2O_3 and α-Mn_3O_4 was considered to be analogous to that of γ-Fe_2O_3 and Fe_3O_4 and for that reason was designated γ-Mn_2O_3.

In order to characterise the compound produced by dehydroxylation of sample A an X-ray diffractometer trace was taken of the product obtained at the end of the first decomposition stop. This is shown in fig.5.2b and did not correspond with the patterns reported by Dubois and Verwey and de Boer. Other authors[15, 134] have presented X-ray line diagrams for γ-Mn_2O_3 and these are reproduced in fig.5.3. It can be seen however, that there is disagreement amongst the various workers and none of the patterns resembles the pattern presented in this work.

Close examination of the X-ray data in fig.5.2b revealed that a large number of the lines could be attributed to α-Mn_3O_4

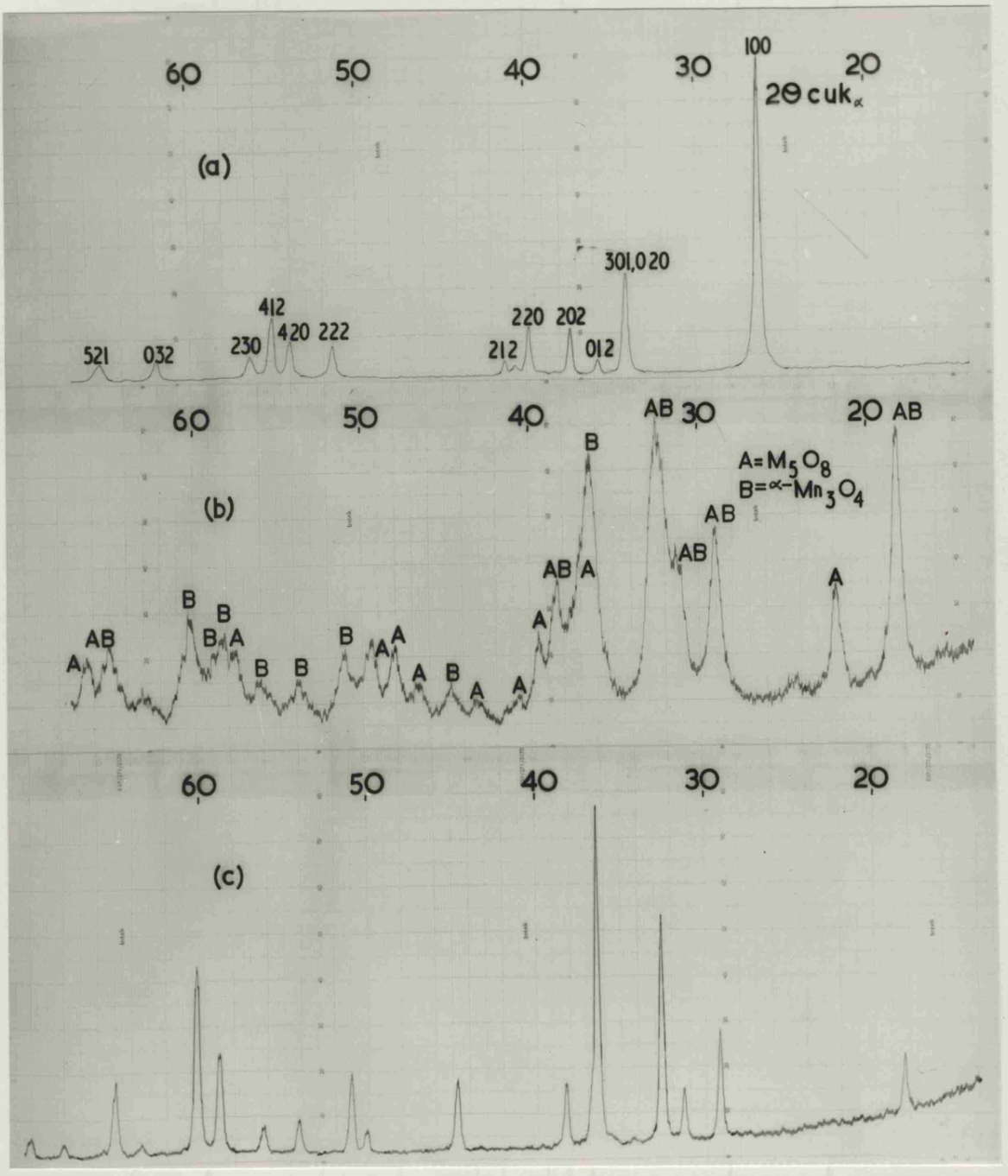

Fig.5.2 X-ray diffractometer traces (Cu K_α) of the products obtained by application of a linear heating programme ($5^oC\ min^{-1}$) to γ-MnOOH (sample A) in vacuum. These correspond with temperatures of (a) 25^o (b) 370^o and (c) 670^oC on the thermal analysis curve in fig.5.1.

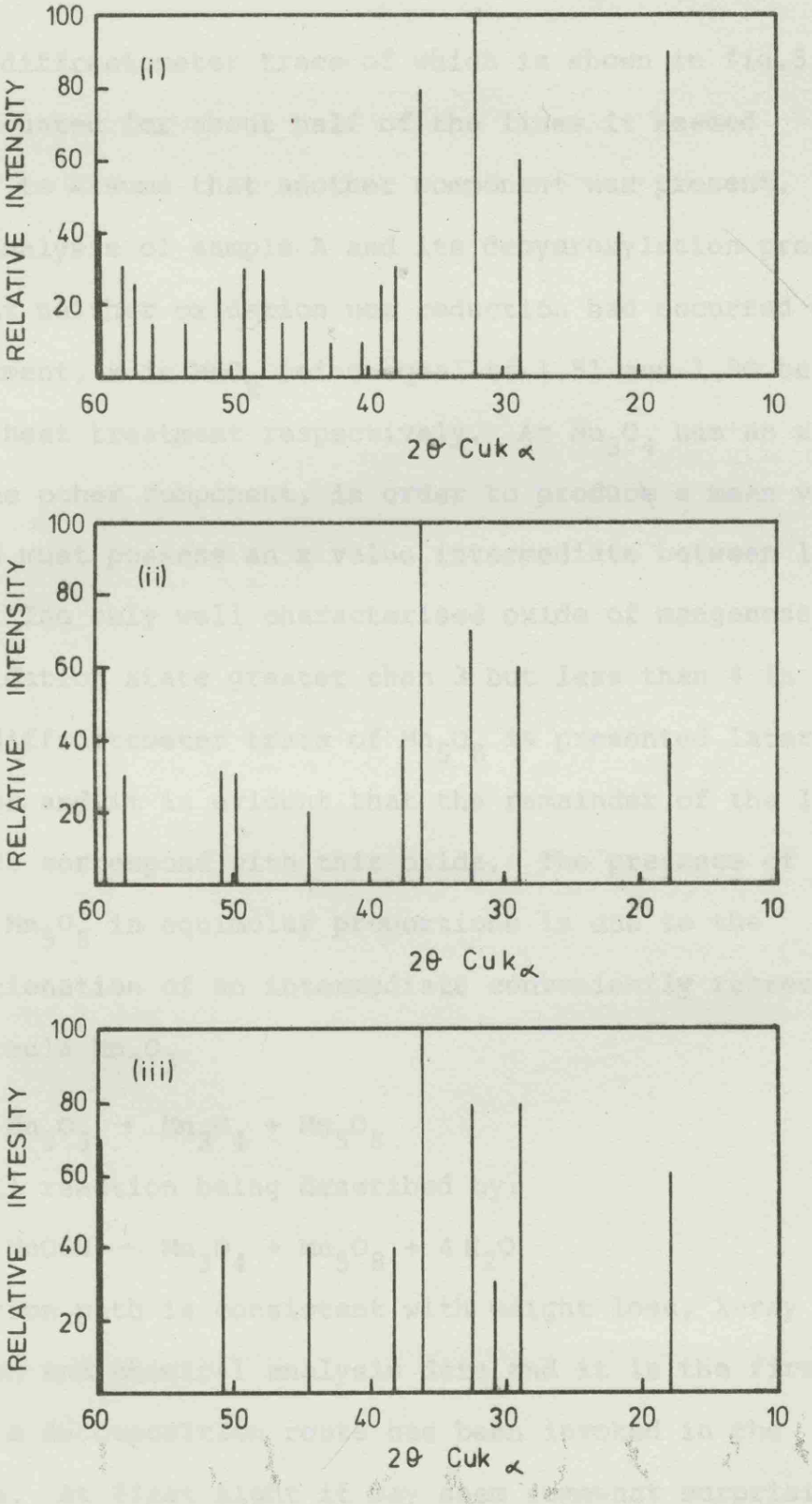

Fig.5.3 X-ray line diagrams for (i) γ-MnOOH (sample A) dehydroxylated in vacuum (ii) γ-Mn_2O_3 prepared by Moore, Ellis and Selwood[15] (iii) γ-Mn_2O_3 prepared by Drotschmann[134].

the X-ray diffractometer trace of which is shown in fig.5.2c. Having accounted for about half of the lines it seemed reasonable to assume that another component was present. Chemical analysis of sample A and its dehydroxylation product showed that neither oxidation nor reduction had occurred on heat treatment, x in MnO_x being equal to 1.51 and 1.50 before and after heat treatment respectively. As Mn_3O_4 has an x value of 1.33 the other component, in order to produce a mean valency state of 3 must possess an x value intermediate between 1.50 and 2.00. The only well characterised oxide of manganese having a mean oxidation state greater than 3 but less than 4 is Mn_5O_8. An X-ray diffractometer trace of Mn_5O_8 is presented later in the Chapter and it is evident that the remainder of the lines in fig.5.2b correspond with this oxide. The presence of Mn_3O_4 and Mn_5O_8 in equimolar proportions is due to the disproportionation of an intermediate conveniently represented by the formula Mn_2O_3

$$4\ Mn_2O_3 \rightarrow Mn_3O_4 + Mn_5O_8 \qquad (5.1)$$

the overall reaction being described by:

$$8\ MnOOH \rightarrow Mn_3O_4 + Mn_5O_8 + 4\ H_2O \qquad (5.2)$$

This reaction path is consistent with weight loss, X-ray diffraction and chemical analysis data and it is the first time such a decomposition route has been invoked in the literature. At first sight it may seem somewhat surprising that the presence of Mn_5O_8 has not been observed in similar studies. A contributing factor, and there are others which will be mentioned later, may be the relatively weak X-ray

diffraction pattern of Mn_5O_8 compared to that of α-Mn_3O_4. Insensitive recordings may reveal the presence of only α-Mn_3O_4 and as the analytical composition of the dehydroxylated product would correspond with a mean valency state of 3 this could have given rise to the claims for a modification of Mn_2O_3 possessing an X-ray pattern almost identical to that of α-Mn_3O_4.

The second decomposition stage results from the decomposition of Mn_5O_8 to Mn_3O_4

$$3\,Mn_5O_8 \rightarrow 5\,Mn_3O_4 + 2O_2 \qquad (5.3)$$

The expected weight loss from equation (5.3) is in good agreement with that found experimentally. An X-ray diffractometer trace of the final decomposition product confirmed that this was α-Mn_3O_4. No data are available in the literature concerning the thermal behaviour of Mn_5O_8 in vacuum. In air or oxygen, however, Oswald, Feitknecht and Wampetich[8] found that decomposition at 550°C to α-Mn_2O_3 occurred. This does not appear to happen in vacuum.

The thermal behaviour of the sample prepared at 25°C (sample B) has also been investigated and the TPD curve obtained in vacuum is shown in fig.5.4. Whereas only two decomposition steps were observed for sample A, sample B appeared to decompose in three distinct stages. The first decomposition step has a maximum rate of weight loss at 255°C and occurs about 40° earlier than for sample A. This results from the smaller particle size of B compared to that of A. The weight loss associated with the initial decomposition process again shows good agreement with

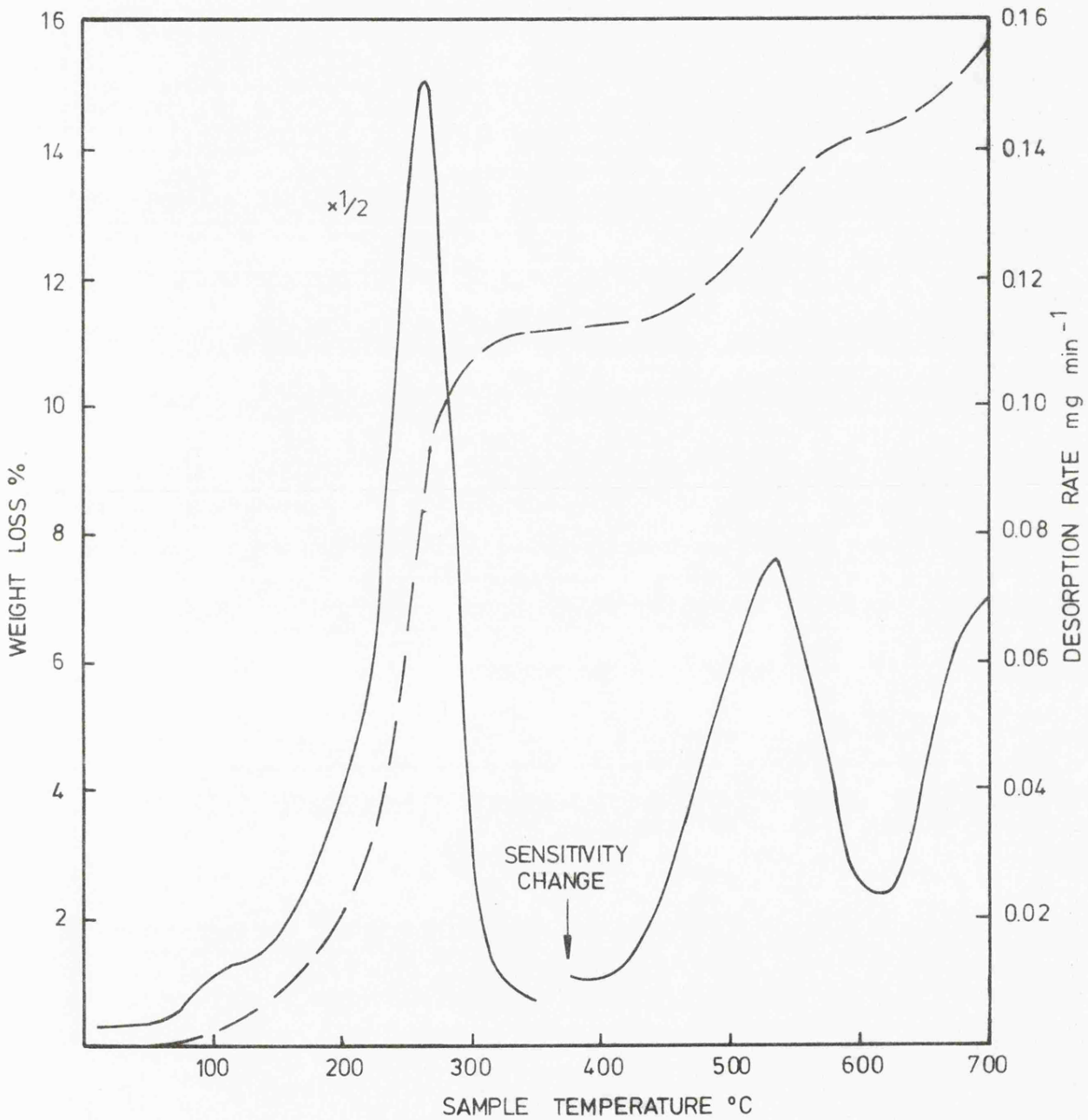

Fig.5.4 Thermal decomposition in vacuum of sample B. Weight loss (— — —) and rate of decomposition (———) curves. Sample weight 60.1 mg.

that expected for the compositional change MnOOH to Mn_2O_3, a marginal increase resulting from the inclusion of surface water which desorbs in the same temperature range. Characterisation of the dehydroxylation product was attempted as for sample A by means of X-ray diffraction. It can be seen from fig.5.5b however, that the diffractometer trace bore little resemblance to that obtained for sample A. Indeed the pattern could not be ascribed to any known oxide of manganese. Before attempting to interpret the two additional decomposition steps the effect of heat treatment on the sample precipitated at 5^oC (sample C) was examined. The TPD curve is illustrated in fig.5.6 and reveals three decomposition peaks as for sample B. As for the two other samples the weight loss associated with the initial decomposition step was related to the dehydroxylation of the oxyhydroxide. Chemical analysis of the dehydroxylation product gave a value for x in MnO_x of 1.50 which confirmed that no change in the mean oxidation state of the manganese ions had taken place on thermal treatment as for sample A. An X-ray diffraction trace of this compound (Fig.5.7b) was similar to that obtained for sample B except for the disappearance of some weak lines present in B and a strengthening of the majority of the remainder. It was tempting to suggest that this compound could correspond only to Mn_2O_3. The weight loss and analytical data were consistent with this hypothesis but the X-ray results appeared to be contradictory. There was some resemblance between this X-ray pattern and that found for α-Mn_2O_3 the common form of Mn_2O_3, but they were clearly not the same compound. No agreement was found between the X-ray data and that reported for γ-Mn_2O_3.

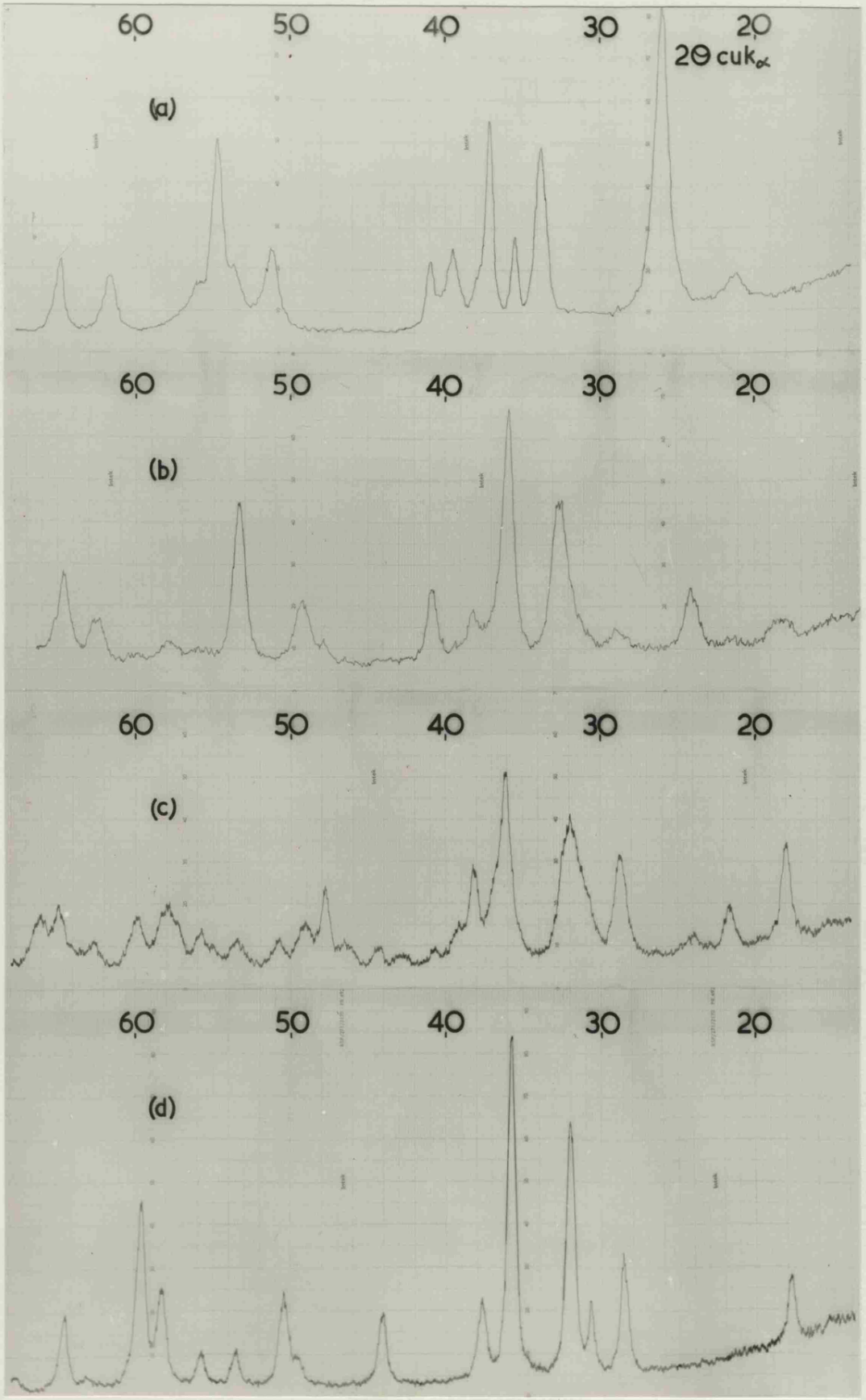

Fig.5.5 X-ray diffractometer traces (Cu K_α) of the products obtained by application of a linear heating programme ($5^oC\ min^{-1}$) to γ-MnOOH (sample B) in vacuum. These correspond with temperatures of (a) 25^o (b) 350^o (c) 520^o and (d) 615^oC on the thermal analysis curve in fig.5.4.

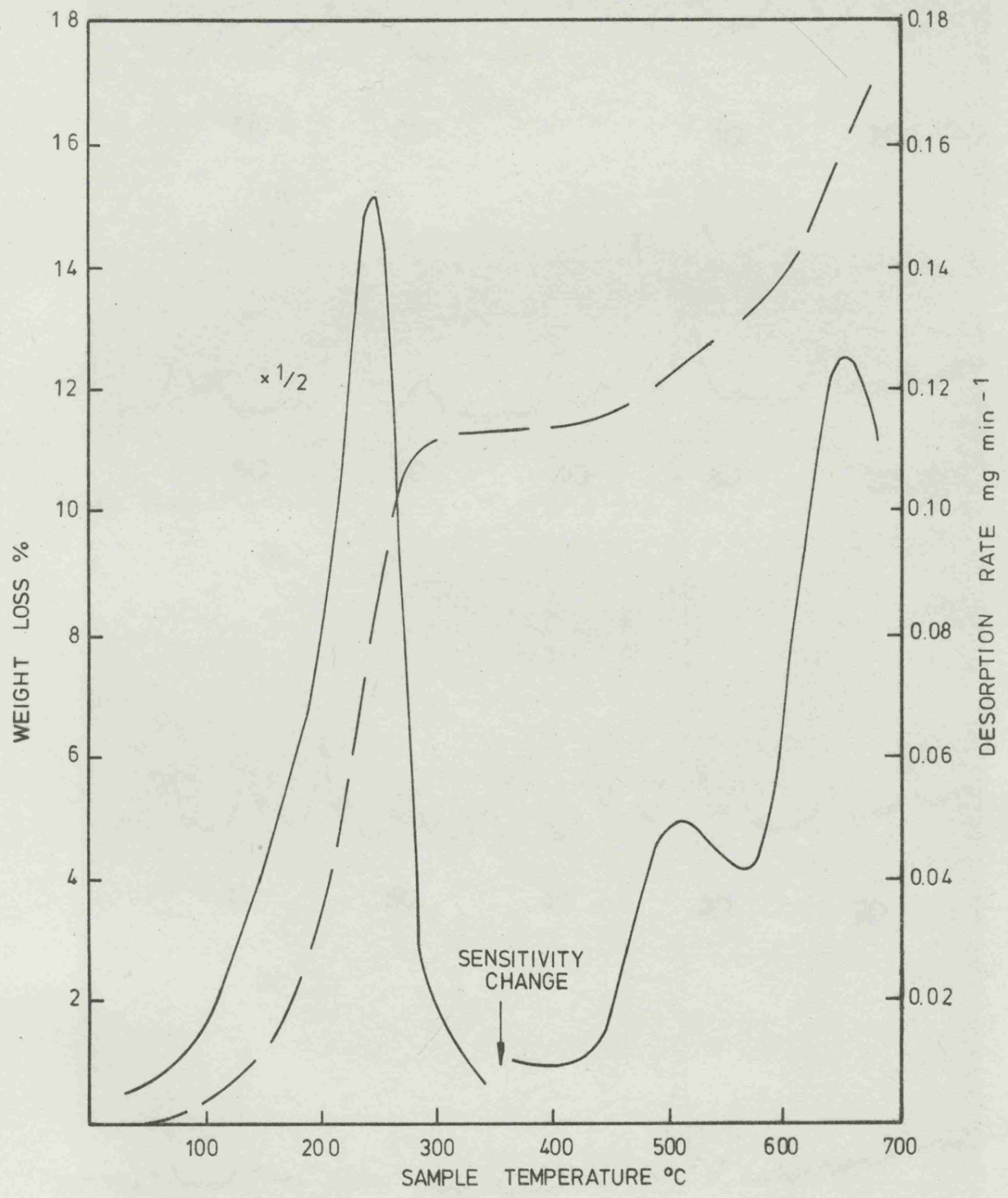

Fig.5.6 Thermal decomposition in vacuum of sample C. Weight loss (— —) and rate of decomposition (——) curves. Sample weight 63.0 mg.

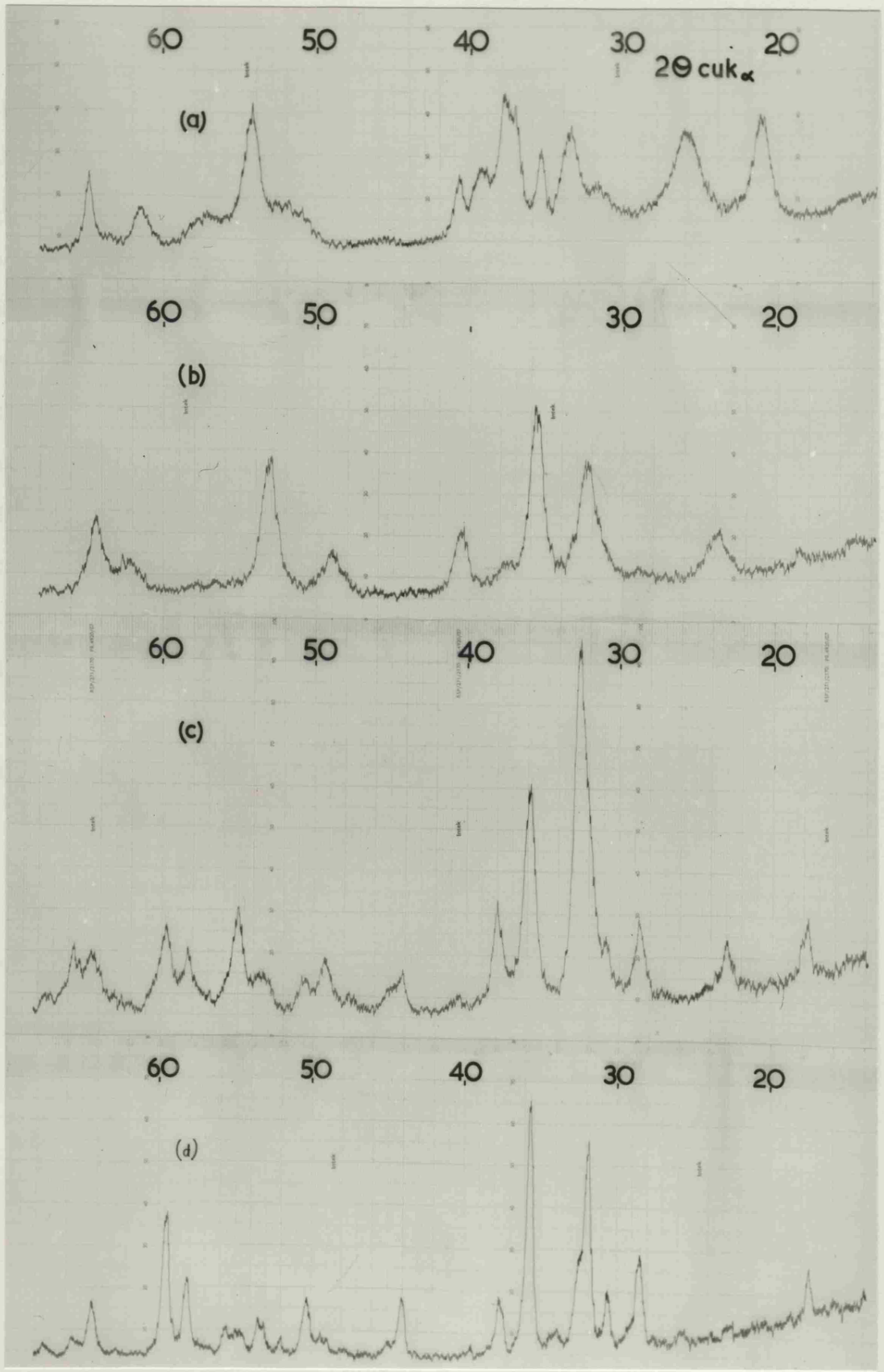

Fig.5.7 X-ray diffractometer traces (Cu K_α) of the products obtained by application of a linear heating programme ($5^oC\ min^{-1}$) to γ-MnOOH (sample C) in vacuum. These correspond with temperatures of (a) 25° (b) 350° (c) 565° and (d) 670°C on the thermal analysis curve in fig.5.6.

Another form of Mn_2O_3 has been described in the literature by Lima-de-Faria and Lopes-Vieira[17] but these results have not to date been substantiated by subsequent workers. These authors studied the transformation of natural groutite (α-MnOOH) at 300°C into β-MnO_2 and observed some weak and diffuse spots on X-ray oscillation photographs which could not be ascribed to β-MnO_2. Some of the spots fitted well into Mn_2O_3 with a corundum structure having a = 4.9 and c = 14.3. Unfortunately no additional X-ray diffraction data were given, which prevented a direct comparison with the trace in fig.5.7b. Following this lead, careful inspection showed that the pattern in fig.5.7b could be indexed on the basis of a corundum unit cell using the ASTM cards of α-Al_2O_3[135] and α-Fe_2O_3[136] and the data are presented in Table 5.1. Lattice parameters were calculated

TABLE 5.1

X-RAY DIFFRACTION DATA FOR Mn_2O_3 - CORUNDUM TYPE

d(Å)	I/I^o *	hkl
3.75	30	012
2.77	65	104
2.52	100	110
2.22	35	113
1.86	25	024
1.72	75	116
1.49	15	124
1.45	45	030 or 300

* These values do not take into account the presence of α-Mn_3O_4

for the sample from the relationship[137]

$$\frac{1}{d^2_{hkl}} = \frac{4}{3}\frac{(h^2 + k^2 + l^2)}{a^2} + \frac{l^2}{c^2} \qquad (5.4)$$

which is valid for crystals with hexagonal unit cells. Approximate values of $\underline{a}$ were obtained by substituting hkl = 110 or 030 from which the mean value of $\underline{a}$ was calculated to be 5.02Å. Values of $\underline{c}$ were found by substituting hkl = 012, 024, 104, 113 and 124 and $\underline{a}$ = 5.02 Å into equation (5.4). The mean value of $\underline{c}$ was calculated to be 14.30 Å. This is in excellent agreement with the results of Lima-de-Faria and Lopes-Vieira.

Apart from possible instability due to Jahn-Teller distortion there does not appear to be any obvious reason why Mn_2O_3 should not crystallise with the corundum structure. Al^{3+}, Cr^{3+}, Ga^{3+} and V^{3+} whose effective ionic radii are smaller than Mn^{3+} and Ti^{3+} which is larger all form oxides of formula M_2O_3 which crystallise with the corundum structure. It was of interest to know if Jahn-Teller distortion was present in the corundum form of Mn_2O_3. A convenient means by which the presence of such a distortion can be detected is from plots of ionic radii versus unit cell volume or a particular lattice dimension for a series of compounds that crystallise with the same structure. Such correlations have been found to be linear or vary in a regular manner if distortion is absent. A relevant example of such a relationship has recently been published by Chenavas, Joubert, Capponi and Marezio[138]. These authors found that a plot of unit cell volume versus ionic radii for a series of oxyhydroxides that crystallised

in the diaspore (α -AlOOH) arrangement varied in a regular manner. The effect of the presence of Jahn-Teller distortion may be illustrated by plotting the lattice parameters for this series of oxyhydroxides as a function of ionic radius and superimposing on this the parameters of α-MnOOH. The values of ionic radii are those given by Shannon and Prewitt[139] and the relationships obtained are shown in fig.5.8. It can be seen that whereas the a axis for α-MnOOH appears 'normal' there is elongation along the b axis and contraction along the c axis suggesting the presence of Jahn-Teller distortion. Application of this method to the oxides possessing a corundum structure produced the relationships shown in fig.5.9. Evidence for the presence of Jahn-Teller distortion is not so convincing as for the diaspore structure but this is likely to be a consequence of the orientation of the octahedra in the corundum structure. This arrangement would not give Jahn-Teller distortion exclusively in the c direction which results in a smaller difference between the expected and observed lattice parameter.

Dehydroxylation of the three samples of manganese oxyhydroxide has led to the formation of three different products. Dehydration of sample A produced an equimolar mixture of α-Mn_3O_4 and Mn_5O_8. Thermal treatment of sample C produced primarily Mn_2O_3 possessing a corundum structure whilst the product resulting from sample B was made up of this modification of Mn_2O_3 and α-Mn_3O_4. In order to understand the reasons for this behaviour it was necessary to examine the nature of the three oxyhydroxides

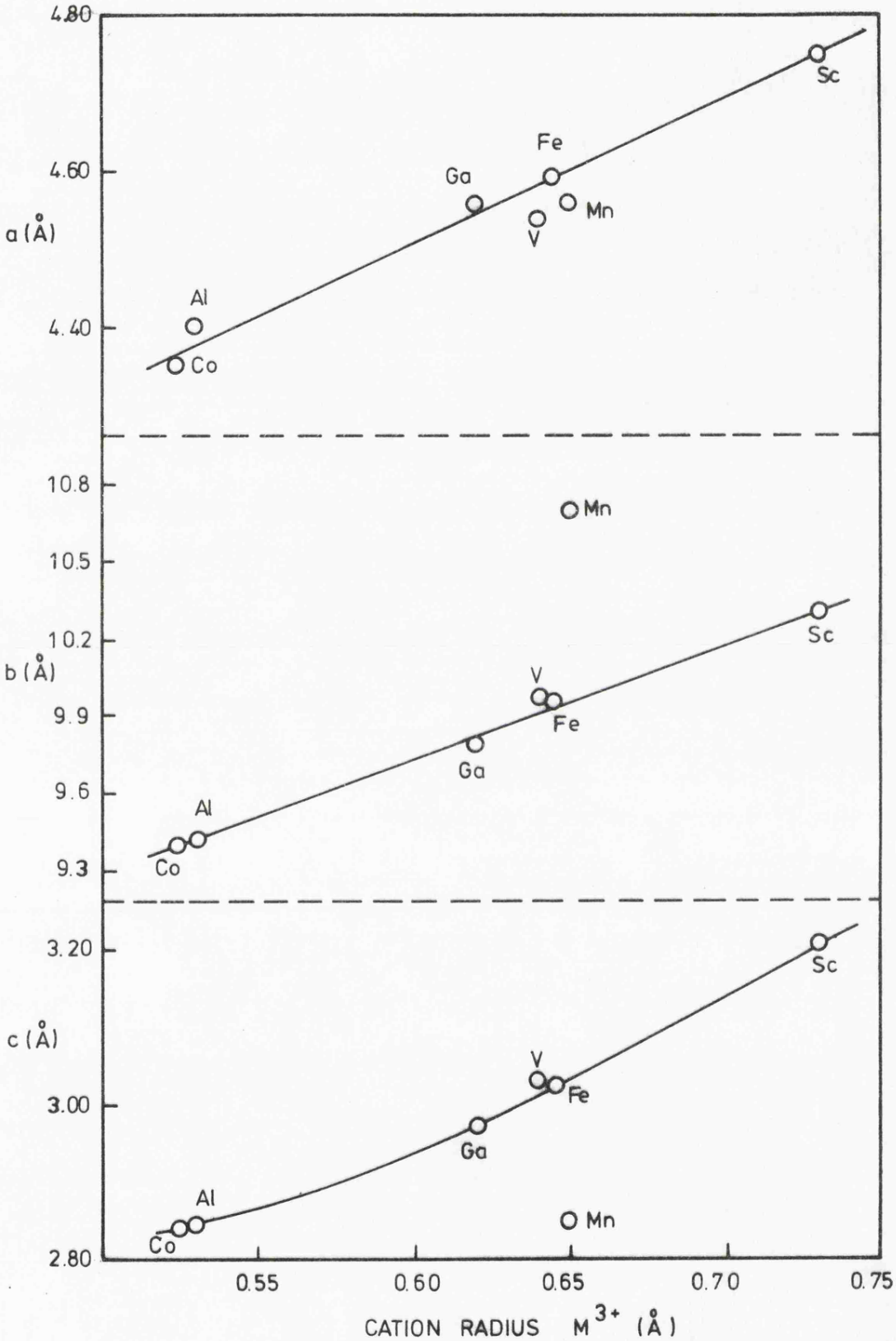

Fig.5.8 Unit cell parameters for oxyhydroxides of formula M^{3+} OOH existing in the diaspore arrangement.

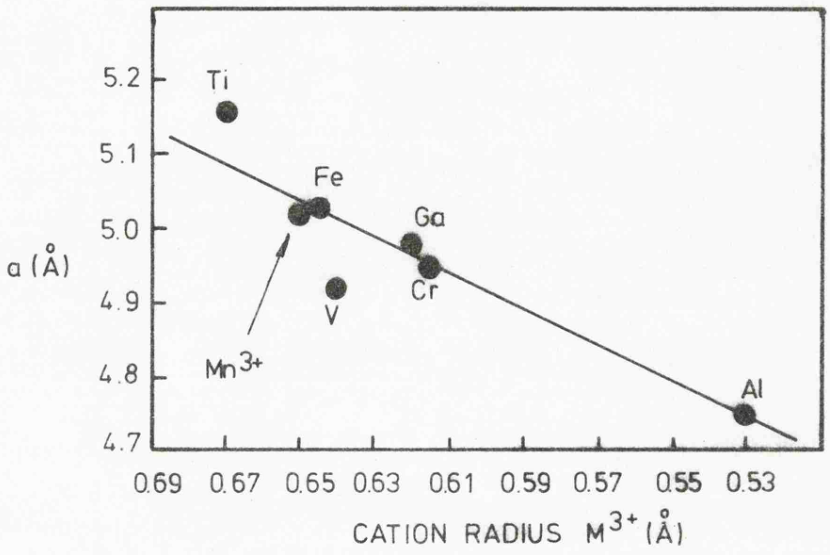

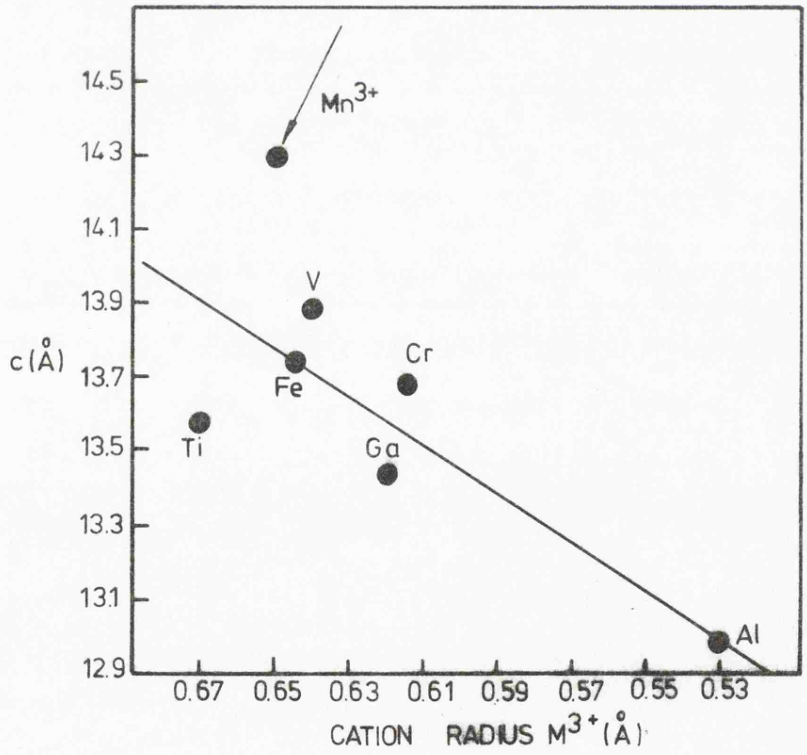

Fig.5.9 Lattice parameters for oxides of formula $M_2^{3+}O_3$ existing in the corundum structure.

more closely. The X-ray diffraction patterns of these materials are shown in figs. 5.2a, 5.5a and 5.7a. That of the sample precipitated at 100°C (Fig.5.2a) was in good agreement with the data given in the ASTM card for natural γ-MnOOH. The trace of sample B (Fig.5.5a) also shows good agreement except that the lines are less intense and considerably broader than those of sample A. Also present is a line at $2\theta = 21.0^{\circ}$ (Cu K_{α} radiation) which cannot be ascribed to γ-MnOOH. The pattern of sample C (Fig.5.7a) is less intense and broader than that of sample B. Although it is indicative of γ-MnOOH the line at $2\theta = 21.0^{\circ}$ has increased in extent and the splitting of certain other lines is apparent.

The presence of a peak at $2\theta = 22^{\circ}$ in synthetic γ-MnOOH has been briefly referred to in the literature. Feitknecht and Marti[140] observed that X-ray patterns of γ-MnOOH samples obtained by precipitation differed slightly from X-ray patterns of natural manganite. A new weak line at low diffraction angles appeared and some weak lines with larger angles of reflection were missing. Gattow[141] reported that the oxidation of an alkaline manganous sulphate solution with hydrogen peroxide produces not γ-MnOOH but materials with rather diffuse X-ray patterns which are slightly displaced from X-ray patterns of natural γ-MnOOH. Also a new strong line appears at $2\theta = 22.0^{\circ}$. He termed these compounds γ' - MnOOH. It appears that it is unnecessary to formulate the existence of γ' - MnOOH but that this consists of a mixture of γ-MnOOH and α-MnOOH.

Additional evidence in favour of samples B and C being mixtures of γ- and α-MnOOH was obtained by refluxing sample C in 1N nitric acid. Giovanoli and Leuenberger[10] have shown that α-MnOOH decomposes to γ-MnO_2 whilst β-MnO_2 is produced from γ-MnOOH. The dioxides may be distinguished by X-ray diffraction. Both γ- and β-MnO_2 were present in the product obtained by application of this procedure to sample C whilst only β-MnO_2 could be detected when sample A was used.

If the assumption that sample A is γ-MnOOH whilst samples B and C consist of mixtures of α- and γ-MnOOH, albeit in different proportions, is correct, then the thermal behaviour may be interpreted as follows: The formation of Mn_5O_8 and α-Mn_3O_4 results from the dehydroxylation of γ-MnOOH whilst the presence of Mn_2O_3 with a corundum structure results from the thermal dehydration of α-MnOOH. Mixtures of γ- and α-MnOOH i.e. B and C, will form Mn_5O_8, α-Mn_3O_4 and Mn_2O_3 the relative amounts depending on the ratio of the two oxyhydroxides.

The decomposition behaviour of samples A, B and C beyond the first decomposition stage is complex. Shown in fig.5.10 are the resulting TPD curves and some interesting trends are immediately obvious. It can be seen that the maximum desorption rate for the second peak decreases with decrease in the sample preparation temperature whilst the third peak behaves in the opposite way, i.e. the maximum desorption rate increases from A → C.

X-ray diffractometer traces of the samples obtained by heating

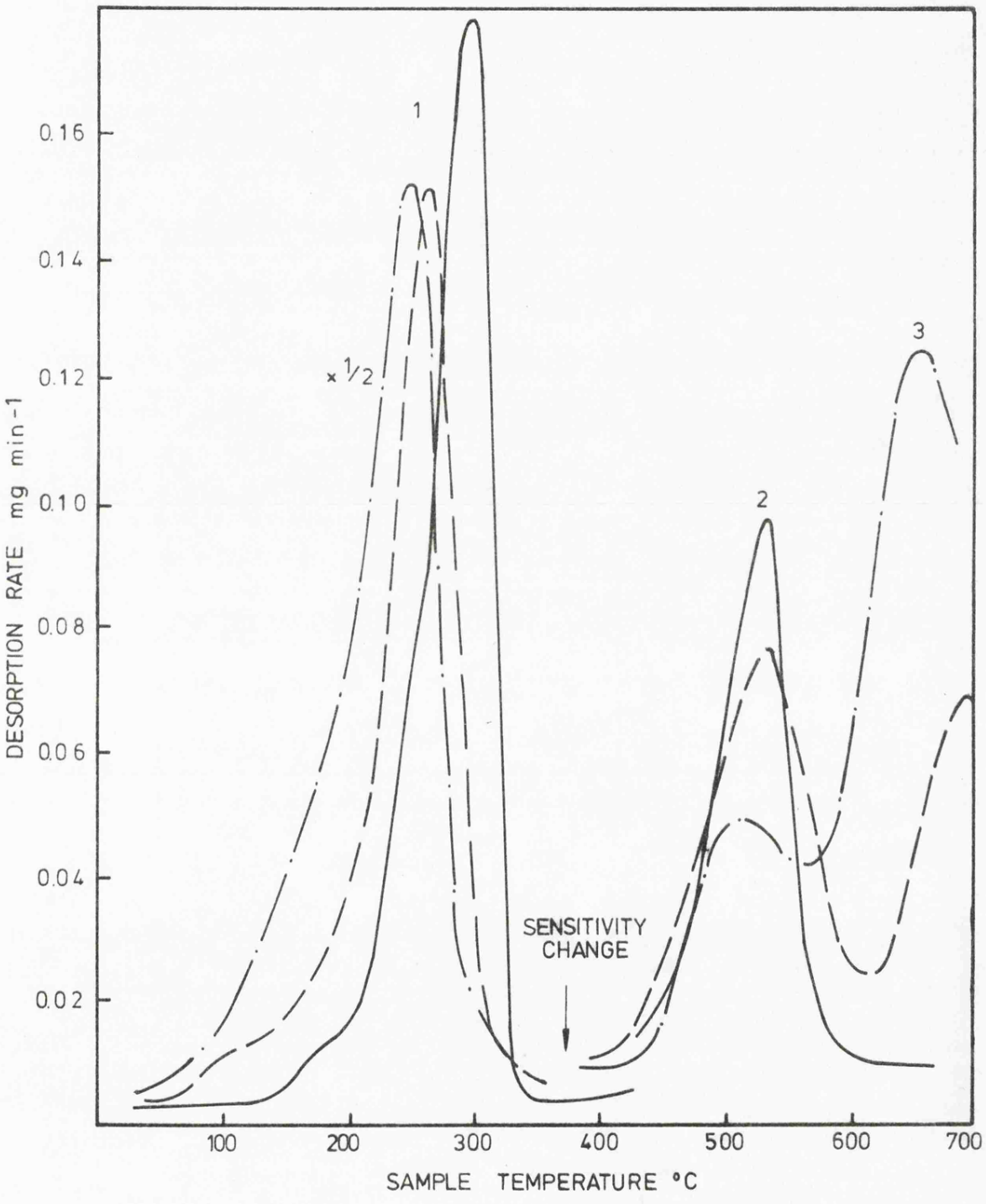

Fig.5.10 Thermal decomposition in vacuum of samples A (———), B (— —) and C (———·).

A, B and C to selected points along their decomposition routes are illustrated in figs. 5.2, 5.5 and 5.7. As mentioned above the sample composition of B midway between the first and second decomposition stages corresponded to a mixture of the corundum form of Mn_2O_3 and α-Mn_3O_4. Although Mn_5O_8 would be expected it was not observed. However, a diffractometer trace of the product formed by heating sample B to a temperature corresponding to the maximum desorption rate of peak 2 (Fig.5.5c) revealed a mixture of Mn_2O_3 - corundum type - , α-Mn_3O_4 and Mn_5O_8. The intensity of the lines attributed to Mn_2O_3 decreased whilst those of α-Mn_3O_4 and Mn_5O_8 intensified. Further heating to 615^{o}C i.e. midway between peaks 2 and 3 produced a compound whose X-ray diffractometer trace indicated the presence of only α-Mn_3O_4 (Fig.5.5d). That this oxide is unlikely to be the sole component was shown by the presence of the third decomposition stage. α-Mn_3O_4 is unlikely to decompose in vacuum in the temperature range of interest and this additional weight loss was probably due to another component. The inability of X-ray diffractometry to reveal the presence of a minor or relatively non-crystalline phase is well known. Fishburn and Dill[142] reported that an X-ray powder pattern of a mixture consisting of three types of manganese dioxide showed the presence of only β-MnO_2 until the other phases present comprised about 50% by weight. An X-ray trace recorded on completion of the TPD run was identical with that obtained on the preceding sample, i.e. only α-Mn_3O_4 could be detected.

The decrease in the height of peak 2 for sample B relative

to sample A could be ascribed to the presence of less Mn_5O_8 as a result of replacing a proportion of γ-MnOOH by α-MnOOH. The corresponding increase in peak 3 was apparently associated with an increase in the amount of the corundum form of Mn_2O_3 produced from the decomposition of α-MnOOH. Although X-ray and weight loss data are consistent with the compositional change $Mn_5O_8 \rightarrow \alpha\text{-}Mn_3O_4$ very little light has been shed on the thermal decomposition path of Mn_2O_3.

The X-ray diffractometer trace of the product obtained by heating sample C to a temperature midway between the first and second decomposition stages (Fig.5.7b) indicated that the corundum form of Mn_2O_3 was the major component. Further heating to a temperature corresponding to the midpoint between the second and third decomposition stages produced a mixture of Mn_2O_3 and $\alpha\text{-}Mn_3O_4$ (Fig.5.7c). However, this modification of Mn_2O_3 possessed the C-sesquioxide structure ($\alpha\text{-}Mn_2O_3$), although one or two low intensity peaks associated with the corundum form were faintly visible. Thus, at a temperature in the region of 450°C, the corundum form of Mn_2O_3 undergoes a phase transition to the more stable C-sesquioxide variety. An X-ray trace of the final TPD product (Fig.5.7d) showed this to be predominantly $\alpha\text{-}Mn_3O_4$, the intensity of the $\alpha\text{-}Mn_2O_3$ lines having diminished but still being faintly visible.

This evidence suggested that the third stage in the decomposition path resulted from the breakdown of $\alpha\text{-}Mn_2O_3$ although this is not entirely consistent with the accepted thermal behaviour

of this oxide. α-Mn_2O_3 is reported[143] to decompose in vacuum at 850°C to α-Mn_3O_4 which is about 150°C above that found for peak 3. However, Grasselly[144] found that α-Mn_2O_3 heated for two hours at 670°C in a carbon dioxide atmosphere produced a mixture of α-Mn_3O_4 and MnO. Chemical analysis showed that the composition of each of the dehydroxylated products obtained from samples A to C (i.e. at the end of the first decomposition stage) could be formulated as $MnO_{1.50}$. If it is assumed that the weight loss encountered beyond this stage was due to the elimination of oxygen then the weight loss for sample C was in excess of that expected from the compositional change $MnO_{1.50} \rightarrow MnO_{1.33}$ (Mn_3O_4). The only well characterised oxide of manganese with a mean oxidation state less than that of Mn_3O_4 is MnO. It therefore appears that under the conditions in which the experiments were conducted α-Mn_2O_3 decomposed directly to MnO as shown below

$$2\,Mn_2O_3 \rightarrow 4\,MnO + O_2 \qquad (5.5)$$

although it must be stressed that this explanation can only be considered as tentative. No chemical or X-ray evidence confirming the formation of MnO could be obtained possibly because of its ease of oxidation.

The results of the investigation into the thermal behaviour in vacuum of γ-MnOOH and mixtures with α-MnOOH may be summarised as follows:

γ-MnOOH decomposed initially to an equimolar mixture of α-Mn_3O_4 and Mn_5O_8 as a result of a dehydroxylation process which can be

represented schematically by equation (5.2). Although this was thought likely to proceed via the formation of Mn_2O_3 no evidence of this was found. A second decomposition stage resulted from the decomposition of Mn_5O_8 to α-Mn_3O_4 as given by equation (5.3). Replacement of γ-MnOOH by α-MnOOH led on thermal dehydration to the formation of a modification of Mn_2O_3 possessing a corundum structure. This oxide underwent a phase transition to α-Mn_2O_3 in the same temperature range as that in which the decomposition of Mn_5O_8 to α-Mn_3O_4 took place. A third decomposition process was considered to result from the thermal decomposition of α-Mn_2O_3 direct to MnO as given by equation (5.5).

5.1.(ii) Oxygen

The thermal dehydration of γ-MnOOH in an oxygen environment has been investigated and the TPD curves obtained for samples A and B are illustrated in fig.5.11. Both samples exhibited a desorption peak in the region of 250^{o}C which was followed by a process involving uptake of oxygen. An X-ray diffractometer trace of the product obtained on completion of the absorption step showed this to be β-MnO_2 in accordance with the expected decomposition path given below.

$$4\,MnOOH + O_2 \rightarrow 4\,MnO_2 + 2H_2O \qquad (5.6)$$

However the weight loss associated with the dehydroxylation step was in excess of that required from equation (5.6) and an oxygen absorption stage unexpected. These curves were reminiscent of the trace obtained from the decomposition of $MnO_{1.54}$ which was described in Chapter 4. The explanation

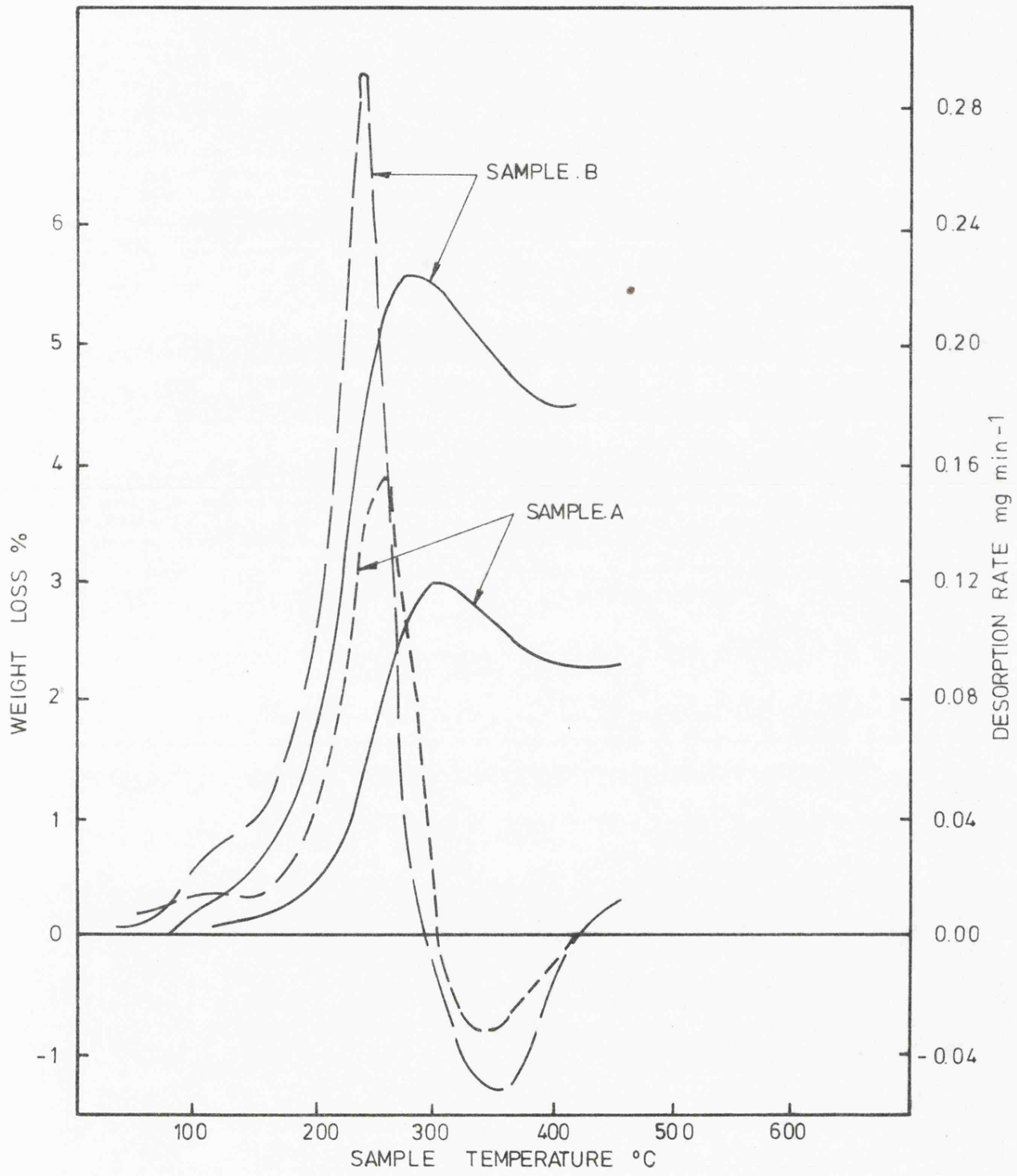

Fig.5.11 Thermal decomposition of γ-MnOOH in oxygen (10 Torr). Weight loss (———) and rate of decomposition curves (– – –). Sample weights: A 112.1 mg , B 111.6 mg.

given to account for that behaviour can be extended to this situation. Sample B which was composed of a mixture of γ- and α-MnOOH produced a larger dehydration step than that of sample A. This was a consequence of the formation of the corundum form of Mn_2O_3 resulting from the dehydroxylation of α-MnOOH. This modification of Mn_2O_3 was previously shown to be capable of existing at this temperature in oxygen (10 Torr) for a finite period of time. The smaller maximum in the TPD curve for sample A was consistent with the formation of a smaller amount of Mn_2O_3. Although this behaviour was indicative of a trace of α-MnOOH present in sample A the X-ray diffractometer trace had failed to detect this.

These results may be compared with two studies reported in the literature. In the most recent publication Sato et al[31] claimed to have established by TG and DTA that synthetic γ-MnOOH dehydroxylated in air to β-MnO_2 via Mn_2O_3 as an intermediate. Although an X-ray diffractometer trace of the γ-MnOOH was indicative of that oxyhydroxide the preparative procedure and its chemical analysis (x in MnO_x = 1.58) suggested that α-MnOOH and probably another component were also present. The evidence presented by Sato et al suggesting that an intermediate formed in the thermal decomposition of γ-MnOOH resulted from γ-MnOOH is therefore considered to be unfounded. It is also difficult to comment on the earlier work of Dubois[13] but it is likely from the mode of preparation that the γ-MnOOH sample investigated contained α-MnOOH which gave rise to the observed desorption - absorption phenomenon.

5.2 Thermal decomposition of α-MnOOH

In an attempt to identify the intermediate formed during the thermal conversion of $MnO_{1.54}$ to MnO_2 described in Chapter 4 a sample of α-MnOOH was synthesised. The X-ray diffractometer trace of the product as mentioned previously was in good agreement with the ASTM data for natural groutite. As the literature contained only a single reference to the vacuum dehydration of synthetic groutite this has also been investigated and the results compared with those of Praliaud, Rousseau and Mathieu[24].

5.2.(i) Vacuum

The TPD curve obtained from the vacuum decomposition of α-MnOOH is depicted in fig.5.12. The presence of two distinct stages in the thermal decomposition process is complicated by partial resolution of the low temperature peak. The first step is ascribed to the dehydroxylation of α-MnOOH but the observed weight loss was in excess of that expected for the compositional change $MnOOH \rightarrow Mn_2O_3$. Further purification of the sample employing a mixture of xylene and industrial methylated spirits[55] in the washing procedure produced no detectable change in the TPD trace. Reducing the sample weight and heating rate to avoid the possibility of the pressure inside the balance case extending into the region where thermomolecular flow forces could be troublesome did not affect the weight loss. X-ray diffractometer traces of the products formed at the end of the first and second stages of the decomposition process are illustrated in fig.5.13. The trace corresponding

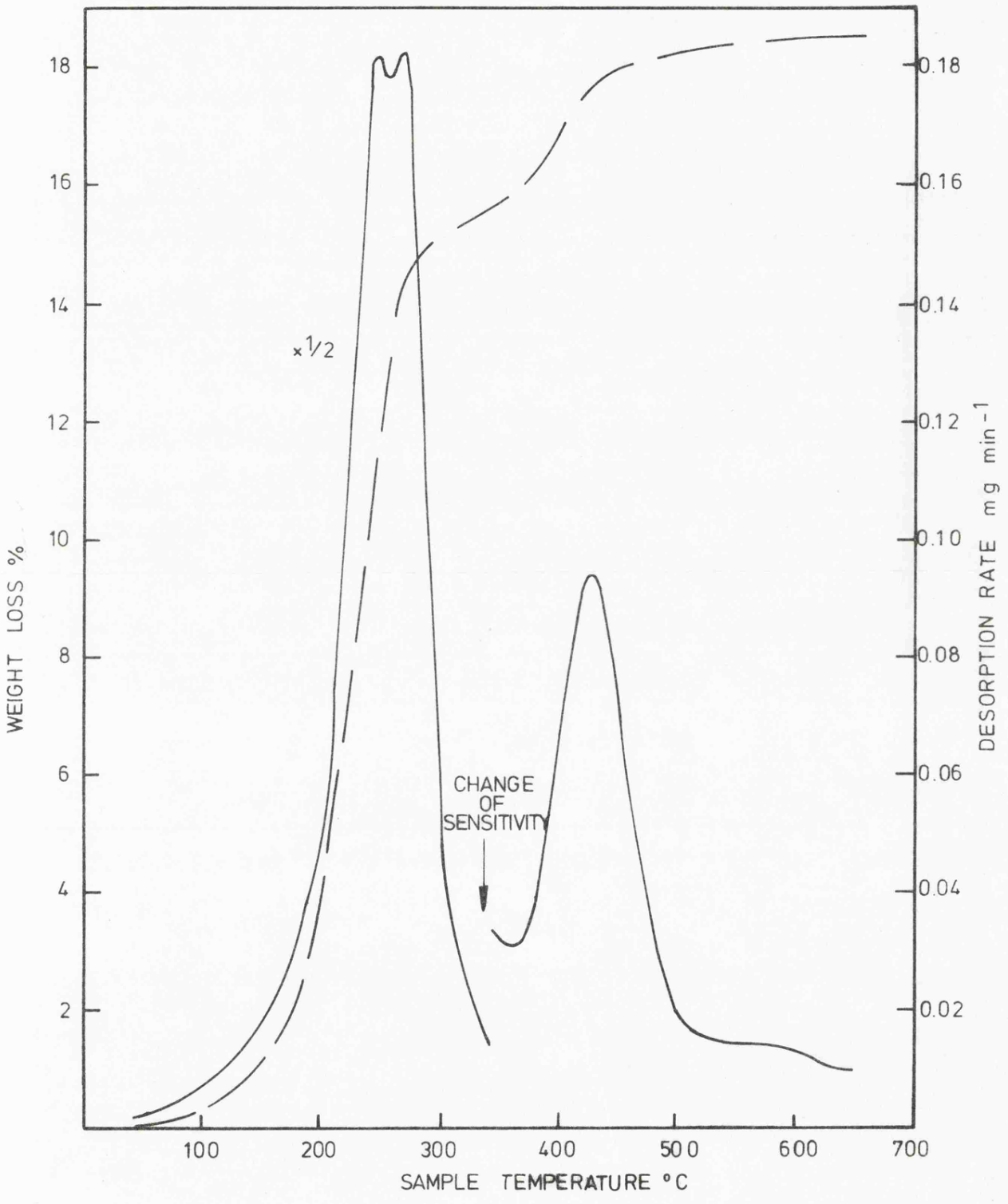

Fig.5.12 Thermal decomposition of α-MnOOH in vacuum. Weight loss (— —) and rate of decomposition (———) curves. Sample weight 61.9 mg.

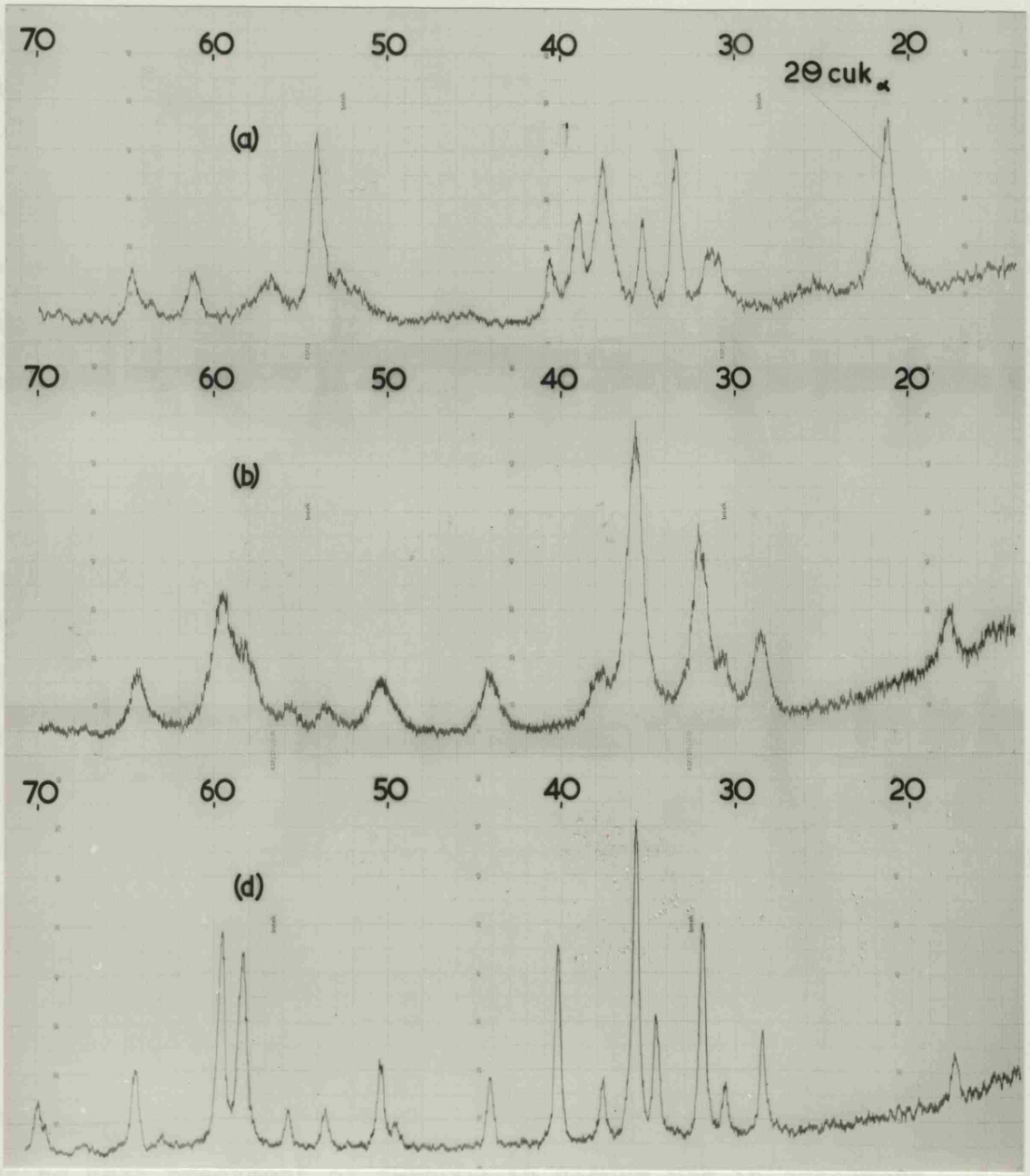

Fig.5.13 X-ray diffractometer traces (Cu K_α) of the products obtained by application of a linear heating programme ($5^oC\ min^{-1}$) to α-MnOOH in vacuum. These correspond with temperatures of (a) 25^o (b) 340^o and (c) 640^oC on the thermal analysis curve in fig.5.12.

to the dehydrated product showed a poor α-Mn_3O_4 pattern rather than the expected Mn_2O_3 diagram whereas the trace taken on completion of the decomposition reaction consisted of a much more crystalline α-Mn_3O_4 phase together with MnO. Chemical analysis of the α-MnOOH indicated that x in MnO_x was 1.45 rather than the ideal value of 1.50. It was likely that the chemical reduction of γ-MnO_2 had not ceased with the formation of α-MnOOH but had continued beyond this stage producing $Mn(OH)_2$ i.e.

$$MnO_2 + H^+ + e \rightarrow MnOOH \qquad (5.7)$$

$$MnOOH + H^+ + e \rightarrow Mn(OH)_2 \qquad (5.8)$$

The presence of MnO in the X-ray diffraction pattern could be accounted for by the decomposition of $Mn(OH)_2$. Although this certainly contributed to the decomposition peak at 260°C X-ray diffraction did not reveal the presence of MnO until after the second decomposition stage. This clearly underlines the inability of the technique in this instance to establish the presence of a relatively non-crystalline phase when this is present as a minor constituent.

The presence of two decomposition stages at 260°C and 430°C during heat treatment of α-MnOOH in vacuum was in agreement with the results of Praliaud, Rousseau and Mathieu[24]. These authors however, claimed that the dehydroxylation of α-MnOOH led firstly to α-Mn_2O_3 which subsequently decomposed at 420°C to α-Mn_3O_4. No X-ray evidence was presented to check these claims but the decomposition temperature of 420°C which they cited for conversion of α-Mn_2O_3 to α-Mn_3O_4 is considerably

below the quoted literature value of 850°C[143].

It is difficult to offer a satisfactory explanation to account for the presence of α-Mn_3O_4 as a result of vacuum dehydration of α-MnOOH. That the X-ray trace was not a true indicator of the sample composition on completion of the first step was evident from a subsequent decomposition process. The formation of the corundum form of Mn_2O_3 was expected but no evidence of this was obtained.

5.2.(ii) Oxygen

The TPD trace from α-MnOOH recorded in an oxygen environment is depicted in fig.5.14. This was similar to the decomposition curve obtained for γ-MnOOH and the chemically reduced γ-MnO_2 sample $MnO_{1.54}$ in that the dehydroxylation reaction leading to the formation of MnO_2 proceeded in two successive stages involving a weight loss - weight gain phenomenon. The main difference in the TPD traces was that the dehydroxylation of α-MnOOH appeared to consist of two components consistent with the findings in vacuum.

Praliaud, Rousseau and Mathieu[24] also looked at the thermal behaviour of α-MnOOH in oxygen. These authors did not observe a weight increase during the dehydration process but their recorded weight loss (∿ 5.5%) was in excess of that expected from the compositional change MnOOH → MnO_2. Their conversion of MnOOH to MnO_2 resulted in the formation of the γ- variety of MnO_2 rather than the β modification found in this study.

Heating the α-MnOOH sample used in this investigation in

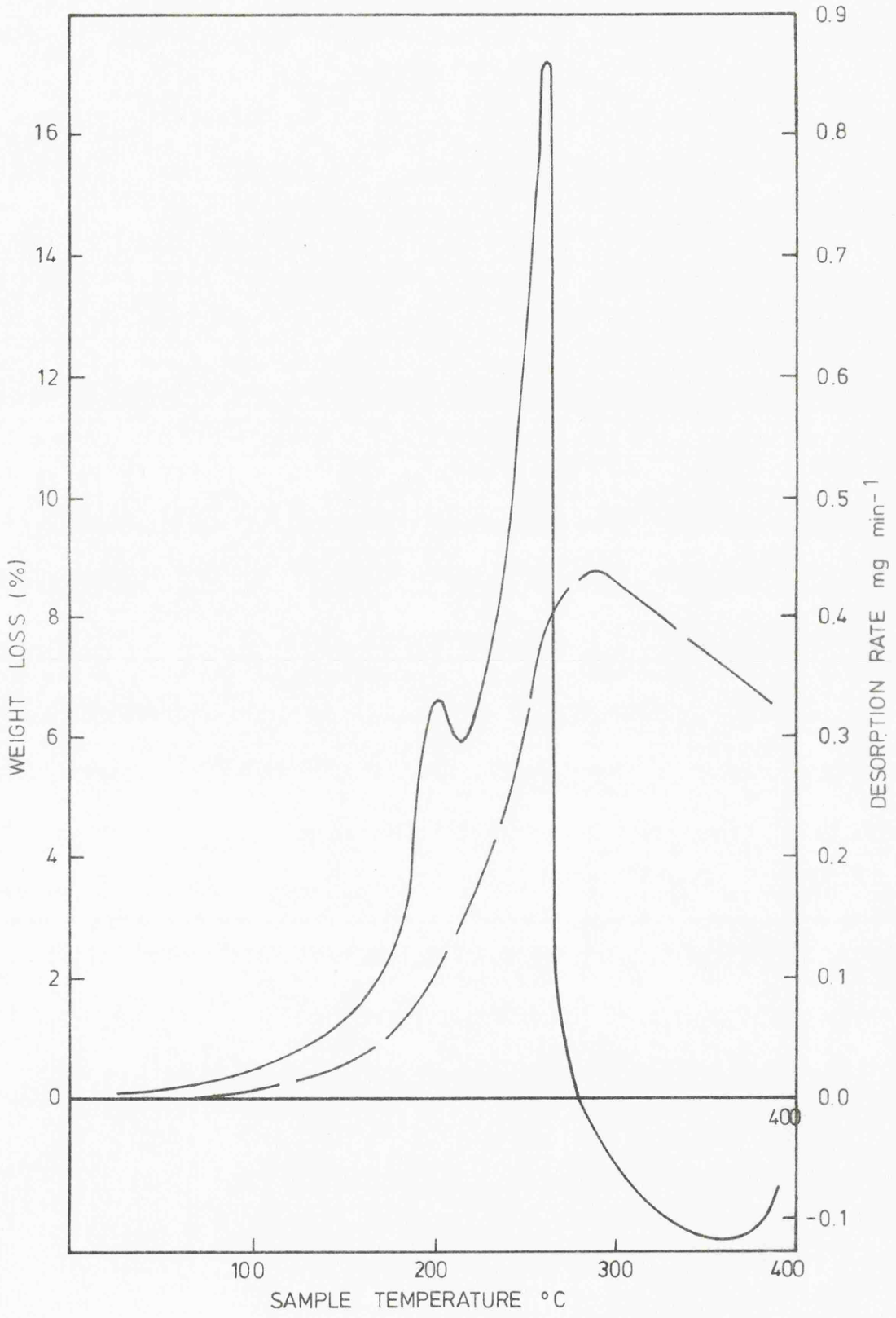

Fig.5.14 Thermal decomposition of α-MnOOH in oxygen (10 Torr). Weight loss (— — —) and rate of decomposition (———) curves. Sample weight 111.6 mg.

oxygen (10 Torr) to a temperature just below that corresponding to the oxygen absorption step produced the corundum form of Mn_2O_3 as described in Chapter 4.

5.3 Thermal decomposition of Mn_7O_{12}

5.3.(i) Vacuum

During the thermal decomposition in vacuum of γ-MnOOH, the formation of Mn_5O_8 as an intermediate was postulated. This was observed to eliminate oxygen at ∿535°C to form α-Mn_3O_4 and was the first time that a vacuum decomposition path had been invoked. It is reported[8] to form α-Mn_2O_3 in an oxygen or air environment but such a reaction path was not found in vacuum.

In order to confirm the decomposition behaviour of Mn_5O_8 an attempt was made to obtain a sample of this oxide by an independent route but preliminary experiments involving oxidation of α-Mn_3O_4[6] were unsuccessful. A sample, however, was kindly supplied by Dr. Giovanoli which had been prepared by controlled oxidation of MnO. Its X-ray diffractometer trace is given in fig.5.15a and showed good agreement with that reported in the literature.

The TPD curve of this sample is given in fig.5.16. Two distinct decomposition steps were observed at 515°C and 665°C the weight losses of which were in the ratio 3:1. This appeared to contradict both the vacuum decomposition mechanism of Mn_5O_8 postulated earlier and that reported in the literature (oxygen atmosphere). X-ray diffractometer traces of the products

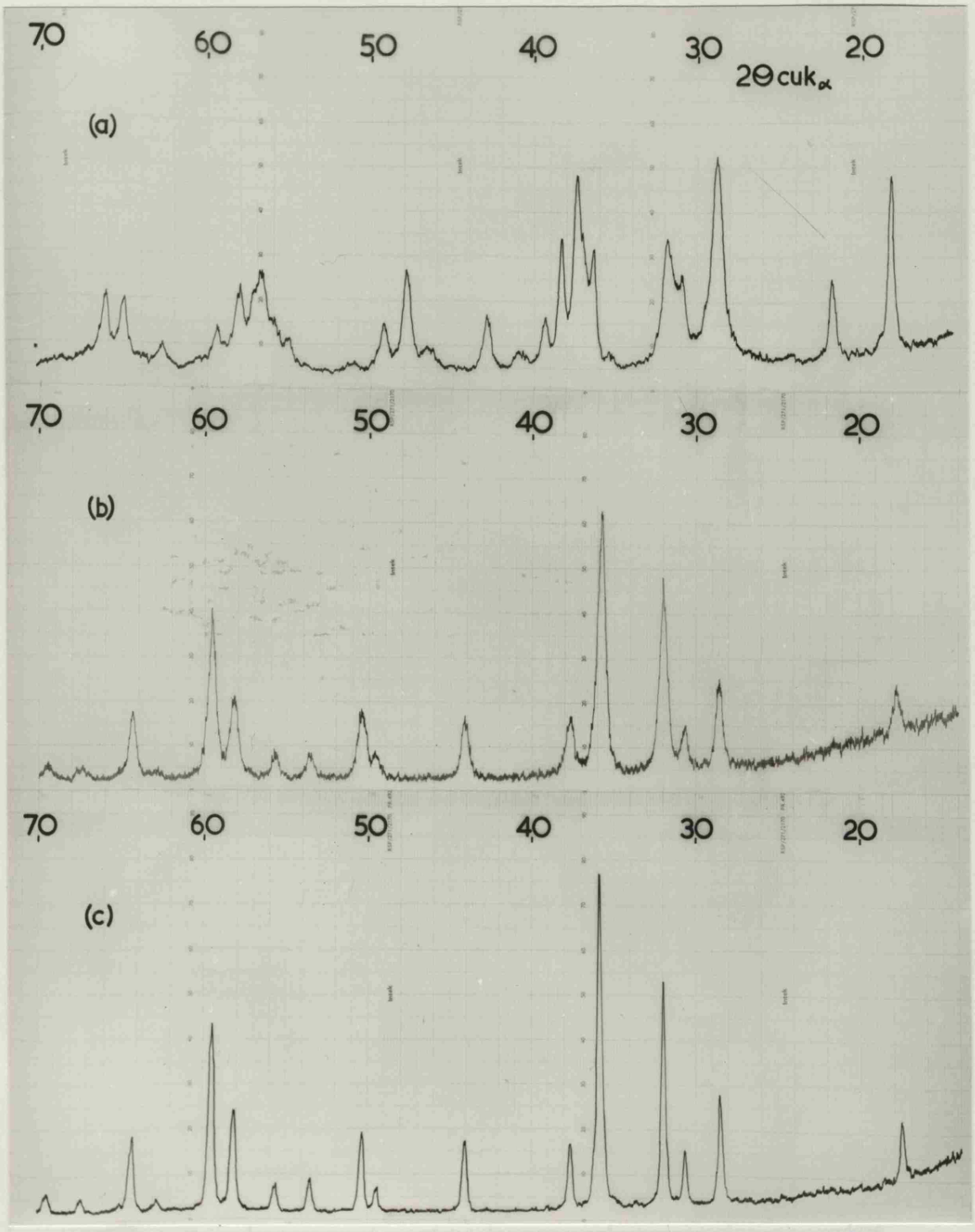

Fig.5.15 X-ray diffractometer traces (Cu K_α) of the products obtained by application of a linear heating programme ($5^oC\ min^{-1}$) to Mn_7O_{12} in vacuum. These correspond with temperatures of (a) 25° (b) 595° and (c) 720°C on the thermal analysis curve in fig.5.16.

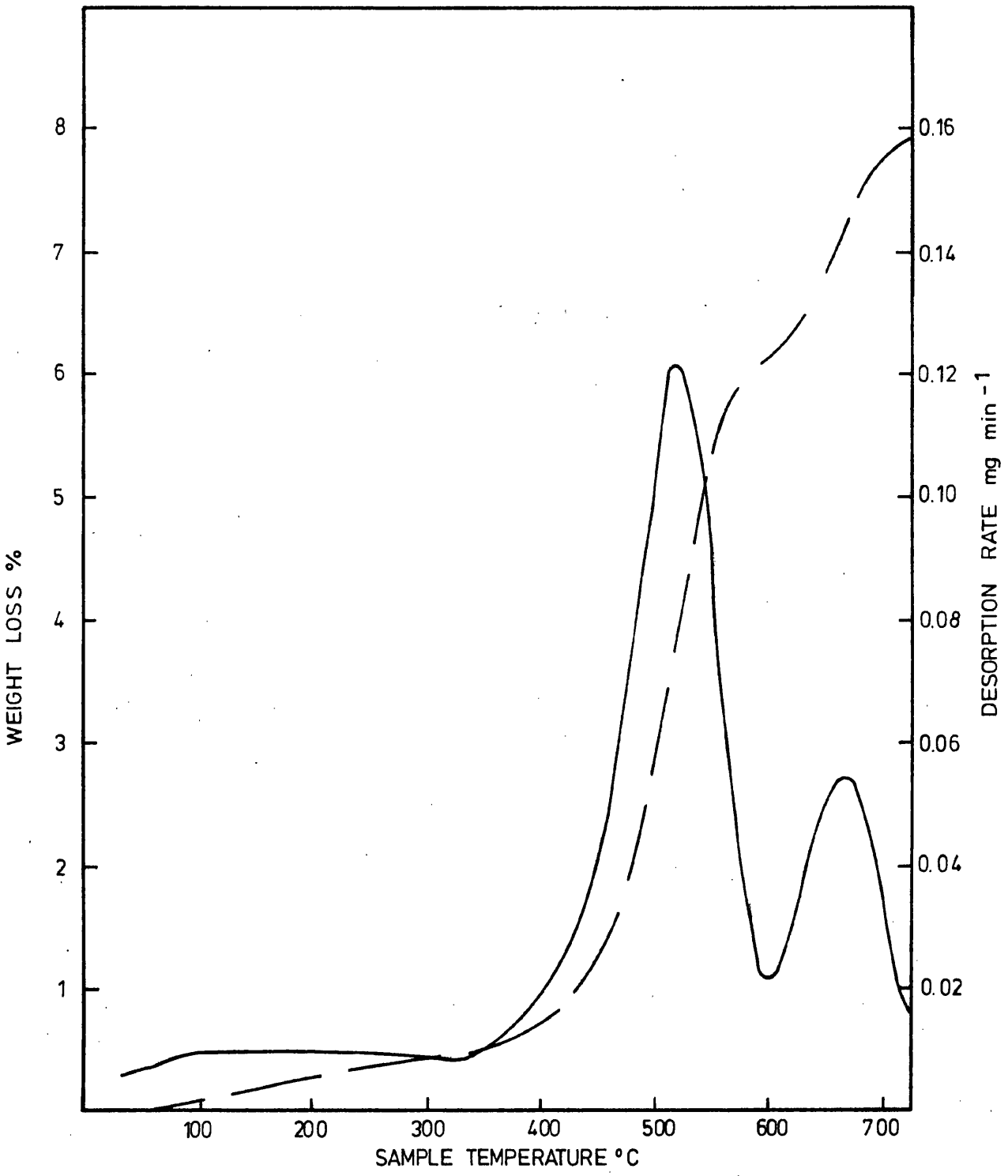

Fig.5.16 Thermal decomposition of Mn_7O_{12} in vacuum. Weight loss (— —) and rate of decomposition (———) curves. Sample weight 55.0 mg.

formed midway between the first and second decomposition steps (Fig.5.15b) and on completion of the second stage (Fig.5.15c) were identical suggesting that α-Mn_3O_4 was the sole decomposition product at both temperatures.

It was tempting initially to suggest that as Mn_5O_8 can be represented by $MnO_{1.60}$ and α-Mn_3O_4 by $MnO_{1.33}$ and that as the weight losses were in the ratio 3:1, the formula of the product midway between the two decomposition steps must be $MnO_{1.40}$. Le Blanc and Wehner[145] found that α-Mn_3O_4 produced by oxidation of MnO could take up oxygen to a composition corresponding to $MnO_{1.42}$ without changing the X-ray pattern which would be consistent with these findings. However the weight losses involved were in excess of those required to support this decomposition route.

Although it was initially assumed that x in MnO_x for Mn_5O_8 was of the order of 1.60 chemical analysis revealed that for the sample supplied by Dr. Giovanoli x = 1.72. A possible reason for this higher oxidation state was that Mn_5O_8 was mixed with a higher oxide of manganese. This could only be MnO_2. To obtain a formula where x = 1.72, 1 mole of Mn_5O_8 must be mixed with 2.1 moles of MnO_2. Close examination of the X-ray diffractometer data obtained on the Mn_5O_8 sample showed that certain lines were relatively more intense than those predicted by the ASTM card. Those lines coincided with the strongest lines of β-MnO_2 which suggested that β-MnO_2 might be present (Fig.5.17). This composition however was

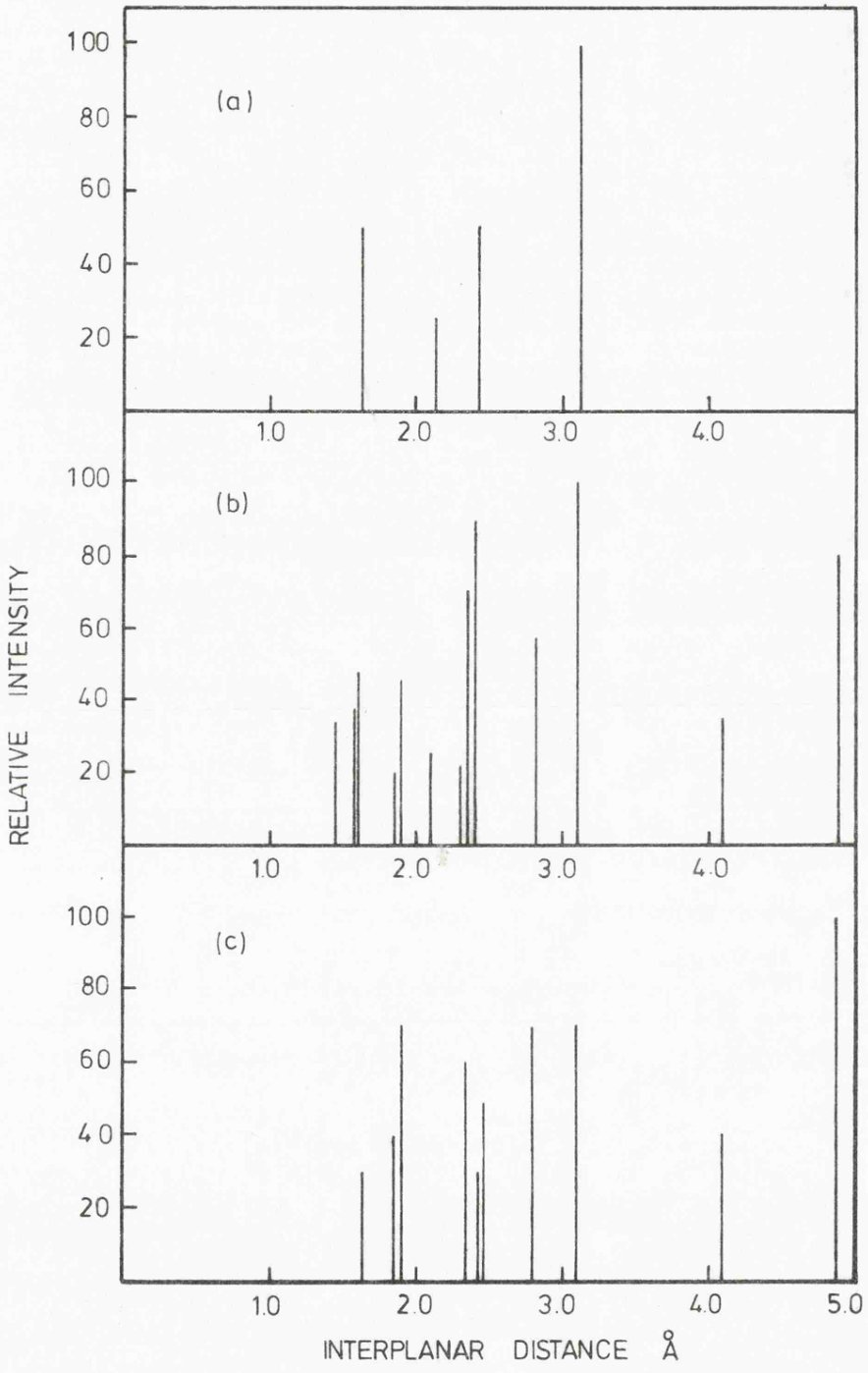

Fig.5.17 X-ray line diagrams of a) β-MnO_2 b) Mn_7O_{12} and c) Mn_5O_8. Lines of relative intensity <20 are not included.

not entirely consistent with the weight loss or X-ray data. If β-MnO_2 were present its expected decomposition product would be α-Mn_2O_3.

$$4\ MnO_2 \rightarrow 2\ Mn_2O_3 + O_2 \qquad (5.9)$$

In the temperature range employed in this study α-Mn_2O_3 would not decompose further to Mn_3O_4. Possible decomposition routes for Mn_5O_8 would be

$$4\ Mn_5O_8 \rightarrow 10\ Mn_2O_3 + O_2 \qquad (5.10)$$

$$3\ Mn_5O_8 \rightarrow 5\ Mn_3O_4 + O_2 \qquad (5.11)$$

with the latter being the most likely. If equations (5.9) and (5.11) accurately described the decomposition route two weight steps in the ratio 1.3:1 with a total weight loss of 6.5% would be expected. However the weight losses were observed to be in the ratio 3:1 with an overall weight loss of 7.9%. If equations (5.9) and (5.10) correctly described the thermal process the agreement between the calculated and observed results would have been worse.

An alternative decomposition mechanism which is completely compatible with the observed experimental behaviour is outlined below. This involved postulating the formation of oxides of manganese whose existence has not been previously reported in the literature. The x value of 1.72 found for the sample of Mn_5O_8 was very close to that of an oxide of formula Mn_7O_{12} (x = 1.714). A possible decomposition route in vacuum for this oxide is given below:

$$Mn_7O_{12} \rightarrow Mn_7O_{10} + O_2 \qquad (5.12)$$

The value of x in MnO_x for Mn_7O_{10} is 1.429 which is in agreement

with the analysis figure for the product obtained midway between the decomposition stages (x = 1.42). Mn_7O_{10} may decompose to α-Mn_3O_4 by the elimination of oxygen and the two decomposition steps may be represented by

$$3\ Mn_7O_{12} \rightarrow 3\ Mn_7O_{10} + 3O_2 \qquad (5.13)$$

$$3\ Mn_7O_{10} \rightarrow 7\ Mn_3O_4 + O_2 \qquad (5.14)$$

The weight losses are seen to be in the ratio 3:1, again in excellent agreement with the experimental results and the overall loss of oxygen calculated from equations (5.13) and (5.14) (7.4%) in good agreement with the observed behaviour (7.7%). Thus it appears that the oxidation of MnO has inadvertently proceeded beyond the formation of Mn_5O_8 to produce an oxide of composition Mn_7O_{12}.

The similarity of the X-ray diffraction data between Mn_7O_{12} and Mn_5O_8 and Mn_7O_{10} and α-Mn_3O_4 is probably significant. Mn_7O_{12} and Mn_5O_8 may be related by a crystallographic shear system based on MnO_2 although some of the facts are difficult to explain. Both compounds may possibly be considered as being members of a homologous series described by the general formula Mn_nO_{2n-2} where n = 5 and 7 for Mn_5O_8 and Mn_7O_{12} respectively. A family of phases with this general formula has recently been found[120] for oxides of chromium where n corresponded to 5, 7, 9 and 11. However, a complete structure determination on Mn_5O_8 showed[9] that the manganese ions were in an oxidation state of +2 and +4 whereas all the crystallographic shear systems based on a rutile structure contain metal ions in the +3 and +4 state.

5.3.(ii) Oxygen

The sample of Mn_5O_8 supplied by Dr. Giovanoli was subjected to a linear rise in temperature in an oxygen environment (10 Torr) and the resulting TPD curve is depicted in fig.5.18 An X-ray diffractometer trace of the product obtained on completion of the single decomposition step showed this to be α-Mn_2O_3. This was consistent with the decomposition behaviour of Mn_5O_8 reported in the literature. However it has been shown above that the sample of Mn_5O_8 used in this study was actually Mn_7O_{12}. The weight loss associated with the decomposition process (4.7%) was in good agreement with the expected oxygen removal resulting from the compositional change $Mn_7O_{12} \rightarrow \alpha$-$Mn_2O_3$ (4.2%).

$$4\ Mn_7O_{12} \rightarrow 14\ Mn_2O_3 + 3O_2 \qquad (5.15)$$

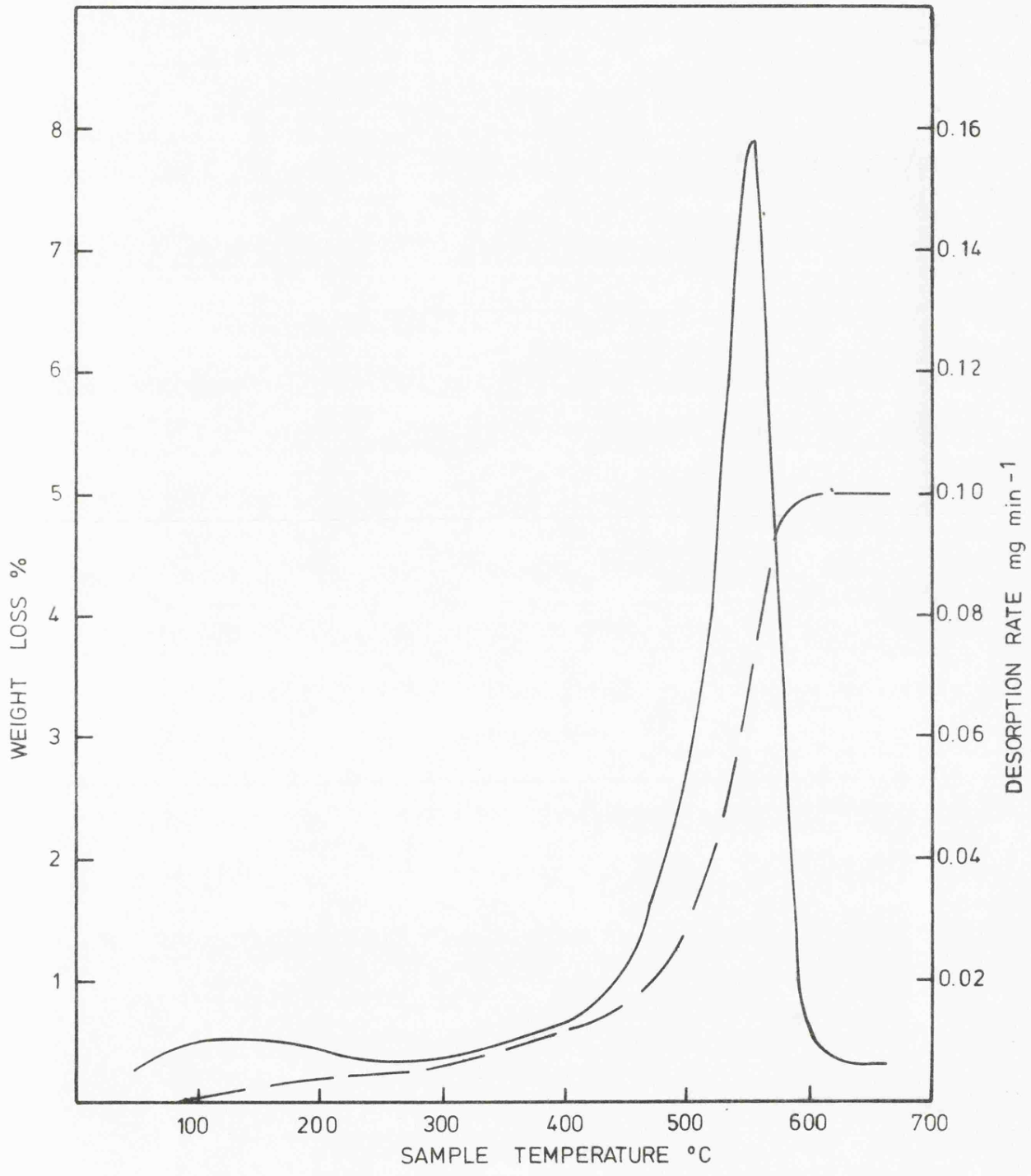

Fig.5.18 Thermal decomposition of Mn_7O_{12} in oxygen (10 Torr). Weight loss (— —) and rate of decomposition (———) curves. Sample weight 60.9 mg.

CHAPTER 6

General Discussion and Conclusions

With the possible exception of chromium, manganese is exceptional amongst the first row transition metals because of the large number of oxides and oxyhydroxides that it can form. Despite this situation manganese oxide chemistry has been neglected compared to numerous studies reported on other oxide systems such as SiO_2, TiO_2 etc. Much of the work relating to manganese dioxide has been superficial and this has contributed to the controversy surrounding many aspects of its behaviour.

The classification of water associated with the dioxide has in particular suffered in this respect. As mentioned in Chapter 1 many authors have investigated the nature of the water associated with manganese dioxide in an attempt to relate this with the electrochemical behaviour of the oxide. Although previous evidence suggested that water played an important role in the discharge mechanism its nature was unclear. In the present work five types of water have been identified. These may be classified in order of the ease by which they were removed from γ-MnO_2 by application of a linear heating programme; (i) physically adsorbed molecular water (ii) molecular water doubly hydrogen bonded to underlying surface hydroxyl groups (iii) chemisorbed molecular water possibly trapped between crystallites during the manufacturing or preparative procedure (iv) surface and bulk hydroxyl groups due to the presence of MnOOH (v) hydroxyl groups associated with $Mn(OH)_4$.

It is unlikely that (i), (ii) or (iii) would influence the

electrochemical characteristics of γ-MnO_2 to an appreciable extent whereas the removal of hydroxyl groups from the lattice might be expected to have a profound effect. In Chapter 3 textural studies showed that above 160°C the BET surface area underwent an appreciable increase in agreement with the work of Praliaud, Rousseau and Mathieu[24]. Application of Sing's α_s method showed that this was due primarily to the generation of a micropore network and that this occurred at the same temperature as hydroxyl groups were removed from the lattice of γ-MnO_2. The marked dependence noted by Sasaki and Kozawa[41] of the capacity of a Leclanché cell on the pretreatment temperature of γ-MnO_2 below 250°C was probably a consequence of a dehydroxylation process.

In Chapter 4 the compounds obtained by partial chemical reduction of γ-MnO_2 were characterised by X-ray diffraction and magnetic susceptibility measurements and their thermal behaviour investigated. These reduced oxides have been the subject of much interest as they are believed to be formed during the discharge step at the cathode of the Leclanché cell. The results suggested that the reduction proceeded in a homogeneous manner from MnO_2 to $MnO_{1.75}$ confirming the earlier work of Gabano et al[19] and Giovanoli, Bernhard and Feitknecht[55]. However, between x = 1.75 and 1.62 a structural reorganisation appeared to take place with the reduction to $MnO_{1.54}$ proceeding via a two phase mechanism. This is contrary to the earlier work of Feitknecht, Oswald and Feitknecht-Steinmann[52] who proposed a homogeneous

reduction throughout the whole of the range and Giovanoli, Bernhard and Feitknecht[55] who reported the existence of a single phase between $MnO_{1.75}$ and $MnO_{1.50}$ albeit different from that between MnO_2 and $MnO_{1.75}$. The reduction mechanism, as well as being studied by X-ray diffraction, has been investigated electrochemically. Thus Bode and Schmier[146] found that the potential of the chemically reduced oxides in potassium chloride solution varied linearly with sample composition and concluded that the reduction was single phase over the entire range. X-ray diffraction patterns of these samples however, appear to be inconsistent with a homogeneous mechanism. The reduction has also been studied electrochemically in an alkaline media by Bell and Huber[147]. These authors claimed that down to $MnO_{1.7}$ the reduction was homogeneous but between $MnO_{1.7}$ and $MnO_{1.47}$ a heterogeneous system was present. In this latter range samples were considered to mixtures of $MnO_{1.7}$ and $MnO_{1.47}$ which is in close agreement with the results reported in this work. An electron microscopic study may well resolve this controversial problem.

Brouillet, Grund, Jolas and Mellet[47] had earlier proposed that the weight loss associated with the decomposition of these compounds in oxygen was independent of sample composition as the loss of water was almost compensated by the absorption of oxygen

$$4\ MnOOH + O_2 \rightarrow 4\ MnO_2 + 2H_2O \qquad (6.1)$$

This decomposition path was confirmed for $x > 1.75$ but below this value this invariance was no longer found. This was

attributed to the formation of Mn_2O_3 as an intermediate during the conversion of MnOOH to MnO_2.

It has been possible to show that the procedure developed by Gregg and Langford[80] for evaluating the micropore contribution of carbons can be applied successfully to selected oxides of manganese. The amount of nonane adsorbed in the micropores calculated as liquid was in good agreement with the quantity of nitrogen. Gregg and Langford however did not find such good agreement, this probably being a consequence of the narrow pores present in their samples.

The thermal decomposition of γ- and α-MnOOH and Mn_7O_{12} has been investigated in Chapter 5 and the decomposition routes shown in Table 6.1. Vacuum dehydration of γ-MnOOH resulted in the formation of Mn_5O_8 and α-Mn_3O_4

$$8\ MnOOH \rightarrow Mn_5O_8 + Mn_3O_4 + 4\ H_2O \qquad (6.2)$$

This was the first time such a reaction path had been proposed. Previous reports suggested that a modification of Mn_2O_3 designated γ-Mn_2O_3 was produced[13] or the decomposition product could not be identified[31]. Increasing the severity of the heat treatment resulted in the decomposition of Mn_5O_8 to α-Mn_3O_4

$$3\ Mn_5O_8 \rightarrow 5\ Mn_3O_4 + 2O_2 \qquad (6.3)$$

There are no reports in the literature concerned with the vacuum decomposition of Mn_5O_8.

By altering the temperature of the medium in which γ-MnOOH was precipitated mixtures of γ- and α-MnOOH were obtained.

TABLE 6.1

THERMAL DECOMPOSITION OF OXIDES AND OXYHYDROXIDES OF MANGANESE

Compound	Mode of Preparation	Environment	Decomposition Path
γ-MnOOH	Oxidation of $MnSO_4$ in alkaline media[10]	Vacuum	$\xrightarrow{300^\circ C}$ α-Mn_3O_4 + Mn_5O_8 + H_2O; $Mn_5O_8 \xrightarrow{545^\circ C} \alpha$-$Mn_3O_4 + O_2$
		Oxygen (10 Torr)	$\xrightarrow{\sim 250^\circ C}$ β-MnO_2
α-MnOOH	Oxidation of $MnSO_4$ in alkaline media	Vacuum	$\xrightarrow{240^\circ C}$ $Mn_2O_3 + H_2O$ (corundum); phase transition $\sim 450^\circ C$; α-$Mn_2O_3 \xrightarrow{670^\circ C} MnO^*$?
		Oxygen (10 Torr)	$\xrightarrow{\sim 250^\circ C}$ (Mn_2O_3 - corundum)* $\rightarrow$ β-MnO_2
α-MnOOH	Chemical reduction of well crystallised γ-MnO_2[19]	Vacuum	$\xrightarrow{260^\circ C}$?
		Oxygen (10 Torr)	$\rightarrow$ Mn_2O_3 (corundum) $\rightarrow$ β-MnO_2
Mn_5O_8	Decomposition of γ-MnOOH	Vacuum	$\xrightarrow{545^\circ C}$ α-$Mn_3O_4 + O_2$
Mn_7O_{12}	Supplied by Dr. Giovanoli. Oxidation of MnO	Vacuum	$\xrightarrow{515^\circ C}$ $Mn_7O_{10} + O_2$; $\xrightarrow{665^\circ C}$ α-$Mn_3O_4 + O_2$
		Oxygen (10 Torr)	$\xrightarrow{555^\circ C}$ α-$Mn_2O_3 + O_2$

All of the decomposition products have been confirmed by X-ray diffraction except those denoted by *

Thermal analysis of these compounds in vacuum led to the formation of a variety of Mn_2O_3 which possessed a corundum structure, together with Mn_5O_8 and α-Mn_3O_4. The presence of this modification of Mn_2O_3 is believed to result from the decomposition of α-MnOOH.

$$2\ MnOOH \rightarrow Mn_2O_3 + H_2O \qquad (6.4)$$

The corundum form of Mn_2O_3 has also been obtained as an intermediate in the oxidation of $MnO_{1.54}$ to β-MnO_2 under similar conditions to those which Lima-de-Faria and Lopes-Vieira[17] used to observe this sesquioxide. The present work has therefore not only confirmed the existence of a corundum form of Mn_2O_3 but has established an alternative route by which this compound may be prepared. The vacuum decomposition of the corundum form of Mn_2O_3 has not been satisfactorily resolved and warrants further study. It appears to undergo a phase transition to the more stable C-type modification before decomposing directly to MnO.

In this present work evidence has been obtained for the existence of two new oxides of manganese namely Mn_7O_{12} and Mn_7O_{10}. The former was initially thought to be Mn_5O_8 as its X-ray diffraction pattern strongly resembled that oxide but recent experimental evidence suggests that this is in fact Mn_7O_{12}. There is a report in the literature[148] describing the preparation and probable structure of an oxide of formula $Mn_7O_{12}.6H_2O$. A detailed investigation of this compound was not carried out but it was reported to be

a mixed valence oxide containing Mn(II) and Mn(IV). Its X-ray diffraction pattern did not correspond to the oxide investigated in the present work.

The similarity between the X-ray patterns of Mn_5O_8, Mn_7O_{12} and β-MnO_2 suggests that these oxides may be related by a crystallographic shear system. It has been pointed out that the corundum type sesquioxides of the transition metals that form crystallographic shear structures i.e. Ti, V and Cr have anomalously short metal - metal distances[120]. It would be of interest to obtain a measure of this metal - metal bonding in the corundum form of Mn_2O_3 in order to see if this is a prerequisite for crystallographic shear phase formation. Prior to establishing the presence of CS structures in manganese oxide systems a reliable preparative procedure for Mn_7O_{12} is required as this was obtained inadvertently by the controlled oxidation of MnO.

The structural relationship between Mn_7O_{10} and α-Mn_3O_4 merits further consideration. The apparent identical nature of their X-ray diffractometer traces suggests that the structures of these two oxides are very similar.

The thermal behaviour of the manganese oxides and oxyhydroxides in an oxygen environment was discussed in Chapter 5. The conversion of the oxyhydroxides to manganese dioxide via a weight loss and weight gain process was shown to proceed via manganese sesquioxide (corundum type) as an intermediate. Although this phenomenon has been previously observed for

MnOOH there are no reports of other oxyhydroxides exhibiting this type of behaviour. A particularly relevant example within this context is the VOOH - VO_2 system.

The synthesis of a modification of VOOH isostructural with α-MnOOH has recently been reported[125]. VO_2 exists in two forms which are structurally similar to γ- and β-MnO_2 and V_2O_3 crystallises with the corundum structure. In contrast to the MnOOH - MnO_2 system however, no anomalies were observed by Muller and Joubert during the thermal decomposition of VOOH to VO_2. Although slightly removed from the situation described above the conversion of CrOOH to CrO_2 is not reported to proceed via Cr_2O_3 as an intermediate step[149]. The difference in behaviour between these structurally similar oxyhydroxides may be a consequence of the mechanism of the water removal and a function of particle size. It would be of interest to investigate these reactions by electron microscopy in order to identify any intermediate formed during the dehydration.

It is evident from the work presented in this thesis that there are many aspects of manganese oxide chemistry that would benefit from a detailed investigation using techniques that have become available in recent years. The preparation of single crystals of many of the oxides mentioned in this work, particularly the corundum form of manganese sesquioxide, would permit accurate structural determinations to be made. It is hoped that this dissertation will stimulate the necessary interest.

REFERENCES

1. Giovanoli, R., Chimia 23, 470 1969.

2. Wells, A.F., Structural Inorganic Chemistry, Third Edition, p.472. Oxford University Press 1962.

3. Wyckoff, R.W.G., Crystal Structures, Vol.1, Second Edition, p.292, Interscience 1964.

4. Dent Glasser, L.S. and Smith, I.B., Mineral Mag. 35, 327 1965.

5. de Wolff, P.M., Acta Crystallog. 12, 341 1959.

6. Feitknecht, W., Pure Appl. Chem. 9, 423 1964.

7. Yamamoto, N., Kiyami, M. and Takada, T., Japan J Appl. Phys. 12, 1827 1973.

8. Oswald, H.R., Feitknecht, W. and Wampetich, M.J., Nature 207, 72 1965.

9. Oswald, H.R. and Wampetich, M.J., Helv. Chim. Acta 50, 2023 1967.

10. Giovanoli, R. and Leuenberger, U., Helv. Chim. Acta 52, 2333 1969.

11. Pauling, L., Z. Krist. 75, 128 1930.

12. Norrestam, R., Acta Chem. Scand. 21, 2871 1967.

13. Dubois, M.P., Ann. Chim. 5, 411 1936.

14. Verwey, E.J.W.and de Boer, J.H., Rec. Trav. Chim. 55, 531 1936.

15. Moore, T.E., Ellis, M. and Selwood, P.W., J. Am. Chem. Soc. 72, 856 1950.

16. Schmier, A. and Sterr, G., Z. Anorg. Chem. 346, 181 1966.

17. Lima-de-Faria, J. and Lopes-Vieira, A., Mineral Mag. 33, 1024 1964.

18. McMurdie, H.F. and Golovato, E., J. Res. Natl. Bur. Std. 41, 589 1948.

19. Gabano, J.P., Morignat, B., Fialdes, E., Emery, B. and Laurent, J.F., Z. Phys. Chem. 46, 359 1965.

20. Gruner, J.W., Am. Mineral 32, 654 1947.

21. Collin, R.L. and Lipscomb, W.N., Acta Cryst. 2, 104 1949.

22. Dent-Glasser, L.S.and Ingram, L., Acta Cryst. 24, 1233 1968.

23. Klingsberg, C. and Roy, R., Am. Mineral 44, 819 1959.

24. Praliaud, H., Rousseau, J. and Mathieu, M.V. Rev. Chim. Minerale 6, 567 1969.

25. Buerger, M.J., Z. Kristallog. 95, 163 1936.

26. Dasgupta, D.R., Mineral Mag. 35, 131 1965.

27. Davis, R.J., Mineral Mag. 36, 274 1967.

28. Kulp, J.L. and Perfetti, J.N., Mineral Mag. 29, 239 1952.

29. Naganna, C., Proc. Indian Acad. Sci. 58, 16 1963.

30. Rode, E.Ya., cited by Mackenzie, R.C. and Berggren, G. in 'Differential Thermal Analysis' (R.C. Mackenzie,ed.) Vol.1, p.271, Academic Press 1970.

31. Sato, M., Matsuki, K., Sugawara, M. and Endo, T., Nihon Kagaku Kaishi 9, 1655 1973.

32. Feitknecht, W. and Marti, W., Helv. Chim. Acta 28, 129 1945.

33. Feitknecht, W., Brunner, P. and Oswald, H.R., Z. Anorg. Chem. 316, 154 1962.

34. Meldau, R., Newesely, H. and Strunz, H., Naturwissenschaften 60, 387 1973.

35. Glemser, O., Ber. Deutsch. Chem. Ges. 72, 1879 1939.

36. Kedesdy, H., Katz, G. and Levin, S.B., Acta Crystallog. 10, 780 1957.

37. Bystrom, A.M., Acta Chem. Scand. 3, 163 1949.

38. Giovanoli, R., Maurer, R. and Feitknecht, W. Helv. Chim. Acta 50, 1072 1967.

39. Kozawa, A. and Powers, R.A., J. Chem. Ed. 49, 587 1972.

40. Kozawa, A., J. Electrochem. Soc. 106, 79 1959.

41. Sasaki, K. and Kozawa, A., J. Electrochem. Soc. Japan 25, 273 1957.

42. Ibid idem 25, 115 1957.

43. Tvarusko, A., J. Electrochem. Soc. III, 125 1964.

44. Covington, A.K., Cressey, T., Lever, B.G. and Thirsk, H.R., Trans. Faraday Soc. 58, 1975 1962.

45. Muller, J., Tye, F.L. and Wood, L.L. in 'Batteries 2' (D.H. Collins, ed.), p.201, Pergamon Press 1965.

46. Glemser, O. and Meisiek, H., Naturwissenschaften 44, 614 1957.

47. Brouillet, Ph., Grund, A., Jolas, F. and Mellet, R. in 'Batteries 2', (D.H. Collins, ed.), p.189, Pergamon Press 1965.

48. Tye, F.L., in discussion of paper by Brenet, J. in 'Power Sources' (D.H. Collins, ed.), p.47 Pergamon Press 1967.

49. Brenet, J., Chartier, P., Dott, M.T., Gross, M., Le Tran, K., and Traore, K., Electrochim Acta 13, 2167 1968.

50. Brenet, J. and Briot, A.M., Rev. Gen. Electr. 61, 405 1952.

51. Le Tran, K. and Brenet, J., C.R. Acad. Sci. 264, 1517 1967.

52. Feitknecht, W., Oswald, H.R. and Feitknecht-Steinmann, U., Helv. Chim. Acta 43, 239 1960.

53. Coeffier, G. and Brenet, J., Bull. Soc. Chim. Fr. 17, 2835 1964.

54. Laragne, J.J. and Brenet, J., Bull. Soc. Chim. Fr. 9, 3499 1968.

55. Giovanoli, R., Bernhard, K. and Feitknecht, W., Helv. Chim. Acta 51, 355 1968.

56. Redhead, P.A., Vacuum 12, 203 1962.

57. Amenomiya, Y. and Cvetanovic, R.J., J. Phys. Chem. 67, 144 1963.

58. Czanderna, A.W., in 'Vacuum Microbalance Techniques', (A.W. Czanderna, ed.), Vol.6, p.129, Plenum Press, New York 1967.

59. Hansen, R.S. and Mimeault, V.J., in 'Experimental Methods in Catalytic Research', (R.B. Anderson, ed.), p.217, Academic Press, 1968.

60. Biegen, J.R., Czanderna, A.W. and Kollen, W., J. Colloid Interface Sci. 34, 406 1970.

61. Eyring, H., Walter, J. and Kimball, G.E., Quantum Chemistry, John Wiley, New York 1944.

62. Petermann, L.A., in 'Progress in Surface Science' (S.G. Davison, ed.), Vol.3, p.1, Pergamon Press, 1972.

63. Yakerson, V.I., Rozanov, V.V. and Rubinshtein, A.M., Surface Sci. 12, 221 1968.

64. Munuera, G. and Stone, F.S., Discuss. Faraday Soc. 52, 205 1971.

65. Stakebake, J.L., J. Phys. Chem. 77, 581 1973.

66. Krylova, I.V., Filonenko, A.P. and Sitonite, Yu.P., Russian J. Phys. Chem. 41, 1526 1967.

67. Sedlak, J.M. and Beebe, R.A., J. Colloid Interface Sci. 47, 483 1974.

68. Brunauer, S., Deming, L.S., Deming, W.S and Teller, E., J. Am. Chem. Soc. 62, 1723 1940.

69. Brunauer, S., Emmett, P.H., and Teller, E., J. Am. Chem. Soc. 60, 309 1938.

70. Everett, D.M., Manual of Symbols and Terminology for Physico-Chemical Quantities and Units, Appendix II, Part 1, Butterworths 1972 and IUPAC.

71. Gregg, S.J. in MTP Int. Rev. Sci. : Phys. Chem. (M. Kerker, ed.), Butterworths, series one 7,189 1972.

72. Lippens, B.C.and de Boer, J.H., J. Catal. 4, 319 1965.

73. Sing, K.S.W., in 'Surface Area Determination' (D.H. Everett and R.H. Ottewill eds.), p.25, Butterworths, 1970.

74. Sing, K.S.W., Chem. Ind. (London) 1520 1968.

75. Baker, F.S., Carruthers, J.D., Day, R.E., Sing, K.S.W. and Stryker, L.J. Discuss. Faraday Soc. 52, 173 1971.

76. Mikhail, R.S.H., Brunauer, S. and Bodor, E.E., J. Colloid Interface Sci. 26, 45 1968.

77. Nicolaon, G.D. and Teichner, S.J., J. Colloid and Interface Sci. 38, 172 1972.

78. Dakri, M.A., Tye, F.L. and Whiteman, J.L. in 'Power Sources' (D.H. Collins, ed.), p.65, Pergamon Press 1967.

79. Le Tran, K., J. Chim. Phys. 64, 922 1967.

80. Gregg, S.J. and Langford, J., Trans. Faraday Soc. 65, 1394 1969.

81. Parfitt, G.D., Urwin, D. and Wiseman, T.J., J. Colloid Interface Sci. 36, 217 1971.

82. Nyholm, R.S., Quart. Rev. 7, 377 1953.

83. Earnshaw, A., Introduction to Magnetochemistry, p.100, Academic Press 1968.

84. Selwood, P.W., Eischens, R.P., Ellis, M. and Wethington, K., J. Am. Chem. Soc. 71, 3039 1949.

85. Ohama, N. and Hamaguchi, Y., J. Phys. Soc. Japan 30, 1311 1971.

86. Ghosh, S. and Brenet, J., Z. Electrochem. 67, 723 1963.

87. Zeilmaker, H. and Drotschmann, C., Batteries 20, 959 1966.

88. Labat, J. and Gabano, J.P., C.R. Acad. Sc. Paris 264, 164 1967.

89. Takahashi, K. and Kozawa, A., in 'Electrochemistry of Manganese Dioxide and Manganese Dioxide Batteries in Japan', (K. Takahashi, S. Yoshizawa and A. Kozawa,eds.), Vol.II, p.23, Electrochemical Society of Japan, 1971.

90. Kozawa, A., in 'Batteries', (K.V. Kordesch ed.), Vol.1, p.385, Marcel Dekker, Inc., New York 1974.

91. Ambrose, J., Ph.D. Thesis, University of Newcastle, 1967.

92. ASTM, X-ray powder diffraction data file 12-733.

93. ASTM, X-ray powder diffraction data file 20-718.

94. Baker, F.S. and Sing, K.S.W., Nature 229, 27 1971.

95. Hagan, A., Ph.D. Thesis, University of Bristol, 1974

96. Czanderna, A.W., in 'Vacuum Microbalance Techniques', (A.W. Czanderna and Katz, eds.), Vol.1, p.129, Plenum Press, New York 1961.

97. Cutting, P.A. in 'Vacuum Microbalance Techniques', (C.H. Massen and H.J. Van Beckum,eds.), Vol.7, p.71, Plenum Press, New York 1970.

98. Alario Franco, M.A., Baker, F.S. and Sing, K.S.W., in 'Progress in Vacuum Microbalance Techniques', (S.C. Bevan, S.J. Gregg and N.D. Parkyns, eds.), Vol.2, p.51, Heyden & Son, 1973.

99. Day, M.A., loc. cit. Ref. 98 p.197

100. Davies, G., Coord. Chem. Rev. 4, 199 1969.

101. Freeman, D.S. and Chapman, W.G., Analyst 96, 865 1971.

102. Lingane, J.J. and Karplus, R.R., Ind. Eng. Chem. (Anal. Ed.), 18, 191 1946.

103. Vetter, K.J. and Jaeger, N., Electrochim Acta 11, 401 1966.

104. loc. cit. Ref. 83 p.92.

105. Lindoy, L.F., J. Chem. Ed. 49, 117 1972.

106. Munuera, G., J. Catal. 18, 19 1970.

107. Carter, G., Vacuum 12, 245 1962.

108. Bunn, C.W., Chemical Crystallography, Oxford University Press, 1961.

109. Jones, P. and Hockey, J.A., Trans. Faraday Soc. 67, 2769 1971.

110. McCafferty, E. and Zettlemoyer, A.C., Discuss. Faraday Soc. 52, 239 1971.

111. Gammage, R.B., Fuller, E.L. and Holmes, H.F., J. Colloid Interface Sci. 38, 172 1972.

112. Doremus, R.H., J. Phys. Chem. 75, 3147 1971.

113. Lima-de-Faria, J., Z. Kristallog. 119, 176 1963.

114. Claveau, A. and Beaulieu, C.E., Mem. Sci. Rev. Metall. 3, 173 1973.

115. Hitchcock, J. and Pelter, P., presented at the Fourth International Conference on Thermal Analysis, Budapest, 1974.

116. Brenet, J., Gabano, J.P. and Seigneurin, M., 16th Congr. Int. de Chimie Pure and Appl. 1957 p.70.

117. Fukuda, M., Nat. Tech. Rep. 4, 321 1958.

118. Wadsley, A.D., Rev. Pure Appl. Chem. 5, 165 1955.

119. Anderson, J.S. in 'Surface and Defect Properties of Solids', Vol.1, p.1, The Chemical Society, 1972.

120. Alario Franco, M.A., Thomas, J.M. and Shannon, R.D., J. Solid State Chem. 9, 261 1974.

121. Fleischmann, M., Thirsk, H.R. and Tordesillas, I.M., Trans. Faraday Soc. 58, 1865 1962.

122. Gabano, J.P., Morignat, B. and Laurent, J.F., Extended Abstracts, Battery Division, Electrochemical Society 1966.

123. Baker, T.W., U.K.A.E. Harwell, personal communication.

124. Klingsberg, C., Ph.D. Thesis, The Pennsylvania State University 1958.

125. Muller, J. and Joubert, J.C., J. Solid State Chem. 11, 79 1974.

126. Evans Jr., H.T. and Mrose, M.E., Am. Mineral. 40, 861 1955.

127. Cimono, A., Lo Jacono, M., Porta, P. and Valigi, M., Z. Phys. Chem. 59, 134 1968.

128. Parks, G.A., Chem. Rev. 177 1965.

129. Payne, D.A. and Sing, K.S.W., Chem. & Ind. 918 1969.

130. Gregg, S.J. and Sing, K.S.W., Adsorption, Surface Area and Porosity, Academic Press 1967.

131. International Critical Tables of Numerical Data, Physics, Chemistry & Technology, Vol.3., First Edition, p.30, McGraw-Hill Book Co. 1928.

132. Jeziorowski, H., Knozinger, H. and Meye, W., J. Colloid Interface Sci. 50, 283 1975.

133. Dubinin, M.M., J. Colloid Interface Sci. 49, 5 1974.

134. Drotschmann, C., Batterien 18, 686 1964.

135. ASTM, X-ray powder diffraction file 10-173

136. ASTM, X-ray powder diffraction file 13-534

137. Bunn, C.W., in 'X-ray Diffraction by Polycrystalline Materials' (H.S. Peiser, H.P. Rooksby and A.J.C. Wilson, eds.) p.344, The Institute of Physics, 1955.

138. Chenavas, J., Coubert, J.C., Capponi, J.J. and Marezio, M., J. Solid State Chem. 6, 1 1973.

139. Shannon, R.D. and Prewitt, C.T., Acta Cryst. 25, 925 1969.

140. Feitknecht, W. and Marti, W., Helv. Chim. Acta 28, 129 1945.

141. Gattow, G., Batterien 16, 322 1962.

142. Fishburn Jr., H.W. and Dill Jr., W.E., Proc. 15th Annual Power Sources Conf. p.98, PSC publications committee, New Jersey 1961.

143. Hardy, A., Bull. Soc. Chim. Fr. 1329 1961.

144. Grasselly, Gy., Acta Mineral. Petrogr. 20, 227 1972.

145. Le Blanc, M. and Wehner, G., Z. Phys. Chem. 168, 59 1934.

146. Bode, H. and Schmier, A., Proc. 3rd Internat. Symp. on Batteries 1962 p.329.

147. Bell, G.S. and Huber, R., J. Electrochem. Soc. 111, 1 1964.

148. Giovanoli, R., Stahli, E. and Feitknecht, W., Helv. Chim. Acta 53, 453 1970.

149. Alario Franco, M.A. and Sing, K.S.W., J. Therm. Anal. 4, 47 1972.